Accuracy in Radiotherapy Dosimetry

Mahmoud Allahverdi, B.Sc., M.Sc.

Ph.D
The University of Edinburgh
1998

DECLARATION

I declare that this thesis has been composed by myself and that the work contained in it is my own.

Mahmoud Allahverdi

September 1998

This work is dedicated
to my dear wife Nasrin and
to my dear daughter Maryam

ACKNOWLEDGEMENTS

The author wishes to thank all those who contributed in the tuition process towards learning the new skills needed for this work. In particular I would like to express my gratitude to my supervisor Dr David Thwaites for his invaluable advice, guidance, criticism and encouragement throughout the course of this project. In addition, I would like to thank Dr Tony Redpath and Dr David Bonnett, the examiners, for their helpful comments and suggestions on the layout and presentation of this thesis.

I am grateful for the technical support of the Mechanical and Electronics workshops and also to Mrs. Aileen McLeod and Mr. Ronnie Turnbull of the Treatment Planning Unit for their assistance. I am thankful to all staff in the Department of Medical Physics and Medical Engineering in the Western General Hospital and the Department of Clinical Oncology (particularly Oncology Physics) for their assistance during my time here. I very much appreciate the head of department Professor W.N. McDicken for his kindness and advice.

I thank all those friends with whom I kept in touch during these last years. Iranian students in Edinburgh and my fellow students deserve a special mention for their support and good advice.

I would like to thank my wife for her tireless patience, encouragement, and supportive attitude throughout the entire programme. I am also very grateful to my mother for her moral support.

The financial support of the government of the Islamic Republic of Iran is very much appreciated.

Abstract

Accuracy in Radiotherapy Dosimetry

The accuracy of radiotherapy is one of the most important aspects of the management of patients with cancer undergoing radiation treatment. The main aim of achieving accuracy is to produce quality in treatment, by ensuring that treatment delivery conforms as closely as possible to prescription. There is a narrow relationship between the probability of local tumour control or normal tissue injury and total absorbed dose. Based on clinical data on these dose effect relationships, an accuracy is recommended of ±3% on absorbed dose delivered at the specification point and ±5% at other points in the target volume (Mijnheer et al 1987, Brahme et al 1988, Thwaites 1992). This is taken to be a requirement at the one standard deviation level and as a final value incorporating all contributing uncertainties up to and including treatment delivery. It is generally taken to be consistent with the ICRU (1976) requirement of ±5% on delivered dose. To meet this, comprehensive quality assurance and quality control programmes are necessary and there are many sets of guidelines in this area (Thwaites et al 1995).

The accuracy achieved in practice can be estimated either by a priori methods or by measurement-based investigation, including dosimetry intercomparisons and audit and also from in vivo dosimetry carried out on groups of patients. The minimum figures obtained from such exercises most probably indicate the best currently achievable precision in delivery of radiation doses to patients in routine practice. The project involves an experimental analysis of achievable accuracy in the different steps of radiotherapy,

including investigations of the basic dosimetry chain, considering the individual steps concerned in dosimeter and treatment beam calibration and some aspects of treatment planning and dose delivery. The results are investigated from these various areas and are analysed in terms of overall achievable accuracy and its relationship to clinical requirements and to quality assurance programmes. It is concluded that required clinical accuracy can be achieved in radiotherapy treatment, but needs careful control at all stages of the radiotherapy process.

In addition a previously-designed geometric phantom, developed for a UK national dosimetry intercomparison and audit system (Thwaites et al 1991), has been used to extensively test achievable accuracy of dosimetry and some basic treatment planning parameters and processes in one department. This has been used as the basis to develop an interdepartmental audit in Scottish and other radiotherapy centres (the so-called Scottish+ audit group, within the UK radiotherapy dosimetry audit network). Also a semianatomic phantom has been developed to allow reasonably realistic audit of various representative treatment sites, including breast, thorax, head and neck, etc. This has been constructed from epoxy-based tissue substitute phantom materials. It has been extensively tested before audit use, by measuring the whole range of possible irradiation situations on five megavoltage photon beams, calculating dose distributions using the Edinburgh in-house treatment planning system and CADPLAN, and comparing measured results to expected values. Some small differences can be linked to the phantom materials. Others can be linked to small discrepancies in the testing department, for example in planning data, machine performance, etc. Others can be linked to problems in the way that planning systems cope with some treatment situations, in particular around inhomogeneities, interfaces, due to lack of scatter, etc. The results coupled with similar results from a geometric phantom and in vivo dosimetry give a good estimate of achievable accuracy within a single department. The interdepartmental audit has shown that there is general agreement of doses within the specified audit tolerances. However, analysis of the results

point-by-point and field-by-field can illustrate problems. The pilot work has established the audit approach and methodology as a valuable system and has provided a baseline set of data for subsequent ongoing routine audit, building on the methods developed.

One significant source of uncertainties associated with the absorbed dose delivered to the patient is due to dose per monitor unit determination for linac treatments. The accuracy of monitor unit determination for dosimetry calculations can be significantly influenced by variations in head scatter and phantom scatter. This becomes more important where the collimator setting and field size on the phantom surface differ or where the beam distribution is altered from the standard e.g. wedged beams, blocked fields, asymmetric fields, irregular and MLC fields. Head scatter factors were measured using plastic build up caps, brass caps, slab phantoms and miniphantoms for different situations to assess and compare the techniques and investigate the effects of secondary electrons. Phantom scatter factors were then derived and compared in different situations to tabulations. The output factors obtained for various configurations of open, wedged, blocked and MLC beams, both for symmetric and asymmetric situations have been investigated and compared to those obtained and used in the standard in-house treatment planning calculation approach and other approaches. The results show that separating head scatter factors and phantom scatter factors for regular and irregular fields provide a more accurate method to calculate monitor units for standard and conformal radiotherapy treatment.

CONTENTS

List of Tables

List of Figures

Chapter 1

1-Introduction

1-1-Developments in Radiotherapy Treatment

The modern practice of radiotherapy has developed since the 1940. Many successive revolutions have happened from that time until now. The first in the early fifties, was the jump from conventional x-rays to high energy photon beams. In this process progress in radiation therapy was largely determined by the production of satisfactory sources, firstly ^{60}Co which is still one of the most common sources for patients' treatment in centres world-wide. The second development was the linear accelerator where technology has improved from year to year. The third development between the sixties and the seventies was the application of computers in radiotherapy particularly in treatment planning. It was followed by the fourth one on diagnostic imaging particularly Computer Tomography (CT), which would not have been feasible without computers. These new equipment and techniques are now used routinely in the majority of radiotherapy centres. Current developments include conformal radiotherapy, both static and dynamic using further sophisticated machinery, and the rapid expansion of the use of information-technology in radiotherapy departments. The purpose of all these advances in radiotherapy has been to improve accuracy and improve quality in patient treatment and in the outcome of treatment. New techniques also show the responsibility of the physicist to continue to work to improve quality in radiotherapy.

1-2-Aim of Radiotherapy

The purpose of treatment of cancer is to remove or kill the cancer cells or to stop their multiplication. There are different types of tumour cells, some grow together to form a solid mass, and some are able to move freely in the blood such as leukaemia or in the

lymphatic system such as lymphomas. Tumour cells are treated in different ways i.e. surgery, chemotherapy, and radiotherapy. For some cases the combination of these modalities can be used. In Europe it has been estimated that out of a hundred cancer patients, approximately 22 will be cured by surgery, 18 by radiotherapy (alone or combined, but with radiotherapy as the major modality), and 5 by chemotherapy (alone or more often, combined with other modalities).

In radiotherapy tumour cells are damaged or killed by ionising radiation e.g. x-ray. The dose required to achieve cell killing is variable, because the cells have different sensitivity to radiation. Also the radiosensitivity of cells varies considerably as they pass through the cell cycle. The tumour cells are always situated close to or within normal tissues. Figure (1-1) shows the viable tumour regions surrounded by vascular stroma from which the tumour cells obtain their nutrient. In some cases, as illustrated, as these regions expand, areas of necrosis appear at the centre. The tumour mass may also spread and infiltrate normal tissues. The radiation tolerance of the normal tissues inside the irradiated volume generally limits the absorbed dose that may be delivered to the target volume. There is often a small margin between the absorbed dose values needed for adequate tumour control and those causing unacceptable complications. Therefore, it is generally not possible to kill all tumour cells. In addition some normal cells generally receive a high dose. The aim of radiotherapy is to maximise dose to tumour cells and at the same time minimise dose to normal tissue cells. Chapter 2 discusses this further.

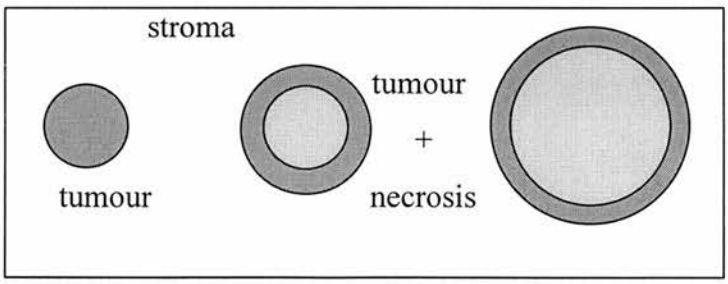

Fig. 1-1: Schematic sections of carcinoma showing the development beyond a limiting distance from the vascular stroma

1-3-Radiobiology of Tumours and Normal Tissues

Different cells (and different individuals) have different radiosensitivies. For tumour cells, the initial steepness of cell survival curves is a significant factor in the clinical response. The effect of ionising radiation on the various normal tissues of the body is variable, both for the dose required to produce damage and in the expression of damage. Normal tissues can be divided into two categories, early responding, e.g. skin, and late-responding, e.g. lung, kidney and spinal cord. Damage to early responding tissues tends to heal, but to the late-responding tissues tend to be more permanent. Some late tissues are very sensitive or the effects are very critical, for example damage to the spinal cord appears as paralysis. Therefore, the radiotherapist seeks to avoid such damage at all costs.

As radiation dose increases, the effects on both normal tissue and tumour increase. The questions then arise as to what level of normal tissue damage (early or late) to the patient can be tolerated; what limiting radiation dose produces this level and what the effect on the tumour is at this dose, i.e. the level of tumour response is determined by the maximum tolerable dose to normal tissues. Because the two effects typically overlap in dose and because at least some of dose-effect curves are steep, the accuracy of treatment dosimetry is critical in determining answers to these questions.

One additional factor in all these questions is that of fractionation, i.e. when the number of fractions is increased or dose per fraction is decreased, the tolerance is increased. Fractionation modification has been used, or is being developed, to try to improve the optimisation of the balance between tumour control and normal tissue damage. It has been suggested to use an increased number of small dose fractions (hyperfraction), given over a conventional overall time to take advantage of the differences between tumour and late normal-tissue responses. Also accelerated fractionation has been suggested, to minimise

repopulation in the tumour. However, whatever the fractionation, the requirement for technical accuracy is still vital.

1-4-Aim of Thesis

It has been estimated that around ten million people in the European Union are alive today after treatment for cancer. Of these, 1-2 million will have recurrent desease and will die of the cancer, while the rest are considered cured. Around half of these cured cancer patients have received radiotherapy (Thwaites et al 1995). Some of these patients will develop some side-effects due to the treatment. Therefore, the further development of radiotherapy is aimed at conformally shaping the high dose regions to the tumour regions with the highest possible precision and at the same time reducing the dose of radiation to the surrounding normal tissue. This requires even higher accuracy in dose calculation and delivery.

One of the most important current questions is then what degree of accuracy is required and how can it be achieved in practice? In addition what degree of accuracy is actually being achieved in practice now? Can the new methods and new techniques improve accuracy in radiotherapy? The aim of this thesis is to investigate some of these questions and to test what achievable accuracy can be obtained in best current radiotherapy practise, in order to support evolving clinical requirements. Inaccuracies, or uncertainties, occur at all the various stages of the radiotherapy process. One major area of this work is the measurement and assessment of what uncertainties are introduced individually at the various stages of the technical radiotherapy process. Such investigations can be carried out in one department to test possible variations between patients, or modalities, or at different times, in a given centre or between centres (quality audit) to test variations which might affect patients treated at different departments. The information obtained can be used to quantify and optimise each step in order to improve accuracy in radiotherapy. Also the information

obtained in all centres can be used to help to optimise radiotherapy in different departments to match the best consistency achievable, by identifying differences or errors in practice.

In general, the results from different stages using measurement in phantoms can be coupled with those from other tests such as in-vivo measurements on patients to allow conclusions to be drawn on the achievable accuracy in a particular department over a wide range of treatment conditions. The results from interdepartmental tests (audit) can improve, or give confidence in, shared or transferred clinical experience from one centre to another.

1-5-Outline of Thesis

Chapter 2 discusses accuracy requirements in radiotherapy. The uncertainties are discussed at each of the various stages of radiotherapy. Chapter 3 experimentally investigates the achievable accuracy at the different stages of the basic dosimetry chain, considering the individual steps concerned in dosimeter and treatment beam calibration. Chapters 4 and 5 present an extensive experimental measurement programme to test achievable accuracy of clinical dosimetry on treatment units for single fields and multi-field planned situations in one department using both geometric and semianatomic phantoms. The semi-anatomic phantom has been developed and tested to be used in further development of interdepartmental audit in Scottish and other centres (in the Scottish+ group). Chapter 5 describes this work and presents initial results from the phantom use. Chapter 6 reviews some commercial 2D and 3D inhomogeneity algorithms against measurement to compare the approaches and evaluate their practical usefulness. In conjunction with the results from the preceding chapters where measured doses were compared to calculated dose distributions using the same algorithms, this can show which situations require more sophisticated algorithms in treatment planning. Chapter 7 reviews the methods for separation of total scatter factor into head scatter factor and phantom scatter factor for different situations. The accuracy of monitor unit determination for dosimetry calculations

can be significantly influenced by variations in head scatter factor and phantom scatter factor. This becomes more important where the collimator setting and field size on the phantom surface differ. Chapter 8 experimentally investigates these approaches and assesses the effects of electron contaminants and electron equilibrium on collimator scatter factors, to compare the various methods of separation of total scatter factor into head scatter factor and phantom scatter factor. Chapter 9 presents the results obtained by separating total scatter factor into head scatter factor and phantom scatter factor for open and wedged beams, blocked fields, MLC and irregular fields, both for symmetric and asymmetric situations. These factors have been investigated and mu/dose calculations compared to those obtained and used in the standard in-house treatment planning calculation approach and other approaches, to quantify the uncertainties in MU calculation in various practical clinical situations. The phantom scatter factors are compared in different situations to tabulation to assess whether these tabulations are generally applicable in all such cases. Chapter 10 summarises the experimental assessment of achievable accuracy for various stages of radiotherapy. Finally, some conclusions are drawn in chapter 11.

Chapter 2

2- Accuracy Requirement in Radiotherapy

2-1- Introduction

The accuracy of radiotherapy is one of the most important aspects of the management of patients with cancer undergoing radiation treatment. Nowadays 2.5 million patients are treated by radiotherapy world-wide in each year. The aim is to achieve local control of the tumour. However, radiation also damages healthy tissue and so a parallel aim is to minimise complications. The required accuracy in radiotherapy is based on information on the relationship between dose and tumour control (TC) and that between dose and normal tissue complications (NTC). Thus, for optimum treatment, the radiation dose must be planned and delivered with a high degree of accuracy. The main aim of achieving accuracy is to produce quality in treatment, by ensuring that treatment delivery conforms as closely as possible to prescription. The purpose of new techniques in radiotherapy e.g. new modalities, conformal therapy, new facilities such as multileaf collimators, etc. is to maximise the dose distribution in the target volume and at the same time minimise the dose to critical tissue. New developments in dosimetry intercomparison, in vivo dosimetry, portal imaging, etc. are intended to verify treatment accuracy. They can also reveal errors and thereby improve quality.

2-2- Accuracy

Accuracy usually refers to deviation of the measured value from its 'true' value. This deviation is considered as a combination of random and systematic errors. Random uncertainties are derived by statistical methods from a number of repeated readings. In the analysis of the results of repeated measurements, it is necessary to show that they are consistent with a given type of distribution, ideally this will be a normal

distribution if there are sufficient observations. In this case the spread can be expressed in terms of the standard deviation.

Systematic uncertainties are estimated by considering the physical effects which influence the results. These uncertainties may be related to the level and effectiveness of the quality assurance programmes of the therapy centre. The first step in the estimation of this uncertainty is for the experimenter to identify those aspects of the measurement that can affect its value. Successful identification of such effects depends very much on experience and judgement. Random and systematic uncertainties are also called type A and B uncertainties (Thwaites 1988). Type A is statistical and can be estimated from repeated independent observation as a standard deviation. Type B uncertainties are not statistical but can be estimated and reported as an effective standard deviation, which is expected to contain the true value in about 70% cases. Systematic uncertainties are important in transferring experience from one centre to another centre, whilst random uncertainties are important in describing the precision of dosimetry in one radiotherapy centre. The overall uncertainties can be obtained by the combined uncertainties as the square root of the sum in quadrature of all components in both categories of uncertainty, as a one standard deviation value.

2-2-1- Relationship between TCP and NTCP with absorbed dose:

For both human normal tissue and tumours the curves of response versus dose have sigmoidal shapes (Fig. 2-1). There is often a steep relationship between the probability of local tumour control or normal tissue injury and total absorbed dose.

According to figure (2-1), D_0 is the intended treatment dose, i.e. selected as a balance between maximising dose to the tumour and at the same time minimising dose to normal tissue to within an acceptable level. Small changes in D introduce large changes in dose response. The separation between the curves is also important (the closer together that the curves are the greater the accuracy required).

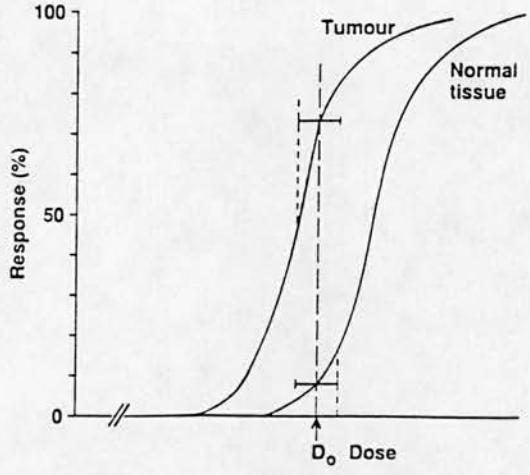

Fig 2-1: Probability of tumour control and normal tissue complication against dose

The required accuracy can be linked to the steepness of the curves, by considering the effect of small changes of dose on NTCP and TCP and whether the changes produced in these are acceptable or no. The steepness of dose-effect curves can be quantified by $\Delta_{P2/P1}$, where P_2 and P_1 are selected relevant values of the percentage of the probability of effect and Δ is the relative percentage increase in dose to produce a change in probability of effect between the two stated values (Goitein 1979). For example, Withers and Peters (1980) calculated for general situations that with reduction of 3% in dose, the probability of tumour cell control decreases from 50% to 25%, and also increases from 50% to 75% probability for an increase of 5% in dose. Mijnheer et al (1987) showed that the relative gradient, $\Delta_{75/50}$ of most clinical curves for local tumour control varies between 10% and 20%, whereas clinical dose-effect curves for normal tissue damage have a $\Delta_{50/25}$ between 4 and 10%. They considered a representative value to be 7.0% for normal tissue damage.

Brahme et al (1988) introduced another factor to represent curve steepness, γ, as the normalised dose gradient according to $\gamma = D\ (dp/dD)$, where γ shows the change in the probability of effect for a given relative change in dose. Based on this definition, when dose increases by 1.0% it produces a probability increase of γ% (Thwaites 1991).

In addition other parameters such as biology variation due to tumour heterogeneity, radiosensivity, staging, and technical parameters such as dose per fraction can affect tumour control probability.

2-2-2- Clinical Requirement on Accuracy

On the basis of considering clinical data on these dose-effect relationships, a required accuracy of ±3% on absorbed dose delivered at the specification point and ±5% at other points in the target volume has been proposed by a number of authors (Mijnheer 1987, Brahme et al. 1988, Thwaites 1992). Mijnheer et al (1987) suggested a value of 7.0% change in dose at the 95% confidence level as the limit on clinically detecting changes in complication probabilities based on the data summarised section 2-2-1. Therefore, setting this as the maximum allowable variation in dose at the 2sd level, a value of 3.5%, one sd level, was recommended as the general accuracy requirement on absorbed dose delivery. Brahme et al (1988) suggested a figure of 3.0%, one relative standard deviation, in order to keep variation in TC probability within acceptable limits by calculating TC variations for various changes in dose, using typical values of tumour γ steepness his calculation model. Therefore, taking both approaches there is good agreement and, a recommended value of ±3% on absorbed dose delivered at the specification point as a 1sd level is selected as the lower of the two. In addition ±4mm is generally required (1sd) in the geometric aspects (Thwaites 1989, 1991). This is based on a priori estimation of minimum achievable geometric uncertainties in typical situations and setting this to the recommended level (AAPM 1984, Thwaites 1991). These are all taken to be requirements at the one standard deviation level and as a final value incorporating all

contributing uncertainties up to and including treatment delivery. This implies that changes will be clinically observable (within a confidence limit of 95%) for dose changes at twice this level, at least for situations described by steeper dose-effect relationships. Brahme et al. (1988) indicated that the largest loss in TC introduced by dosimetric inaccuracy is found at the highest TC probabilities. This also implies that the accuracy requirement on each step (from basic dosimetry to patient dose delivery) of the whole process must be suitably less than the overall accuracy recommendations.

2-2-3- Quality Assurance Recommendations

In order to achieve the required accuracy in radiotherapy, quality assurance and quality control programmes have an obviously important role in reducing uncertainties and improving accuracy. There are many national and international recommendations concerned with this, for example the recent guidelines from ESTRO (Thwaites et al. 1995).

2-2-3-1- Quality Assurance and Quality Control

According to WHO (1988):
"Quality assurance is concerned with all those procedures that ensure consistency of the medical prescription as regards dose to the target volume, together with minimal dose to normal tissue, minimal exposure of personnel, and adequate patient monitoring aimed at determining the end result of treatment".
The aim of quality assurance is to guarantee the performance of a process within a certain stated specification.

Quality control, is the process of measurement and comparison with existing standards and the actions necessary to modify those parameters that are found lower than the accepted level of quality. Quality assurance and quality control programmes must be based on the general clinical requirements and the accuracy deemed

clinically necessary in the overall radiotherapy process, in order to produce the quality in treatment that is demanded in practice. Before the establishment of any quality control programmes a number of questions must first be addressed (Thwaites 1992). These include consideration of:

- what needs to be tested;
- at what frequencies at each level;
- to what tolerance and action levels;
- and using what methods, equipment and time.

The tolerance level is specified based on clinically required accuracy. An action level is often approximately twice the corresponding tolerance level, depending on the situation and the parameter. Frequencies of tests may change in different situations and recommendations, but there are minimum criteria that must not be ignored. The WHO (1988) provided one set of minimum recommendations for quality control in radiotherapy for use in centres world-wide. It can be concluded from the wide literature of recommendations that quality assurance and quality control systems are necessary to achieve good accuracy in radiotherapy treatment. However good the QA and QC recommendations (quality standards) it is also necessary to test how well these standards are met.

2-2-3-2- Quality Audit

Quality audit is an independent review at any level of the radiotherapy process to identify and quantify errors. Independent implies that the methods for review must be independent of the process and procedures under consideration, e.g. independent equipment, independent methods and ideally independent personnel. External audit would require external personnel. However many types of audit can be implemented within a department (internal audit). Quality audit can be carried out at any level in radiotherapy i.e. dosimetry, planning system performance, target volume selection and treatment prescription, planning procedures, patient positioning, dose delivery etc. However, the most frequent audits in the literature are using dosimetry

intercomparison in reference conditions (beam calibration) with a few other situations included. Quality audit as such is wider than a dosimetry intercomparison, it can include a wider set of parameters (Johansson et al. 1986; EORTC 1989; RPC, Hansson et al $1991_{b,c}$; CHART, Aird et al 1994). Additional characteristics which can distinguish audit from dosimetry intercomparison are: quality standards would be necessarily pre-defined, in terms of tolerance levels and possibly action levels; procedural audit would be included by discussion questionnaire and inspection, feedback from auditors to the centre would be necessary, with any points for action identified, and a response from the centre would be required where appropriate (Thwaites 1996, Bonnett et al 1994). In general, dosimetry intercomparisons have provided the basis of practical dosimetry audit methodology, and also have introduced improvement e.g. the UK dosimetry intercomparison (Thwaites et al 1992).

Practical quality audit can be implemented by visits using ionisation chamber dosimetry or mailed systems using TLD or film (Hansson and Johnsson 1991_c, Davis and Faesster 1993, Bonnett et al 1994, Allahverdi and Thwaites 1996_b, Thwaites and Allahverdi 1997). However, mailed systems can only use a simple questionnaire, and limited measured values. In addition measurements with ionisation chambers, relative to TLD are more flexible and more precise. Audits based on visits can also include more comprehensive procedural audit, more parameters and can vary these parameters as required. However, TLD will often be the preferred organisational basis of audit systems with a wide geographical spread (e.g. IAEA, RPC and EORTC). Quality audit networks have now been established nationally and internationally, which link the different approaches e.g. European/IAEA (Bridier et al 1993, Hansson 1993 and Dutreix et al 1993) and UK audit network (Thwaites and Williams 1994_a, Thwaites 1994_b, Thwaites 1996). Quality audit can be carried out in one department (intra-departmental audit) or between departments (inter-departmental audit) nationally or internationally. Essentially any checking or verification system that is implemented in addition to routine quality programmes in one department, can be defined as a type of audit. In these situations the distinction

between quality assurance and quality audit become blurred. However, it must be stressed that quality audit programmes are not to be used instead of quality assurance programmes but are complementary to them. Quality audit between centres or countries can be carried out at different levels of radiotherapy to measure the achieved consistency between centres.

The quality at the final step of dose delivery to the individual patient can be checked by portal imaging systems for positioning and using in vivo dosimetry for dose as a quality audit programme. In vivo dosimetry and portal imaging systems can reveal uncertainties at the end point of treatment delivery and lead to improvements in local accuracy. These can be coupled with other quality audit at appropriate levels in the radiotherapy process to improve overall accuracy.

2-3- Sources of uncertainties from calibration to dose delivery

Each step in the dosimetry measurement chain, from the basic physics and dosimetry standards underlying beam calibration to the radiation treatment of the patient, contributes to the uncertainty of the absorbed dose delivered to the irradiated tissue. These steps are summarised as follows:

I-Basic Dosimetry:

Accuracy of absorbed dose measurement depends on the quality of radiotherapy equipment, dosimeters and published dosimetry protocols. Different steps in the basic dosimetry chain are as follows:

- Primary standard (NPL) + physical constants
- Secondary standard (SSDL) or secondary standard transfer instrument
- Reference chamber (centre)
- Field instruments (centre)
- Beam calibration (centre)

II- Single Fields:

- Beam data, treatment machine performance, relative dosimetry
- beam quality
- depth dose
- profile, isodose
- dose variation with field size, shape, etc.
- effects of beam modifiers e.g. wedge, blocks, tray, etc.
- effect of different parameters, e.g. oblique incidence, etc.

III- Treatment Planning (centre):

- Beam Data
- Patient Data, specification of volumes etc.
- Calculation algorithms, including inhomogeneity algorithms
- Different Planning Computing Systems performance
- Difference between tissue material to water
- acceptability of plan, criteria, tolerance, etc.

Today most treatment planning is computerised. Therefore, uncertainties, particularly random errors, reduce in comparison to those errors possible in hand planning. However, computers introduce a risk of new errors.

A knowledge of cross-sectional anatomy is very important for accurate treatment planning. Firstly, for determination of treatment volume, body contour, tumour, inhomogeneities, secondly for determination of the position of critical organs for their protection, and thirdly for determination of quantitative information on densities of different materials. For these reasons the wide introduction of CT systems for treatment planning purposes has improved the accuracy of patient data. In addition recent advances in imaging systems particularly MRI may be helpful.

IV: Patient Treatment (centre)

- set up
- immobilisation
- organ motion
- repeatability day to day
- machine stability day to day
- etc.

In the set up, attention must be given to the comfort and immobilisation of the patient. The uncertainties are due to organ motion and patient movement, and therefore the change of the relative position of the target volume during the course of the treatment. Other types of uncertainties in this category may be introduced by machine inaccuracy producing displacement of one or several fields relative to target volume at nominal distance (i.e. isocentric accuracy, light field agreement, jaw alignment, etc.). These errors must be identified and analysed with respect to their contribution to the overall uncertainty in the patient dose. Portal imaging is useful for determining geometric and dosimetric uncertainties at the final step. In vivo dosimetry is useful for estimation of uncertainties related to both the set up of the patient and the treatment unit parameters. Currently, diodes are increasingly used for determination of entrance and exit dose that has provided good results (Leunens et al $1990_{a,b}$ and 1991, Heukelom et al $1991_{a,b}$ and 1992, Millwater et al 1994 and 1998).

Looking at the above list, it can be concluded that firstly uncertainties can occur in any of the different levels of radiotherapy, and secondly the reduction of the overall uncertainty to the required level requires careful control of uncertainties at each step and requires a multidisciplinary collaboration of the whole team of radiotherapist, physicist, engineer and radiographer.

2-4- Evaluation of Uncertainties

The accuracy achieved in practice can be estimated by a priori methods and by measurement-based studies, including dose intercomparisons, which can be carried

out at various levels of the technical radiotherapy process to define errors and uncertainties at each of those stages. This can be coupled with other evidence on achievable accuracy e.g. audit and in vivo dosimetry results. Combining this information can give a good indication of overall accuracy likely to be realised in the clinical situation. The minimum figures obtained from such exercises most probably indicate the best currently achievable precision in the delivery of radiation doses to patients in routine practice. Larger figures indicate situations where improvement is indicated to encourage development towards the minimum figures.

2-4-1- Review of Dosimetry Intercomparisons

Dosimetric intercomparisons can define errors and evaluate the consistency of dosimetry between centres. Many different types of dosimetry intercomparisons have been carried out with simple geometric and anatomical phantoms. Several dosimetry intercomparisons have been made between a few centres to compare dosimetry protocols (Almond et al 1972). Mattsson (1985) carried out a comparison for absorbed dose determination to water using different dosimetry protocols. They showed that differences between dosimetry protocols increase if non-standard ionisation chambers and phantom materials are used.

The majority of intercomparisons have been carried out at the reference point (or close to reference conditions) to provide information on basic dosimetry and protocol differences up to and including beam calibration (Wittkamper et al 1987, Johansson K A 1987, Hansson et al 1991_a, Thwaites et al 1992). Some recent results are summarised in Thwaites et al 1992 and Thwaites 1993 showing the mean deviation in measured dose to expected values up to 2.4% with standard deviations within 1.3 to 3.3%. Overall, most mean deviations in measured dose compared to expected are within ±1.0% with standard deviations on the distributions of between 1% and 10%.

Some intercomparisons have been carried out in non-reference conditions to assess additional uncertainties in single beams, including the presence of beam modifiers.

Wittkamper et al (1987) investigated the accuracy of relative dose distribution in a water phantom. The results were in good agreement except for wedged beams and in off-axis planes which showed larger deviations. Overall, the mean deviation of measured to calculated values for open, wedged, oblique beams etc. are within 3.0% with standard deviations within 1.0% to 3.0% (Thwaites et al 1992).

Some more complicated intercomparisons have been designed to assess the overall uncertainties close to the end of the dosimetry chain using geometric and anatomic phantoms for multiple planned beams. Measured dose values have been compared with calculated values based on the local beam data and treatment planning system (Johansson K A 1987, Wittkamper et al 1988, Van Bree et al 1991, Thwaites et al 1992, Thwaites and Williams 1994_a, Thilander and Jhansson 1994). For example Thwaites et al (1992) carried out a dosimetry intercomparison in 64 radiotherapy centres using a geometric phantom in the UK. The mean deviation between measured and calculated values were 1.008 and 1.011 for homogeneous and inhomogeneous phantoms with standard deviations 2.7% and 3.4% respectively, and 89 percent of the results were within 5% unity. Some intercomparisons have also included mechanical checks of treatment equipment (Hoornaert et al 1993).

2-4-2- Other Evidence on Achievable Accuracy

2-4-2-1- In vivo Measurement

Regular measurements of dose or positional information throughout treatment can provide information on the relative overall uncertainties within a given centre. In vivo dosimetry and portal imaging systems provide tools both to improve the data on uncertainties and to lead to improvement in accuracy. On-line in vivo dosimetry can check the absorbed dose in real time. Today semiconductors (p-type diode) are mainly used, in suitable encapsulation as build up. Diodes are put on the surface skin and entrance and exit doses are measured. An overall check of basic dosimetry, treatment unit parameters, planning and calculation methods and daily set up of the

patient can be determined by the combination of entrance and exit dose. The entrance point is defined as the point along the central axis of a beam at a depth of the Dmax, and the exit point is defined as the point along the central axis of the beam at a distance Dmax from the exit surface of the phantom. Readings are linked to these doses by calibration of the diode against ionisation chamber in these positions.

Leunens et al (1990_b) obtained the results of entrance doses by diodes in 230 patients. They showed that the sources of inaccuracies detected by entrance dose measurement are related to errors in the algorithms for dose calculation, treatment unit and set up errors or human mistakes. Table (2-I) summarises the results of in-vivo measurements for different sites.

Table 2-I: summary of results of in-vivo measurements for different sites

Reference	Site	No.	situation	Mean	S.D.%
Leunen et al (1990_b)	Head and Neck	230	entrance	1.003	2.5
Millwater et al (1993)	Head and Neck		entrance exit	1.004 0.976	2.7 4.8
Leunens et al (1991)	Breast	920 490 430	global modern old unit	1.007 0.999 1.014	3.2 2.2 3.7
Heukelom et al (1991_b)	Breast	14 14 14 14	phantom * patient* patient phantom	0.980 0.991 1.056 1.00	0.6 1.3 2.6 1.4
Ciocca et al (1991)	Breast	33 48 18	ref. point off axis off plane	0.966 0.968 0.968	3.8 4.3 7.6
Heukelom et al(1992)	prostate	18	specific point	1.005	1.7

**isocentre*

Milwater et al (1994, 1998) obtained good results for head and neck. Other authors have obtained good results in breast and pelvic sites (Ciocca et al 1991, Leunen et al 1991, Heukelom et al 1991, 1992). The review of these studies showed that the main deviations are systematic errors related to errors in the algorithms for dose calculation, treatment planning and set up.

2-4-2-2-Portal Imaging Studies

Portal imaging can verify positional aspects of treatment. Different techniques of portal imaging such as film, fluoroscopic detectors, linear arrays of diodes, and matrix ionisation chambers are used. The limitation of images at these beam qualities is that there is relatively low contrast for megavoltage radiation. Some authors (Mitine et al 1991 and 1993, Weltens et al 1993) suggested the main errors or systematic errors can be determined at the first session of treatment. They believed that the first check is appropriate, because the accidental errors or human mistakes do not affect the next set up. Some other authors criticise this assumption (Lebesque et al 1992, Denham et al 1993). They realised that it is not possible to find a discrepancy between simulator and portal image, unless day to day deviations be defined. Table (2-II) gives some examples of the results of simulator to treatment unit differences for different sites. The specific values reported will relate to the particular immobilisation techniques used and their effectiveness, patient movement, organ movement, reproducibility of set up in different departments, etc.

For day-to-day variation on the treatment unit, Tienhoven et al (1991) reported the average of the standard deviation in 41 fractions in 12 patients of tangential breast. The average standard deviations were weighted for the number of fractions per patient (3-5, mean 4). Table (2-IIIa) shows the weighted average standard deviation and maximum deviations for day-to-day variation on treatment unit. Other studies show similar variations for other sites (Table 2-IIIb).

Table 2-II: Average difference (distance) between simulator and portal imaging with standard deviation

	site	Av. displac.	S.D. mm
Mitine et al	Head and Neck		
(1991)	-AP	1 mm	4.5
	-craniocaudal	2 mm	4.0
Dunscumbe et al	Prostate	3.5 mm	4.5
(1993)			
Tienhoven et al	Breast		
(1991)	-AP	2.1 mm	2.8
	-craniocaudal	1.3 mm	4.7
Weltens et al	mantle field		
(1993)	-craniocaudal	1 mm	5.2
	-lateral	1 mm	3.8

Table (2-IIIa): The weighted average standard deviation and maximum standard deviations for day-to-day variation in treatment unit

Parameter	weighted average SD	maximum deviation(mm)
central lung distance	1.7 mm	4.2
central beam edge to skin distance	2.2 mm	4.9
cranoicaudal distance	1.8 mm	3.6
lateral source-skin dist.	5.3 mm	11.5

Table (2-IIIb): Average displacement and standard deviation for portal images taken throughout treatment (interfraction variations)

	Site	average displacement	S.D. (mm)
Dunscombe et al	Head and Neck	1.9	3.3
1992			
Weltens et al	Mantle		
1993	-craniocaudal	*	3.4
	-lateral	*	2.6
Mitine et al	Head and Neck		
1991	-AP	0.1	3.0
	-craniocaudal	0.5	2.5

** not reported in the publication*

2-5- Quality Audit Networks

There are more than 3000 megavoltage radiotherapy facilities world-wide of which not more than 50% participate in some level of quality audit by an independent expert (Hansson and Jarvinen, 1994). There is a need for quality audit programmes which cover all aspects of radiotherapy dosimetry from basic dosimetry to the patient dose delivery. Because of geographic problems both mailed dosimetry systems and on-site reviews are suitable for the most comprehensive audit, and the most rapid resolution of discrepancies. Now, quality audit networks have been established and developed by IAEA/WHO and by EORTC and ESTRO as well as by various national bodies. These programmes recommend that audits should be performed on a regular basis. The frequency of audit depends on the radiotherapy centre and its equipment and methods. Ideally annual audit is recommended in this network, but also that the frequency should not be worse than one visit in every five years (Dutreix et al 1993).

2-5-1- Quality Audit Network in the UK

The UK radiotherapy physics audit network is now well established, with seven network groups and co-ordinated by the IPSM (now IPEM). It is based on visits, using ion chambers as the measurement method, and auditing at least machine calibration, some single field parameters and simple multi-field planned irradiations, in a geometric phantom (IPSM photon dosimetry phantom, Thwaites et al 1992). In addition procedural audit of dosimetry and quality control procedures, and records are incorporated (Bonnett et al 1994, Thwaites 1996). The general approach has been to use interdepartmental audit involving mutual co-operation with peer professionals from other centres.

The different groups have evolved at different paces and in rather different directions. However, the IPEM co-ordinating role ensures a basic common minimum content to the system. One of the major groups is the so-called Scottish+ group, based in Edinburgh and including all Scottish centres and Carlisle, Belfast, and Newcastle. These centres are developing a hierarchical audit system, in the sense that annual audit visits are undertaken but different levels of the dosimetry chain are included at each visit. The Edinburgh centre is the co-ordinator and measuring centre and also is participating in the development and testing of the IAEA and the European systems, thus providing a link between the UK network and these international networks.

2-6- Summary and Conclusion

The purpose of radiotherapy is to eradicate a tumour without causing unacceptably severe damage to healthy tissue. High accuracy is required because, the steepness and separation of the dose effect curves for tumour control and normal tissue complication curves result in potentially large changes in TCP or NTCP for relatively changes in dose. Considering clinical data on these dose effect relationships, an accuracy is recommended of ±3% on absorbed dose delivered at the specification

point and ±5% at the other points in the target volume. This is a requirement at the one standard deviation level and applies to final patient dose, incorporating all contributing uncertainties up to and including treatment delivery. It is consistent with the ICRU (1976) requirement of ±5% on delivered dose. To meet this, comprehensive quality assurance and quality control programmes are necessary and there are many sets of guidelines in this area.

The accuracy achieved in practice can be estimated by a priori methods to analyse uncertainties at the various stages in radiotherapy and by measurement based studies, including dose intercomparisons, which can be carried out at various levels of the technical radiotherapy process to define errors and uncertainties at each of those stages. In vivo dosimetry, portal imaging and internal and external quality audit are additional complementary systems which can assist in identifying and quantifying uncertainties, as well as picking up actual or potential problems in the local quality system. The overall accuracy can be achieved in practice by incorporation of all these aspects in radiotherapy.

Chapter 3

Uncertainties at the end of the Basic Dosimetry chain and experimental assessment of achievable accuracy in Basic Radiotherapy Dosimetry

3-1-Introduction

Overall uncertainties must be considered at all stages from the primary standard laboratory up to and including dose delivery to the patient. Different studies have shown (Johansson 1982_a, Mijnheer et al 1987, Brahme 1988, Thwaites 1993) that the determination of the absorbed dose at the reference point (beam calibration) still remains as one of the significant sources of uncertainty in the absorbed dose to the target volume in radiotherapy. In particular it introduces uncertainties linked to the physical constants and standards labs calibration. Provided different centres use the same values these only affect absolute accuracy, but not precision. However if different labs use different methods and procedures and different countries or centres use different values of physical constants, this introduces differences in dosimetry to different patients. In addition if different radiation modalities are used (n, p, etc.) other uncertainties may be introduced. Beam calibration lies at the interface between basic dosimetry and clinical dosimetry. Any effect her will have effects on all the subsequent steps of radiotherapy treatment. The relevant steps for this stage have been summarised by Thwaites (1993) as follows:

a) The establishment of dosimetry standards, including the basic physical data and procedures involved in the determination of the required dosimetric quantity in the radiation beams to be used for instrument calibration at the standards laboratory;

b) The calibration of a local reference instrument against standards and of clinical field instruments against this local reference at the hospital, enabling the dosimetric quantity to be transferred from standard laboratory to user in a traceable manner (in many countries this also involves a further step between primary standard laboratory and secondary standard laboratory; in the UK this transfer is direct from PSL to hospital);

c) The determination of absorbed dose to water in the treatment beam in reference conditions, following an accepted dosimetry protocol and using a calibrated field instrument (beam calibration). National protocols are used to obtain more consistent absorbed dose calibration dosimetry procedures, instrumentation and physical data.

However, differences exist between different protocols. The main causes of these differences are due to different values of interaction coefficients and factors, mainly stopping power ratios and various perturbation corrections and through the different steps in the calibration. Other sources of differences are the procedures used in the dosimetry protocols to select input data used, for example the specification of the quality of the beam etc. Protocols which use $TPR\ ^{20}_{10}$ as a specification of the beam quality provide a consistent method of selection of stopping power ratios for different energy photon beams.

The accuracy achieved in practice can be estimated by a priori methods or by measurement based investigations, including dose intercomparisons, which can be carried out at various levels of the technical radiotherapy process and which can define errors and uncertainties experimentally at those stages. This section discusses an experimental analysis of achievable accuracy in the different steps up to and including dosemeter and treatment machine calibration. Specific studies have been carried out to separate effects in different stages. The experimentally assessed values can then be compared to a priori estimates.

3-2-Dosimetry Protocols for Megavoltage Photon Beams

The main uncertainties are introduced in the calibration of the measuring instrument in a standard radiation beam, and the absorbed dose determination in the radiotherapy beam. To achieve more accurate and consistent values in these two important steps, national and international protocols and codes of practices (e.g. AAPM 1983, IAEA 1987, CFMRI 1987, NCS 1989, IPSM 1990) are used in different countries.

The majority of current dosimetry protocols are based on the so called N_d formalism, that determine a calibration factor for absorbed dose to air in the ion chamber from an air kerma calibration factor N_k or an exposure calibration factor N_x (equations 3-1 and 3-2). Absorbed dose to water or medium can then be obtained by using water/air stopping power ratios based on Bragg-Gray cavity theory (equation 3-3). The different steps between the calibration of ionisation chambers at the dosimetry laboratories and the determination of absorbed dose to water in photon beams at hospitals introduce significant uncertainties.

$$N_k = N_x\,(W/e)/(1-g) \qquad \text{(eq. 3-1)}$$

$$N_d = N_k\,(1-g)\,k_{att}\,k_m \qquad \text{(eq. 3-2)}$$

$$D_w = M\,N_d\,(S_{w,\,air})_u\,(\Pi\,p_i)_u \qquad \text{(eq. 3-3)}$$

N_k is an air kerma calibration factor, N_x an exposure calibration factor and N_d is a calibration factor which is derived from the exposure or air kerma calibration factor and represents the factor to convert to absorbed dose to the air in the chamber cavity. W is the average energy expended to produce an ion pair in dry air, e is electronic charge, g is the fraction of energy of secondary electrons that is converted to bremsstrahlung in air, k_{att} is a correction for absorption and scattering in the wall, build up cap and central

electrode of the ionisation chamber, at calibration quality, k_m is a correction factor for the difference in composition between the wall plus the build up cap and air again at the calibration quality, $S_{w, air}$ is the ratio of water to air mass stopping power and Πp_i is the product of the correction factors to be applied to the measurements in the phantom, both these are for the measurement beam quality (Williams and Thwaites 1993).

3-2-1-Protocol Differences

There are differences between protocols. These differences are due to the differences in selection methods, to the selection of different values of physical constants, the inclusion or omission of particular factors, the values of data incorporated, the way the user must select data etc. Some studies have compared the absorbed dose to water by using the recommendations of different protocols to measurements using the same set of measuring equipment (Mattson 1985, Mijnheer and Wittkamper 1986, Huq and Nath 1990, Weatherburn and Nisbet 1991).

Weatherburn and Nisbet (1991) have divided protocol discrepancies into two areas: 1) the different format of equations used in the various codes/protocols, and 2) the numerical values of the factors used in each protocol. They arbitrarily used the AAPM protocol as a standard for comparison of other protocols. They considered if all equations were equivalent, then one would expect to obtain the same numerical value for conversion factor at a particular radiation quality, regardless of which protocol was employed. They found that the AAPM equation gave values consistently 0.5% higher in a systemaic way than results derived from equations used in other protocols.

Huq and Ravinder (1990) in comparing between the IAEA protocol (1987) and the AAPM protocol (1983) showed that the differences are within 0.5-1%. The main differences are that the IAEA protocol uses some correction

factors e.g. for the aluminium central electrode which the AAPM ignores, and the stopping power ratios selected by the IAEA protocol are 0.5% different to those in the AAPM protocol. The IAEA values are from more recent Monte Carlo calculations and are expected to be more accurate.

Other sources of discrepancy between the protocols are different numerical values of various constants selected by various protocols. The value of the mean energy required to produce an ion pair, W is different in various dosimetry protocols. For example HPA and NACP protocols use 33.85 J/C, AAPM 33.73 J/C, and IAEA, CFMRI, NCS, and SSRBRP 33.97 J/C, which give up to 0.7% deviations. One other parameter is the fraction of energy of secondary electrons that is converted to bremsstrahlung in air (g). The value of g changes from 0.2% to 0.5% in different dosimetry protocols. Another inconsistency between protocols is introduced by choosing stopping power ratios of water to air from different recommended values. AAPM and CFMRI use restricted stopping power ratios recommended by Cunningham and Schultz (1984). The HPA used unrestricted electron stopping power data by Berger and Seltzer (1982). The IAEA protocol has taken basic stopping power data from Berger and Seltzer (1982) and Monte Carlo calculation by Andreo and Brahme (1986) to apply them to the appropriate spectra.

Stopping power ratios are energy dependent. The majority of protocols use $(TPR)^{20}_{10}$ as the beam quality specifies to choose stopping power ratios but some protocols use the nominal MV energy of the photon beam to do this. Uncertainties may either be increased in this group of protocols, because the nominal MV photon energy of the beam can be derived from the attenuating properties of the beam, or from the accelerator characteristics. However, the same 'MV' may be used for different quality beams. For example Owen (1991) showed that the targets and flattening filters used at NPL, and possibly at other dosimetry laboratories, are much thicker than those which are used in the hospitals and therefore the spectrum is significantly different for the same

accelerating potential. Therefore the same "MV" applies, but the different spectra would require significantly different stopping power ratios. On the other hand, Andreo (1986) showed the different correlation between beam quality and water/air stopping power ratios for different target and filter combinations. Protocols that select water/air stopping power ratios with nominal MV, can introduce uncertainties due to different target design between the centres and primary standard dosimetry laboratory. For example Weatherburn and Nisbet (1991) observed that the NPL beam of 8MV was equivalent to a clinical photon beam of 6MV, and the 19MV beam energy corresponds to 16MV.

It can be concluded that the major sources of discrepancies between protocols are in the different sets of stopping power ratios recommended, disagreements in the other data used by different protocols e.g. displacement correction factor, omission of particular factors, different equation formalism, and the way the user must select those data. Table (3-I) summarises the sources of discrepancies for different dosimetry protocols relative to AAPM protocol (Nisbet 1994).

Table (3-I): Discrepancies for different protocols relative to AAPM protocol on 6MV photon beams

protocol	overall discrep.	(1-g)	calibrat. correct.	$(S/\rho)_{w,\,air}$	perturb. F	equat.
CFMRI	+0.5%	+0.3%	+0.4%	-0.3%	+0.6%	-0.4%
DIN	+2.5%	0.0%	+0.3%	+1.5%	+1.0%	+0.6
HPA	-0.7%	0.0%	-	-	-	-0.7%
IAEA	0.0%	+0.2%	+0.7%	-0.9%	+0.3%	-0.2%
NCS	-1.1%	+0.2%	+0.6%	-0.9%	-0.7%	-0.4%
NACP	+0.1%	+.1%	+0.4%	+1.0%	-0.9%	-0.4%
SEFM	-0.6%	+0.1%	+0.2%	0.0%	-0.5%	-0.4%
SSRBRP	+0.4%	+0.2%	+0.7%	-0.9%	-	-0.4%

Despite the discrepancies between protocols for the dosimetry of megavoltage photon beams, there is generally good agreement between modern protocols, to within ±1.0% (Mattsson and Johansson 1985, Mijnheer and Wittkamper 1986, Thwaites 1993). The development of dosimetry techniques e.g. calorimetry in the NPL in the UK permit considerable improvements in the direct determination of the absorbed dose to water in a water phantom leading to direct "N_w" protocols. Later in this chapter the accuracy of Nw protocols is discussed which is better than that of Nd protocols. Also recent improved calculation of stopping power ratios by Monte Carlo methods shows a good view of improvement and consistency between protocols.

It is desirable that countries using older protocols revise their protocols or adopt the modern protocols that use the latest techniques and data. The International Atomic Energy Agency (IAEA) has stated that:
There is an urgent need for a unified and easily executable code of practice to be used world-wide for the measurement and determination of absorbed dose from radiation beams.
This is a desirable objective, but only several countries have PSDLs and the other countries must use transfer standard instruments. Some countries such as the UK base their protocols on only one transfer instrument to the hospitals (NE 2561/2611) in order to minimise uncertainties by using common instrumentation and so may not be flexible enough for other approaches. The other reason is that in some countries such as the UK dosimetry is based on the water absorbed dose calibration (N_w), whilst the majority of protocols still are based on air kerma calibration (N_k). Therefore there are reasons for differences in approach. However, many countries are currently considering changes from air kerma calibration based protocols to absorbed dose to water calibration based protocols. This should further reduce differences.

3-2-2-New Code of Practice in the UK

The national physical laboratory (NPL) in the United Kingdom has established a calibration service in terms of absorbed dose to water (IPSM now IPEM, 1990). Absorbed dose to water is calibrated directly by the NPL for ^{60}Co gamma ray beam and 4-19 MV x-ray beams with quality indices 0.57-0.79. The graphite calorimeter has two disadvantages. Firstly, calorimeter readings are spaced over about thirty minutes, and secondly the calorimeter measures absorbed dose to graphite in a graphite phantom, whereas what is required for the calibration of a radiotherapy dosemeter is absorbed dose to water in a water phantom. In order to avoid the time consuming operation of the calorimeter for calibrating the secondary standard chambers (hospital reference) directly, three "working standard" ionisation chambers (type 2561) are calibrated against the calorimeter in a graphite phantom. Then the hospital secondary standard chambers are calibrated against these three chambers based on a water absorbed dose calibration. The field chambers are then calibrated against the secondary standard, again directly in terms of absorbed dose to water but in hospital beams when the hospital reference chamber is returned to the hospital.

The national primary standard dosimetry laboratories (PSDL's) have enhanced their efforts in developing water absorbed dose calibration. Boutillon et al (1993) have compared different PSDL's and concluded that the laboratories involved in the comparison use quite different methods e.g. calorimetry, Fricke solution, chemical method, and ionimetric systems in determining absorbed dose to water which have uncorrelated or very weakly correlated uncertainties. This study shows that they agree, including the NPL graphite calibration within ±0.5% giving confidence that the accuracy is high.

The Institute of Physical Sciences in Medicine (IPSM now IPEM, 1990) has provided a dosimetry protocol based on the NPL absorbed dose to water

calibration. Later in this chapter the component uncertainties in the basic dosimetry chain for water absorbed dose calibration protocols are discussed and shown to be less than those for air kerma calibration protocols.

3-3-Uncertainty Estimation in Basic Dosimetry

Uncertainties have been estimated by different authors (Loevinger and Loftus 1977, Johansson 1982_a, IAEA 1987, Brahme 1988, Andreo 1990, and Thwaites 1993).

Loevinger and Loftus 1977 considered two situations: a radiotherapy centre with "best practises" as an optimal model and also a lower accuracy centre as a minimal model. Johansson (1982) considered eight steps for beam calibration:

1) Determination of air kerma in a cobalt 60 gamma ray beam with the primary standard instrument;
2) Calibration of the secondary standard instrument;
3) Determination of air kerma at a SSDL with the secondary standard instrument;
4) Calibration of the reference instrument at the SSDL;
5) Determination of air kerma with the reference instrument;
6) Calibration of the field instrument at the centre;
7) Calculation of the absorbed dose to air ionisation chamber factor, N_d, for the field instrument;
8) Determination of absorbed dose at the reference point in water at the Radiotherapy centre (RTC) with the field instrument.

Johansson (1982) concluded that steps 1, 6, 7, and 8 contribute significantly to the overall uncertainties. In steps 1, 7, 8 uncertainties are due to stopping power ratios that contribute significantly to the overall uncertainties. Uncertainties in steps 2-5 may be considered negligible.

IAEA (1987) and Brahme et al (1988) estimated uncertainties up to beam calibration in two steps. The uncertainties in step 1 refer to the calibration of the ionisation chamber in terms of air kerma. This is mainly carried out in standard laboratories except for field instrument calibration which is done in the hospital (from 1-5 in Johansson 1982). The uncertainties in step 1 were estimated to be 1% by IAEA (1987) and Brahme et al (1988). Uncertainties during step 2 are introduced by the user in selection of interaction coefficients and input parameters (see section 3-6). One reason is the possibility for confusion in the use of absorbed dose conversion and correction factors. After revision of stopping power ratio values, Andreo (1990) estimated a lower uncertainty up to and including beam calibration at the reference point in step 2. Andreo (1990) obtained an overall uncertainty of 1.6% for cobalt 60 gamma ray beams and 2.5% and 2.8% for high energy photon and electron beams respectively (section 3-6). This constitutes a significant decrease compared with the previous estimations (Johansson 1982, IAEA 1987, Brahme 1988).

The results of Andreo (1990) show again the main source of uncertainties in step 2. The user introduces a large proportion of these uncertainties. Therefore it can again be concluded that a main section of uncertainties in air kerma protocols (Nk or Nd) are introduced in the hospital by the user.

The NPL (UK) calibration service based on the direct absorbed dose to water standards for megavoltage photon beams, and the associated Institute of Physical Sciences in Medicine (IPSM now IPEM, 1990) dosimetry protocol, claims smaller uncertainties than the air kerma based approach. Thwaites (1993) estimated the uncertainties at the end point of beam calibration as 1.3% and 1.6% for cobalt 60 and megavoltage x-ray beams respectively using the Nw protocol.

3-4-An Experimental Analysis of Basic Dosimetry

To achieve a high accuracy in radiotherapy, stability of both standard and field instruments is very important. Constancy tests can be carried out using a radioactive test source to check long term consistency.
The transfer of calibration from standard to field chambers in hospital X-ray beams in a Perspex phantom is carried out at a fixed FSD and 5cm depth (7cm depth for higher energy). Errors in calibration of field chambers can be due to instability of both secondary standard and field chambers. Uncertainties due to setting up and instability of machine output may contribute as well.

Part of the uncertainties in beam dose delivery is introduced from the variation in monitor chamber response and monitor unit calibration. It is recommended that deviations between the monitor reading and the determined absorbed dose values should be less than 2.0%. Weekly (or more frequent) checks of the machine output should be carried out. If the deviation is larger than 2.0% and less than 5.0%, the measurement should be repeated on the next day and adjustments made if still outside 2%. When the deviation is larger than 5%, the output should be adjusted immediately.
The appropriate contribution to an uncertainty estimate for the therapy unit monitor is long term instability or variation, although it has been suggested that the short term instability should also be used in combination (Thwaites 1993) where appropriate.

An experimental analysis of basic dosimetry for assessment of achievable accuracy and possible improvement of radiotherapy accuracy was carried out, as follows, by measuring or analysing:

-long term consistency of reference chamber calibration;

-consistency check source tests of secondary standard (short and long term);

-consistency check source tests of field instruments (short and long term);

-monitor unit calibration (short and long term) variation;

-variation of beam calibration at reference point

all uncertainties quoted in the following are at the one standard deviation level.

3-4-1- Methods and Materials

In the UK system, the local reference chamber (secondary standard chambers) must be calibrated against the primary standard every three year. The long term consistency of the local reference chamber (2560/2561) used in Edinburgh was assessed from the records from 1975 to 1992 of N_k calibration factor for ^{60}Co (or 2MV). Short term consistency of the secondary standard and 2571 Farmer type ionisation chamber were tested by carrying out Sr-90 check source measurements 3 times per day at 9am, 2pm, and 5pm regularly during two weeks. The long term stability of the secondary standard and field ionisation chambers were obtained using analysis of departmental check source test records from October 1988 to February 1994 and from August 1991 to February 1993 for the secondary standard and the other ionisation chambers respectively.

A 2571 Farmer type ionisation chamber was calibrated against the secondary standard in a 6MV photon beam over two weeks (once per day) to assess short-term stability of the Farmer chamber calibration factor. A standard Perspex phantom with two holes at 5cm depth and two perspex sheaths was used for this calibration. The ratios of readings, taking means of values with the chambers swapped in position following standard procedures, were calculated for a 10x10 field size and 100cm FSD. The long term variation of calibration of the chambers against the secondary standard was obtained using analysis of departmental records from September 1989 to June 1994.

The short term variation for the monitor unit calibration of MV treatment machines was measured using a RMI 451 phantom and a Farmer chamber at 5cm depth, 10x10 field sizes, and 100cm FSD. The absorbed dose at 5cm depth was normalised to maximum depth and compared with expected values. The long term variation of monitor unit calibration for all machines in the department was obtained by using analysis of output departmental records from September 1993 to October 1994. These ratios have been measured once per week.

3-5- Results

Figure (3-1) shows, the long term consistency of the local reference chamber in terms of its NPL-supplied air kerma (K_a) calibration (N_k) at ^{60}Co or 2MV x-rays. The results show a variation (1sd) of 0.15%. The random error quoted by the NPL on the calibration of the reference chamber is 0.2% (1sd).

Figures (3-2 and 3-3) show the short term variation of S_r check source measurements for the secondary standard and Farmer type ionisation chamber (S/N 2048) connected to a NE 2620 (D2) electrometer. The standard deviation for the secondary standard and Farmer chamber are 0.04% and 0.09% respectively. The means are 1.0005 and 1.0006. Figure (3-4) shows the long term stability of strontium check source measurement for the secondary standard. The mean value obtained is 0.3% deviation from the expected value with standard deviation of 0.16% from October 1988 to February 1994. There is a decreasing trend in this curve from 1991 which was eventually found to be due to damage to the chamber insulator. The long term stability of field ionisation chambers was obtained using analysis of departmental records from August 1991 to February 1993 (Fig. 3-5). Table (3-II) shows the standard deviation of different combinations. Maximum values of sd are 0.3%. It can be seen from Figures (3-1 to 3-5) and Table (3-

II) that the stability of standard and field chambers are very good over both short and long term.

Figure (3-6) shows the short term deviation of a Farmer ionisation chamber calibration factor obtained against the secondary standard over two weeks (once per day) at the end of the day. The mean calibration factor obtained using two separate water proof sheaths was 1.2592 and 1.2613 (difference 0.2%) both with standard deviation of 0.2% for a 10x10 field size and 100cm FSD.

The long term variation of field chambers' calibration factors obtained against the secondary standard were found to be up to 0.2% at the 1 sd level over periods from September 1989 to June 1994 (Table 3-III and Fig. 3-7). This is less than the 0.4% uncertainties that were estimated by IAEA (1987), Brahme (1988), Andreo (1990) and 0.6% according to Table (3-IV) by Thwaites (1993). In general, the stability of chamber factors calibrated against the secondary standard chamber shows standard deviation of 0.2% ±0.1% which again shows good stability of the chambers used in the department.

The treatment machines in the department giving MV photon beams are; RDL Dynaray 4MV (1975), an ABB CH6 MV (1989), a RDL 9MV (1981) and an ABB CH20 (6, 16MV, 1989). During the course of this work a Varian V600 was also installed (1997). Short term deviations of monitor unit calibration on a 6MV (CH6) machine are shown in figure (3-8) over two weeks. The mean deviation was obtained as -0.8% with standard deviation of 0.1%. The long term variation of monitor unit calibration was obtained by analysis of the measured weekly output records in the department from September 1993 to October 1994 Figures (3-9 to 3-13). The long term variation of monitor unit calibration for different machines is typically 1.0% at the 1sd level, with a variation machine-to-machine between 1.2% and 0.7%.

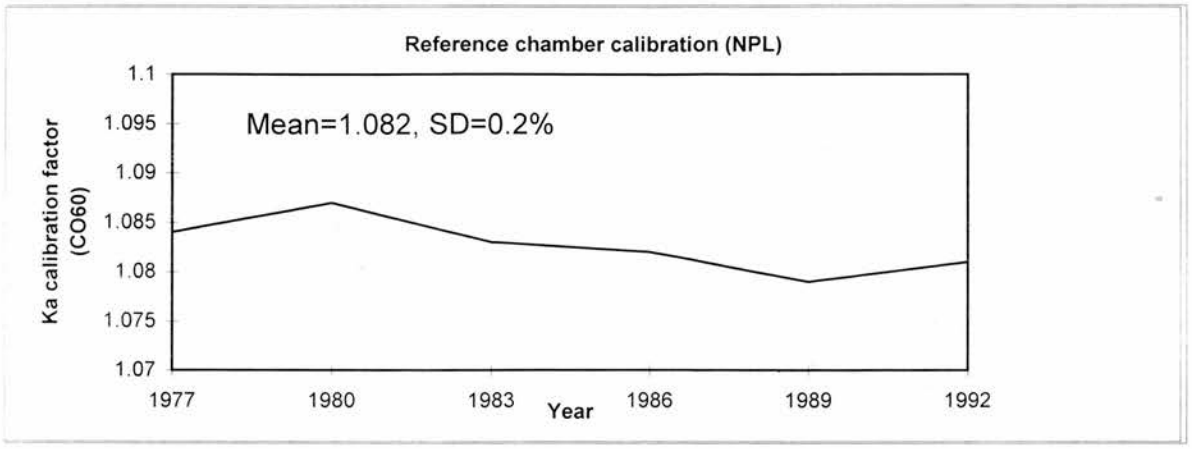

Fig. 3-1: Long term consistency of reference chamber by analysis of NPL supplied factors

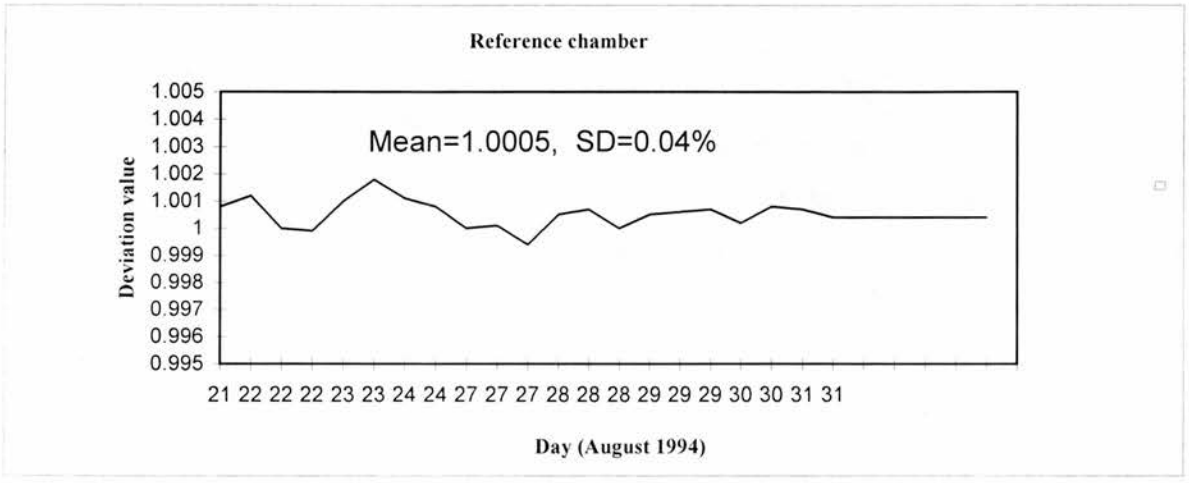

Fig. 3-2: Short term consistency of reference chamber by Sr check source measurements

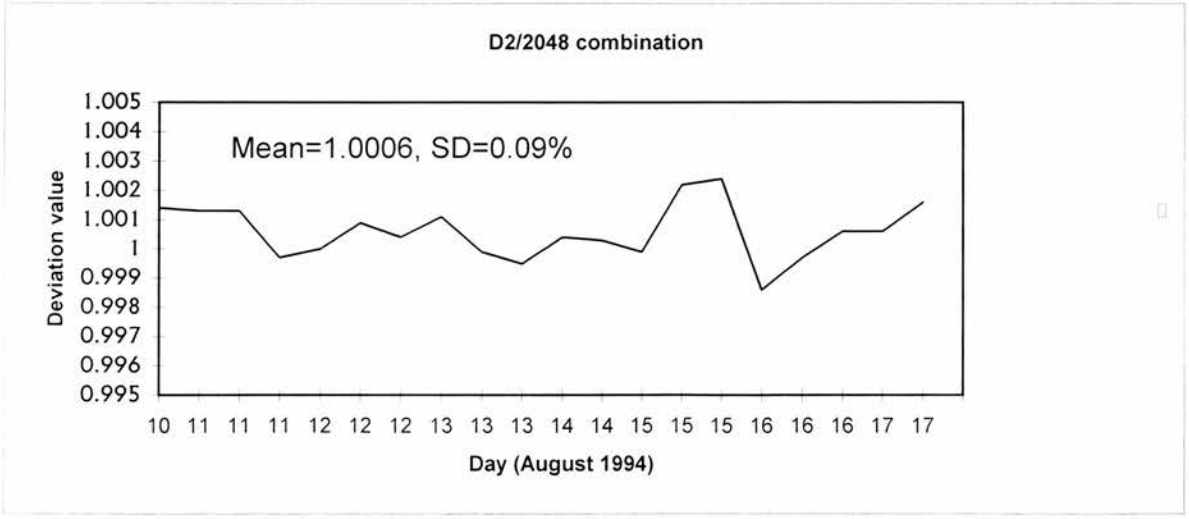

Fig.3-3:Short term consistency of D2/2048(Farmer chamber)by Sr check source measurements

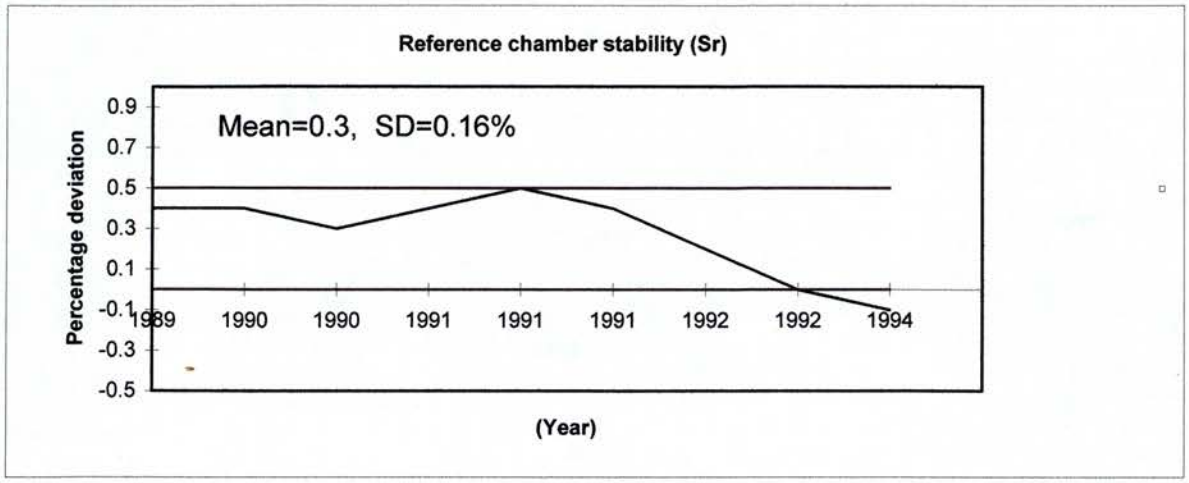

Fig. 3-4: Long term stability of reference chamber

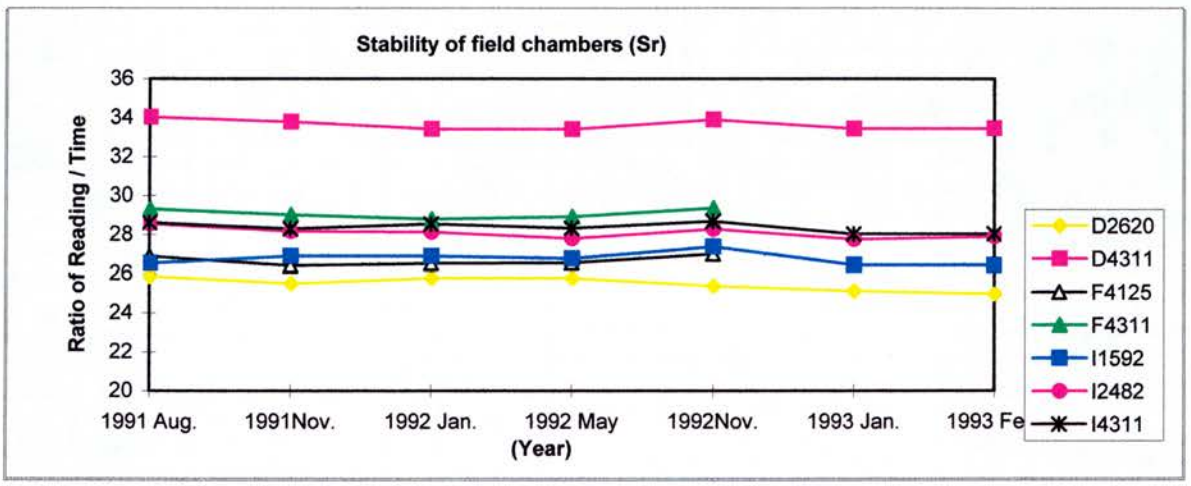

Fig. 3-5: Long term stability of field chambers by using Sr check soı measurements

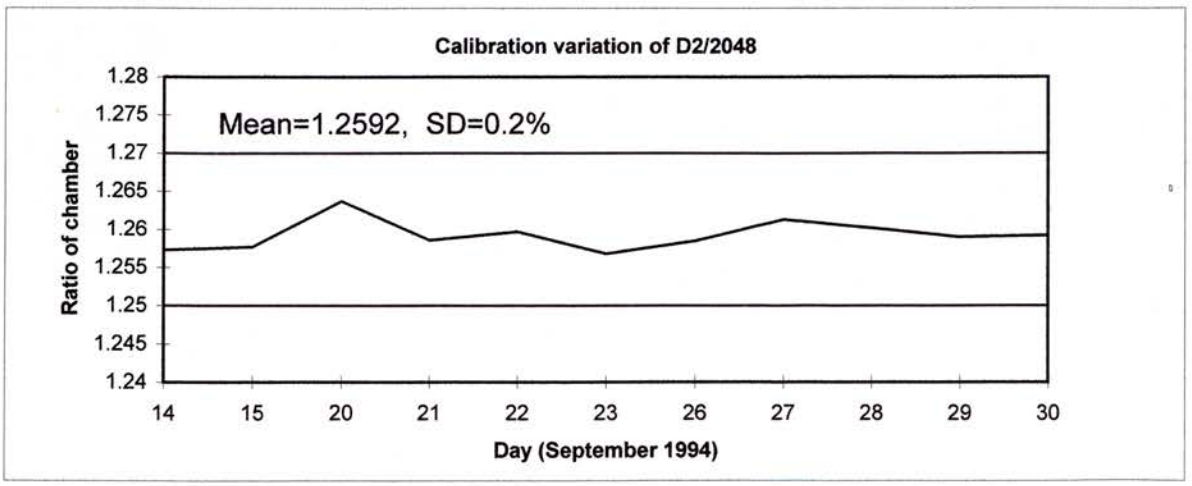

Fig. 3-6: Short term calibration variation of Farmer chamber against secondary standard

Table 3-II : Long term stability of field chambers using Sr check source

comb.	Aug. 91	Oct. 91	Jan. 92	May 92	Oct. 92	Jan. 93	Feb. 93	SD %
I2484	28.54	28.16	28.12	27.79	28.26	27.75	27.88	0.3
I1592	26.53	26.88	-	26.76	27.37	26.44	26.42	0.3
I4311	28.61	28.30	28.54	28.32	28.67	28.02	28.04	0.3
D4311	34.03	33.78	33.42	33.40	33.90*	33.43	33.44	0.3
D2620	25.86	25.49	25.77	*	25.37	25.11	25.96	0.3
F4125	26.89	26.41	26.52	26.54	27.00	-	-	0.3
F4311	29.30	29.01	28.79	28.91	29.35	-	-	0.2

** cap broken*

Table 3-III: Long term deviation of calibration of field chambers against secondary standard

combin.	Sept. 89	Mar.90	Mar.91	June 91	Aug. 92	June 94	S.D. %
I2484	1.064	1.028*	1.027	-	1.026	1.023	0.2
I1592	1.043	1.045	1.049	1.057*	1.057	1.055	0.3, 0.1
D1-4311	-	-	1.216	-	1.220	1.219	0.2
D1-771	-	1.016	*	-	1.006	1.005	0.1
D1-4125	-	-	-	-	1.254	1.255	0.1
D1-119	-	-	-	-	1.260	1.261	0.1
F-4125	1.072		1.075	-	1.074	-	0.1
F4311	1.044	1.042	1.041	-	-	-	0.2
I4311	1.020	1.018	1.016	-	-	-	0.2

**cap broken*

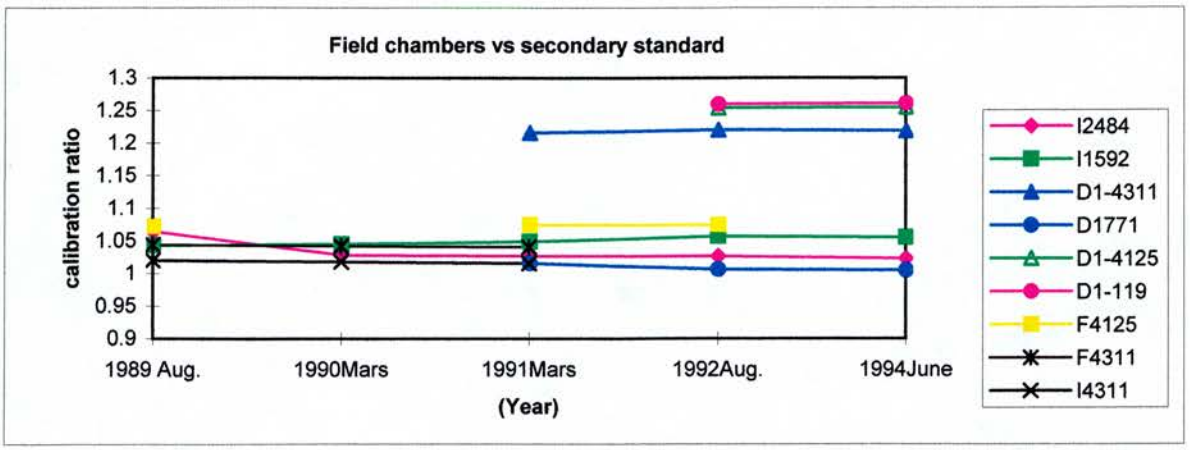

Fig. 3-7: Long term deviation of field chambers against secondary standard

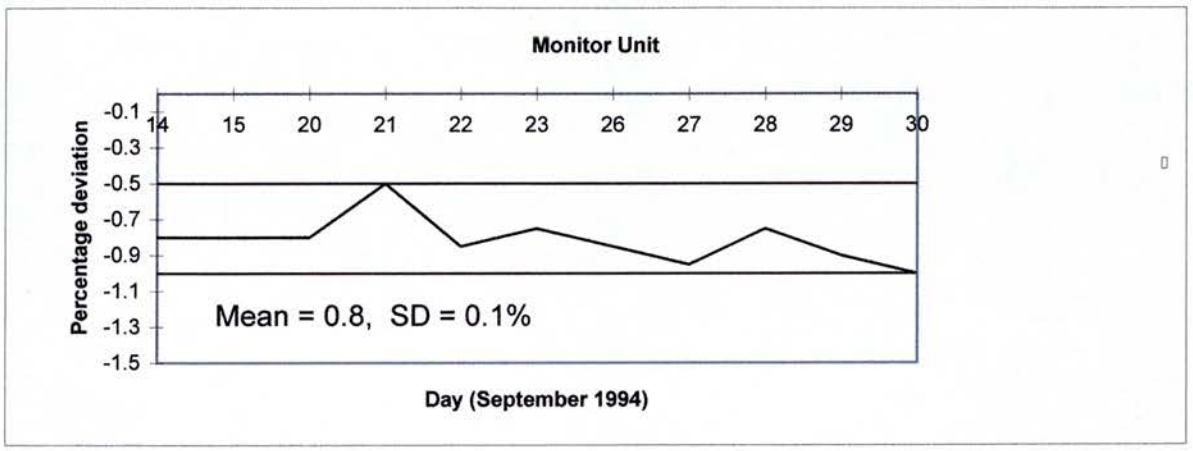

Fig. 3-8: Short term stability of monitor unit calibration for 6MV machine

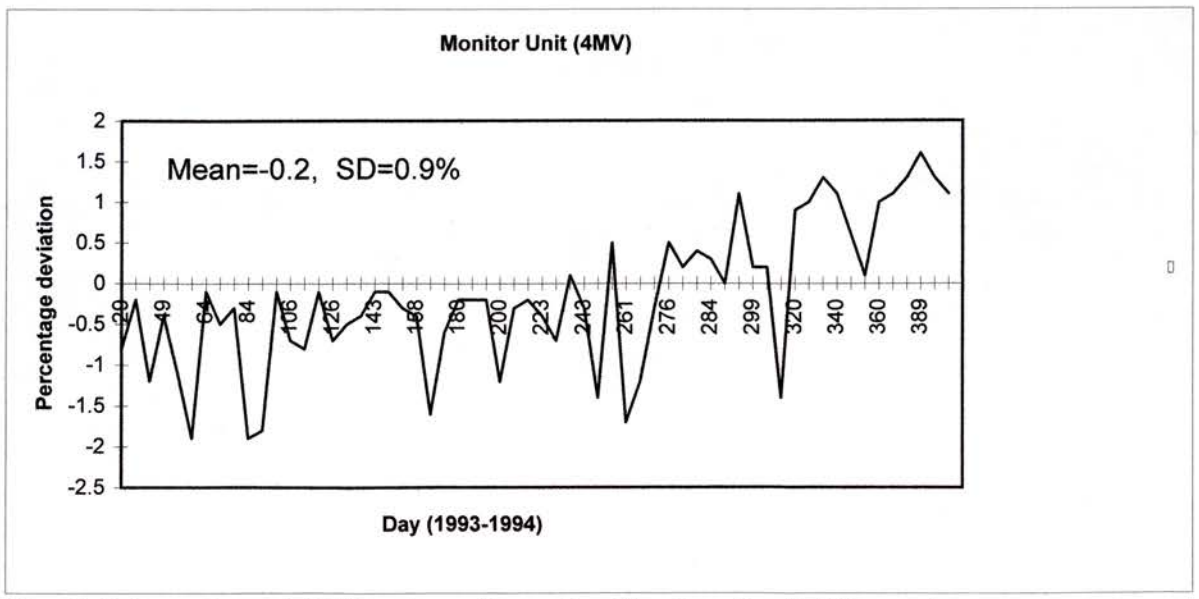

Fig. 3-9: Long term stability of monitor unit calibration for 4MV machine

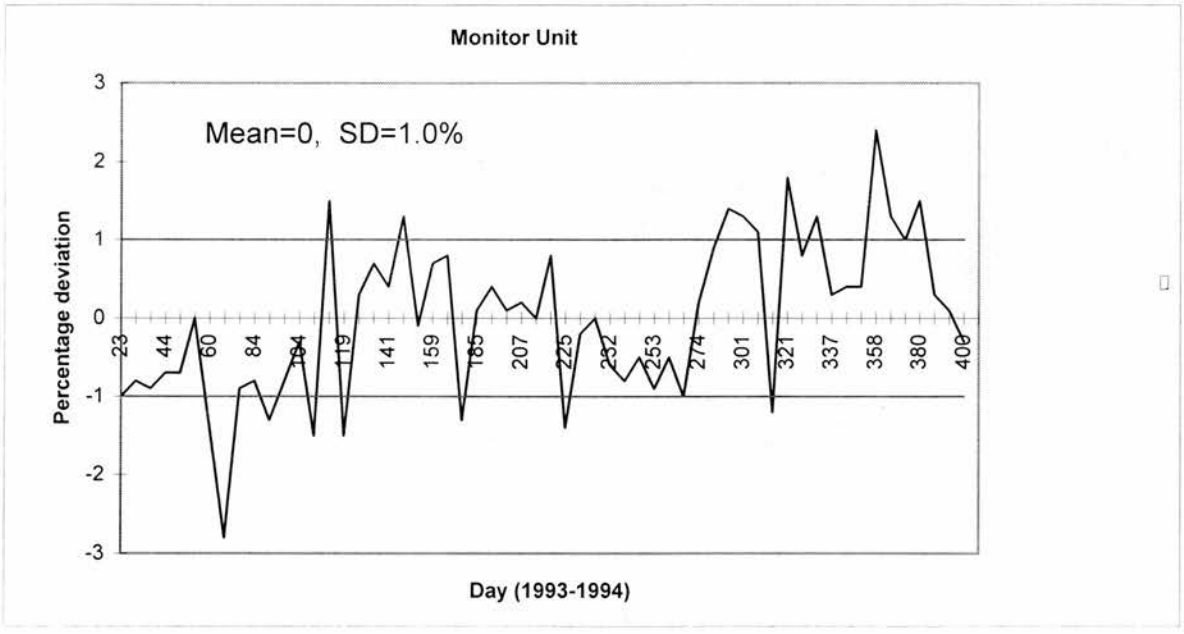

Fig. 3-10: Long term stability of monitor unit calibration 6MV(CH6) photon beam machine

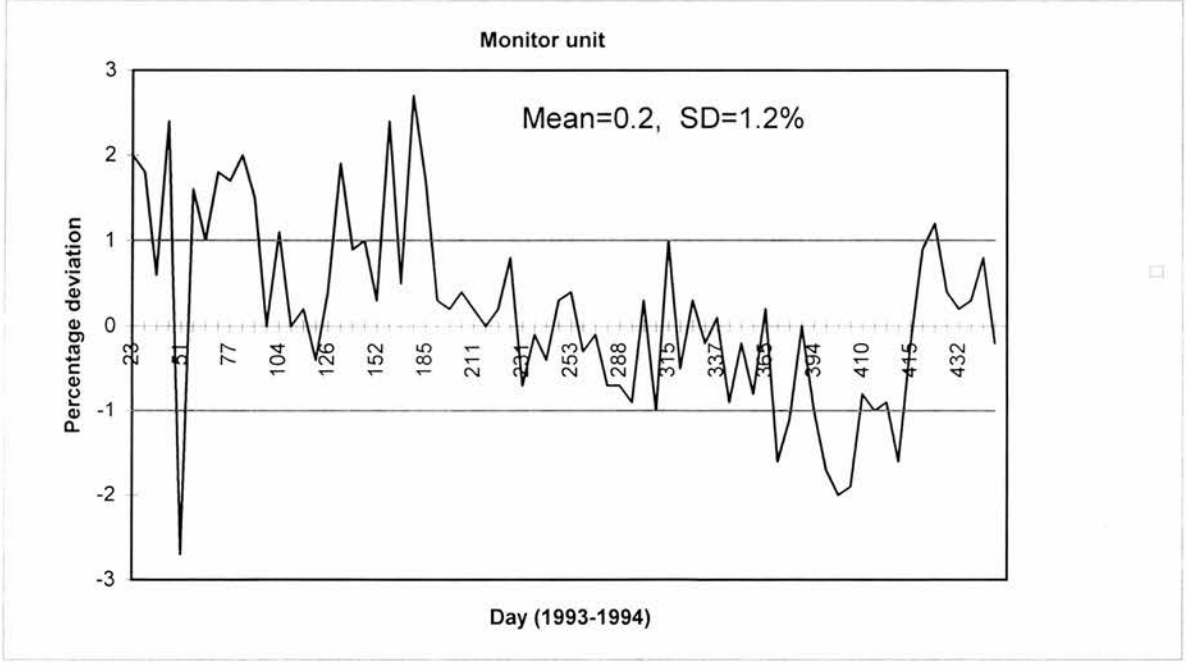

Fig. 3-11: Long term stability of monitor unit calibration for 6MV (CH20) photon beam machine

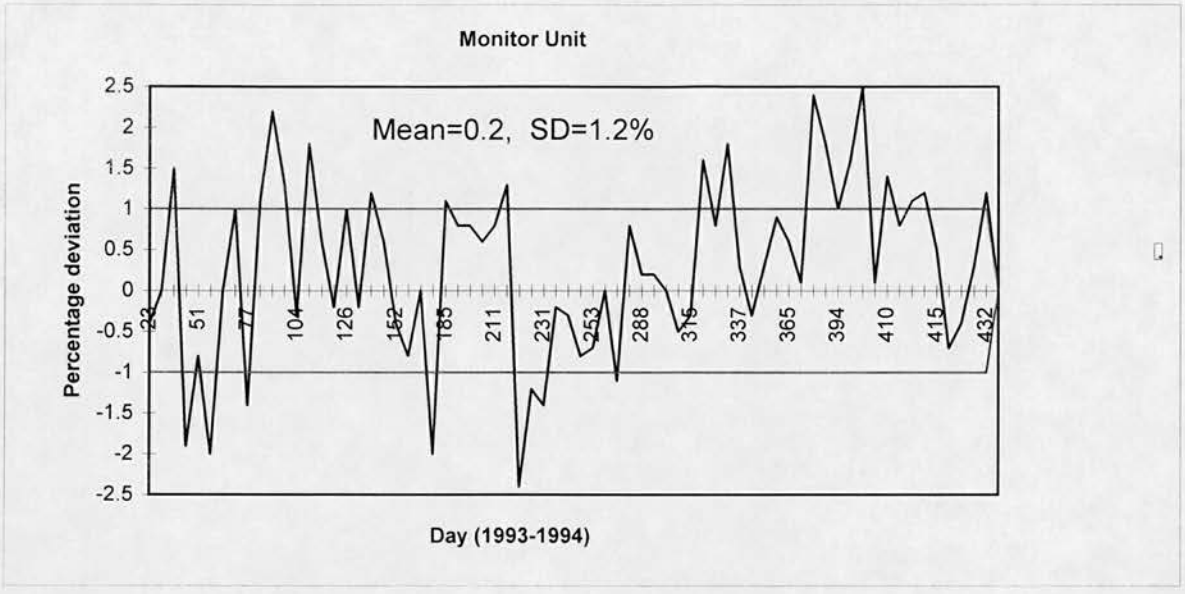

Fig. 3-12: Long term stability of monitor unit calibration for 9MV photon beam machine

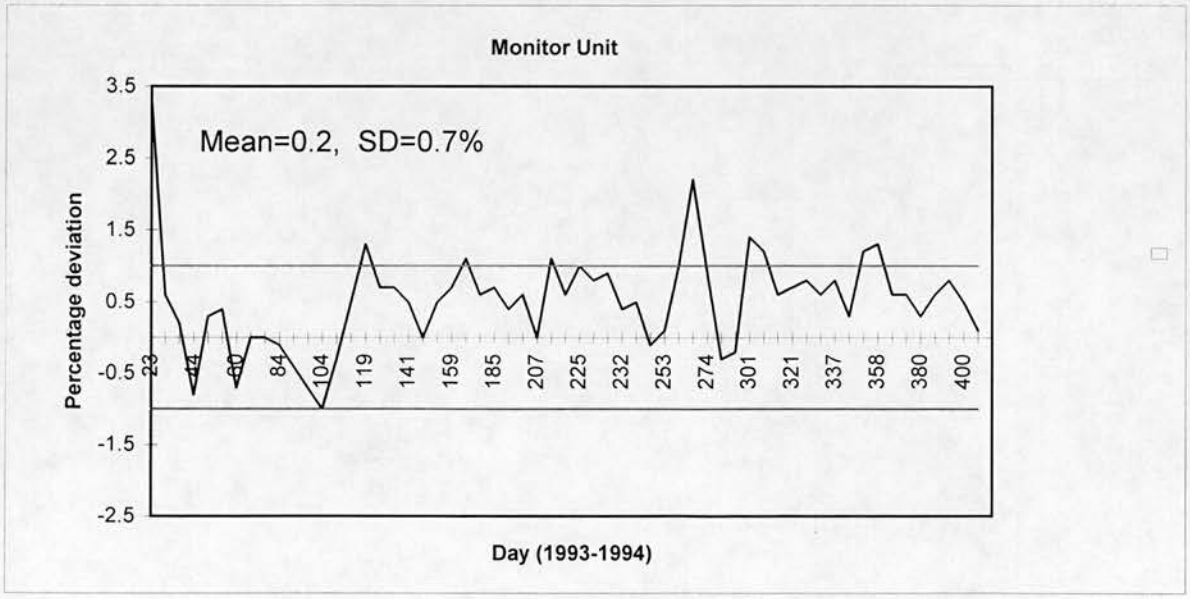

Fig. 3-13: Long term stability of monitor unit calibration for 16MV photon beam machine

The standard deviation of monitor unit calibration for the 6MV (ABB CH6) accelerator was 1.0%, which is in good agreement with estimated values by Thwaites (1993). The long term variation of monitor unit calibration is the appropriate uncertainty to apply for machine stability and must be assumed in the final step when the absorbed dose is delivered to the patient. An analysis of the figures for the newest linac (Varian V600) from May 1997 to March 1998 shows a s.d. of less than 0.5%.

Table 3-IV: Estimated combined uncertainties, up to beam calibration for x-ray photon beams

	Air kerma based (estimated values)			$N_{d,w}$ based (estimated & experimental)		
Protocol	IAEA, 1987	Brahme1988	Andreo1990	Thwaites1993	exp. 1996	source exp.
1	0.5	0.5	0.5			
2	0.3	0.3	0.3	0.7	0.7	NPL exp.
3	0.3	0.3	0.3		0.25	Rec. & exp
4	0.5	0.5	0.5			
5	0.5	0.5	0.5	0.6	0.2	Records
6	2.6	2.5	1.4			
			Monte Carlo			
7	1.0	1.0	1.0	0.8	0.6	Rec &exp
8	1.5	1.5	1.5	1.0	1.0	Records
Total	3.4	3.3	2.5	1.6	1.4	

[1=physical constant, 2=calibration secondary standard, 3=calibration reference instrument, 4=transfer K_{air}, 5=calibration field instrument, 6=physical constant and user factor, 7=field instrument, 8=monitor unit]

3-6- Discussion

Table (3-IV) shows the measured and estimated combined uncertainties, up to and including beam calibration for megavoltage photon beams. Estimated uncertainties in N_w protocols are smaller than N_d protocols. This is confirmed by the measured values obtained in this work.

The National Physical Laboratory (NPL) in the UK uses a calorimeter for water absorbed dose determination for MV photon dosimetry standards. The estimated total uncertainties of different steps at the NPL are quoted at 0.7%

(of which random uncertainties contribute approximately 0.2% and systematic contribute approximately 0.7%). Additional to this, we measured 0.25% inconsistency of reference chamber calibration from 1975 to 1992, which must be added to 0.7% uncertainties by NPL. The uncertainty of air kerma based absorbed dose for physical constants and primary standards in N_k or Nd protocols e.g. IAEA (1987), Brahme (1988), and Andreo (1990) have been shown in Table (3-IV). Brahme (1988) and IAEA (1987) used an estimation of 1.5% error for stopping power ratios, but Andreo (1990) after revision of stopping power ratios by Monte Carlo calculation, estimated uncertainty 0.4%. After this development uncertainties due to stopping power ratios in physical constants ($k_m k_{att}$) was decreased from 1.5% IAEA (1987) and Brahme (1988) to 0.7% of Andreo (1990).

Over a number of years, the response of an ionisation chamber may change, therefore the stability of the secondary standard and field chambers must be checked against a radioactive source regularly. Johansson (1982_a) estimated 0.2% variation for a secondary standard and 1.1% for field chambers. This can be compared with the measured values in this work. The long term variation of stability of the secondary standard is 0.3% (±0.2%, 1sd, Fig. 3-4). The variation of stability of field chambers in the department is shown in Fig. (3-5) and Table (3-II), which are near 0.3%.

Short term stability of both secondary standard and Farmer chamber are measured at 0.04% and 0.09% respectively which is considered negligible. It can be seen from Figures (3-1 to 3-5) and Table (3-II) that the stability of both standard and field chambers are good. Also the long term variation of field chambers' calibration factors against the secondary standard were good within 0.2% (Fig. 3-7 and Table 3-III).

Uncertainties in field instrument measurements is the sum (quadrature) of the inconsistency of dosimeters, field instrument calibration against secondary standard and set up errors obtained experimentally as follow:

-consistency check of secondary standard	0.2%
-consistency check of field instrument	0.3%
-consistency of field instrument against secondary standard	0.2%
-uncertainty in temperature, pressure, distance	0.5%

The uncertainty in recombination, polarity, and non-linearity is estimated at 0.1% for each one. The cumulative uncertainties obtained are approximately 0.7% which is near the estimated values by other workers.

The deviation of monitor unit calibration is appropriate to the estimate of uncertainties in machine stability. Johansson (1982_a) estimated a 0.5% uncertainty for the dose monitor calibration of the accelerator over a period of 1 or 2 days or during the period when measurements under reference conditions are carried out. The long term stability can be assumed in the final step when the absorbed dose is delivered to the patient as the time from beam calibration to patient treatment may be anything from short to long. He estimated 1% uncertainty in the final step for the long term stability. Brahme (1988)and Andreo (1990) estimated the therapy monitor unit uncertainties at 1.5% for X-ray and electron beams. Thwaites (1993) estimated 0.5% and 1.0% uncertainties for short and long term stability of calibration of the dose to monitor unit factor. He suggested that the appropriate uncertainties for the therapy monitor unit are those for long term instability, but the short term uncertainties should be used in combination. The short term instability of X-ray beams in our measurements on a 6MV unit was obtained at 0.1% over two weeks (once per day), which is less than the 0.5% estimated by Johansson (1982_a) and Thwaites (1993). The long term instability of monitor unit calibration from analysis of departmental records from September 1993 to October 1994 were obtained at 1.0% . The maximum standard deviation was 1.2% for 6MV on Linac20 and minimum sd was 0.7 % for 16MV. Monitor unit calibration uncertainties on the other accelerators also showed

an uncertainty of approximately 1.0% which is in agreement with the estimated values by Thwaites (1993).

Uncertainties at the end point of beam calibration for megavoltage X-ray beams have been estimated by different authors (Johansson 1982_a, IAEA 1987, Brahme 1988, and Andreo 1990) according to Table (3-IV). All these estimated values are based on air-kerma-based Nd protocols. Overall values (1sd) were from approximately 3.5% to 2.5% for Andreo (using revised stopping power ratios estimates).

Thwaites (1993) estimated combined uncertainties in the basic dosimetry chain, using the N_w calibration and IPSM code of practice (1990) at 1.6% for X-ray beams. This can be compared with the above air kerma based calibration estimates. Accumulated uncertainties from the present experimental work show a cumulative value of 1.4%, which supports the estimated values of Thwaites (1993). Therefore, it can be concluded that the N_w method is the more accurate by around 2% compared to the N_d (N_k) protocols. Table (3-IV) shows that the estimated values for N_w protocols and the experimental results support each other, and are complementary. The results of this work demonstrate the range of deviations experimentally, to illustrate the consistency achievable in practice. It quantifies actual uncertainties obtained in one department in clinical conditions and underpins the estimated values. It may be noted that an equivalent value for ^{60}Co, removing the monitor unit uncertainty but including timer uncertainties of from 0% to 0.5%, will be approximately 1%.

Based on the comparison between our measurements and the estimated values by different authors, it can be concluded that there is good agreement in most cases between measured and estimated values. This agreement is better for N_w calibration and the IPSM code of practice (1990) than air kerma

calibration and N_d protocols. Therefore, N_w protocols are more accurate as well as simpler to apply than N_d protocols (Allahverdi and Thwaites 1996_a).

3-7-Conclusion

-The experimentally obtained uncertainties in basic dosimetry and the estimated values based on a water absorbed dose calibration and protocol support each other;

-Basic dosimetry based on absorbed dose to water calibration protocols are more accurate than air kerma calibration protocols;

-Overall uncertainties in basic dosimetry, up to and including beam calibration, for megavoltage x-ray beams are measured at 1.4% (implying also a consistent value for ^{60}Co should be approximately 1%).

Chapter 4

4-Uncertainties in Clinical Dosimetry and Development of Interdepartmental Audit using a simple Geometric Phantom

4-1-Introduction

The absorbed dose to the patient may be different from stated because of e.g. the determination of the absorbed dose in the reference condition, the calculation of the absorbed dose distribution, the set up of the patient and the stability of the treatment units. Errors are both systematic and random. There are uncertainties on all steps within any centre and other uncertainties between centres. These latter uncertainties are important for transferring experience or comparing results between centres. They can be measured by inter-departmental dose intercomparison. According to recent world-wide investigations (Svensson et al 1990) sponsored by IAEA and WHO, about 15% of all cancer patients treated with radiation receive an inadequate dose due to systematic uncertainties in dose delivery. Quality assurance and quality control programmes have an important role in reduction of uncertainties. Many quality assurance programmes have been introduced in recent years such as AAPM 1984, 1994; IPSM 1988; WHO 1988; IAEA 1989; Shaw 1993; Thwaites et al 1995.

Despite having these programmes in radiotherapy departments, errors can still occur in different levels of radiotherapy. One recommendation to complete the circle of these programmes is to use quality audit. Quality audit is an independent review of different levels of the radiotherapy process which can identify and quantify errors. Such a programme is implemented by external personnel, or at least persons who are not responsible for the performance of the product or process under review. In chapter 2 the idea of quality audit was introduced and some approaches such as dosimetry intercomparisons, in

vivo dosimetry, and portal imaging were discussed. Dosimetry intercomparison as a common quality audit of radiotherapy dosimetry has been studied by a number of authors e.g. (Johansson 1986, 1987; Wittkamper 1986, 1987; Sipila 1992; Thwaites 1992, 1994_b). Some authors have extended the basic approach to include a wider set of parameters in quality audit (CHART, Aird et al 1993, Bonnett et al 1994, Thwaites 1996). For example Bonnett et al (1994) has developed an audit based on annual mutual interdepartmental audit, where the audit process comprises four sections: procedural audit and examination of records; measurement of samples of data, including chamber intercomparison, mechanical alignment and dosimetric measurements over a range of parameters on one machine per centre on a photon beam and a range of electron beams; a report on the examination and measurement; and the response of the audited department.

Because of the important role of quality audit in radiotherapy, today quality audit networks are being developed internationally (e.g. IAEA) to link the various studies and exercises under way. Also some countries such as the U. K are developing audit network programmes in different levels of the dosimetry chain using a series of phantoms from simple geometry to some semianatomic designs.

In addition to interdepartmental audit programmes to achieve consistency between the centres, intradepartmental audit can be done in a department. "Essentially any checking or verification system which is implemented in addition to those deemed necessary for the achievement of quality in any part of the process could be defined as a type of audit "(Thwaites 1994_b).

This chapter discusses both interdepartmental and intradepartmental audits, using a geometric phantom. The first section investigates problems encountered due to treatment planning algorithms. Potential errors due to different planning algorithms are quantified against measurement to

determine those situations for which more sophisticated algorithms are required. The next section considers a quality audit programme for identifying discrepancies and uncertainties and for ensuring that these discrepancies are within the audit system's predetermined limits.

4-2-UK dosimetry Intercomparison

Dosimetry intercomparison is a method of quality audit that can reveal errors and assess consistency between centres. The IPSM megavoltage photon dosimetry intercomparison in the UK was started in 1987 and was finished in 1992 visiting all 65 centres in the UK (Thwaites et al 1992). This intercomparison provided a baseline set of data for the use of local audit programmes, and also provided a basis for the methodology and development of audit programmes. The purpose of the photon dosimetry intercomparison in the UK was to measure the consistency of clinical dosimetry in all UK radiotherapy centres, and quantify uncertainties, with the aim of improving practice.

Recently, a national electron dosimetry intercomparison in follow up to the photon dosimetry intercomparison was carried out in fifty three centres in the UK (Nisbet and Thwaites 1997). The aim of this intercomparison was to develop a methodology for clinical dosimetry intercomparison of electron beams and to measure the consistency between centres for this modality (90% of UK radiotherapy centres). The results of this intercomparison again provided a standard base line set of data against which individual centres can compare.

4-3-Development and Analysis of Audit Methods

Out of the dosimetry intercomparisons in the UK a quality audit network in the UK has been established. One major development group is the Scottish+

group (based in Edinburgh), including all Scottish centres, Newcastle, Carlisle and Belfast. This audit system has implemented a hierarchy of dosimetry tests to be assessed in a sequential method with different phantoms, as follows:

-Basic dosimetry at the reference point (geometric phantom);
-Single field parameters (geometric phantom);
-Simple multi-field planned irradiations (geometric phantom);
-Complex multi-field planned irradiation (semi-anatomic phantom).

A previously designed geometric phantom developed for the UK national dosimetry intercomparison (Thwaites et al 1992) has been modified and used to extensively test achievable accuracy of dosimetry within a given department and some basic treatment planning parameters and processes in one (Edinburgh) centre. Secondly, the proposed audit testing has been evaluated experimentally in Edinburgh to test the methodology and phantom before use in other centres. Thirdly, interdepartmental audit has been carried out to measure consistency between centres, and finally (chapter 5) the development of a semi-anatomic phantom has been carried out for further stages of the hierarchic audit. The audits also include procedural checking of departmental dosimetry and quality control methods, frequencies and tolerances but that is outside the scope of this work.

4-4-Materials and Methods:

A phantom similar in design to the original IPSM photon dosimetry intercomparison phantom was used. The phantom was made in three 6-cm thick sections of epoxy-resin water equivalent material (WTI St. Bartholomew's hospital). It had six 2 cm diameter removable water equivalent material plugs to accept a Farmer type ionisation chamber and a 8 cm diameter lung equivalent insert which can be replaced by a water

equivalent insert (Fig. 4-1c). One hole was used for the reference point measurements and five points for the planned dose distributions.

The ionisation chamber used was a Farmer type 2571 (SN2048), with graphite wall, connected to a Nuclear Enterprises 2620A (SN-249) electrometer. The chamber was calibrated against a secondary standard chamber which had been calibrated at the NPL in terms of N_w. The IPSM code of practice (1990) was used to derive absorbed dose to water. Repeated Sr consistency check measurements for the field ionisation chamber and the secondary standard chamber showed 0.09 % and 0.04 % (1sd) respectively, and repeated calibrations of the ionisation chamber against the secondary standard showed 0.2 % (1sd) as discussed in chapter 3. Recombination correction factors and correction factors for differences between phantom material and water, although small, were used throughout.

The outline of the phantom contour was manually transferred to the treatment planning computer using a digitizer. Plans were made in x-ray beams of 4 to 16MV using the Edinburgh in-house TPS and the Cadplan system. Measurements were carried out on four linear accelerators at 4, 6,9, and 16 MV energy photon beams.

4-4-1- Planning algorithm tests in a single department (Intra-departmental audit):

Tests on dosimetry at reference point, and on three-fields planned dose distributions were carried out on each machine. The multifield irradiations were carried out for the planned distributions. The phantom was irradiated in reference conditions; i.e. field size 10x10 at the surface, and 100 cm FSD and with the chamber at the reference point. The reference point was situated on the central axis of the beam at 5 cm deep (Fig 4-1a). The chamber axis was positioned at the depth of the reference point and the effective centre

longitudinally of the chamber was positioned at the reference point and a dose of 2 Gy was given at this point as calculated using the departmental planning data.

The mean of five readings for each point was corrected for temperature and pressure and converted to dose. The standard daily output factor was determined before and after each set of measurements, and the results of the measurement were adjusted according to this value. The measurements were compared with expected values from tabulated and calculated planning data.

An irradiation was planned to give a uniform dose distribution with 3-fields according to figure (4-1b). The dose distribution was measured at the five points of the phantom shown. The cross section and the target volume chosen are shown in figure (4-1b). The dose to be delivered to the central point of the planned dose distribution was specified to be 2 Gy and was calculated using the centre's treatment planning systems. Field sizes of 10x10 cm^2 were used for each field. Field 1 was an open field for all energy beams and wedge angles for fields 2 and 3 for the different energy beams were as below, selected to optimise the distribution.

	4MV	**6MV**	**9MV**	**16MV**
field 2	45°	60°	50°	60°
field3	55°	60°	50°	60°

Typical plans for 6 and 16 MV is shown in Figures (4-1d and 4-1e) calculated by the in-house TPS and Cadplan system respectively. Comparison of measured values with calculated values can quantify uncertainties in planning algorithms. Different inhomogeneity algorithms were used, i.e. Batho, ETAR and modified ETAR methods. These methods will be discussed in chapter 6.

An inhomogeneity correction factor, defined as the ratio of the dose in a heterogeneous phantom to the dose at the same point in a homogeneous phantom, was measured and compared to the calculated values using various

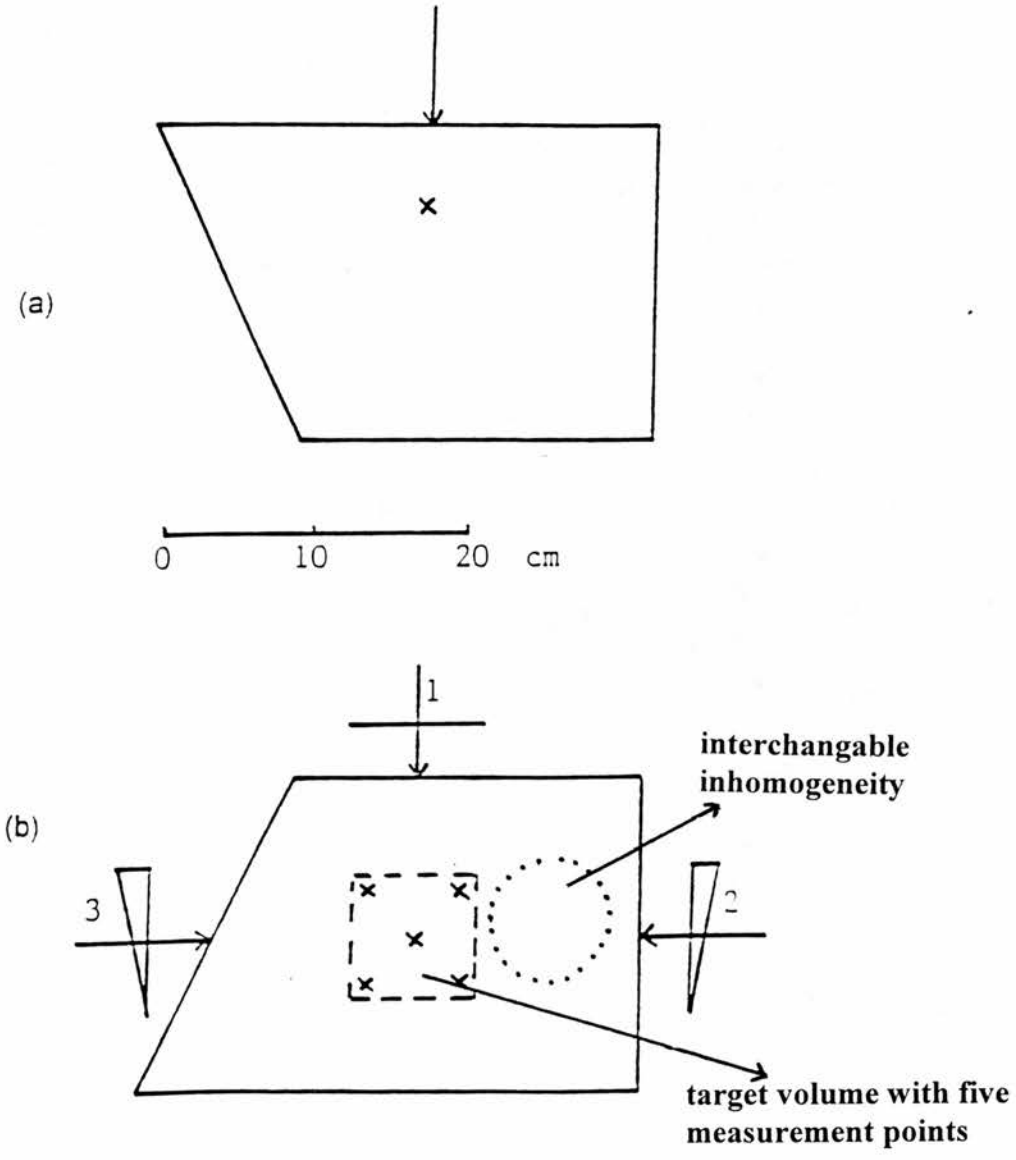

Fig. 4-1: The water equivalent geometric phantom. a) at the reference point and b) orientation for 3 field with target volume and inhomogeneity

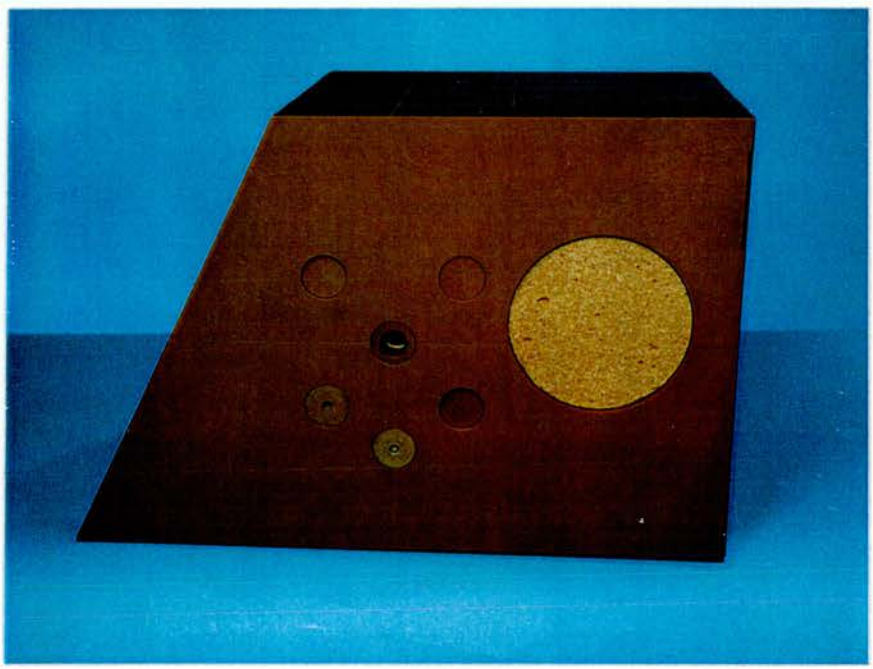

Fig. 4. 1c: The geometric phantom with lung insert

Fig. (4-1d): The cross section of 3-field dose distribution in geometric phantom by in-house treatment planning system

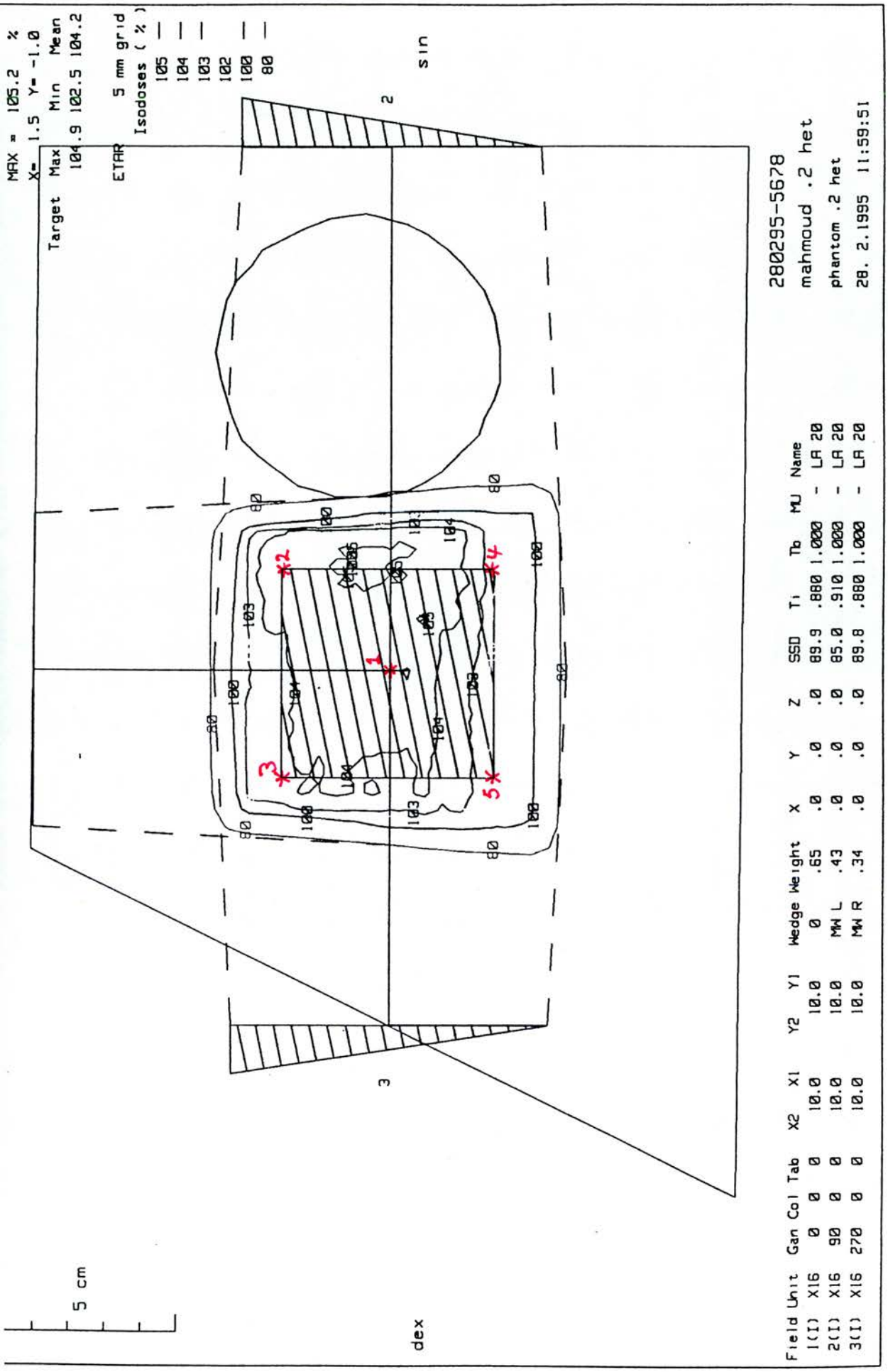

Fig. (4-1e): The cross section of 3-field dose distribution in geometric phantom by Cadplan system

the correction factor for the ETAR method (Sontag and Cunningham 1978). The inhomogeneity correction factor for modified ETAR was obtained using software which had been developed and implemented in-house relatively recently (Redpath and Thwaites 1992). None of these algorithms take account of electronic equilibrium at media boundaries.

For a more detailed analysis of the uncertainties associated with the planning algorithms in these situations the ratio of measured to calculated values were considered field by field. It is important to verify the dose from each single beam, because the average (multifield) values can be acceptable while the error of a single beam may not be acceptable or one beam may contribute more significant errors than other beams. For example modified beams such as wedged beams and oblique incidence beams may introduce greater uncertainties. Any such discrepancies may point to limitations in the dose planning algorithms or the planning data, or the performance of the treatment machine, etc. in these situations.

4-4-2- Interdepartmental Quality Audit:

Similar intercomparisons between measured dose and planned doses for this centre plus seven other centres in the Scottish+ group were compared in an interdepartmental audit programme. This audit was intended to detect discrepancies and evaluate uncertainties at the reference point, for single fields and in 3 field planned dose distributions. Audit of basic dosimetry parameters e.g. quality index, field size variation and wedged beams were considered in single fields. The centres used their local planning system and planning and machine data and calculated dose and absorbed dose distributions for the required measuring situations.

For single field reference point tests, all MV machines in each department have been measured. For the 3-field planned irradiations the ratios of measured to calculated values for one machine per centre (except Edinburgh) were calculated, where the machine was chosen by the centre. Both the homogeneous and the lung inhomogeneity situations were tested. The aim was to ensure by review that absorbed dose at the reference point and for 3 field planned situations were within 3 % and 5 % respectively of that stated by the centres. These tolerances have been obtained by examining the s.d. of the results from the photon dosimetry intercomparisons in the U. K (Thwaites et al 1992). They are similar to tolerance which also have been proposed by RPC (USA) and EORTC (1989).

The total variations in these distributions are caused by variations in the stated absorbed dose values and by experimental uncertainties introduced by the review. However the latter are expected to be relatively small.

4-4-3-Uncertainties

Uncertainties of the audit dosimetry are estimated to be 0.5 % due to random errors in pressure, temperature, dosimeter response, and in setting of distance (Thwaites et al 1992). Random uncertainties estimated for X-ray monitor calibration variation are up to 1.0 % for the photon beams (see section 3-5).

4-5-RESULTS :

4-5-1- The Results of Planning Tests in a single Department:

(a) Reference point:

The ratios of measured to calculated dose values at the reference point were obtained as (4MV=0.995, 6MV=0.995, 6MV= 0.994, 9MV=1.013 and 16MV=0.991) for the different energies. The mean ratio of the measured to calculated dose values at the reference point for all energies is obtained as

0.998 with standard deviation of 0.008 and minimum and maximum values of 0.993 and 1.013. The results were in good agreement with small variations. Deviations can be increased if different field sizes are used. Individual values looking at variation of repeated measurement (5 times) have a sd obtained at 0.3% to 0.6% and for repeated determinations obtained at 0.2 to 0.6%, which combining gives overall uncertainties of 0.4% to 0.8% (1SD).

(b) Dose distribution (3 field):

For the 3 field planned dose distributions a planning system was used which had been developed by the Edinburgh centre (Redpath et al 1977) and which is used as the routine TPS in the department. Figures 4-2, 4-3 and 4-4 show the histograms of the ratios of measured to calculated dose in five points of the dose distributions in isocentrically irradiated homogeneous and inhomogeneous phantoms and as a fixed FSD irradiation of a homogeneous phantom, combining the data for all quality beams. The spread of the differences between measured and calculated dose values were larger in the inhomogenoues phantom than in the homogenous phantom.

Table (4-Ia) shows the mean ratio (all points) of measured to calculated values with the standard deviations for different machines. According to this data the 4 MV accelerator gave the best agreement between measurement and planning calculation, and with the lowest standard deviation.

Correcting the figures for the measured reference point values give the data in Table (4-Ib), i.e. this normalises out the differences observed due to the basic calibration, thereby giving a comparison of the measured to calculated *relative* values.

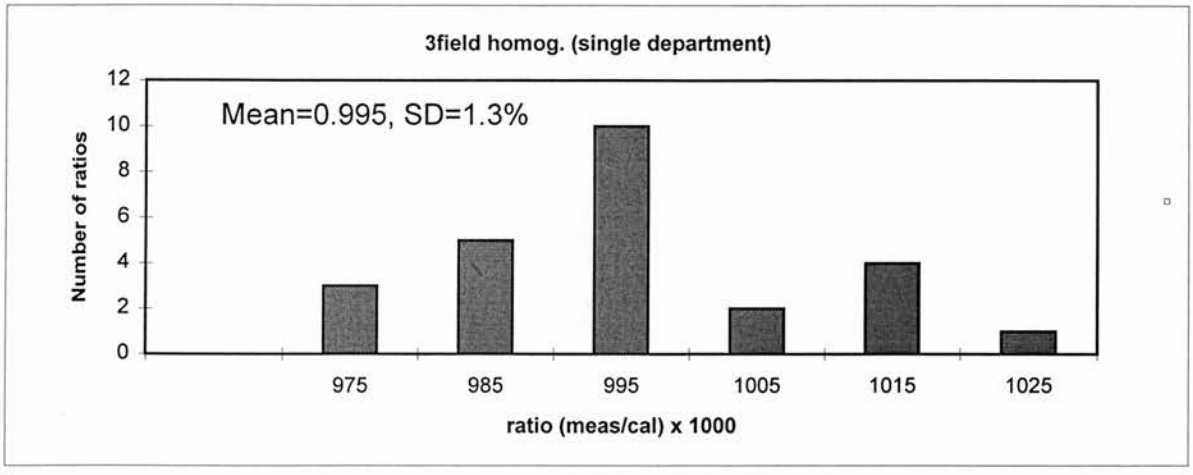

Fig. 4-2: Meas/cal dose results for 3 field planned irradiation in homogeneous phantom and an isocentric set up

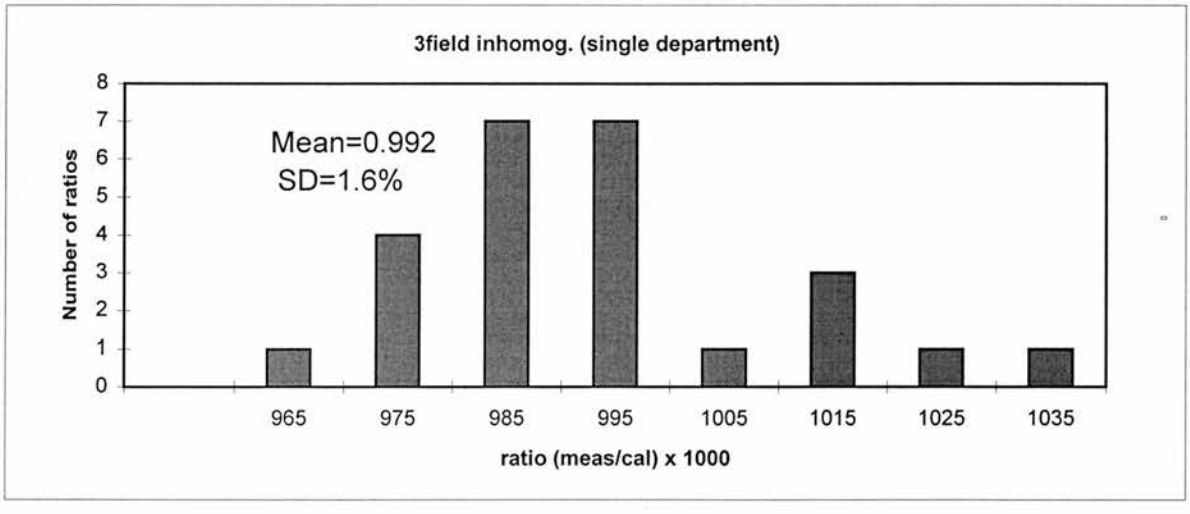

Fig. 4-3: Meas/cal dose results for 3field planned irradiation in inhomogeneous phantom an for an isocentric set up

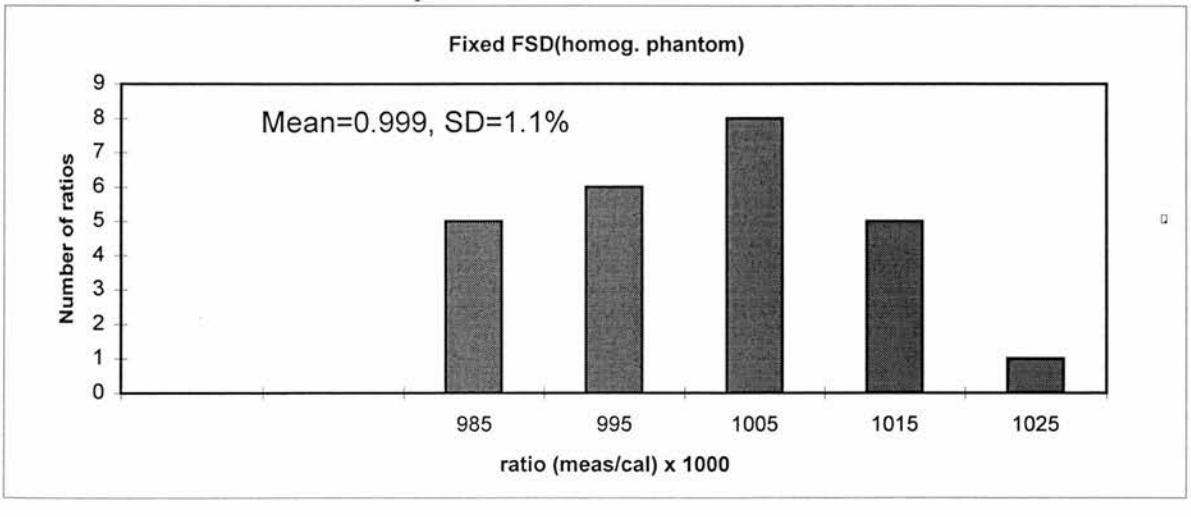

Fig. 4-4: Meas/cal dose results for 3field planned irradiation in homogeneous phantom and

Table 4-Ia: The mean ratio of measured to calculated values of homogeneous and inhomogeneous phantom and standard deviation for 3 fields for different machines (isocentric)

Energy	homogeneous phantom		inhomogeneous-phantom	
	Mean	S.D.	Mean	S.D.
4 MV	0.995	±0.003	0.991	±0.006
6MV-CH6	0.985	±0.009	0.980	±0.012
6MV-CH20	0.985	±0.005	0.982	±0.010
9MV	1.016	±0.007	1.019	±0.007
16MV	0.993	±0.009	0.986	±0.009
Overall	**0.995**	**±0.007**	**0.992**	**±0.009**

The figures also illustrate the consistency of the dose distribution values relative to the reference point dose for both the homogeneous and the inhomogeneous phantom situations. The results show an overall good agreement between measured and calculated values. Besides the conclusions on local dosimetry the generally small differences between measured and calculated dose values also gives confidence in the phantom and methodology.

Table 4-Ib: Distribution of the ratio of the result at homogeneous and inhomogeneous phantom to the measurement at the reference point

Energy	homogeneous/ref. point	inhomog./ref. point
	Mean	Mean
4 MV	1.00	0.996
6MV-CH6	0.990	0.985
6MV-CH20	0.991	0.988
9MV	1.003	1.006
16MV	1.002	0.995
Overall	0.997±0.006	0.994±0.008

(c) 3-field distributions; different planning systems

Figures 4-5 (A-F) show the ratios of 3 field measured to calculated dose values, combining data for the different energies, for the three different planning systems using different inhomogeneity algorithms(Batho, ETAR, and modified ETAR). A, C and E are for the homogeneous phantom. B, D and F for the phantom including the lung equivalent inhomogeneity. All are isocentric irradiation.

Table 4-II shows the mean ratio of measured to calculated dose values with standard deviation, maximum and minimum values using the different planning algorithms for homogeneous and inhomogeneous phantoms.

Using any of these methods in these simple situations gives reasonably good agreement. The power law method, equivalent TAR method and modified ETAR method give mean values close to unity with SD of 1.6%, 1.7%, and 2.7% respectively.

(d) 3-field distributions; field-by-field

Single fields from 3 field beams were considered, in order to assess the worst case situations for prediction of dose delivered to the five points of the phantom. Figures 4-6 (A-F) show single field histograms for the isocentric method for beams 1, 2 and 3 respectively from figure (4-1b). The figures show the two cases of homogeneous (A, C, E) and inhomogeneous (B, D, F) phantoms. As expected errors in the inhomogeneous situation are a little larger than in the homogeneous phantom. Figures 4-6 (G-I) also show single field histograms for the fixed FSD method for beams 1, 2, and 3 again numbered as in figure (4-1b).

Table 4-II: The deviations of measured and calculated dose values based on different planning algorithms:

a: Homogeneous phantom

	Mean m/cal	**S.D. %**	**Minimum**	**Max.**
Batho	0.995	1.3	0.975	1.025
ETAR	0.990	1.5	0.960	1.030
METAR	0.994	1.9	0.970	1.040

b: inhomogeneous phantom

	Mean m/cal	**S.D. %**	**Minimum**	**Max.**
Batho	0.992	1.6	0.964	1.030
ETAR	0.993	1.7	0.970	1.040
METAR	0.994	2.7	0.970	1.060

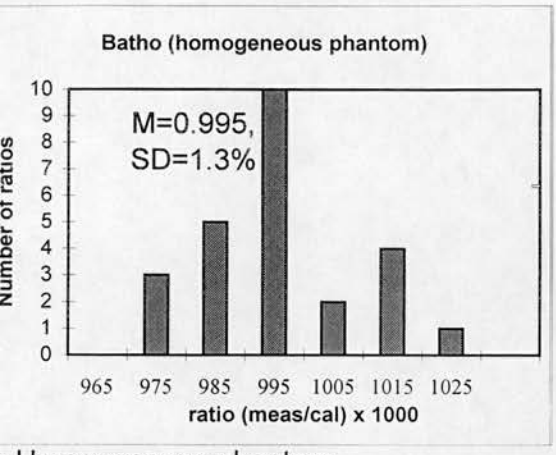

: Homogeneous phantom

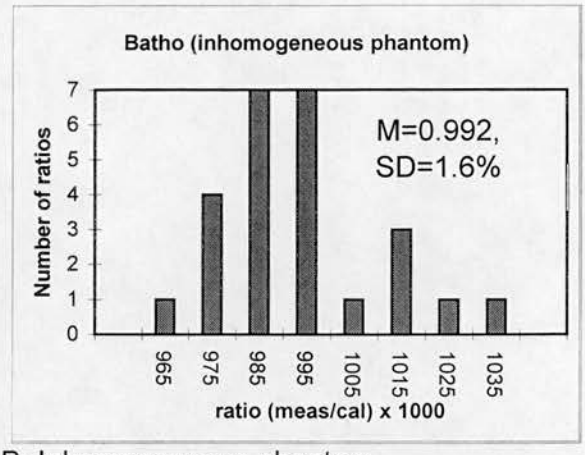

B: Inhomogeneous phantom

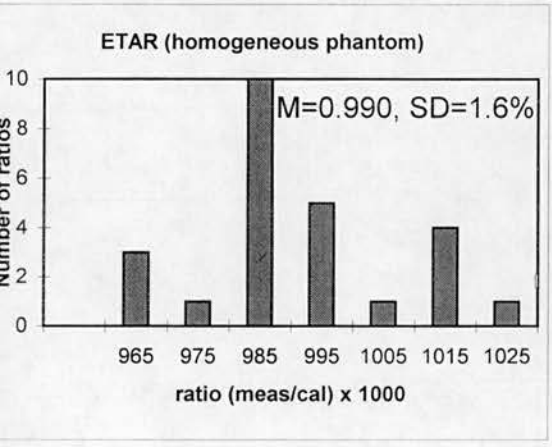

: Homogeneous phantom

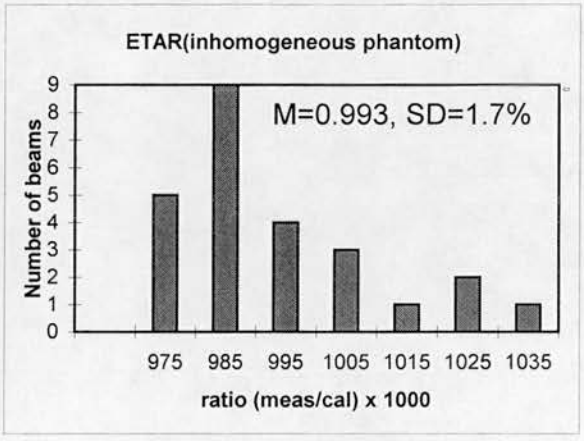

D: Inhomogeneous phantom

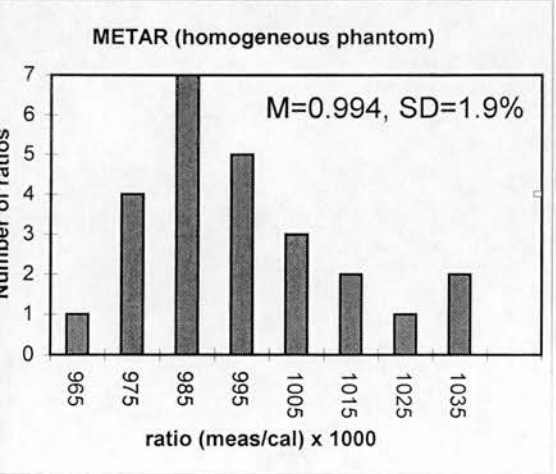

Homogeneous phantom

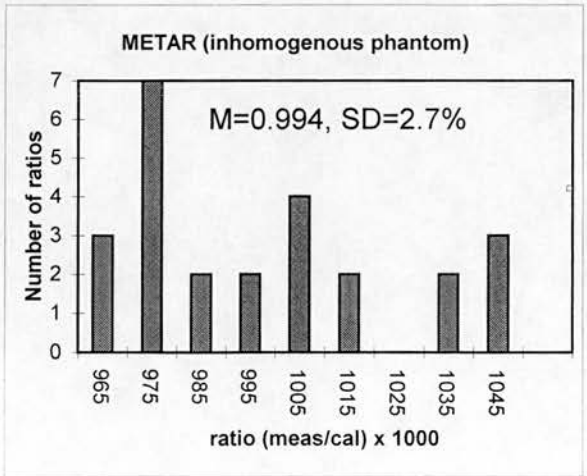

F: Inhomogeneous phantom

g. 4-5 (A-F): Measured to calculated dose ratios for 3-field distributions for different anning systems

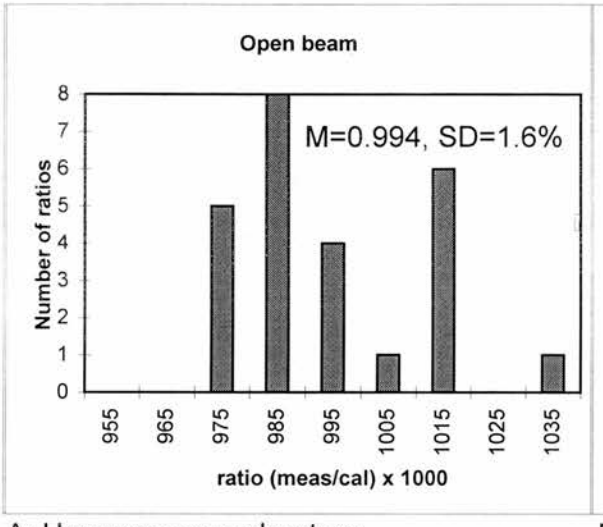

A: Homogeneous phantom

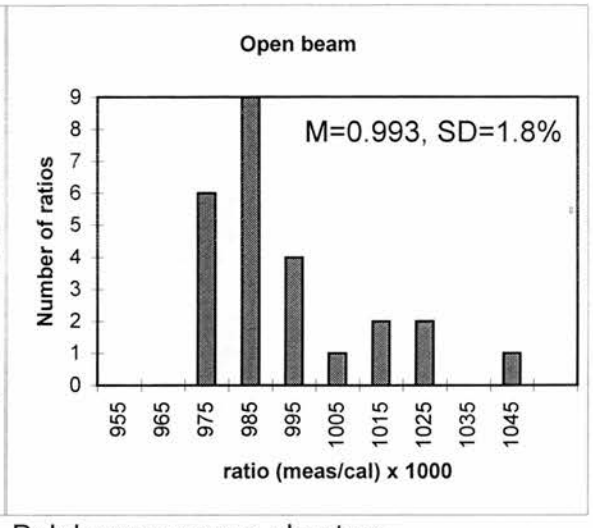

B: Inhomogeneous phantom

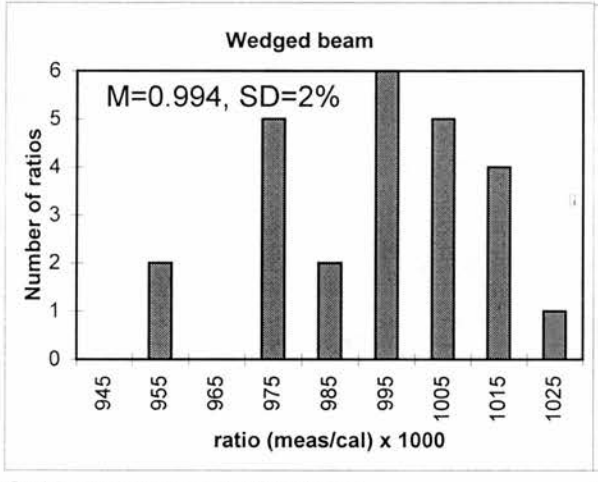

C: Homogeneous phantom

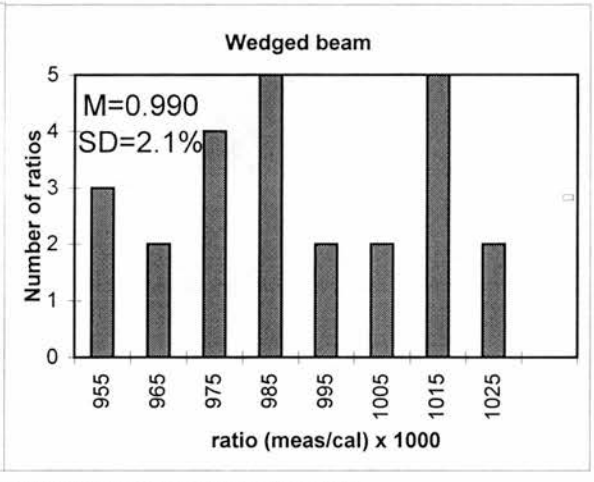

D: Inhomogenous phantom

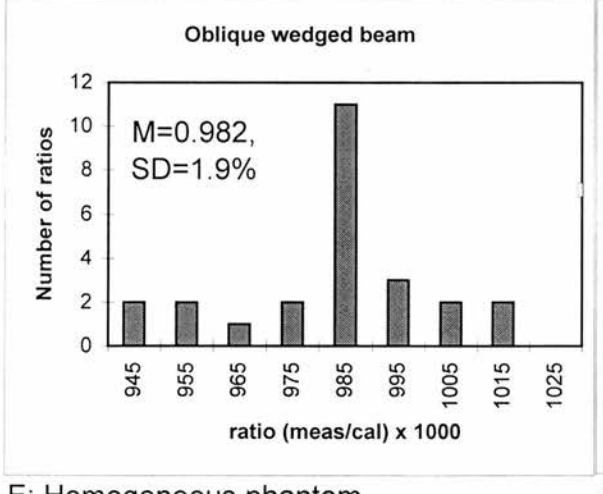

E: Homogeneous phantom

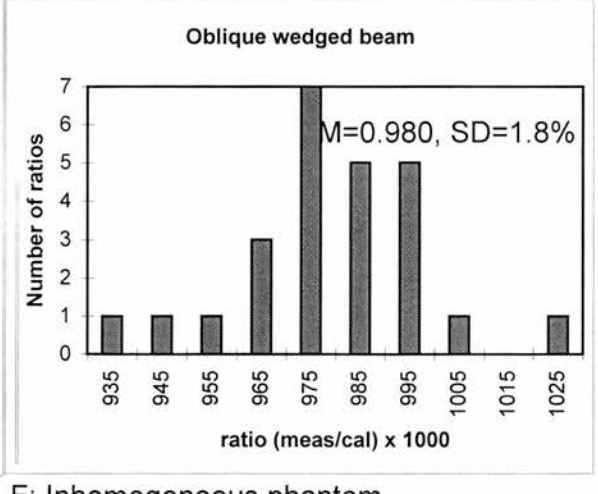

F: Inhomogeneous phantom

Fig. 4-6 (A-F): Measured to calculated dose results for single fields in homogeneous and inhomogeneous phantoms (isocentric method)

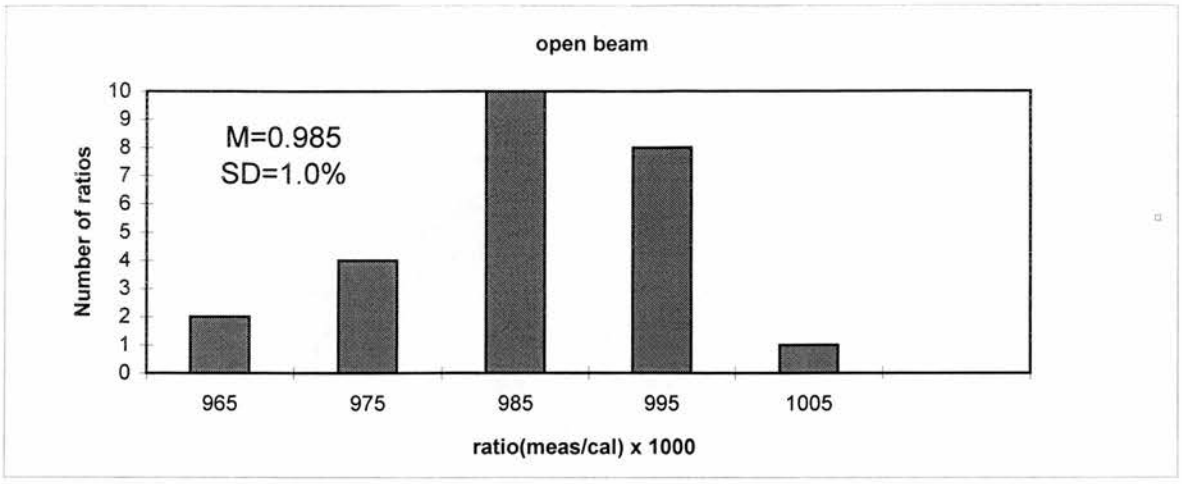

G: Homogeneous phantom

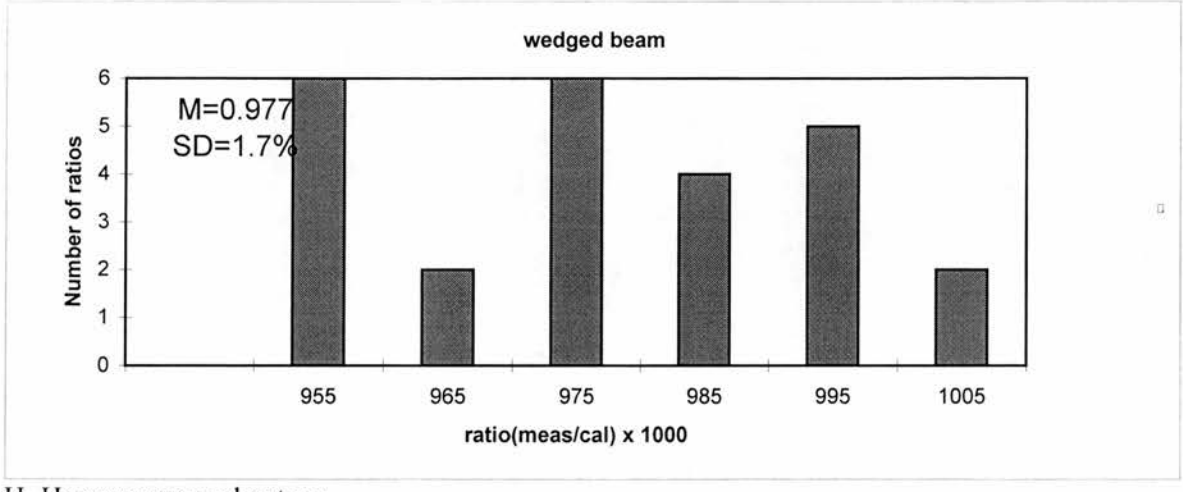

H: Homogeneous phantom

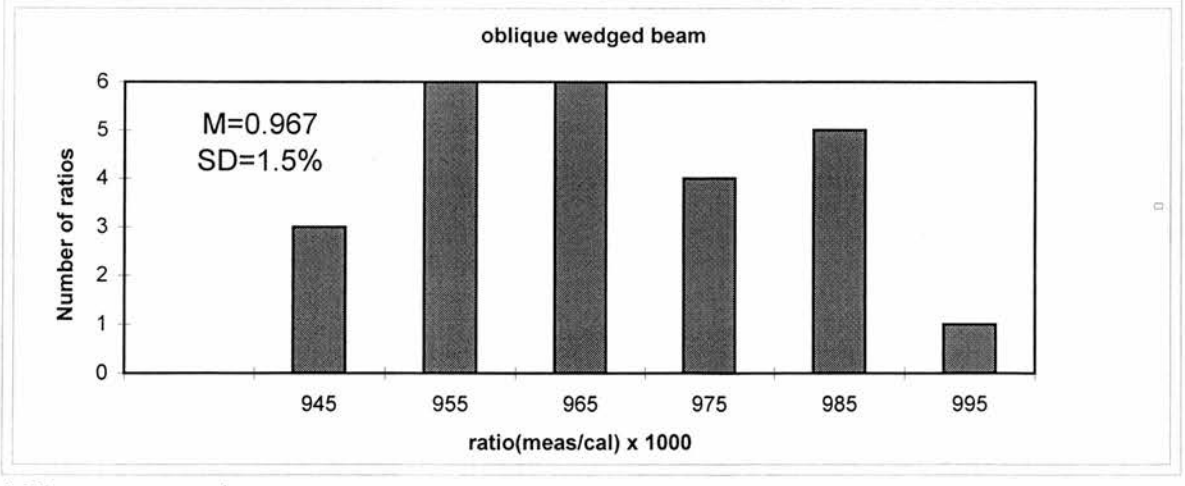

I: Homogeneous phantom

Fig. 4-6 (G-I): Measured to calculated dose results for single fields in homogeneous phantom (Fixed FSD technique)

The mean ratio of measured to calculated doses in the open beam (field 1) for homogeneous and inhomogeneous phantom were 0.994 and 0.993 respectively with standard deviations of 0.016 and 0.018. The mean values of measured to calculated doses in wedged and oblique wedged beams for the homogeneous phantom were 0.994 and 0.982, and for inhomogeneous phantom 0.990 and 0.980 with standard deviations of 0.021, 0.019, 0.021, and 0.018 respectively (Table 4-III). For the isocentric irradiations, mean dose ratios are insignificantly different for open and perpendicular wedged beams. However, the mean dose ratios for oblique wedged beams are lower. Considering standard deviations, there were differences observed between the open and wedged beams, but no significant difference between wedged and oblique wedged beams. Deviations for wedged beams may be due to planning algorithm limitations for wedged beams, misalignment of central beam axis with wedge axis, and changes in wedge position.

Table 4-III: The results of measured to calculated dose values for single fields

a: Homogeneous phantom (isocentric) [Figs. 4-6, A, C, E]

Meas./Calcul.	**Mean**	**S.D. %**	**Min.**	**Max.**
Open beam	0.994	1.6	0.976	1.018
wedged beam	0.994	2.0	0.959	1.030
oblique wedged	0.982	1.9	0.946	1.015

b: Inhomogeneous phantom (isocentric) [Figs. 4-6, B, D, F]

Meas./Calcul.	**Mean**	**S.D. %**	**Min.**	**Max.**
Open beam	0.993	1.8	0.972	1.041
wedged beam	0.990	2.1	0.958	1.020
oblique wedged	0.980	1.8	0.937	1.027

c: homogeneous phantom(fixed FSD) [Figs. 4-6, G, H, I]

Meas./Calcul.	Mean	S.D. %	Min.	max.
Open beam	0.986	1.0	0.963	1.008
wedged beam	0.977	1.7	0.950	1.010
oblique wedged	0.967	1.5	0.946	0.991

4-5-2- Results of Interdepartmental Quality Audit Using the Geometric Phantom:

(a) Reference point

The dose measured at the reference point for 8 centres in the Scottish+ audit group (including Edinburgh) has been audited against the dose stated by the centres. Figure 4-7 shows the ratio of the measured to calculated doses. Good agreement was found between the measured and stated dose values which are all within the tolerance values set up for the group (UK network). The average ratio of measured to calculated dose values is 0.998 with a standard deviation 0.013. Table 4-IV compares the results of this work with other reported dosimetry audits. The last column of this table shows the range of minimum to maximum ratio observed of measured to calculated dose values (spread).

Table 4-IV: The results of different dosimetry intercomparisons at the reference point

Reference	Region	protocol	No.	Mean	S.D.	spread
Johansson-1982[b]	Scandinavia	NACP	50	1.017	0.023	0.10
Johansson-1986	Europe	NACP	16	1.024	0.033	0.14
Wittkamper-1987	Netherland	NCS	40	1.008	0.020	0.10
Hansson-1991[d]	USA	AAPM	740	1.008	0.019	0.14
Thwaites-1992	UK	HPA	100	1.003	0.015	0.10
Hoornaert-1993	Belgium	NCS	21	1.006	0.023	0.08
Thilander-1994	Sweden	NACP	184	1.004	0.020	0.11
This work-1996	Scottish+	IPSM	22	0.998	0.013	0.05

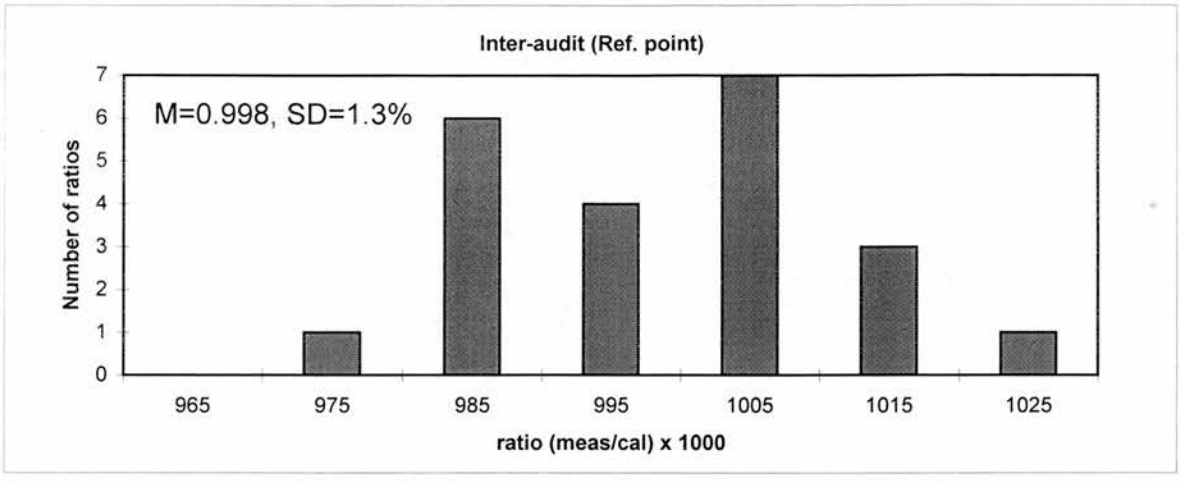

Fig. 4-7: Measured to calculated dose results at reference point

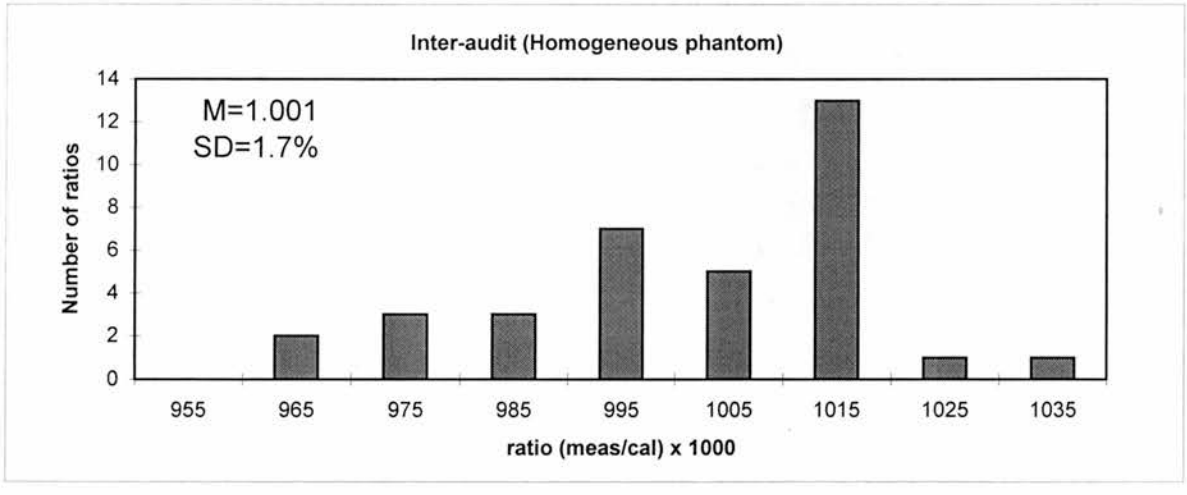

Fig. 4-8: Measured to calculated dose results for 3-field irradiation of the homogeneous geometric phantom

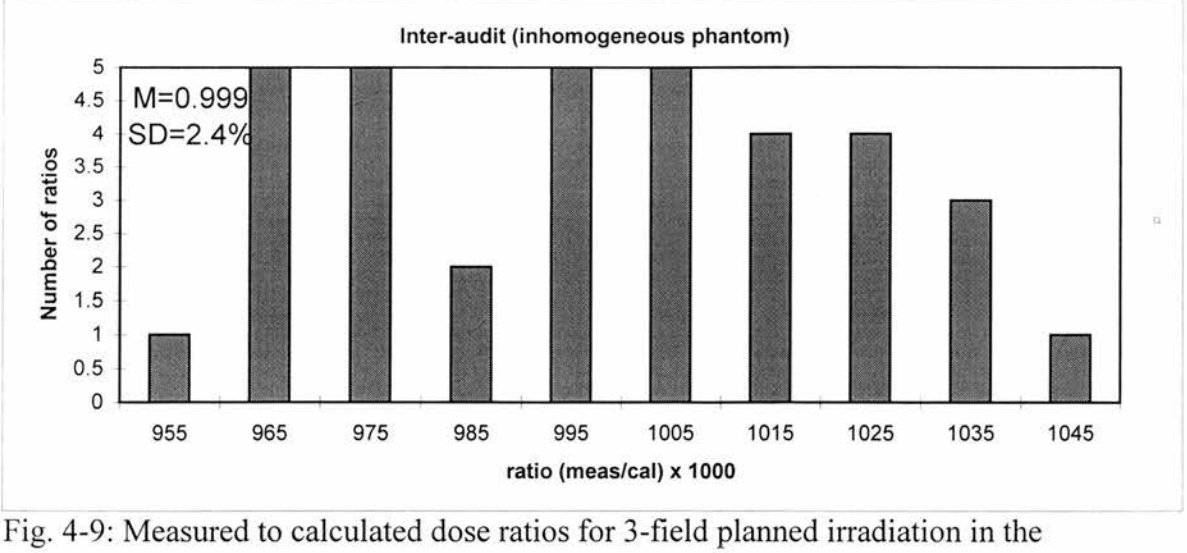

Fig. 4-9: Measured to calculated dose ratios for 3-field planned irradiation in the inhomogeneous geometric phantom

(b) Other single field points

The results for other single field parameters demonstrated that the measured values in non reference conditions including wedged beams and varying field sizes are in good agreement with stated values (see chapter 5). The mean ratio of measured to calculated values obtained is 0.999 with a standard deviation of 1% for all other single field situations.

(c) 3-field irradiations

The histograms of figures 4-8 and 4-9 show the distribution of results of 3-field planned measurements for the homogeneous and inhomogeneous geometric-phantoms in all centres. The differences between measured and calculated values were again all within the pre-set audit tolerances. The mean ratio of measured to calculated dose values obtained in the different departments for the 3 field dose distributions in homogeneous and inhomogeneous phantoms are 1.001 and 0.999 with standard deviations of 0.017 and 0.024 respectively. Table 4-V compares these results with other dosimetry audits where the 'sites' listed have been obtained using phantoms of varying complexity to simulate those areas of treatment. The standard deviation of the ratio of the measured to calculated values for the inhomogenoues phantom is larger than for the homogeneous phantom. This may be partly due to the choice of effective density for the inhomogeneity, and partly due to the errors in inhomogeneity planning algorithms.

Table 4-V: The results of different dosimetry intercomparisons at other point of dose distribution using phantoms to simulate various sites.

reference	Region	Year	site	No.	Mean	SD
Worsnop 1968	USA	1968	Lung	16	+	0.069
Johansson 1987	Sweden	1984	Bladder	15	1.002	0.031
Johansson 1987	Europe	1982-86	Tonsil	19	1.035	0.032
Wittkamper,1987	Netherland	1985	Prostate	18	1.015	0.015
SSRBMP-1984	Switzerland	1984	Lung	13	1.005	0.062
Thwaites 1992	UK	1987-91	Homog.* Inhomog.	62 62	1.008 1.001	0.027 0.034
Van Bree 1994	Netherland	1990-91	breast	21	0.999	0.015
this work	UK	1994-5	Homog.* Inhomog.	8 8	1.001 0.999	0.017 0.024

* *geometric phantom*

\+ *no true mean reported, only relative distribution values*

4-6-Discussion

4-6-1- Planning Algorithms Tests in one Department:

(a) Reference point

The IPSM geometric phantom was used to test treatment planning algorithms and to quantify discrepancies against measurements.

"As an integral part of treatment delivery, uncertainties in the treatment planning process contribute directly to uncertainties in patient doses, for which specification of accuracy requirement exist "(Mijnheer et al 1987).

The mean ratio of measured to calculated dose values at the reference point is 0.998 with a standard deviation 0.008. The mean value of this ratio is close to unity. This implies that no major systematic errors exist in the calibration, performance and operation of the machines or similarly in the phantom and methodology used. Part of the observed standard deviation is contributed by the experimental uncertainties. Even though no overall major systematic differences exist the results do imply that differences of up to 2% may exist between different beams.

(b) 3-field irradiation

An intradepartmental audit programme was carried out in 3 planned field irradiations to test different algorithms in the department. The IPSM geometric phantom with an exchangeable epoxy-resin/lung insert has been used. The results of the ratios of measured to calculated values (Fig. 4-2, 4-3, and 4-4) indicate the deviations observed between measurement and calculation for isocentric and fixed FSD methods. The mean computed dose was within 1.0% of measurement in all cases. The computed dose for the individual points was generally higher than measured dose but by within 3.0% (more than 90% cases) for both homogeneous and inhomogeneous phantoms. Considering standard deviations, there are no significant

differences between the isocentric method and the fixed FSD method (Table 4-III, a-c). However, mean dose ratios for fixed FSD tend to be lower than for isocentric. The reasons for the generally small discrepancies observed can not at this stage be separated, but could arise for any stage of the process.

Because of this observed systematic difference between calculation and measurement, the 3 field dose distributions were analysed in detail by single fields. As shown in figures 4-6 (A-F) for the isocentric irradiations and figures 4-6 (G-I) for the fixed FSD irradiations deviations in mean dose ratios are insignificantly different for open and perpendicular wedged beam. However the mean dose ratios for oblique wedged beams are lower. Considering standard deviations, the ratio of measured to calculated values for wedged beams are generally larger than open beams. But there is no difference between wedged and oblique wedged beams (Table 4-III). From this analysis it can be concluded that there is generally good agreement between measured and calculated values in the department, however wedged beams introduce generally larger uncertainties. The reasons for this increased uncertainty may be due to planning algorithm limitations for wedged beams, misalignments of central beam axis with wedge axis, and small changes in wedge position.

(c) 3-field irradiations; different planning algorithms

As shown in figures 4-5 (A-F) the spread and standard deviation of the ratio of measured to calculated values in the inhomogeneous phantom are generally larger than the homogeneous phantom. Inhomogeneity correction factors were measured and calculated for three planning algorithms. Equivalent TAR and modified ETAR take account of the density, position, and shape of an inhomogeneity, but power law methods (Batho) only take account of the density and position of the inhomogeneity. Neverless, the Batho method, Equivalent TAR and modified ETAR all give good overall agreement with measured values in this relatively simple phantom with SD of 1.6%, 1.7% and

2.7% respectively. Typically agreement at individual points is within about ±3% of measurement (see chapter 6).

Measured uncertainties (sd) due to inhomogeneity algorithms are near the same for Batho and ETAR methods, but rather larger for the modified ETAR method (Tables 6-I and 4-II). From these tables it can be concluded that the Batho method is good enough for relatively large inhomogeneities in relatively simple situations.. More complicated situations will be considered in a semi-anatomic phantom in the next step.

4-6-2-Interdepartmental Quality Audit :

The results of this work are the first round of audit within the Scottish+ audit group. The aim is to identify errors and to ensure that any discrepancies are within the IPSM network tolerances, based on the dosimetry intercomparison in the U. K (Thwaites et al 1992).

(a) Reference point

The ratio of measured to calculated dose values at reference point are shown in the histogram of figure 4-7. This ratio is 0.998 with standard deviation 0.013. All individual results were within the predetermined tolerances, showing good agreement in basic dosimetry in the centres of this group.

The results of this study show better sd than previous dosimetry intercomparisons (Table 4-IV), partly because the centres are all now using the new code of practice (IPSM 1990) for measured absorbed dose which is less ambiguous than other protocols (Allahverdi and Thwaites 1996_a).

The best consistency is achieved where centres use a single standard

laboratory and a single clear-cut dosimetry protocol. Thwaites (1993) estimated a consistency of 1.6 % (1sd) for centres using a single standard laboratory and a single unambiguous dosimetry protocol based on ion chamber dosimetry. The measurement consistency of this study between centres in the Scottish+ group which uses the new code of practice and the NPL calibration service is 1.4 % which is near the estimated consistency by Thwaites (1993). This indicates good agreement between the results of this audit with estimated values. Such an agreement indicates that the consistency of basic dosimetry in the centres involved is essentially limited by the expected random uncertainties, i.e. there are no further contributions to inconsistency. The standard deviations reported in Table(4-IV) indicate a range from 1.3% to 3.3% for megavoltage x-ray beams. Some reports e.g. IAEA/WHO Svensson (1990) showed the standard deviation of observed distributions is 6.7% if results from all countries are included. Further analysis showed the standard deviations from individual countries vary from 1.8% to 9%. The data obtained up to 1987 showed that 50% of all participants had deviated more than 5%, 26% of centres more than 10% and 5% of centres more than 30% from the IAEA reference. These variations show that much larger inconsistencies can arise and therefore there is a need for careful implementation of dosimetry protocols, practices and quality assurance in all beams available in a particular centre. Some of the problems observed, of course, are due to lack of resources, personnel, training etc. However the present results indicate achievable accuracy. The effect on radiotherapy outcome of 'simply' improving basic calibration to these levels of accuracy in those centres surveyed by IAEA/WHO would be significant.

The interdepartmental results of mean 0.998, SD 0.013 can be compared with the single centre results. The mean ratio of measured to calculated dose values at the reference point for the single (Edinburgh) centre was obtained as 0.998 with standard deviation of 0.008.

(b) Non reference point single field situations

The mean ratio of measured to calculated dose values for non-reference measurements in single fields were near unity with standard deviation of 1.0% (chapter 5). Thus no significant systematic differences were observed between measured and stated dose values for single fields in all centres.

(c) 3-field irradiations

Figures 4-8 and 4-9 show the ratio of measured to calculated dose values in 3-field planned irradiations for all centres. This ratio for homogeneous and inhomogeneous phantoms respectively is 1.001 and 0.999 with standard deviations of 0.017 and 0.024. The sd have improved since the IPSM UK-wide photon dosimetry intercomparison (Thwaites et al 1992). The range of standard deviations in Table 4-V shows the requirement to establish comprehensive quality assurance and quality control programmes. The fact that the standard deviations obtained in this study are smaller than those obtained in the earlier UK photon dosimetry intercomparisons may be due partly to the usual observations that uncertainties in a second check audit are reduced because problems identified in the fist audit have been rectified and because the audit itself promotes greater attention to quality, and partly due to the reduction of uncertainties in basic dosimetry as discussed above. Since the original UK intercomparison most centres have adapted the single (1990) dosimetry protocol and most centres have reconsidered quality assurance in detail following DOH (Department of Health) guidance on the importance of quality systems in the UK.

Larger discrepancies between measured and calculated values were observed for the inhomogeneous phantom. This is in part due to the choice of density by the different departments for the inhomogeneity and also due to inhomogeneity planning algorithms. (The outline and inhomogeneity structures of the phantom were transferred to individual computer planning systems by digitizer. The centres were given the true density of the

inhomogeneity, but some centres chose to use different values to suit local practice). Even so the differences are small and all measurements were within audit tolerances (5%).

In general from this audit it can be concluded that all stated dose values in these centres are in agreement with audit measured values within the audit system's predetermined tolerances and are therefore satisfactory within the terms of the audit. Looking below these tolerance values, the individual values raise some points which departments may wish to investigate further.

4-7-Conclusion

A quality audit of dosimetry was carried out in one department and also between centres to quantify uncertainties and to check the consistency of dosimetry between the centres involved. The extensive results in one department have demonstrated some problems in clinical dosimetry and treatment planning. For example the use of wedge filters and the presence of inhomogeneities produce additional uncertainties between the calculated and measured absorbed doses.

The discrepancies observed in this intercomparison at the reference point and for multi planned fields are smaller than in previously reported studies. This may be due to using one single standards laboratory and one clear code of practice in all centres, to increased attention to quality or to the original audit itself. The results of this audit show that all stated dose values in these centres are in agreement with audit measured values within the audit system's predetermined tolerances and are therefore satisfactory within the terms of audit. The smaller observed sd in this audit compared to the previous UK dosimetry intercomparison shows that dosimetry audit programmes provide a basis for improving quality in treatment dosimetry.

The systematic and random uncertainties observed in this audit and compared to those reported in other dosimetry intercomparisons show that quality assurance and quality control programs must be focused on all steps of radiotherapy and they also provide some reference measures of achievable accuracy and precision in reasonably well resourced and staffed departments.

Chapter 5

5-The Development of a Semianatomic Phantom to Evaluate Departmental Accuracy and Expand the Quality Audit System

5-1-Introduction

The idea of quality audit has been discussed in the previous chapter, as based on a simple geometric phantom. Various quality audit dosimetry programmes or dosimetry intercomparisons have been reported to test the uncertainties in treatment planning by using more complicated anatomic phantoms and geometric phantoms such as Wittkamper et al (1987), Johansson et al (1987), Van Bree (1992), Sipila (1992), Thwaites et al (1992) and Thilander et al (1994). Some authors have carried out audits involving more parameters at different levels of the radiotherapy process (Mills et al 1992, Aird et al 1994, Bonnett et al 1994, Thwaites and Allahverdi $1995_{a,b}$ and 1997, Allahverdi and Thwaites 1996_{b} and 1997). The Scottish+ group set up a programme to carry out different levels of dosimetry audit over a 5 year cycle. The previous chapter covered the first and second steps including beam quality, beam calibration, single field parameters, and basic practical planning methods and data by using a geometric phantom. This chapter discusses the next steps including development of a semianatomic phantom to test more complex situations that are closer to the level of treatment dose delivery. Tolerances in this audit are again based on the results of the UK photon dosimetry intercomparisons (Thwaites et al 1992), and the results of steps 1 and 2 of the group's audit programme.

A semianatomic phantom has been designed, to still be reasonably simple but with shapes and structures to simulate some common treatment sites, including breast, head and neck, thorax, etc. It has been extensively tested on five megavoltage photon beams in the range 4 to 16 MV in one centre (Edinburgh). On the one hand this can be seen as testing the phantom and methodology. On the other hand the results, coupled with those from the geometric audit phantom and from in vivo dosimetry

measurements on patients enable an assessment of achievable accuracy in a single department. After this the phantom has been used in auditing other departments.

5-2-Methods and Materials:

5-2-1-Design of semianatomic phantom

A semianatomic phantom was designed to allow reasonably realistic audit of various representative treatment sites, including breast, thorax, head and neck, etc (Thwaites and Allahverdi 1995_b and 1997, Allahverdi and Thwaites 1996_b and 1997). The aim was to move along the dosimetry chain to test more complex situations. The shape of the geometric phantom was very simple but still intended to test some clinically realistic parameters. It was used to test reference point dosimetry and some simple multi-field planned situations (previous chapter). The semi-anatomic phantom can be used as a next step after the geometric phantom to test a number of planned irradiations simulating different typical clinical situations. Tests using a semianatomic phantom can be incorporated with the previous simpler tests in comparing audit results. Anatomic phantoms can be used as a further step after a semianatomic phantom. The advantage of the semianatomic phantom compared to an anatomic phantom is that the construction and shape of the semianatomic phantom is simpler. In addition setting up of the different sites of the semianatomic phantom is easier than for an anatomic phantom. The shape of the phantom is such that it allows modified future audits closer to the point of patient dose delivery, for example by incorporating additional measurement points inside the inhomogeneities, by modifying external shape, etc.

The cross section of the phantom is shown in Fig. (5-1). The phantom has 3 sections (each 6cm thick) with length and width of 30 cm and 20 cm respectively. The dimensions and shape were selected so that the phantom would allow many different treatment techniques. The right upper area of the phantom is like a breast, and the whole phantom with two lungs is close to the realistic clinical treatment of a thorax. The left side of the phantom resembles the head and neck in dimensions.

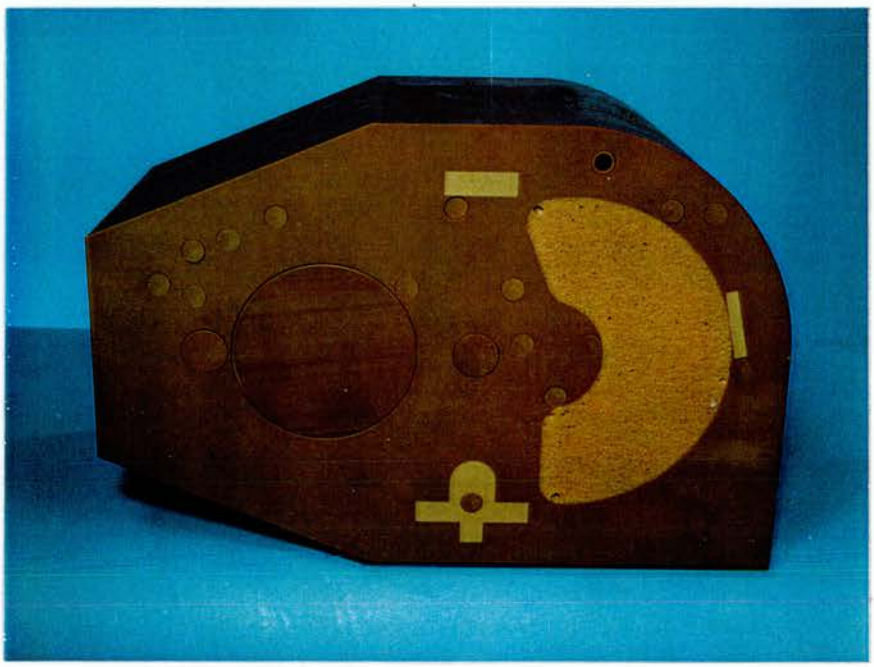

Fig. 5. 1a: The semianatomic phantom with 'water' insert

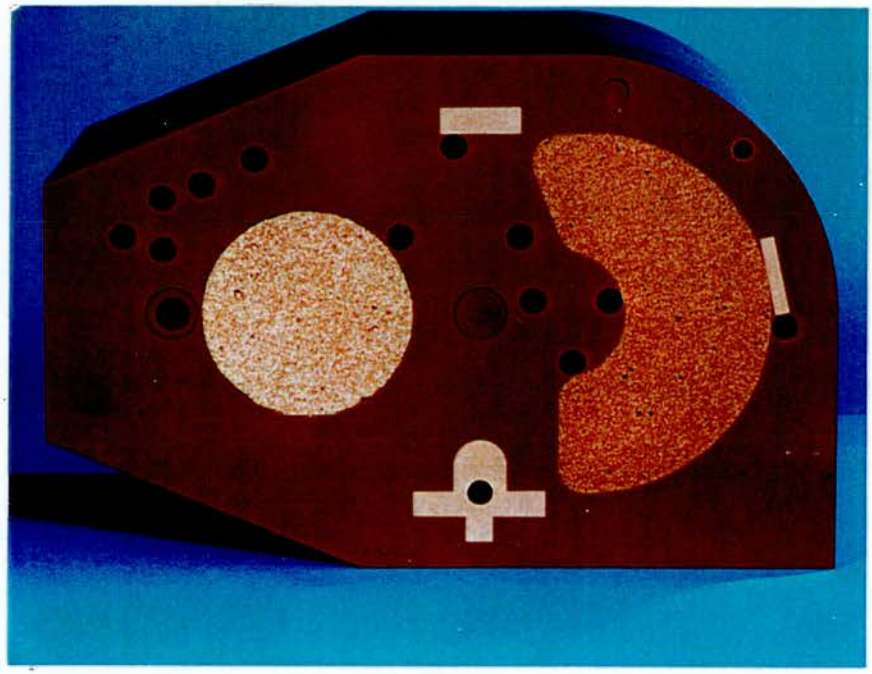

Fig. 5. 1b: The semianatomic phantom with lung insert

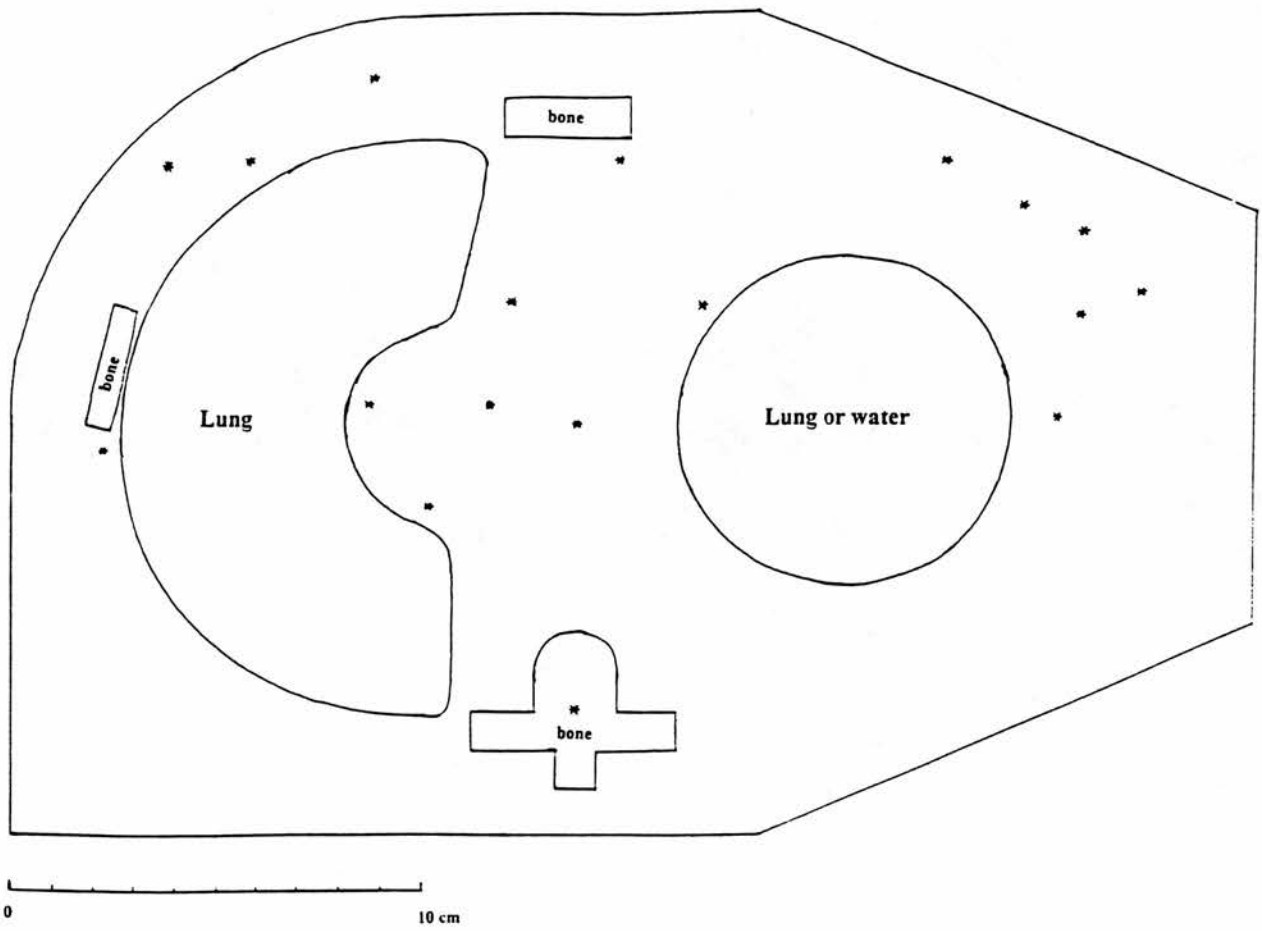

Fig. 5-1c: Schematic of the semi-anatomic phantom

The phantom was designed to satisfy these criteria. The construction was then commissioned from St Bartholomew's hospital, London. The phantom was made from the epoxy resin water equivalent material (MTI) developed by Barts. The differences between this phantom material and water have been checked and are typically less than 0.5% for different energy photon beams (Allahverdi and Thwaites 1995_c, Allahverdi et al 1996_c). The phantom contains fixed lung and bone substitute inhomogeneities of representative sizes and densities made from Barts epoxy-based materials. A 8cm diameter hole accepts the water equivalent insert from the IPSM geometric phantom and this can be replaced by the 8cm diameter core of lung equivalent material, when the phantom is used for thorax simulation.

The total number of measurement points in the phantom are currently eighteen, all of which are positioned in the water equivalent material of the phantom except one point in the representative spinal cord position. The phantom enables the provision of additional measurement points inside inhomogeneities, etc., by adding holes in future work and also will allow future shape modification. The cylindrical holes' size was drilled at 1cm diameter to take rods accepting the PTW chamber (0.125cc), except two points drilled at 2cm size to accept the Farmer chamber rods from the geometric phantom. One hole was drilled inside the spinal-cord point and several holes were drilled besides the lungs and bones to evaluate inhomogeneity effects. The radius of the PTW chamber is small, and is suitable for positioning close to inhomogeneity interfaces.

5-2-2-Initial Tests

5-2-2-1-Computer Tomography (CT)

The outline of the phantom has been obtained by both available methods (i.e. simulator CT and CT scanner) used for imaging patients in the department. Images from Computer Tomography (CT) were transferred to the Cadplan treatment planning system and those from simulator scanning were transferred to the standard

in-house planning system which is used in the department. The image resolution from the CT scanner is 512x512, then this is reduced to 256x256 in the in-house planning system and Cadplan system. The pixel size is around 1.5-2 mm^2.

The dimensions and densities of the phantom were obtained from CT images as a check. The electron density of different tissue materials was obtained using a calibration curve of CT numbers against density. Usually, these calibration curves are bilinear with one linear portion for soft tissue and another one for bony tissue. Here, electron density for soft tissue (CT numbers < 1100) is obtained by:

a) 0.00100 x CT numbers + 0.0

and for bony tissue (CT numbers >1100) is obtained by:

b) 0.00048 x CT numbers + 0.57200

The CT numbers and electron densities for the different materials of the phantom are shown in Table 5-I.

Table 5-I: CT numbers, electron density and dimensional errors of phantom structure

CT NO.	**Modal**	**density**	**Cadpln (mm)**	**standard (mm)**
phantom	1000	1.0	1.0	2.0
fixed lung	239	0.24	1.0	2.0
remov lung	263	0.26	0.5	2.0
spinalbone	1436	1.26	1.0	3.0
bone	1495	1.29	1.0	2.0

In terms of hardware, errors due to geometrical distortions and the transfer of data from simulator scanning or CT scanning to the treatment planning computer contributes to the dose uncertainties. According to the results in Table 5-I dimensional errors associated with CT simulator images and transfer in to the standard planning system (last column) are greater than those for the CT scanner and

transfer into the Cadplan system, where these are quoted for maximum errors typically linked to maximum dimensions.

5-2-2-2-Measurements for testing of phantom

Initial tests to check out the phantom and methodology were carried out for a range of x-ray energies from 4MV to 16MV. The ionisation chambers used were the same as for all subsequent measurements, i.e. a PTW 0.125cc ionisation chamber and a Farmer type 2571, with graphite wall, connected to a Nuclear Enterprises 2620A electrometer. The chambers were calibrated against a secondary standard which had been traceably calibrated at the NPL. The IPSM code of practice (1990) was used to derive absorbed dose to water. The mean of several readings (at least 3) for each point was corrected using temperature, pressure, recombination correction and phantom correction factors where appropriate. The output was determined before and after each set of measurements and the results of the measurements were adjusted according to mean measured output. It should be mentioned that the phantom corrections are small, the phantom being in agreement with water measurements to within a few tenths of a percent for MV photon beams.

Table 5-II shows some mean ratios of measured to expected doses at the isocentre. The mean ratio of measured to calculated dose values for all sites and energies at the isocentre was obtained as 0.992 (sd 1.6%). Therefore, these initial tests gave an underlying confidence in the phantom and methodology as no significant systematic errors were found.

Table 5-II: The ratio of mean measured to calculated dose values at isocentre point

Energy	Mean ratios
4MV	0.993
6MV	0.995
9MV	0.990
16MV	0.987

5-2-2-3-Intradepartment Planning Tests

Different 'sites' of the phantom were tested with different energies on five megavoltage photon beams in the range 4 to 16 MV. The measured values were compared with expected values, using the Edinburgh in-house TPS and Cadplan planning system. These tests are as follows:

-Breast

Two tangential beams are used for breast cancer in most centres. One problem of this method is the effect of the low density of a section of lung which is involved in the treatment volume and the effect of any air included in the fields, depending on technique (Fig. 5-2). For this reason, the breast volume of the semianatomic phantom was chosen such that it includes a section of lung to evaluate the inhomogeneity algorithms in these situations and for surface curvature was representative of real situations. Four points were chosen in the breast volume, one point at or close to isocentre and the other points were situated at or close to lateral and medial high dose spots or close to the interfaces. Tests were carried out on 4 MV and 6 MV photon beams according to clinical treatment situations.

-Thorax

Thorax treatment was considered using two "lungs" present in the phantom for two situations: 1) a 3-field brick and 2) a more realistic clinical treatment using typical beam directions (here called oblique chest). Two wedged beams and one open beam were used isocentrically in each method (Figs. 5-3 and 5-4). Eight points were considered in the thorax region, five points in the target volume and three points outside of the target volume. All points were measured using a PTW chamber in a 1cm plug, except the isocentre point in the 3 field brick technique using a Farmer chamber inserted in a 2cm plug. In the thorax region the low density lung significantly alters the dose distribution; different calculation algorithms to account for such inhomogeneities will be discussed in chapter 6. Several measurement points were considered at interfaces between lungs or bones and the water equivalent

material of the phantom to evaluate the inhomogeneity algorithms used in these fairly realistic situations. As mentioned above the images of the semianatomic phantom have been obtained by computer scanning (CT) as well as simulator-CT and input to the TPS. Therefore, the densities of internal organs in addition to detailed anatomical contours, can be obtained precisely. Therefore, improved inhomogeneity algorithms such as ETAR can be used and evaluated.

-Brain

The left side of the phantom is intended to resemble head and neck in dimensions, when the 8cm diameter core of water equivalent material is replaced. Two opposed wedged fields were used isocentrically (Fig. 5-5). The isocentre point was measured using a Farmer chamber, and five other points were measured using the PTW chamber.

-Right angle wedged pair

The left upper corner of the phantom was chosen to irradiate a right angle wedged pair. Two wedged beams were used isocentrically and three points were measured (Fig. 5-6).

-Parotid

A section of phantom was given an irradiation similar to a parotid treatment (Figs. 5-7 and 5-8). Two wedged beams were used isocentrically for two situations. In one situation the beam directions are similar but the isocentre is shifted such that the corner of phantom was included in the irradiated area (Fig. 5-7).

Example of plans for all these situations are given in Figs. 5-2 to 5-8. Typical beam numbering and measurement point numbering are shown. For all these irradiations the dose was measured and compared for each single beam, because the tolerance may be acceptable for multifield totals, while the error of a single beam may not be acceptable or one beam may contribute more significant errors than other beams. The aim was to determine worst cases in different situations to assess the phantom and to assess possible errors in the treatment planning algorithms.

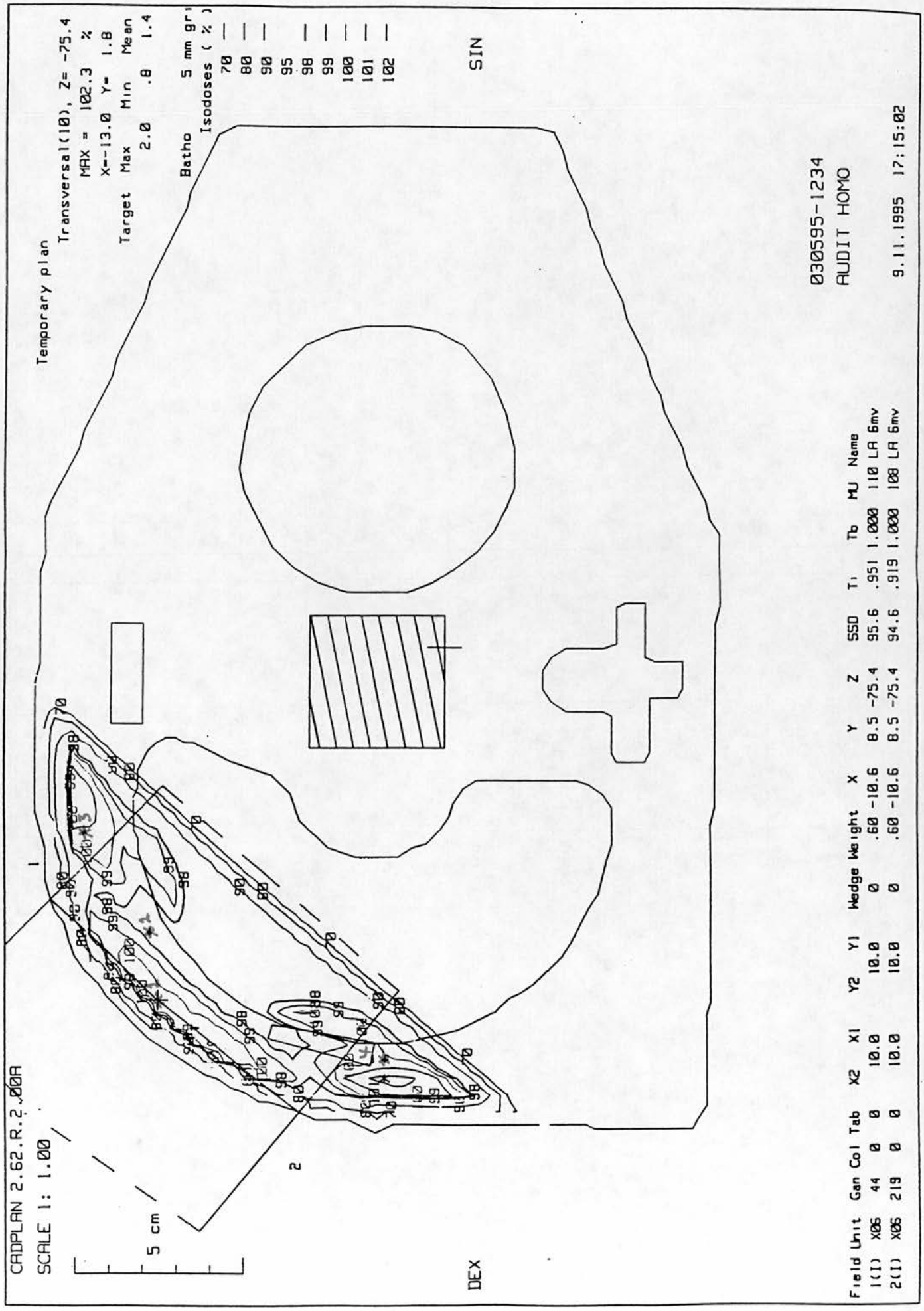

Fig. 5-2: The cross section of Breast in semianatomic phantom

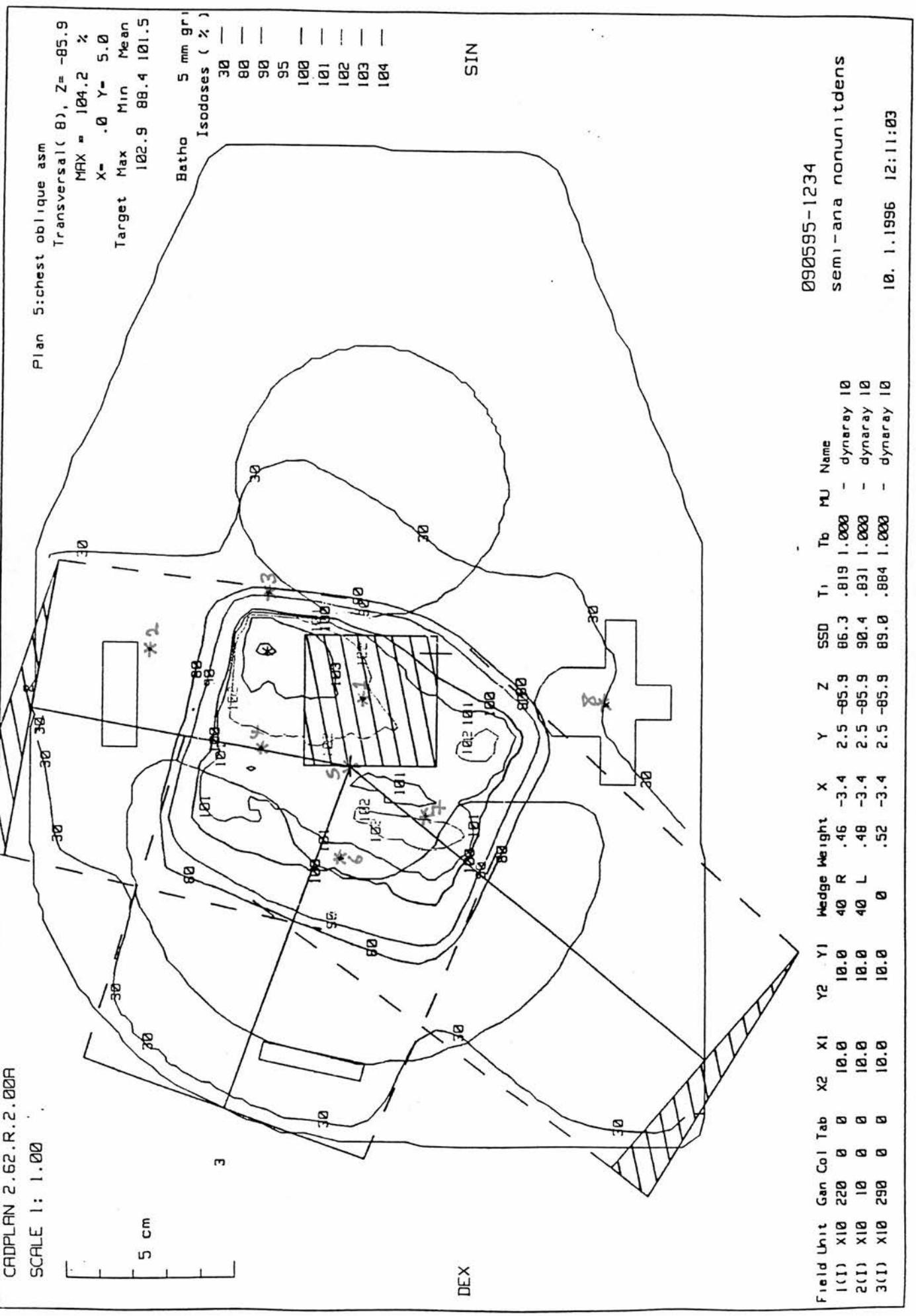

Fig. 5-3: The cross section of Thorax (clinical situation) in semianatomic phantom

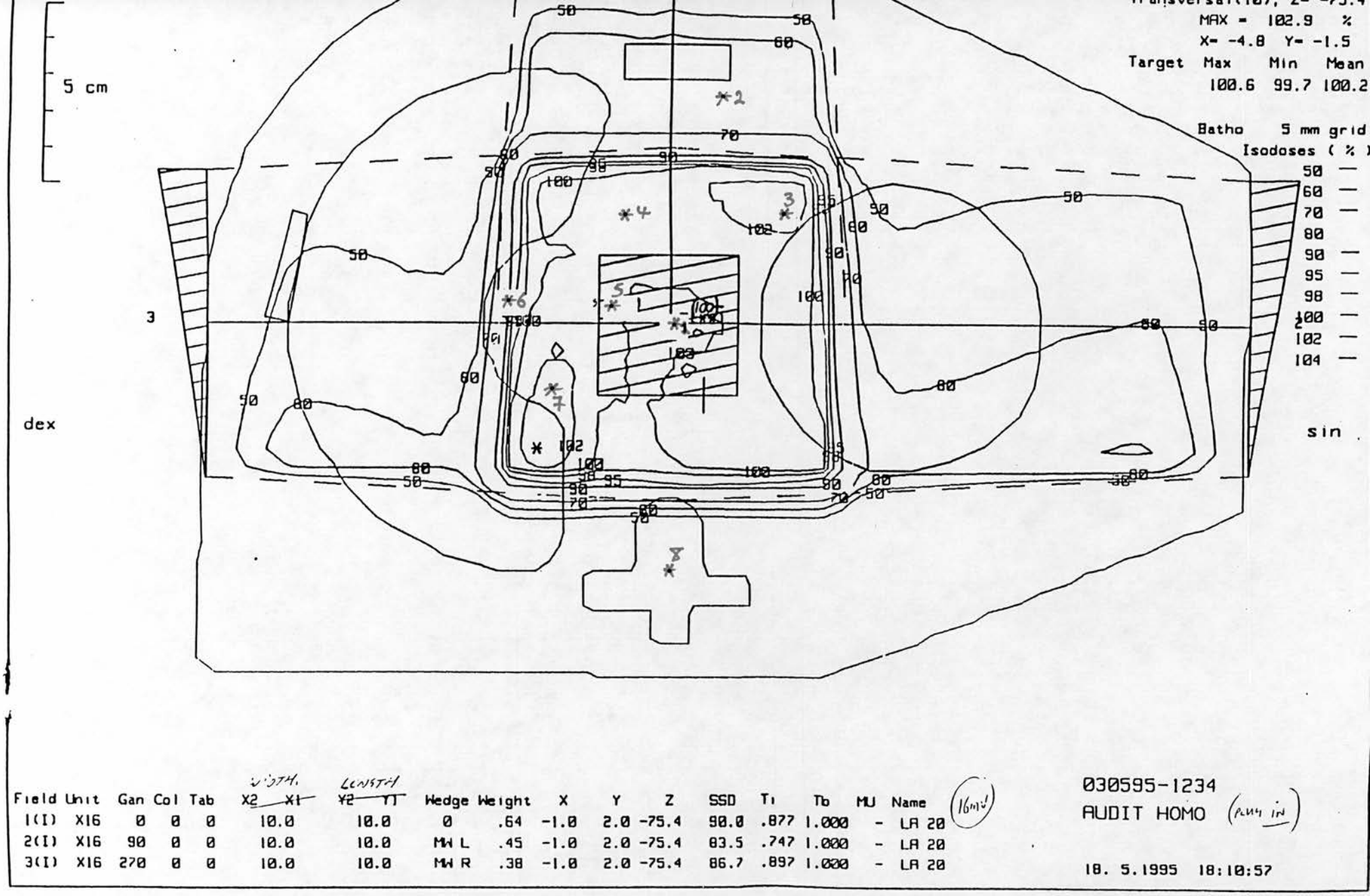

Field	Unit	Gan	Col	Tab	X2	X1	Y2	Y1	Wedge	Weight	X	Y	Z	SSD	T1	Tb	MU	Name
1(I)	X16	0	0	0	10.0		10.0		0	.64	-1.0	2.0	-75.4	90.0	.877	1.000	-	LA 20
2(I)	X16	90	0	0	10.0		10.0		MW L	.45	-1.0	2.0	-75.4	83.5	.747	1.000	-	LA 20
3(I)	X16	270	0	0	10.0		10.0		MW R	.38	-1.0	2.0	-75.4	86.7	.897	1.000	-	LA 20

Fig. 5-4: The cross section of Thorax (3 brick field) in semianatomic phantom

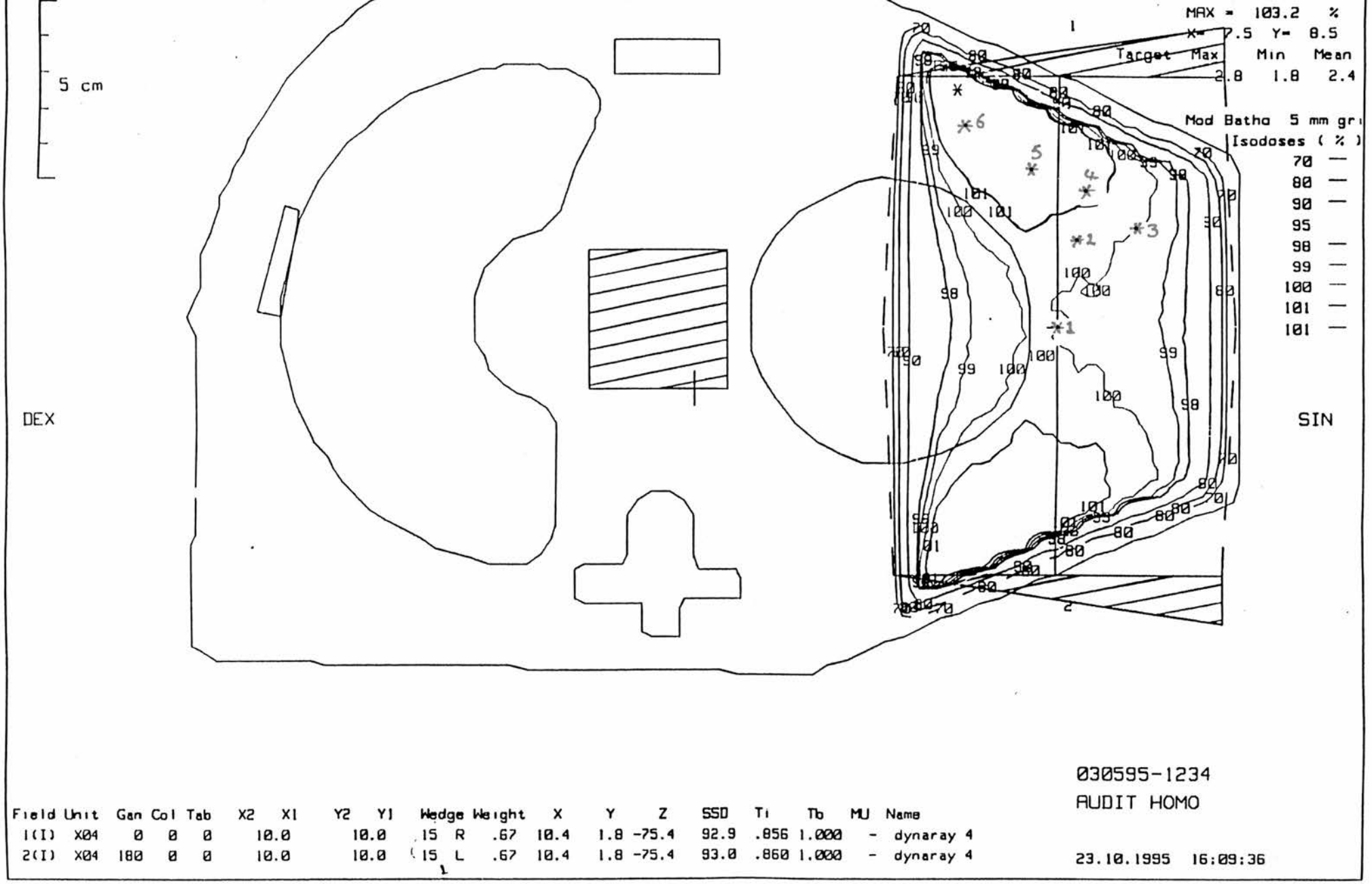

Field	Unit	Gan	Col	Tab	X2	X1	Y2	Y1	Wedge	Weight	X	Y	Z	SSD	Ti	To	MU	Name
1(I)	X04	0	0	0	10.0		10.0		15 R	.67	10.4	1.8	-75.4	92.9	.856	1.000	-	dynaray 4
2(I)	X04	180	0	0	10.0		10.0		15 L	.67	10.4	1.8	-75.4	93.0	.860	1.000	-	dynaray 4

Fig. 5-5: The cross section of head in semianatomic phantom

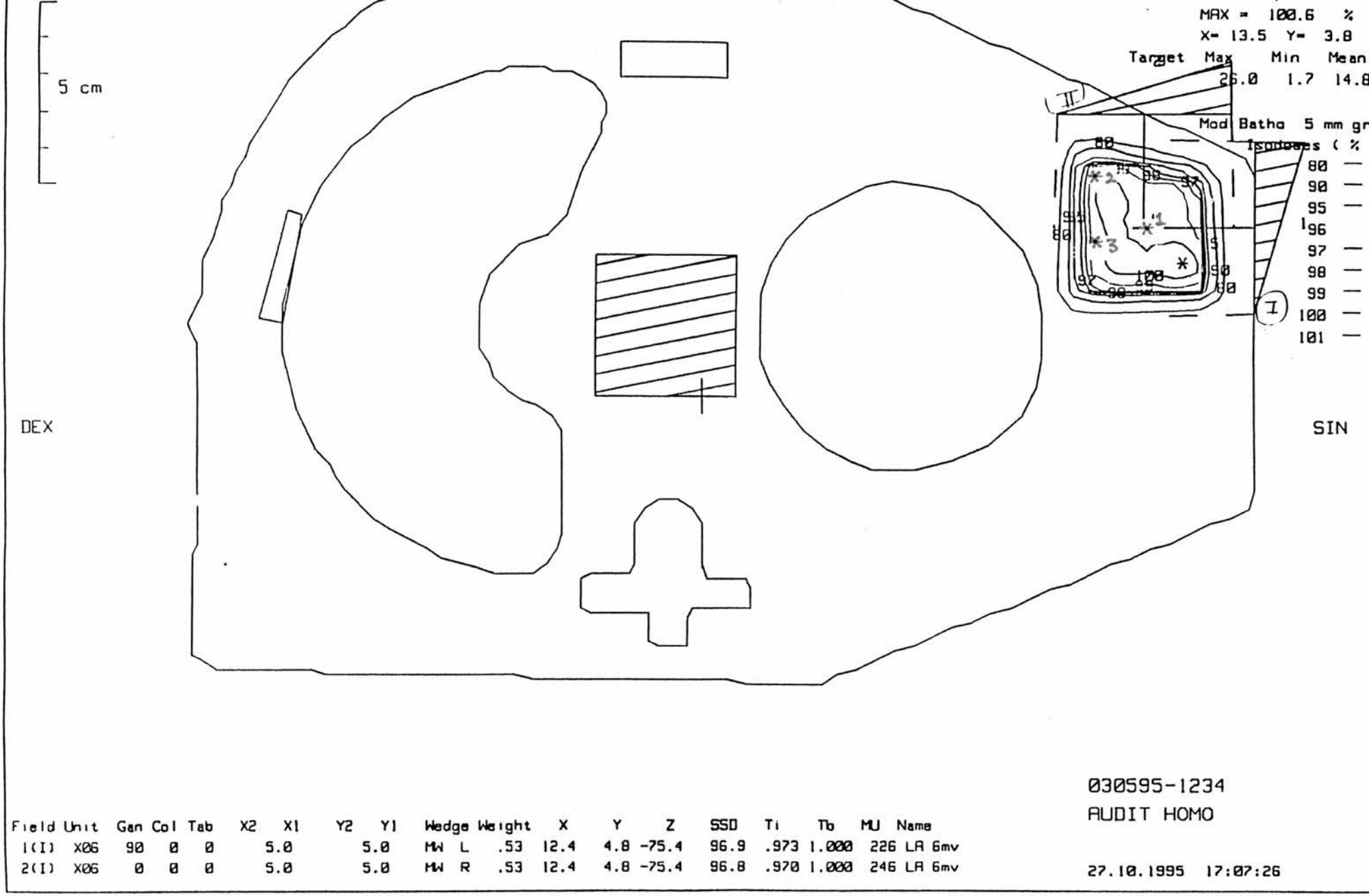

Field	Unit	Gan	Col	Tab	X2	X1	Y2	Y1	Wedge	Weight	X	Y	Z	SSD	Ti	Tb	MU	Name
1(I)	X06	90	0	0		5.0		5.0	MW L	.53	12.4	4.8	-75.4	96.9	.973	1.000	226	LR 6mv
2(I)	X06	0	0	0		5.0		5.0	MW R	.53	12.4	4.8	-75.4	96.8	.970	1.000	246	LR 6mv

Fig. 5-6: The cross section of right wedge angle beam in semianatomic phantom

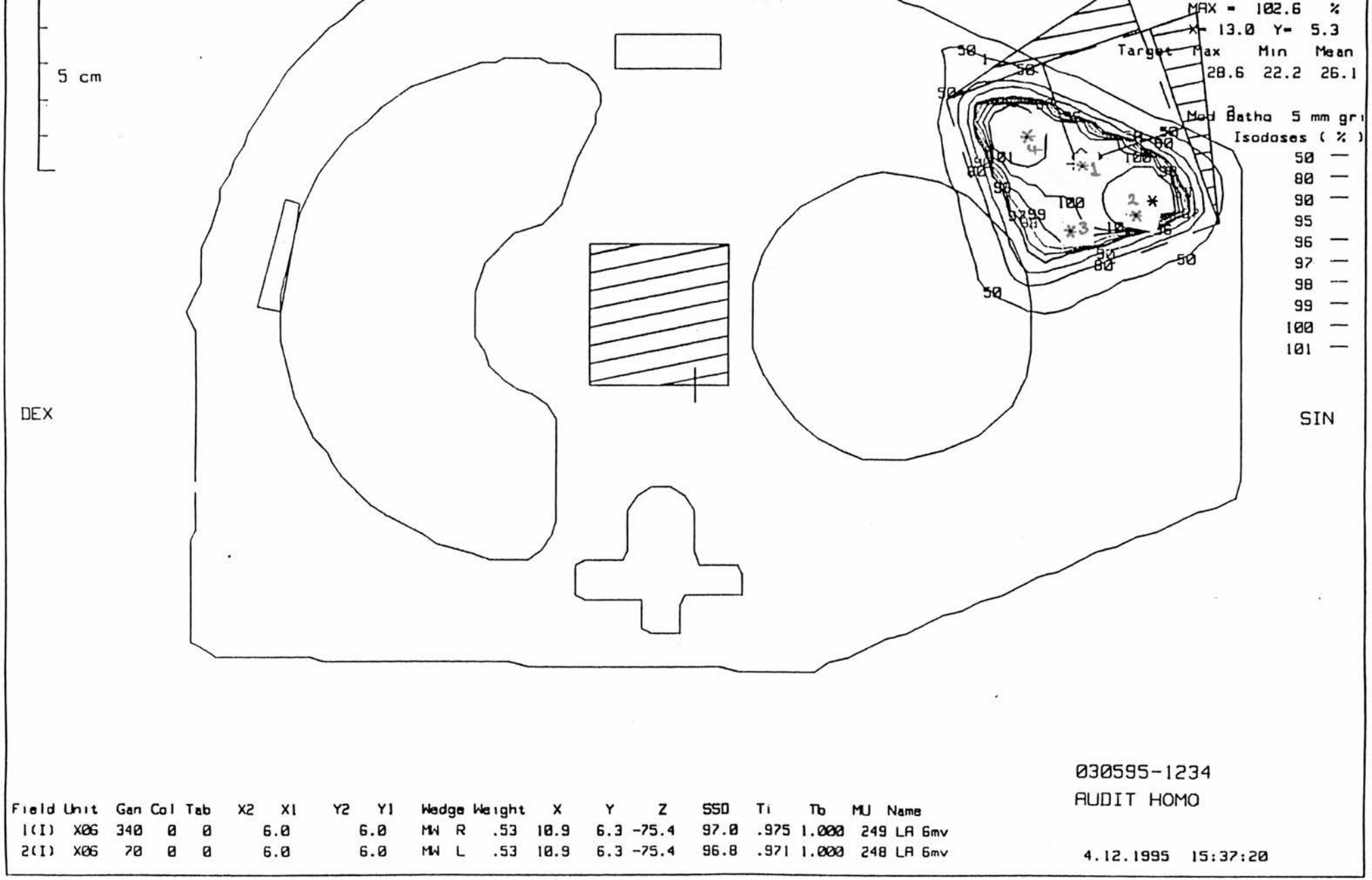

Field	Unit	Gan	Col	Tab	X2	X1	Y2	Y1	Wedge	Weight	X	Y	Z	SSD	Ti	Tb	MU	Name
1(I)	X06	340	0	0		6.0		6.0	MW R	.53	10.9	6.3	-75.4	97.0	.975	1.000	249	LA 6mv
2(I)	X06	70	0	0		6.0		6.0	MW L	.53	10.9	6.3	-75.4	96.8	.971	1.000	248	LA 6mv

Fig. 5-7: The cross section of parotid in semianatomic phantom

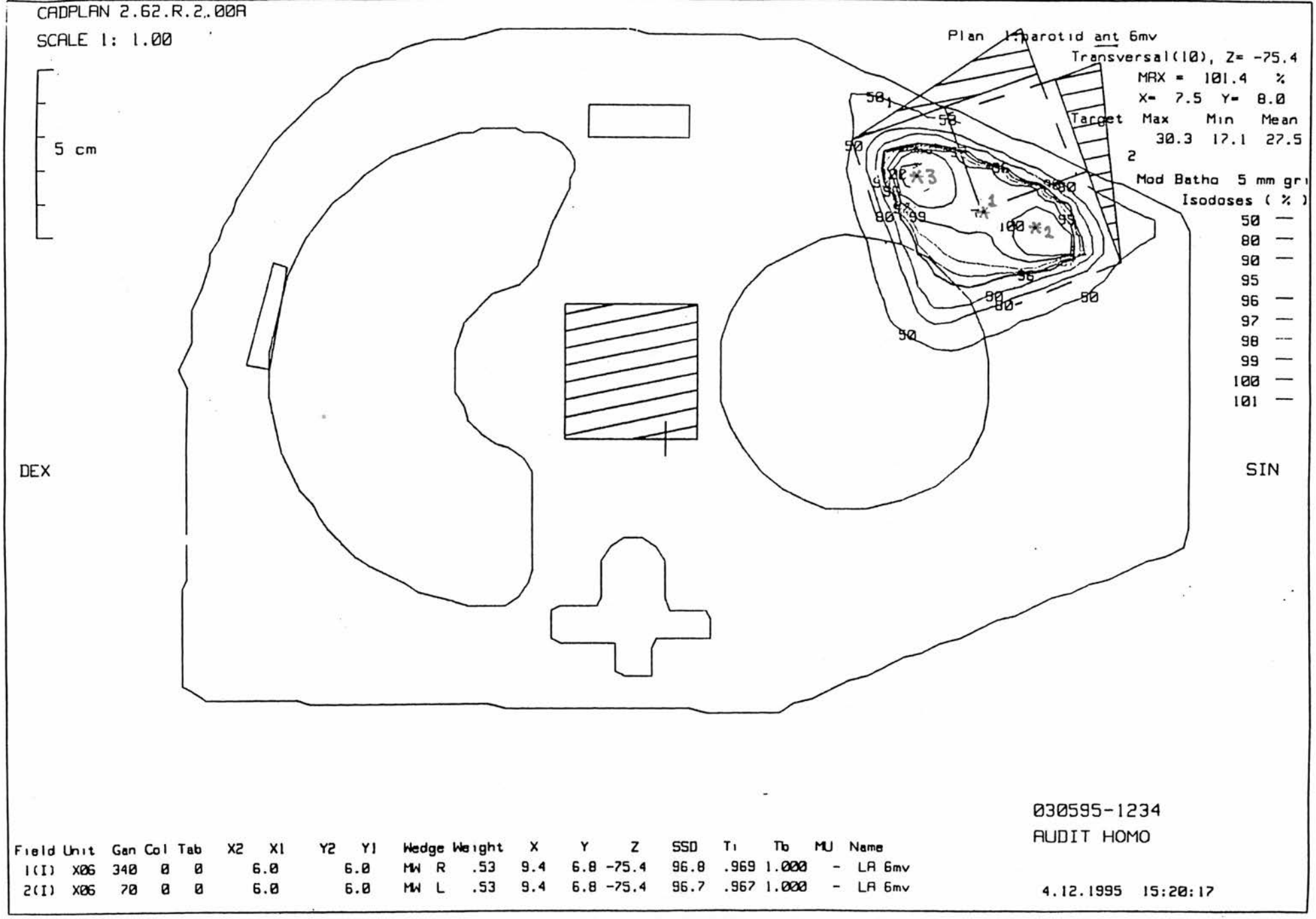

Field	Unit	Gan	Col	Tab	X2	X1	Y2	Y1	Wedge	Weight	X	Y	Z	SSD	T1	Tb	MU	Name
1(I)	X06	340	0	0		6.0		6.0	MW R	.53	9.4	6.8	-75.4	96.8	.969	1.000	-	LA 6mv
2(I)	X06	20	0	0		6.0		6.0	MW L	.53	9.4	6.8	-75.4	96.7	.967	1.000	-	LA 6mv

Fig. 5-8: The cross section of Parotid in semianatomic phantom

5-2-3-Methods for inter-departmental Audit

As a first round of audit using the semi-anatomic phantom, the outlines of the phantom, inhomogeneity structures and target volumes for thorax and breast were entered onto a life-size figure and were mailed to participating centres. The planning team in each centre was asked to plan according to their own individual treatment criteria to provide a uniform dose distribution to the target volume. The centres had freedom to choose beam energy, field size, beam directions, etc. The inhomogeneity densities were provided, but again the centres could choose to use these values or others.

The cross sections of the breast volume and the target volume of the thorax treatment are seen in figures 5-2 and 5-3. For the thorax, all centres used a 3 field technique, one open and two wedged fields isocentrically, but selected different beam directions. Also all centres used two tangential breast fields isocentrically for the breast irradiation, but the isocentre point was at different points for each centre, following these specific techniques.

The measurements were carried out as part of an audit visit in one day, typically later afternoon and evening including the phantom measurements plus other audit tasks. These measurements were as follows:

I-comparison of audit pressure measurement and local pressure statement (audit tolerance 0.3%);
II-audit beam calibration in reference conditions, 100FSD, 10x10 field, 5cm deep in phantom, 200 MU (audit tolerance 3.0%);

III-simple audit of geometric parameters, in parallel with set up of geometric and semi-anatomic phantoms; including

-Optical distance indication (ODI) vs lasers at 100fsd (tolerance 2mm)

-Measured vs predicted fsd on planned fields (tests input of phantom toTPS, in combination with some aspects of set up and machine geometric parameters) (Tolerance 5mm);

-Measured light field sizes (audit tolerance 3mm)

IV-Tests on delivery of dose to planned near-clinical situations in the semianatomic phantom (this tests a combination of data acquisition, TPS performance, MU calculation, set up and machine performance);

V-procedural audit on the quality assurance and methods used in the department for the treatment planning system and the treatment planning process (by discussion with local staff).

All tolerances in this audit are based on the UK photon dosimetry intercomparison sd (Thwaites et al 1992) and the audit group results (sd) from steps 1 and 2 or a UK national QA guidelines (IPSM/IPEM). A report or description of the audit, including all measurements made, calculated values, procedures used and total results were sent to the host department. Moreover, required specific recommendations and comments arising from the audit accompanied this report. The differences noted between the host and the visitors concerning any aspect tested can improve quality in the centre if the reason can be identified and improved and also it can help in planning expansion of future audit.

5-3-Results

5-3-1-Intra departmental

The results of extensive tests on four megavoltage photon beams in the range 4 to 16 MV in one centre (Edinburgh) is shown in Table 5-III. The first column of the table shows the 'anatomical site' of the phantom and the second column indicates the overall number of points inside the target volume for each site (Figs. 5-2 to 5-8). The points out of the target volume and on the edges of beams, where small errors in set up could produce large errors between measured and calculated values, are not

Table 5-III: The measured to calculated dose values and standard deviations for different sites of semianatomic phantom

anatom. sites	Points (TV)	field	energy	Cadplan Mean	Cadplan SD%	stand. Mean	stand. SD%
Thorax*	5	2wedged	4	0.991	1.1	0.998	0.9
3field		+	6	0.980	0.6	0.988	0.5
brick		1 open	9	0.973	0.8	0.976	0.6
lungout)			16	0.983	0.6	0.988	0.6
thorax#	5	2wedged	4	1.001	0.8	1.00	0.6
3 field		+	6	0.986	0.9	0.986	0.8
brick		1 open	9	0.979	0.9	0.980	0.5
(lungin)			16	0.989	0.8	0.983	0.7
Thorax*	5	2wedged	6	0.991	1.3	0.994	1.1
oblique		+	9	0.976	0.5	0.978	0.7
lungout)		1 open					
Thorax#	5	2wedged	6	0.992	1.2	0.992	1.1
(lungin)		+	9	0.980	0.5	0.985	0.6
		1 open					
Head	6	2wedged	4	1.013	1.4	1.002	1.4
			6	0.985	1.4	0.980	1.4
Breast	4	2wedged	4	0.964	0.7	-	-
			6	0.993	1.3	-	-
parotid	3	2wedged	4	0.991	1.4	0.989	1.4
ant.			6	1.001	0.3	1.005	0.8
Parotid	4	2wedged	4	0.991	1.6	0.989	2.0
post.			6	1.00	0.7	1.004	0.5
rightang	3	2wedged	6	1.006	0.4	1.013	0.4
wed.pair							

** density = 1.0 # density = 0.25*

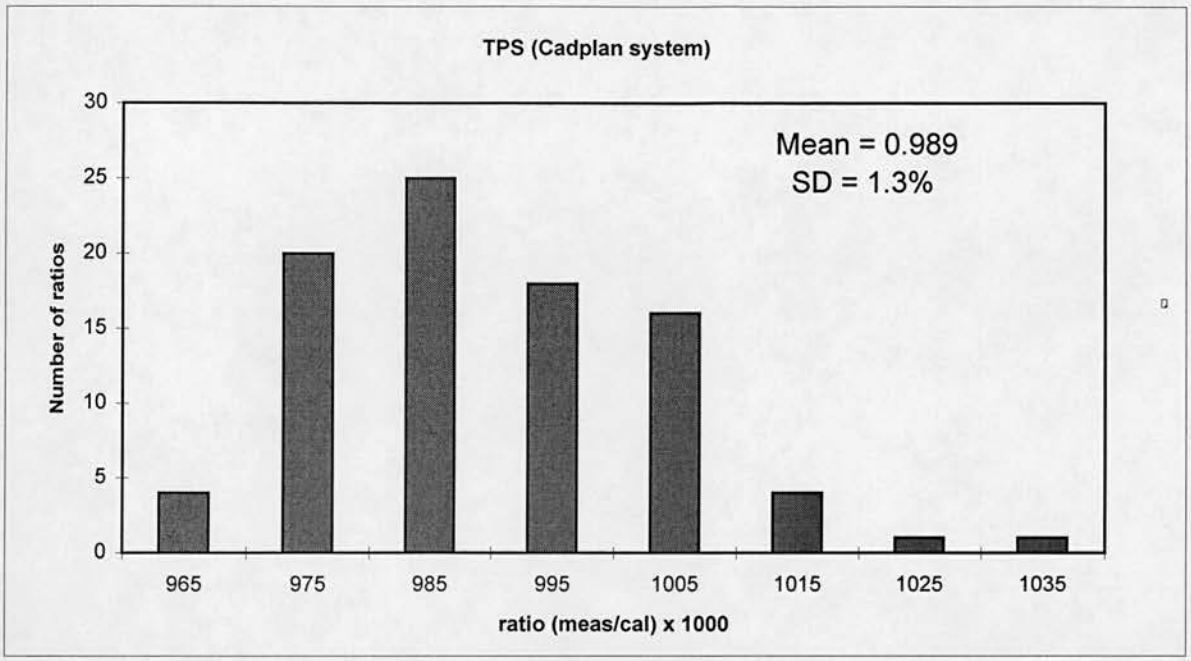

Fig. 5-9: Measured to calculated dose ratios for all points (TV) in one department

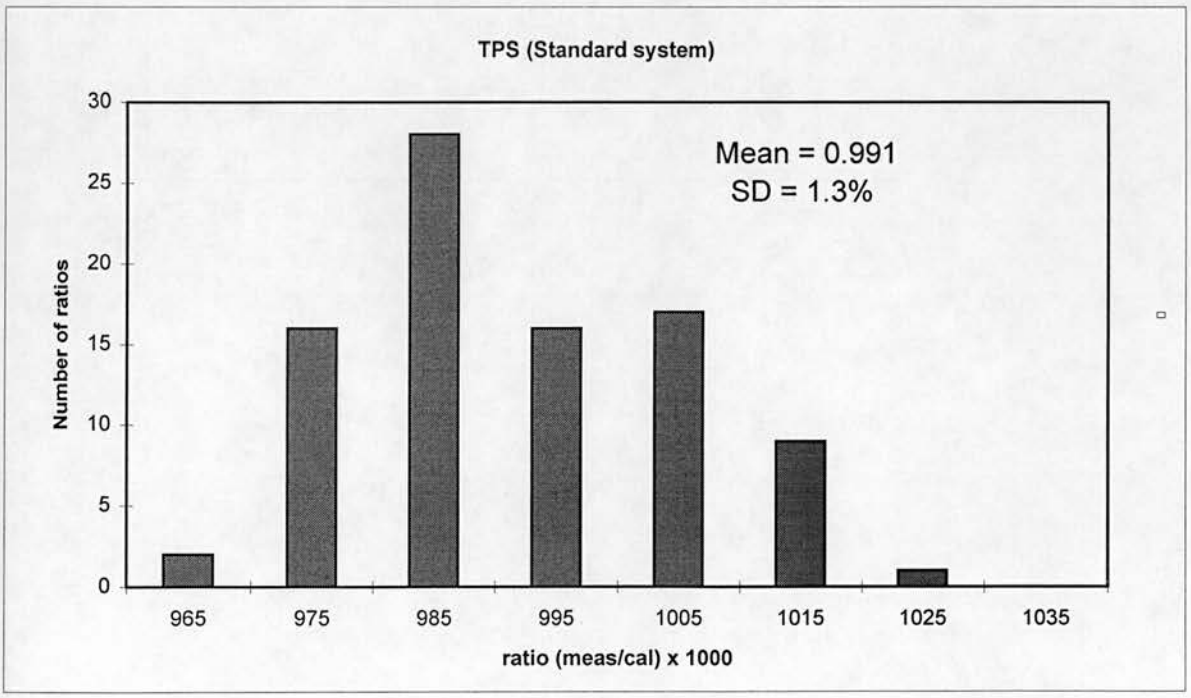

Fig. 5-10: Measured to calculated dose ratios for all points (TV) in one department

considered here. The thorax has been considered using two situations, "lung-in" and "lung-out" (see 5-2-2-3). The combination of fields are shown in the third column and the energy (MV) of the photon beams are shown in the fourth column. The mean ratios of measured to calculated dose values with standard deviations for the different sites of the semianatomic phantom are then given comparing to the planning calculations for both the Cadplan system and the standard system in house. The mean ratios in Table 5-III are the average of measured to calculated dose values from several points in each site.

The overall mean ratios of measured to calculated dose values (all beams, all sites, all points inside the target volume) obtained are 0.989 and 0.991 with standard deviations 1.3% for both the Cadplan system and standard system respectively (Figs. 5-9 and 5-10). When points outside the target volume of the thorax including inside the 'spinal cord' were considered, the mean ratios of total points in the phantom were obtained as 0.990 and 0.996 with standard deviations of 1.4% and 2.0%.

Table 5-IV shows the minimum and maximum deviations of measured to calculated dose values for the two treatment planning systems for individual measurement points from all fields involved combined. The values of worst cases for the Cadplan system (column 2) are also gives by analysis of single fields to illustrate the maximum deviations for specific fields. Note that for the thorax 3-field brick, maximum percentage deviations are given for TV points alone and for out-of-TV points. The latter at (2.5-3.5%) essentially are due to points near the edges of beams as discussed above.

According to Table 5-III the means of all the measurement points in different sites of the phantom show agreement between the stated and calculated values within 3% except for 4MV breast, where the difference is due to lack of scatter. In almost all cases the measured doses tended to be less than calculated. However, the analyses of single fields (Table 5-IV) show some larger discrepancies between measured dose

Table 5-IV: The minimum and maximum deviations of measured to calculated dose values (multi-field) and worst cases of single fields

anatomical sites	energy	Cadplan system worst cases *(single field)*	Cadplan system Min. *(multi-field)*	Cadplan system Max. *(multi-field)*	standard system Min. *(multi-field)*	standard system Max. *(multi-field)*
Thorax 3field brick (Target volume)	**4**	**4.4**	**-1.1**	**1.0**	**-1.1**	**1.3**
	6	**-5.1**	**-2.7**	**-0.5**	**-2.5**	**-0.4**
	9	**-6.0**	**-2.9**	**-0.5**	**-2.7**	**-1.5**
	16	**7.6**	**-2.2**	**0**	**-2.4**	**-0.6**
Thorax 3field brick (All points)	**4**	**-27**	**-2.8**	**1.0**	**-1.1**	**4.1**
	6	**36**	**-2.7**	**0.1**	**-2.5**	**3.4**
	9	**30**	**-2.9**	**1.4**	**-2.7**	**2.2**
	16	**35**	**-2.2**	**0.3**	**-2.4**	**1.4**
clinical thorax (Target volume)	**6**	**-4.6**	**-2.6**	**0.6**	**-2.1**	**0.5**
	9	**-5.3**	**-2.5**	**-1.4**	**-2.3**	**-1.3**
clinical thorax (All points)	**6**	**-**	**-3.7**	**0.6**	**-2.1**	**6.0**
	9	**-**	**-2.5**	**0.2**	**-2.3**	**4.5**
Head	**4**	**3.9**	**-0.7**	**3.1**	**-1.8**	**2.0**
	6	**-3.5**	**-2.2**	**-0.9**	**-3.1**	**-1.7**
Breast	**4**	**-5.7**	**-3.4**	**-1.3**		
Parotid (ant.)	**4**	**-3.6**	**-2.5**	**0**	**-2.6**	**0.1**
	6	**-1.0**	**-0.2**	**0.4**	**0.1**	**1.4**
Parotid (post.)	**4**	**-4.0**	**-3.1**	**0.4**	**-0.3**	**1.3**
	6	**-1.1**	**-0.7**	**0.9**	**-0.2**	**1.0**
right wedge angle beam	**6**	**-4.3**	**0.3**	**1.0**	**1.1**	**1.8**

and calculated dose values. Figure 5-11 shows all the deviations of measured to calculated dose values of single fields for different sites of the phantom comparing to Cadplan calculations (all points are inside the target volume). The mean ratio obtained of measured to calculated dose values for all points (inside the target volume) is 0.989 with a standard deviation of 2.3%, i.e. considering single field data the sd is larger than considering multi-field.

The main reasons for discrepancies in these situations are expected to be due to inhomogeneity algorithms, beam modifiers, interfaces and points near the edge of beam. Inhomogeneity algorithms will be discussed further in the next section. The analysis of single fields for thorax for points 2 and 8 showed larger deviations for fields 2 and 3 (Fig. 5-4). This is more significant for 16MV photon beam. Points 2 and 8 are near the edge of beams 2 and 3 where small errors in set up could produce large errors in comparison. In addition for higher energy beams such as 16MV, other problems are expected to arise near inhomogeneity due to lack of electronic equilibrium. The results show that total deviation (multifield) can be within tolerance, whilst the error for single beams may be out of the tolerance. Depending on the situation of each particular beam, one beam may contribute more significant errors than other beams.

5-3-2-Interdepartmental Audit

Table 5-V compares the audit pressure statements. The audit system values were calibrated (to within ±0.1%) against Edinburgh University Meteorology Department's system. The consistency of the audit barometer was checked before and after audit visits by comparison with Edinburgh's mercury-in-glass system. According to Table 5-V all local pressures in this audit were within the predetermined tolerance value (0.3%).

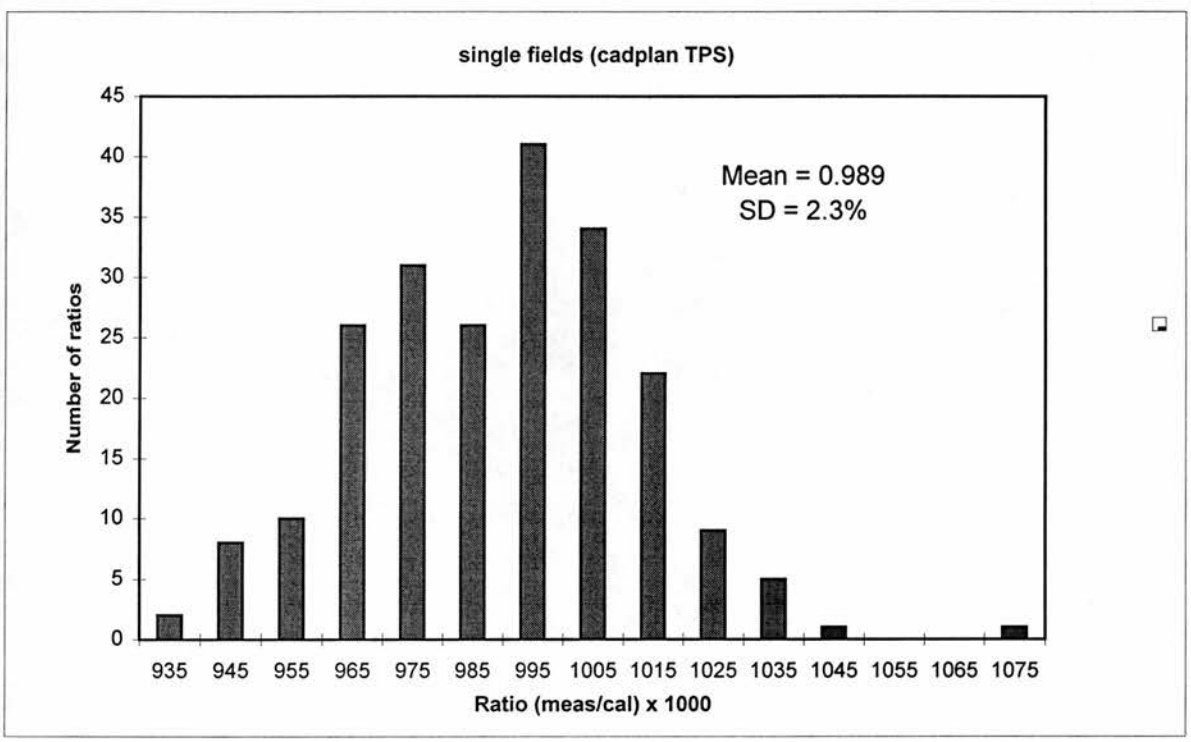

Fig. 5-11: Measured to calculated dose ratios for all sites and points (inside the target volume) in one department

Table 5-V: Percentage deviation between the audit and local pressure statements

centre	*1*	*2*	*4*	*6*	*7*	*9*
comparison (agreement to within)	0.2%	0.1%	0.2%	0.2%	0.1%	0.2%

Table 5-VI compares the ratios of measured to calculated dose values for beam calibration reference conditions; 10x10 field, 100FSD, 5cm deep in phantom and 200 monitor unit. These were straight comparisons as the equipment was found, uncorrected for the centre's daily output correction. These figures were used to normalise the multi-field phantom results.

Table5-VI: The ratios of measured to calculated values at the reference conditions

centre	*1*	*2*	*2*	*4*	*6*	*6*	*9*	*9*
Energy (MV)	6	6	10	6	6	6	6	15
Ratio	0.997	1.007	1.033	0.986	0.983	0.993	0.987	0.993

Most ratios in Table 5-VI are within tolerance values of dosimetry intercomparison in the UK (3%). The mean ratio of measured to calculated dose values obtained is 0.997 with a standard deviation of 1.6%. The results of the simple tests of geometric parameters which may affect calibration are shown in Table 5-VII. These tests were carried out in parallel with the set up of the geometric and semianatomic phantom. These parameters are also all within the predetermined tolerances.

Table 5-VII: The results of the simple tests of geometric parameters

centre	*1*	*2*	*4*	*6*	*9*	*tolerance*
ODIvs laser (100fsd)	<1.5	<2	<1.5	<1.5	<1	2mm
comparison of fsd	<2	<4	<2	<2	<2	5mm
meas.light field size	<2	<2	<2	<2	<2	3mm

Treatment planning tests were carried out on the breast and thorax sites for the first round of audit. The centres had the freedom to choose field sizes and direction of beams, beam wedge, etc.

Figures 5-12 and 5-13 show the ratio of measured to calculated dose values for breast volume and target volume of the thorax. The mean ratios obtained of measured to calculated dose values for breast and target volumes of thorax were 0.997 and 0.982 respectively with standard deviations 3.6% and 1.6%. Larger deviations were observed when the measured points lay outside the target volume of the thorax, including inside the spinal cord. When all the points of the thorax were considered i.e. both, inside and outside the target volume, the mean ratios of measured to calculated dose values obtained was 0.984 with a standard deviation of 3.6% (Fig. 5-14), and for all points of breast and thorax taken together 0.988 with a standard deviation of 3.6%. Table 5-VIII shows the mean, minimum and maximum ratios of measured to calculated dose values with standard deviations of thorax and breast for each centre. All the mean results for both breast and thorax are within the audit tolerances of 5% except some individual points show greater discrepancies. These are discussed in detail in section (5-4-2). Some sd are significantly larger than the typical values. These are due to either out-of-target-volume points or no correction being made for lung (see section 5-4-2).

Table 5-VIII: The mean, minimum and maximum ratios of measured to calculated dose values and SD of thorax and breast for each centre

	Thorax				**Breast**			
centre	**Mean**	**SD%**	**Min.**	**Max.**	**Mean**	**SD%**	**Min.**	**Max.**
1	0.982	2.1	0.945	1.00	1.014	6.2	0.963	1.098
2	0.972	3.0	0.911	1.00	1.002	1.8	0.976	1.017
4	1.00	2.6	0.963	1.051	1.006	4.5	0.967	1.059
6	0.972	2.4	0.915	0.991	1.015	5.0	0.966	1.074
7	0.985	1.2	0.963	1.006	0.963	0.8	0.952	0.971
9	0.992	7.7	0.898	1.111	0.970	0.8	0.960	0.978

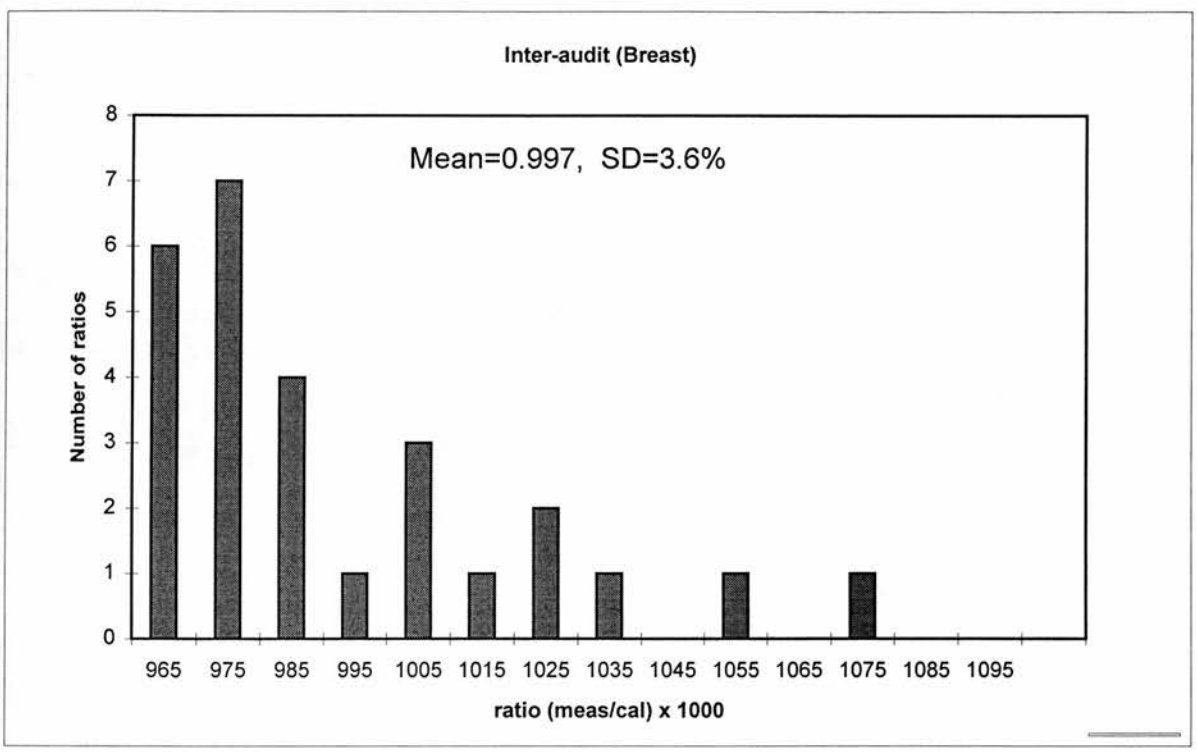

Fig. 5-12: Measured to calculated dose ratios for Breast in interdepartmental audit

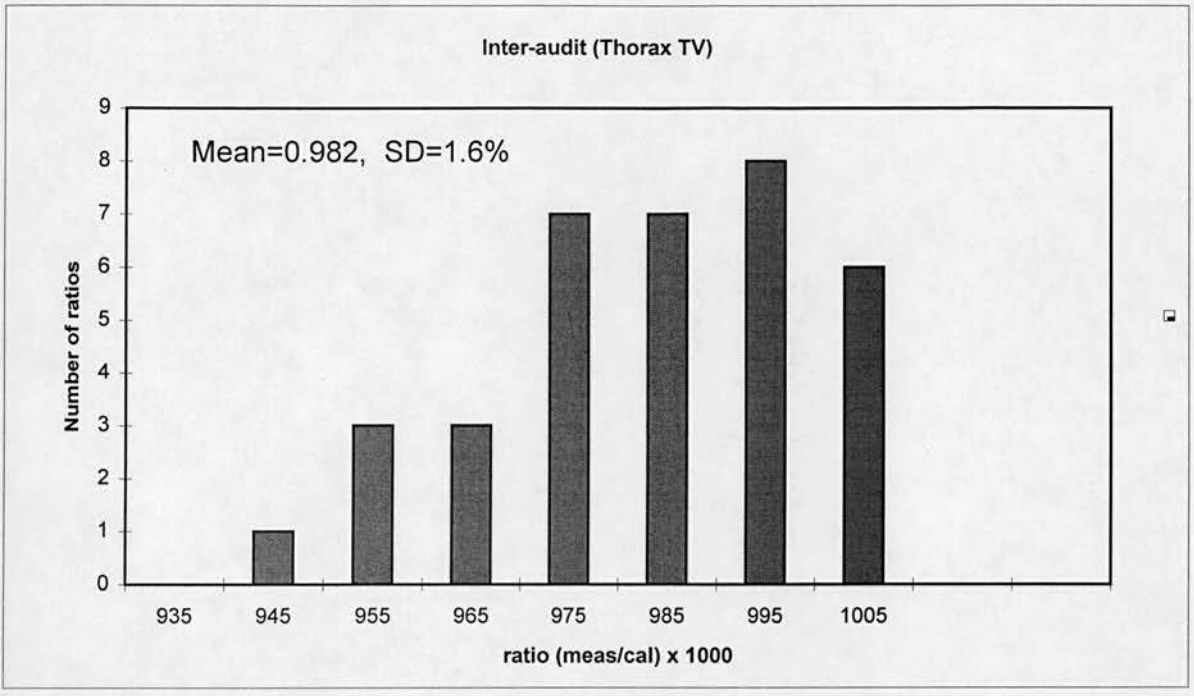

Fig.5-13: Measured to calculated dose ratios for Thorax (TV) interdepartmental audit

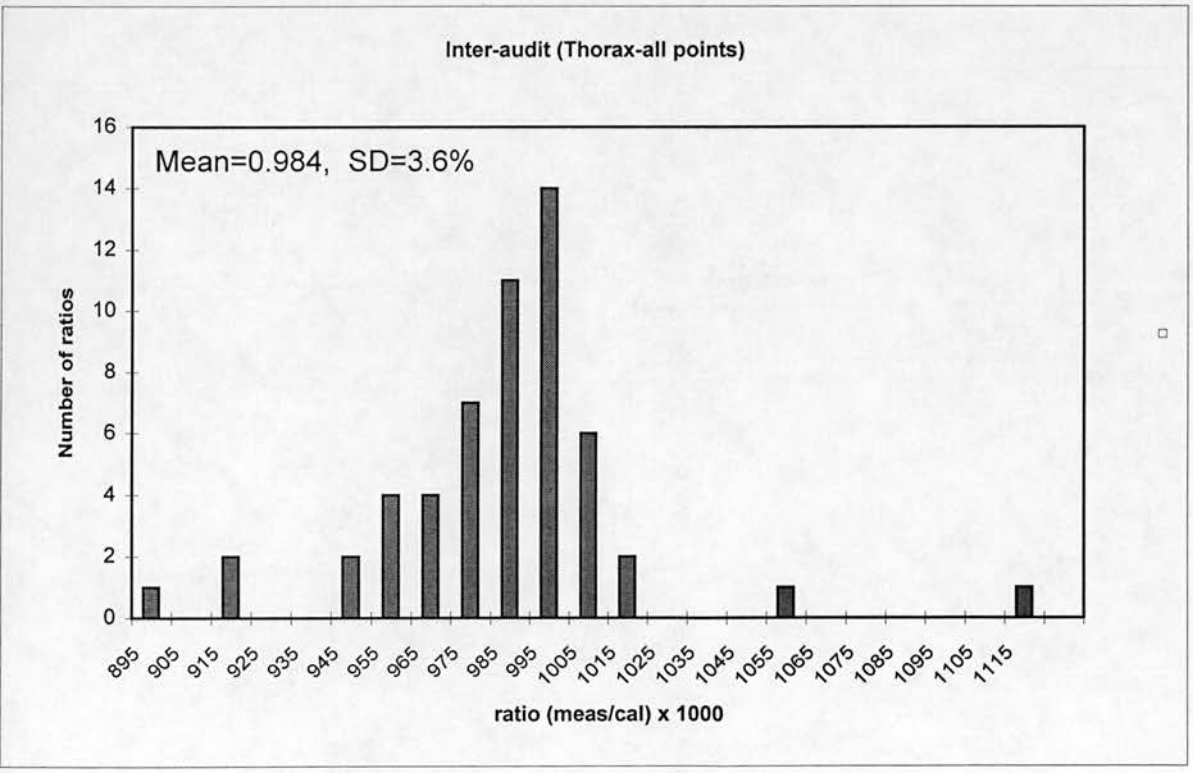

Fig. 5-14: Measured to calculated dose ratios for Thorax (all points) interdepartmental audit

Table 5-IX shows mean, standard deviation and spread for different levels of radiotherapy dosimetry from basic dosimetry up to and including the treatment planning level from the results of the geometric and the semianatomic phantom for

Table 5-IX: Mean, SD, and spread of results at different levels of radiotherapy dosimetry from basic dosimetry to patient dose delivery for a single centre and for the Scottish+ group centres

	Mean	**SD%**	**Spread**
Reference point			
one department	**0.998**	**0.8**	**0.02**
Inter department	**0.998**	**1.3**	**0.05**
other single f. points			
one department	**0.999**	**1.0**	**0.07**
Inter department			
3 F. geometric phantom			
a)Homogeneous			
one department	**0.995**	**1.3**	**0.05**
Inter department	**1.001**	**1.7**	**0.06**
b)Inhomogeneous			
one department	**0.992**	**1.6**	**0.06**
Inter department	**0.999**	**2.4**	**0.07**
Semianatomic phantom			
one department			
a)conventional TPS			
-TV	**0.991**	**1.3**	**0.03**
-total points	**0.996**	**2.0**	**0.09**
b)Cadplan TPS			
-TV	**0.989**	**1.3**	**0.06**
-total points	**0.990**	**1.4**	**0.07**
Intra department			
thorax (TV)	**0.989**	**1.0**	**0.04**
thorax(total points)	**0.989**	**1.2**	**0.05**
breast	**0.977**	**1.8**	**0.06**
Inter department			
thorax(TV)	**0.982**	**1.6**	**0.06**
thorax(total points)	**0.984**	**3.6**	**0.21**
breast	**0.997**	**3.6**	**0.15**

the single centre and for the Scottish+ group centres. Overall it shows good achievable accuracy in a single department up to the level of patient dose delivery in relation to the required accuracy. Also the consistency between centres is good, in particular most of the results of the different centres show agreement within the predetermined audit tolerances.

5-4-Discussion

The results from the geometric phantom tests (previous chapter) showed the achievable accuracy for different steps of radiotherapy in a single department, and the achievable consistency between centres. To develop the audit system for testing more complex situations in treatment planning, closer to the level of treatment dose delivery to the patient, a semianatomic phantom has been developed, which simulates various practical clinical treatment situations (Fig. 5-1). The different sites of the phantom were measured in a single department and also between centres (Figs. 5-2 to 5-8).

5-4-1-Intra Departmental

The images of the phantom from CT and simulator CT were transferred to two treatment planning systems. The initial tests using CT (Table 5-I) showed the precise density of the phantom structure and inhomogeneities. The geometrical deviations transferred by CT were less than those from the simulator, therefore the Cadplan system (based on CT) can give more precise values from this point of view (Table 5-I). Also the initial testing of the phantom gave confidence in the phantom itself and in the methodology (Table 5-II).

Table 5-III shows the mean ratios of measured to calculated dose values with standard deviations from different simulated sites of the semianatomic phantom for

both treatment planning systems. With consideration of points inside the target volume, the total mean ratios of measured to calculated dose values obtained were 0.989 and 0.991 with standard deviations of 1.3% for Cadplan and standard in-house systems (Figs. 5-9 and 5-10). This shows that the measured values are in good agreement with the expected values except for several individual points (Table 5-IV) and also that the distribution is achieved with a good precision. The two treatment planning systems show essentially the same results, but when points outside the target volume were considered, the total mean ratios of measured to calculated dose values obtained were 0.990 and 0.996 with standard deviations of 1.4% and 2.0% for Cadplan and standard systems respectively. The points outside of the target volume for the thorax irradiations are at inhomogeneity interfaces, edges of beams and one point inside the spinal cord. Of course in the edge of beam small errors in the experimental set up can produce large errors between measured and calculated values.

Breast

All the ratios of measured to calculated dose values show good agreement with expected values except for points 1 and 2. The main reason for deviations is that these points receive lower doses than expected values, due to lower scatter from the lung than predicted by the inhomogeneity algorithms and also reduced scatter from the air outside the breast area.

Thorax

Two situations were considered as thorax irradiations: 1-a typical clinical situation, 2-a three field brick. In situation 1 points 2,3 and 8 are outside the target volume (Fig. 5-3) and these show the major discrepancies. Point 2 lies under the bone inhomogeneity for beam 1. Point 3 is near the interface with the lung inhomogeneity. Also this point lies in the beam edge of fields 1 and 2, and small geometrical changes due to set up or input to the TPS can change the value from that calculated. Point 8 lies within the spinal cord and this point lies in low dose areas particularly for fields 1 and 3. The analysis of single fields, for other points of the thorax which are within

the target volume, shows good agreement between measured and calculated values, except for points 4, 5 and 7. Points 4 and 5 show the major deviations from field 2. These points lie under the lung inhomogeneity, while beam 2 passes through the lung. Moreover, the Batho algorithm was used in both TPS for inhomogeneity correction, which may be not adequate for this situation. Point 7 lies near the interface of the lung inhomogeneity. It shows large deviations for field 1, because this point lies on the fan line of field 1 which passes through the narrow gap between the bone inhomogeneity and the edge of the large lung.

In the 3 field brick situation for the thorax, points 2,6 and 8 are outside the target volume (Fig. 5-4), which show the major deviations. Points 2 and 8 show similarly large deviations as seen and discussed for situation 1 of the thorax. Point 6 lies in the edge of beam 1, and small geometrical changes due to set up or input to the TPS, can change the value from that calculated. This point also lies near the interface of the lung inhomogeneity. Analysis of single fields showed that the other points in the target volume of the thorax irradiation are in agreement with expected values except for points 5 and 7. Point 5 lies on the fanline of field 1 which passes through the narrow gap between the bone inhomogeneity and the edge of the large lung. Point 7 lies under the lung inhomogeneity interface for beam 2 also.

Head

All the results of multifield and single field comparisons for head and neck show good agreement between measured and calculated dose values for 4MV and 6MV photon beams.

Right angle wedged pair

All the measured to calculated values show good agreement for both multifields and single fields.

Parotid

A parotid type set up was considered for two situations in the semianatomic phantom, with the second one having the isocentre shifted more laterally to involve the discontinuous phantom corner. Three and four measurement points were used respectively. For both situations all the measured values showed good agreement with expected values.

Testing the phantom and methodology, and estimation of* achievable *accuracy in one department

The results from different sites of the semianatomic phantom showed there is no significant overall systematic difference between measured and calculated values for both the Edinburgh in house TPS and the Cadplan system. The standard deviations on the overall distributions are 1.3% for both systems (Fig. 5-9 and 5-10). For individual sites and energies according to Table 5-III, the mean ratios are from 0.964 to 1.013 with standard deviations from 0.3% to 2.0% . The analysis of multifields and particularly single fields for each site of the phantom (Fig. 5-11) showed overall confidence in the phantom and methodology and in the department's dosimetry. The major discrepancies were observed for some points of the thorax, particularly when the measured points outside the target volume were compared with expected values. The main reason for this is in the way that planning systems cope with some treatment situations, in particular around inhomogeneities, interfaces, due to lack of scatter, edge of beam, etc. Other reasons for discrepancies can be due to uncertainties and variations in machine performance and in treatment planning data. It could possibly be due to the phantom material. However, it has been show that there is no systematic discrepancies due to the phantom; based on experimental testing it is expected that the results will agree with water phantoms to within a few tenths of a percent for MV photon beams (Thwaites and Allahverdi 1995$_c$;

Allahverdi, Thwaites and Nisbet 1996$_c$). Corrections have been applied to the measurements to take this into account.

In general it can be concluded that there is no significant overall systematic differences between measured and calculated values, for all sites and energies. The results point by point from multifields and field by field shows a good achievable accuracy in this single department (Figs 5-9 to 5-11), with an overall standard deviation of 1.3% on the delivery of planned realistic treatments to a phantom.

Table 5-IX shows the results from beam calibration up to and including the treatment planning level. It shows good agreement between measured and calculated values for the different steps of radiotherapy dosimetry up to patient dose delivery. These results coupled with other results from in vivo dosimetry in patients can show the overall achievable accuracy in one department. For example Blyth et al (1997) measured entrance and exit doses with diodes on patients treated for head and neck malignancies in this same department. The measured doses were compared to expected doses. The standard deviation on the results of both entrance and exit dose measurements obtained were 3.0% and 3.5% respectively. These results coupled with the results from geometric and semianatomic phantom intercomparisons (Table 5-IX) show that 3.5% (1SD) at the isocentre and 5% (standard deviation) at other points is a reasonable value which can be achieved in agreement with the clinical requirements on accuracy. For example combining reference point sd (0.8%) with target volume sd (1-1.6%) and with in-vivo measurement sd (3.25%) gives total uncertainties (1sd) of 3.5%-3.7%. It is expected that the field by field sd on the in-vivo measurements is an overestimate of patient target volume sd (Blyth et al 1997, Millwater et al 1998) and so these overall figure may be realistically reduced to around 2.8-3.1% in optimal conditions for accurate single centre target volume dose s.d.

5-4-2-Interdepartmental Audit

The results of interdepartmental audit by geometric phantom (previous chapter) showed that the results at different levels of beam calibration and some basic radiotherapy planning processes are generally in agreement within the predetermined tolerances. The main problems observed were due to inhomogeneities and beam modifiers, especially wedged beams. The semianatomic phantom was designed to audit more complex situations as close as possible to the level of treatment delivery to the patient. The phantom simulates some clinical sites like thorax, breast, head and neck, parotid, etc. For evaluation of the final steps of radiotherapy dosimetry, anatomical phantoms and in vivo dosimetry on the patient can be used (Johansson et al 1987, Wittkamper et al 1987, Van Bree et al 1992). At this first round of audit visits using the semianatomic phantom, thorax and breast sites were evaluated.

The basic parameters checked in the audit almost all lay within the tolerance values. The mean ratio of measured to calculated reference dose values obtained was 0.998 with standard deviation 1.3%. The first audit visit (Thwaites et al 1992) reported the mean ratio of measured to calculated values as 1.003 with standard deviation 1.5%. The sd from the current measurements is slightly smaller, indicating a possible small improvement in consistency. More significantly, the spread (minimum to maximum) of measured to calculated dose values is smaller than the first visit and smaller than other reported dosimetry intercomparisons at the reference point. Therefore, this indicates an improvement in quality and consistency between centres at the second check of audit. The distribution differences are similar to those found in other dosimetry quality audits reported in the literature (Table 4-IV) and are within the audit tolerances. The differences between single and multi-centre results (sd of 0.8% and 1.3% respectively) indicate the increasing uncertainties centre to centre (effectively a 1% sd distribution of mean values centre to centre).

The simple tests of geometric parameters were carried out in parallel with set up of geometric and semianatomic phantoms. For all measured situations, the FSD was

checked against the plan value. This folds in an element of checking of outline input, of set up and of alignment of lasers and machine geometrical parameters. In all centres these agreed to within audit tolerances (Table 5-VII), giving high confidence in the application of quality control programmes for these parameters.

Breast and thorax were chosen for testing in the first round of audit. The distribution of ratios of measured to calculated values are shown in figures (5-12 and 5-13). The mean ratio of measured to calculated dose values obtained were 0.997 and 0.982 with standard deviations of 3.6% and 1.6% for breast and thorax target volume respectively. All the ratios show agreement between the locally stated or calculated values and the audit measured values within the predetermined audit system tolerances except for a small number of individual points (Table 5-VIII), where deviations of up to ±10% were observed (as discussed below). Figure (5-14) shows the distribution of measured to calculated values for the thorax site with the addition of points both inside and outside the target volume. The mean ratio of measured to calculated dose values obtained was 0.984 with a standard deviation 3.6%. The major discrepancies are observed for points 2,3 and 8 outside the target volume.

The results of point by point and field by field analysis for each centre can indicate the main problems depending on their limitations in treatment planning and procedures. Approximately all centres used the same techniques for plans of thorax and breast as Edinburgh with small differences in beam directions and field sizes. In the results for all centres a correction was applied to account for differences between audit measured dose in calibration conditions and locally stated dose in these conditions to separate this out from basic planning uncertainties. In general all the parameters tested in all centres show agreement between the locally stated or calculated values and the audit measured values within the audit system's pre-set tolerances and are therefore satisfactory within the terms of the audit.

Centre 1

In the breast irradiation, point 4 is outside tolerance both before (at +11.7%) and after (at +9.8%) correction for the audit measured beam output. This point lies below a significant thickness of lung when viewed along a field (medial) fan line passing through the point. As the standard procedures for breast planning in this centre do not include lung corrections and as this plan followed these procedures, then it would be expected that this point will receive a higher dose than calculated. Point 3 will show a similar qualitative effect from field 2 (lateral), but to a lesser degree, given the field angles and lung position. Points 1 and 2 will tend to receive lower doses than expected due to lower scatter from the lung than predicted in a lung-free calculation.

For the thorax irradiation, point 8 (cord) is outside audit tolerance (at -5.5%) when the measurements are corrected for audit measured beam output. However, point 8 lies close to the beam edge of field 1 (and to a lesser extent field 2), so small geometric discrepancies (in TPS input, set up or treatment machine) could lead to changes. In addition it lies within a bone inhomogeneity, which is not taken into account in the standard planning approach for this irradiation in this centre.

Centre 2

One point (point 3) in the thorax three-field irradiation lay outside the tolerance of 5%, at 6.8% low on the basis of the raw dose measurement and 8.9% low when this was corrected for the audit measured beam calibration. Looking at the individual field measurements for this point, it is field 1 which contributes a low dose to this point, at approximately 30% low in each case; the other fields being within 5% of calculated. Point 3 lies exactly on the beam edge of field 1. Therefore, any small error in input to the TPS, or in set up, or in exact position of the radiation field edge could significantly alter the value from that calculated. A rough estimate of the total displacement, from whatever combination of causes, required to cause this difference results in 2-2.5 mm.

centre 4

After correction of the breast irradiation measurements, to take into account the audit measured beam calibration, point 4 is outside tolerance (at +5.9%). The reason is the same as point 4 in centre 1 for breast.

For the thorax irradiation, point 2, which lies outside the target volume, is just outside audit tolerance (at +5.1%) when the measurements are corrected for audit measured beam output. It lies close to the beam edge of field 3 (posterior oblique), so small geometric discrepancies (in TPS input, set up or treatment machine) could lead to changes. The bulk of the dose to this point is given by field 1 (lateral anterior oblique). The choice of field 1 direction puts this point just under the tip of the anterior bone inhomogeneity, on a field 1 fan line. This may give rise to deviations between calculated and delivered dose, as may for example, differences between expected and actual beam profiles, depth doses, etc.(for this beam and this position).

Point 7 lies just on tolerance, for the raw measured doses. Applying the correction based on the audit measured beam calibration brings this point within tolerance.

centre 6

After correction of the breast irradiation measurements, to take into account the audit measured beam calibration, point 4 is outside tolerance. The reason is the same as point 4 in centres 1 and 4 for breast.

Point 8 (cord) in the thorax irradiation has a lower measured dose than predicted (by approximately 9%). Possible causes include: bone inhomogeneities not accounted for, modelling of penumbra dose from fields 2 and 3, depth dose or beam profiles at this depth from field 1. This point also lies close to the edge of beam 3, any small

errors in input to TPS, in set up or in exact position of the radiation field edge could significantly alter the value from that calculated.

centre 7

This was described in detail in the single department evaluation (previous section).

centre 9

For the thorax irradiation, applying a correction for the audit measured beam calibration, brings point 6 just into audit tolerance (at -5%). The other points remain outside tolerance: 2 (-10.2%), 3 (+11.1%), 7 (-5.7%), and 8 (+10.8%). Point 2 lies close to the edge of beam 2 (the posterior oblique plain field and wedged fields), any small errors in input to the TPS, in set up, or in exact position of the radiation field edge could significantly alter the value from that calculated. Approximately 1.5 to 2 mm total displacement, from whatever combination of causes, would be sufficient to cause the observed difference.

Similarly point 3 lies almost exactly on the edge of field 1 (the anterior plain and wedged fields) and field 3 (anterior oblique). The bulk of the dose to point 8 (cord position) is from field 1. Field 2 is observed to contribute approximately the same as field 3 to this point, at approximately 4% of the dose from field 1. Possible sources of observed difference could be, for example, depth doses or wedge profiles at this depth for field 1, inhomogeneity correction effects to this point, modelling of penumbra for field 2 and field 3.

Points 6 and 7 lie inside the target volume. Point 6 is only marginally outside the 5% tolerance on the raw measurement and is brought just into tolerance by the application of a correction based on the audit measured beam calibration. Point 7 is still marginally outside tolerance after this correction. Given the choice of field directions in the plan, point 7 lies on a fan line of field 1 which passes almost tangentially through the narrow gap between the anterior bone inhomogeneity and the edge of the large lung. This may give rise to problems for the inhomogeneity algorithm. In addition small changes in relative positioning may be expected to give rises to differences between delivered dose and calculation. Both these points will

receive reduced scatter from the adjacent lung, which a 2-D inhomogeneity correction algorithm would not necessarily predict well. These effects would be mirrored in clinical practice.

Overall results: achievable accuracy between departments

The total results from beam calibration to treatment patient dose delivery for a single centre and for Scottish+ group audit centres have been summarised in Table 5-IX. As expected, uncertainties are increased from the initial stages to the further stages and from a single to multiple centres. Standard deviations for multi-centre audit from beam calibration to end point of treatment delivery to a phantom are from 1.3% for reference dose to 2.4% for dose delivery to target volume (and to 3.6% when all points are considered), showing a good view of achievable accuracy up to patient dose delivery. A similar estimate to that made before for a single department (see section 5-4-1 and taking the same in-vivo sd) gives overall figures of 3.8-4.2%. Reducing the in-vivo figures in the same way reduces this to 3.2-3.7% as an estimate in optimal conditions of centre to centre target volume dose sd.

The results from other centres also show generally good agreement within audit tolerances and are therefore satisfactory within the terms of the audit. The main reason for this agreement is that these centres use extensive quality programmes, quality assurance and quality control, in their centres. However, this audit highlighted some problems in treatment planning systems and algorithms. This can aid in the development of the next steps of the audit programme to continue to promote high quality in treatment.

5-5-Conclusions

Despite having quality assurance and quality control programmes in centres, errors and uncertainties occur in different levels of radiotherapy dosimetry from beam

calibration to dose delivery to the patient. Quality audit is a tool to identify systematic errors and provide a basis for quality improvement. The audit network in the UK now has been established with seven geographic groups. The Scottish+ group, based in Edinburgh, has developed a hierarchical approach, testing different levels at each visit. As part of this, a semianatomic phantom has been developed to allow reasonably realistic audit of various representative treatment sites, including breast, thorax, head and neck, parotid, etc. It is made from epoxy-resin tissue substitute materials, contains lung and bone and is drilled to take ionisation chamber inserts.

The initial testing gives general overall confidence in the phantom and methodology. There are no systematic discrepancies due to the phantom. The mean ratios of measured to calculated doses, using the Edinburgh in house TPS and Cadplan, in the target volumes for all sites and energies was obtained at 0.990 with a standard deviation of 1.3%. For individual sites and energies, the mean ratios are from 0.973-1.013 with standard deviations of 0.3%-2.0%. When points outside the target volume of the thorax were considered, uncertainties were increased. The analysis point by point, field by field and analysis of single fields showed that major discrepancies can be linked to problems in the way that planning systems cope with some treatment situations, in particular around inhomogeneities, interfaces, edge of beams, etc. Others can be linked to small discrepancies in the department's dosimetry or processes, for example in planning data, machine performance, etc. The results, coupled with other results, from geometric phantom audit (previous chapter) show a good view of achievable accuracy up to patient dose delivery within a single department, with achievable sd on target volume dose being less than 3% in optimum conditions.

The mean ratio of measured to calculated dose values from two rounds of interdepartmental audit in the target volumes were obtained as 0.982 (breast) and 0.997 (thorax) with standard deviations of 1.6% and 3.6% respectively. This shows that there is general agreement of doses within the specified audit tolerances, and

generally satisfactory performance within the terms of the audit. However, analyses of the results point by point and field by field can illustrate problems. The results and overview of this audit show that it is necessary for all centres to participate regularly in audit to obtain confidence and high quality in treatment. The results also show that an achievable sd on target volume dose can be less than 3.5% centre to centre in optimum conditions.

Chapter 6

6-Evaluation of Uncertainties in Treatment Planning Inhomogeneity Algorithms

6-1-Introduction

One source contributing uncertainties to the patient dose delivery is the calculation of dose in a patient. Beam modelling in computerised radiotherapy planning refers to the efforts to set up formalisms for the manipulation of dosimetric data for calculating the dose at each point in the patient (ICRU 1987). The calculation algorithms for the homogeneous patient can be categorised in different ways e.g. matrix models (Milan and Bently 1974); analytical beam models (Van de Geijn 1972); models based on the separation of primary and scattered radiation (Cunningham and Beaudion 1973) and superposition methods. Superposition methods incorporating Monte Carlo methods, consider and accurately model electron and photon transport, at the expense of very long computation times (Mackie et al 1990).

Significant advances have been made in the development of three dimensional (3D) treatment planning information and display techniques using Computerised Tomography (CT) and 3D calculation algorithms. The development of CT produced a revolution in treatment planning by providing accurate geometric and physical data for tumour and normal tissue localisation. In dose calculation, the CT numbers are related to the electron density of the corresponding tissue at each voxel (Prasad et al 1979, Hobday et al 1979, Battista et al 1980), giving precise input data for use in inhomogeneity correction algorithms.

The dose calculation has no exact mathematical solution, all calculation methods are based on approximate models. For this reason, computer methods are used for obtaining better approximations in acceptable time. Some of these methods are better for some applications than others. The validity of treatment planning

calculations can be judged by careful experimental testing. Computer methods reduce uncertainties in comparison to manual methods. However, computers introduce a risk of new errors e.g. corruption of beam data and patient data, algorithms and errors due to hardware components. Of course quality assurance and quality control programmes reduce the uncertainties in computer planning (Westerman et al 1984, Wittkamper et al 1988, Van Dyk et al 1993, IPEM 1994, AAPM 1994).

In practice, a patient is different from the homogeneous situation both in shape and composition. The problem of the shape is essentially the same as an inhomogeneity. An air gap due to the surface shape can be considered to be an inhomogeneity. Some authors have reviewed inhomogeneity calculation algorithms (Purdy and Prasad 1983, Wong et al 1991, Purdy 1992, Redpath et al 1993, Aspradakis 1996). One significant source of uncertainties in planning is related to the inhomogeneity algorithms, as the calculation algorithms for a heterogeneous medium are only approximate. The question arises; which one of these algorithms is the best or in which situations to particular algorithms perform acceptably well. Many algorithms in radiation treatment planning systems are still based on empirical methods (1D and 2D) developed up to 30 years ago. 1D methods can frequently lead to errors of 10-15% and 2D algorithms, e.g. the Batho method can lead to errors of 5-10% (Wong et al 1991). To reach the recommended accuracy of at least ±5% in the delivery of absorbed dose to a target volume in a patient, the dose calculation must be better than ±5%.

The purpose of this chapter is review some commercial inhomogeneity calculation algorithms and test against measurement in two relatively simple, but clinically relevant situations to obtain an indication of the magnitude of uncertainties associated with these situations.

6-2-Dose Calculation Models

Dose calculation models are based on measured data in water (i.e. central axis depth doses, tissue air ratios, beam profiles at selected depth, etc.), and a correction for inhomogeneities is applied. The most applicable method is based on the assumption of the separation of primary component and scattered radiation (Cunningham and Beaudion 1973). The primary and scatter components are calculated separately, and the total dose at any point is obtained by summing these. This method is better for lower energy photons, where the range of secondary electrons is smaller and where electronic equilibrium exists. However, for higher energy photon beams, the range of secondary electrons is larger particularly in the vicinity of low density inhomogeneities (e.g. lung and air cavities) and for where there is no electronic equilibrium. At present the conventional methods do not take account of disequilibrium situations within inhomogeneities and at sites close to interfaces and this can lead to significant dose calculation errors. Some authors have discussed and used Monte Carlo codes and convolution techniques in the region of electronic disequilibrium (Mackie et al 1984, Boyer and Mok 1985, Kijewski et al 1986, Woo et al 1990, Ahnesjo 1991, Bortfeld et al 1993, Haider and El-Khatib 1994). Tawfiq and El-Khatib (1994) used parameters from experimental measurements without the use of the Monte Carlo code systems.

The following sections briefly review conventional algorithms before the experimental tests are discussed.

6-2-1-One Dimensional Methods Based on Water Equivalent Depth

These methods take into account path length and field size but do not take account of the position and shape of the inhomogeneity. All these methods first calculate dose under the assumption that there is complete water equivalence, and then determine a correction factor C by:

$$C = \frac{\text{Dose in heterogeneous phantom}}{\text{Dose at the same point in homogeneous water phantom}}$$

1-Ratio of Tissue Air Ratios (RTAR)

In this method a correction factor can be obtained by using the ratio of two tissue air ratios:

$$C = [TAR (d_{eff}, r)]/[TAR (d, r)] \quad (6\text{-}1)$$

Where d is true depth, d_{eff} is the effective depth or the water equivalent depth, and r is effective beam radius for the beam used.

2-Equivalent Path Length (EPL)

This simple method calculates correction factors by using water equivalent depth (radiological depth). This depth is scaled by the effective density relative to water of the medium along the primary ray. The method uses percentage depth doses and the correction factor can be obtained by:

$$C = P [(d_{eff}, W, F) / (d, W, F)] . [(F+d_{eff}) / (F+d)]^2 \quad (6\text{-}2)$$

Where d is true depth, W is field size and F is FSD.

3-The Attenuation coefficient Method

In this method the correction factor can be obtained by:

$$C = Exp. [-\mu (d - d_{eff})] \quad (6\text{-}3)$$

Where d is true depth, d_{eff} is the water equivalent depth and μ is the effective linear attenuation coefficient for the photon energy and field size used.

6-2-2-Two Dimensional Methods:

6-2-2-1-Original Power Law (Batho) Method

This method was suggested by Batho (1964), where one correction factor was proposed for a point lying below an inhomogeneity, but within tissue like material as follows:

$$C = \{[TAR\ (d_1, r)] / [TAR\ (d_2, r)]\}^{1-\rho} \qquad (6\text{-}4)$$

where d_1 is equal to the depth of the calculation point below the lower interface of the inhomogeneity, d_2 is the depth of the point below the top interface of the inhomogeneity, and ρ is the electron density of the inhomogeneity. A more general form of the correction factor was developed by Sontag and Cunningham (1977) as follow:

$$C = \{[TAR\ (d_1, r)]^{(\rho 1 - \rho 2)} / [TAR\ (d_2, r)^{(1-\rho 2)}]\}.\ [(\mu_{en} / \rho)^{\rho 1}] / [(\mu_{en} / \rho)^{\rho 2})] \qquad (6\text{-}5)$$

Where d_1 and d_2 are the same as in (6-4) and ρ_1, ρ_2 are electronic densities relative to water of the inhomogeneity and the surrounding material (Fig. 6-1). The second ratio in this equation is a ratio of mass absorption coefficients accounting for differences in effective atomic numbers.

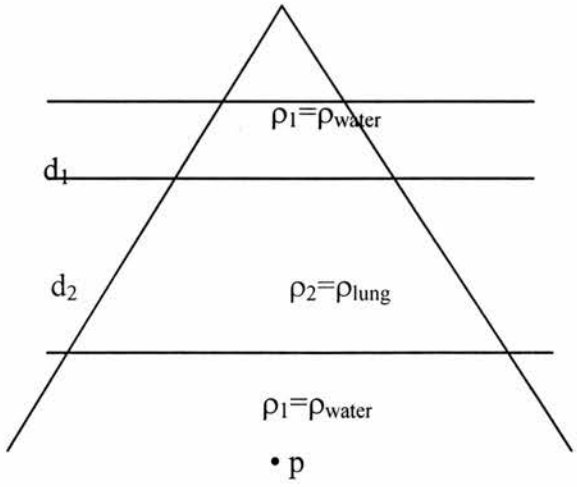

Fig. 6-1: The irradiation geometry in the power law method

This method takes account of the position of a calculation point relative to an inhomogeneity. It does not take account of the lateral dimension or shape of an inhomogeneity, or backscattered radiation originating from the material below the point of calculation. The scattered radiation is considered indirectly, as it depends on the lateral extent of the material above the point of dose calculation. When the lateral extent of the inhomogeneity is less than the beam width, the power law gives significant errors. Therefore, this method is more accurate for small field sizes.

The power law method assumes only Compton interactions. In higher energy photon beams where there is a significant amount of pair production, significant errors can occur with this method (Sontag and Cunningham, 1977). However, the pair production effect is not very significant in the normal range of megavoltage photon beams used in clinical situations. It can be concluded that the Batho method is good for lower energy megavoltage photon beams and smaller field sizes. Despite having significant errors with this method, the Batho method is still used in routine treatment planning due to its simplicity, speed, and less demanding memory and computation requirements. A number of experimental works (Young and Gaylord 1970, Sontag and Cunningham 1977, Webb and Fox 1980, Cassell et al 1981, Lulu and Bjarngard 1982, Wong and Henkelman 1982, El-Khatib and Battista 1984, Webb and Casell 1985, Thomas 1991) have improved the method and shown that Batho is more accurate than 1D simple methods.

6-2-2-2-Modified Batho Method

El-Khatib and Battista (1984) showed good agreement between the Batho method and that obtained by experimental values when TAR_s were replaced by TMR'_s. However, their results for 6MV photon beams showed an underestimation for the power law correction in lung. Thomas (1991) considered the calculation of dose near interfaces for energies greater than ^{60}Co where the interface distance is less than the build up distance corresponding to the beam energy. He replaced TMR (d,r) with TMR ($d+d_b$, r), where d is depth and d_b is build up depth for the particular energy,

and r is field size. This modification of the Batho method gave better agreement with measured data and improved significantly its performance for high energy photon beams.

6-2-3-Three Dimensional Methods (3D)

Several methods in this category have been developed using 3D CT density information.

6-2-3-1-The Equivalent Tissue Air Ratio (ETAR) Method

Sontag and Cunningham (1978) developed the equivalent tissue air ratio method. This method takes account of size, shape, density, and position of structures in the body by using the information from a series of CT scans. The shortcoming of all 1D and 2D (methods) are due to the fact that they do not take account of the lateral scatter in dose calculation. The ETAR method takes account of both effective depth and effective field size. A modification factor can be expressed by:

$$C = [TAR (d', r')] / [TAR (d, r)] \qquad (6\text{-}6)$$

where d is depth and r is radius, d′ and r′ are the scaled values for these two quantities. This scaling was proposed by O'Connor (1957) who stated:

"A beam irradiating a homogeneous but non-water equivalent phantom is equivalent to a beam irradiating a water phantom with all linear dimensions such as depth and field size scaled in proportion to the density (electron density) of the non water equivalent material."

This theorem states that:

$$TAR[d, r]_{\rho} = TAR [\rho \times d, \rho \times r]_{\text{unit density}} \qquad (6\text{-}7)$$

For example the TAR for a 10x10 field at depth 10 cm in a medium of density ρ = 0.4 would correspond to the TAR in a unit density medium for depth of 4 cm and

field size 4x4 cm (Leavit 1982). This scaling can be expanded to separate zero area TAR and SAR terms.

$$TAR[d, 0]_{\rho} = TAR[\rho.d, 0]_{\text{unit density}} \quad (6\text{-}8)$$

$$SAR[d, r]_{\rho} = SAR[\rho.d, \rho.r]_{\text{unit density}} \quad (6\text{-}9)$$

Where the primary term (zero area TAR) is calculated for the effective depth to the point

$$d' = [d \Sigma \rho(j)]/n \qquad (j = 1, 2, ...n) \quad (6\text{-}10)$$

where there are n discrete inhomogeneity elements of equal length such as CT pixels, each with relative electron density $\rho(j)$. The scatter term is determined by scaling the beam radius to $r' = r \times \rho'$, where ρ' is the effective density and is a weighted average relative density over the entire irradiated volume. This can be expressed by:

$$\rho' = \Sigma \Sigma \Sigma W(i, j, k) \cdot \rho(i, j, k) / \Sigma \Sigma \Sigma W(i, j, k) \quad (6\text{-}11)$$

Where $\rho(i, j, k)$ is the density of element (i, j, k) in the 3D matrix of CT numbers, and W(i, j, k) is a weighting factor which expresses the relative importance of each element in contributing to the scatter dose at the point of the calculation. This method reduces the volume integration (3D) to a planar summation (2D calculation). More detail is discussed in Sontag and Cunningham (1978). A number of experimental works (Sontag and Cunningham 1977,1978; Tatcher and Palti 1981, Mackie et al 1984, El-Khatib and Battista 1986, El-Khatib et al 1989) have shown that the ETAR method is more accurate than 1D and 2D methods, and that it is valid over the entire range of energies used for radiotherapy. The method uses CT numbers, thus it does not need to obtain an outline of internal structures of the patient with its associated errors and loss of information.

6-2-3-2-Modified ETAR

Redpath and Thwaites (1992) developed a new scatter method based on the principles of the ETAR method, which takes account of the 3 dimensional shape, position, and composition of the inhomogeneity. Modified ETAR (METAR) defines the amount of scattered radiation that reaches a point of calculation from the other points in the irradiated volume. It models single scatter and multiple scatter separately, using realistic parameters based on the physics of scattering with attenuation by inverse square law and taking account of inhomogeneities at the point of scattering. The method has included three improvements for increasing the speed of calculation. Firstly they considered reducing the 3D calculation to 2D using a plane at an effective distance from the calculation plane. This was not chosen arbitrarily as in ETAR, but was calculated by weighting the distance of all neighbouring slices with the relative amount of scattered radiation originating from them and reaching the calculation plane. Secondly it considers that the scatter reaching any point originates only from a defined region about that point instead of the whole of the irradiated volume. They considered that the scatter radiation is generated from points which were at a distance less than 5cm in the lateral and forward direction from each point calculation. Thirdly the number of scatter points was linked to a maximum of 1000 regardless of size of patient cross section. The improvement in this model in comparison with ETAR is that the relative scattered photon contribution to a point originating from all scattering sites in both a homogeneous and a heterogeneous medium, is estimated, taking into account single and multiple scatter separately, and using fewer approximations and simplifications, e.g. the scatter from different density materials is modelled better. In addition the model takes into account change in primary dose and here scatter due to presence of beam modifying devices or inhomogeneities.

6-2-3-3-Differential Scatter-Air Ratios (DSAR)

The volume integration of differential scatter air ratios (DSAR) method was introduced first by Beaudion (1968) and Cunningham(1972) and further developments have been reported by Larson and Prasad (1978) and Redpath (1995).

This method considers the total amount of scattered radiation from individual volume elements which are determined by differentiating measured SAR's in water. For the heterogeneous medium, DSAR's are adjusted according to the change in primary and scatter fluence, and the change in density at the scatter site. The DSAR implementation used in this work is that due to Redpath (1995), in which the scatter component of dose in a homogeneous unit density medium can be calculated using a scatter integration technique (Clarkson 1941) together with a table of differential scatter air ratios. The total scatter contribution to each point of the medium can be obtained by summing the DSAR contribution from sector integration region. For inhomogeneous medium the scatter component can be calculated by modifying the DSAR's before summing over the beam portal. The modification takes account of changes both in the primary and scatter component due to the presence of non unit-density inhomogeneities in the irradiated volume. TAR's are modified to account for changes in primary due to relative electron density variations along the path between the source and the calculation point. DSAR's are modified to account for the variations in the primary photon fluence along the path between the source and the scattering element.

The delta volume (DV) method is an extended form of DSAR. The scatter contribution is divided into a first and multiple scatter component. This method is more accurate than other commercial methods (Wong and Purdy 1990, Wong and Henkelman 1983), but the computation time is long.

6-2-3-4-Convolution and Monte Carlo Methods

The shortcomings of commercially implemented 3D methods to date are due to the fact that they are based on photon transport models only which assume local energy deposition for dose calculation. Therefore, there can be significant errors particularly for higher energy photon beams in disequilibrium regions such as inhomogeneity interfaces. Point spread array methods (Mackie et al 1985) and differential pencil beam methods (Mohan et al 1986) consider both photon and electron transport for

dose calculation. For these methods, the input dose distributions are calculated from Monte Carlo modelling. These methods model more accurately the electronic disequilibrium situations at inhomogeneity interfaces and cavities. The shortcoming of superposition methods is that they are currently not practical for routine clinical use because of their long calculation time.

6-3 Methods and Materials

Different inhomogeneity calculation algorithms were compared with measured dose values. Doses were measured in two situations by using the geometric phantom and an RMI (water equivalent plastic) slab phantom. The changes in dose are usually local to the vicinity of the inhomogeneity and inside the inhomogeneity. The perturbation of secondary electrons at the interfaces is the main cause of changes and this is more noticeable for the higher energy photon beams. The primary beam inside the inhomogeneity is increased (if lower density), but the scattered radiation is decreased due to a decrease in scattering material. At present, commercial 3D calculation methods provide calculations of the primary photon and scattered photons, but they do not take into account the effects due to the secondary electrons. This can produce significant errors particularly in critical situations. The aim of this section is evaluate dose calculation models used in 2D and commercial 3D methods against measurement, particularly at interfaces and inside an inhomogeneity. Two relatively simple phantom situations are tested, but simulating clinically relevant situations.

Geometric Phantom

The IPSM photon dosimetry intercomparison phantom was used as described in chapter 4. It has a 8cm diameter lung substitute material insert which can be replaced by water equivalent material. Therefore, the phantom was used for two situations, both as a homogeneous and an inhomogeneous phantom. Doses were measured at the five points in the phantom (Fig. 6-2). The dose to be delivered to the central

point of the planned dose distribution was specified to be 2 Gy for a 3-field irradiation.

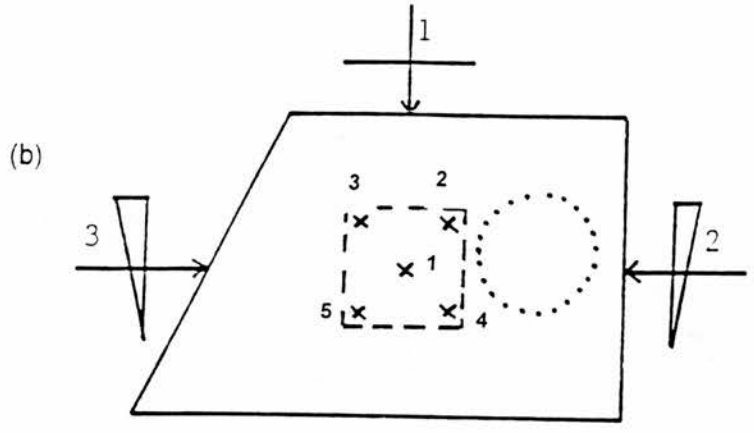

Fig. 6-2: The geometric phantom with 5 measurement points

An inhomogeneity correction factor was defined as the ratio of the dose in a heterogeneous phantom to the dose at the same point in a homogeneous phantom. The different available inhomogeneity calculation algorithms (Batho, ETAR and METAR methods) were compared and quantified against measured values. Different energy photon beams of 4, 6, 9, and 16 MV were used. The Batho method is used in the standard TP system of the department, and ETAR is used in the Cadplan system. The data of the METAR method is available from the in house developed system (Redpath and Thwaites 1992)

Slab interface Phantom

At present, commercially available inhomogeneity algorithms do not take account of the electronic disequilibrium at media boundaries. Therefore, significant errors can occur for these situations. For this purpose a slab phantom was designed according to figure (6-3). The central axis was situated within the cork with density 0.25 with a distance of 1 cm to the water/cork interface. The slab RMI phantom was used as water equivalent unit density material. The dose was measured at points along the central axis. The ratio of the dose in the inhomogeneous phantom to that at the same location in a homogeneous phantom was determined as a correction factor. The correction factors were obtained at two field sizes 5x5 and 10x10 for 6 and 16 MV x-

ray beams. Different inhomogeneity algorithms (Batho, ETAR, METAR, DSAR and modified Batho methods) were quantified against measured values. The DSAR used in this work was the implementations-reported by Redpath (1995) as described in section (6-2-3-3). For both phantoms, doses were measured with a Farmer type 2571 ionisation chamber. The distance between phantom surface and cork is 3cm, and the thickness of cork is 14cm. A thickness of 10cm RMI phantom was used as backscatter material. All measurements were carried out at 100FSD.

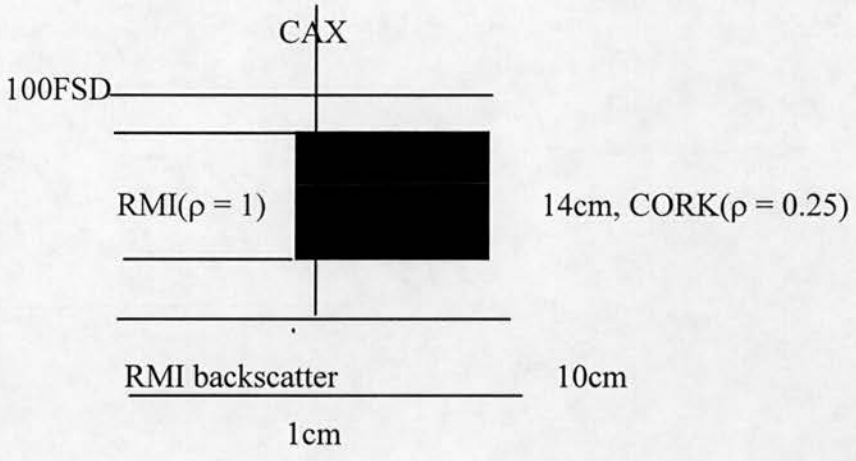

Fig. (6-3): Geometry used to obtain experimental data. Dose measured at different depth on central axis (CAX).

6-4-Results

Geometric Phantom

Inhomogeneity correction factors were measured and calculated for five points in the phantom. The low density lung insert affects both the primary and the scatter component of the radiation beam. The primary beam is increased due to increased transmission through the low density structure. The scatter radiation is decreased due to a decrease in scattering material. Table (6-I) shows comparison between measured correction factors with those obtained from different inhomogeneity calculation algorithms for the three field distributions as a test of a relatively realistic clinical situation, looking at the overall effect on dose from the 3-fields.

Table (6-II) compares the measured correction factors for the single fields with those obtained by the Batho algorithm. The measured differences in field I and III give an indication of the uncertainties on the measurements and point selection for calculation, as only insignificant differences are expected on three fields. field II of course, passing through the inhomogeneity has large correction factor and the differences between measured and calculated are up to 3.0%.

Table (6-I): Correction factors (CF) for different inhomogeneity algorithms (3-field) and measured correction factors

MV	points	Meas. 3field	Batho	Devi. %	ETAR	Devi. %	MET AR	Devi. %
4	1	1.059	1.069	+0.9	1.070	+1.0		
4	2	1.048	1.053	+0.5	1.052	+0.4		
4	3	1.043	1.050	+.07	1.045	+0.2		
4	4	1.017	1.019	+0.2	1.004	-1.2		
4	5	1.027	1.023	-0.4	1.010	-1.7		
6	1	1.054	1.059	+0.1	1.054	0.0	1.064	+0.9
6	2	1.044	1.050	+0.5	1.049	+0.5	1.040	-0.4
6	3	1.040	1.040	+0.6	1.041	+0.1	1.053	+1.3
6	4	1.019	1.019	0.0	1.00	-0.8	0.995	-1.3
6	5	1.019	1.019	+1.1	1.010	-0.8	1.006	-1.2
6L20	1	1.055	1.059	+0.4	1.054	-0.1	1.064	+0.9
6L20	2	1.047	1.050	+0.3	1.049	+0.2	1.040	-0.7
6L20	3	1.045	1.040	-0.5	1.041	-0.4	1.053	+0.8
6L20	4	1.009	1.019	+1.0	1.00	-0.9	0.995	-1.4
6L20	5	1.020	1.019	-0.1	1.010	-1.0	1.006	-1.4
9	1	1.050	1.040	-0.1	1.039	-1.0	1.046	-0.4
9	2	1.034	1.045	+0.7	1.040	+0.6	1.038	+0.4
9	3	1.036	1.045	+0.9	1.034	-0.2	1.035	-0.1
9	4	1.016	1.015	-0.1	1.010	-0.6	0.996	-0.2
9	5	1.023	1.015	-0.8	1.008	-0.8	1.005	-1.8
16	1	1.031	1.040	+0.9	1.040	+0.9	1.044	+1.3
16	2	1.026	1.033	+0.7	1.030	+0.4	1.028	+0.2
16	3	1.031	1.035	+0.4	1.027	-0.4	1.034	+0.3
16	4	1.006	1.010	+0.4	1.010	+0.4	1.001	-0.5
16	5	1.010	1.020	+1.0	1.010	0.0	1.010	0.0

Table (6-II): Comparison between measured correction factors (CF) and calculated values (CF) from Batho algorithm for single fields

	Field I		Field II			Field III	
points	measured	calculated	measured	calculated	devia.%	measured	calculated
4MV							
1	0.991	1.00	1.231	1.257	2.1	1.005	1.00
2	0.998	1.00	1.186	1.210	2.0	0.995	0.997
3	0.995	1.00	1.223	1.256	2.7	1.009	1.002
4	0.997	1.00	1.050	1.052	0.2	0.990	1.009
5	1.005	1.001	1.102	1.086	-1.5	1.00	1.00
6MV							
1	0.998	1.00	1.227	1.227	0	0.996	1.00
2	1.003	1.001	1.169	1.171	0.2	0.995	1.00
3	1.004	1.00	1.211	1.227	1.3	0.995	0.998
4	0.997	0.997	1.031	1.035	0.4	0.990	1.00
5	0.999	1.003	1.065	1.067	0.2	0.999	1.00
9MV							
1	1.010	1.00	1.181	1.193	1.0	1.010	1.00
2	0.980	1.00	1.148	1.137	-1.0	0.995	1.00
3	1.010	1.00	1.167	1.188	1.8	1.004	1.00
4	1.007	1.00	1.044	1.032	-1.1	0.994	1.00
5	1.010	1.001	1.070	1.063	-0.7	0.996	1.001
16MV							
1	0.993	1.00	1.147	1.157	0.9	0.992	1.00
2	0.992	1.00	1.126	1.100	-2.3	0.982	1.00
3	1.00	1.00	1.160	1.156	-0.3	1.004	1.00
4	0.994	1.00	1.032	1.034	0.2	0.990	1.00
5	0.995	1.00	1.055	1.055	0	0.998	1.00

Slab Interface Phantom

The correction factors on the central axis of the beam (Fig. 6-3) are plotted as a function of depth from 1 cm inside the cork to 4 cm below the cork (Fig. 6-4 to 6-7). These figures show that the Batho and modified Batho methods generally underestimate the dose, while the other calculation algorithms generally overestimate the dose within the inhomogeneity up close to the inhomogeneity boundary, except for a 5x5 field size for the 16 MV photon beam. If no correction is made, uncertainties can be introduced from 15% to 35%.

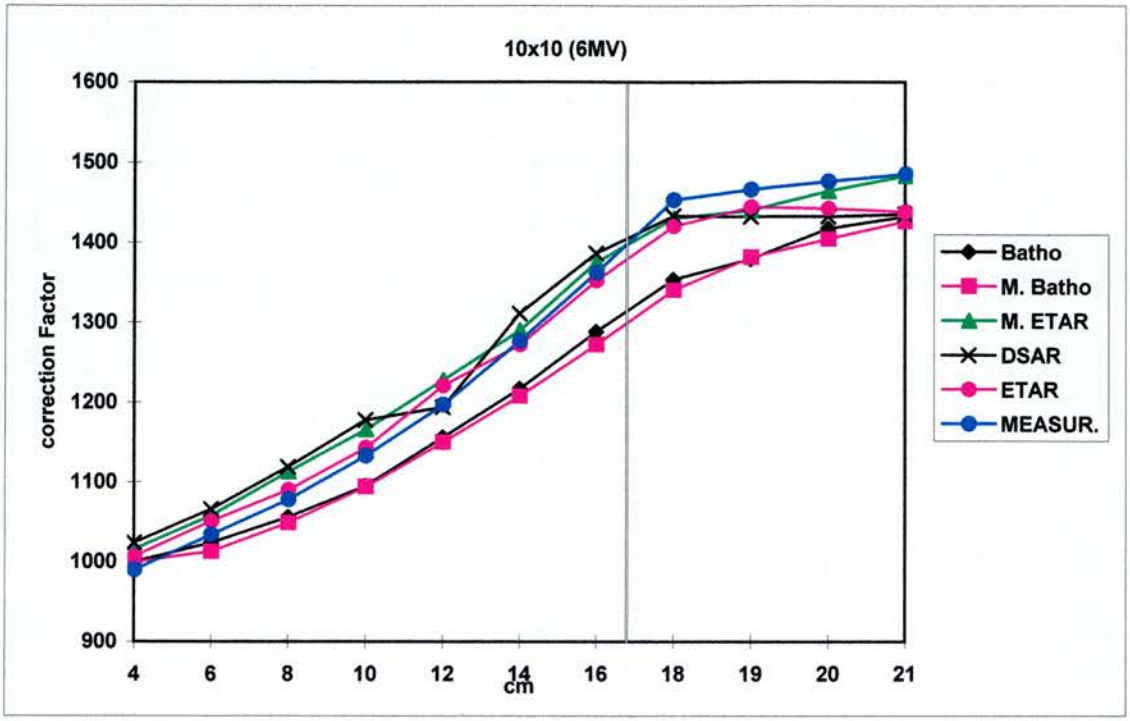

Fig. 6-4: Correction factors for points along the central axis lying both within and below a 14cm cork inhomogeneity

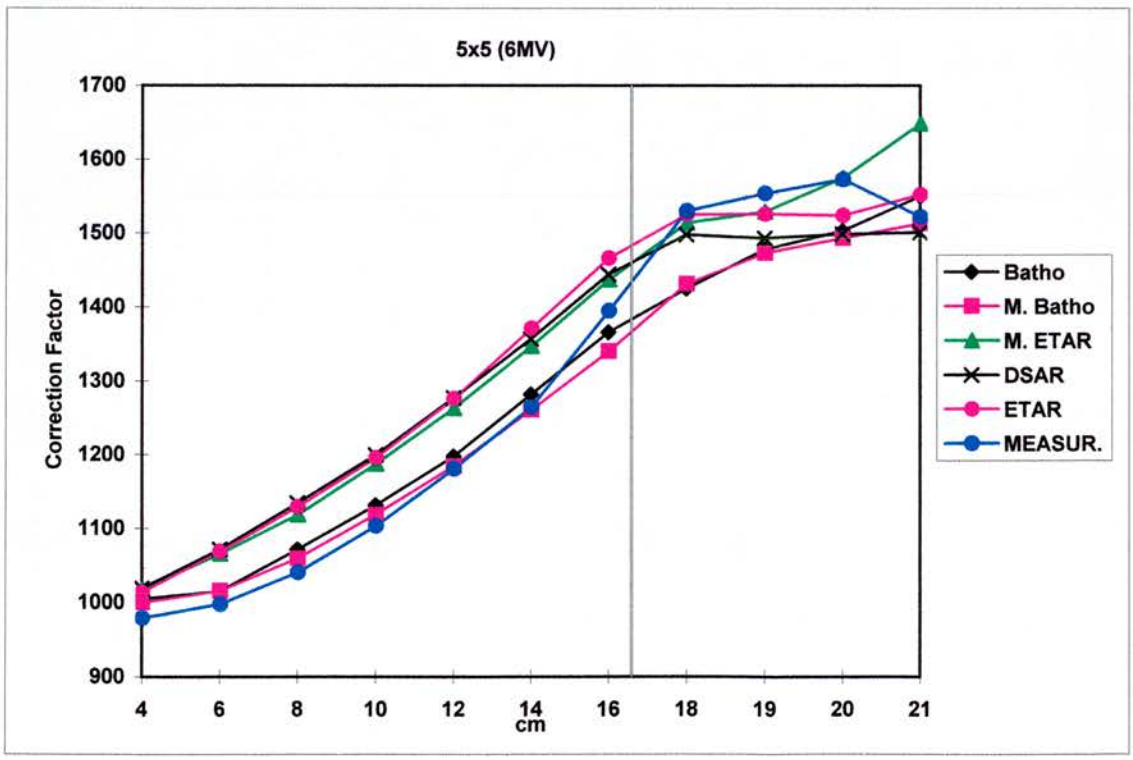

Fig. 6-5: Correction factors for points along the central axis lying both within and below a 14cm cork inhomogeneity

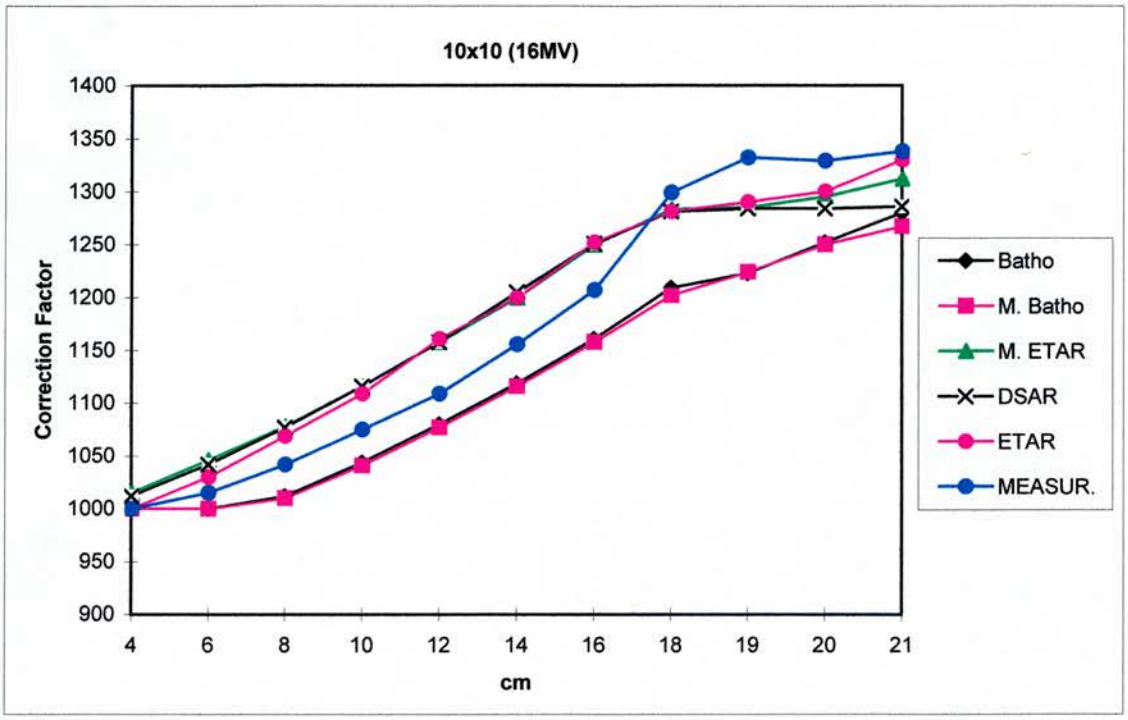

Fig. 6-6: Correction factors for points along the central axis lying both within and below a 14 cm cork inhomogeneity

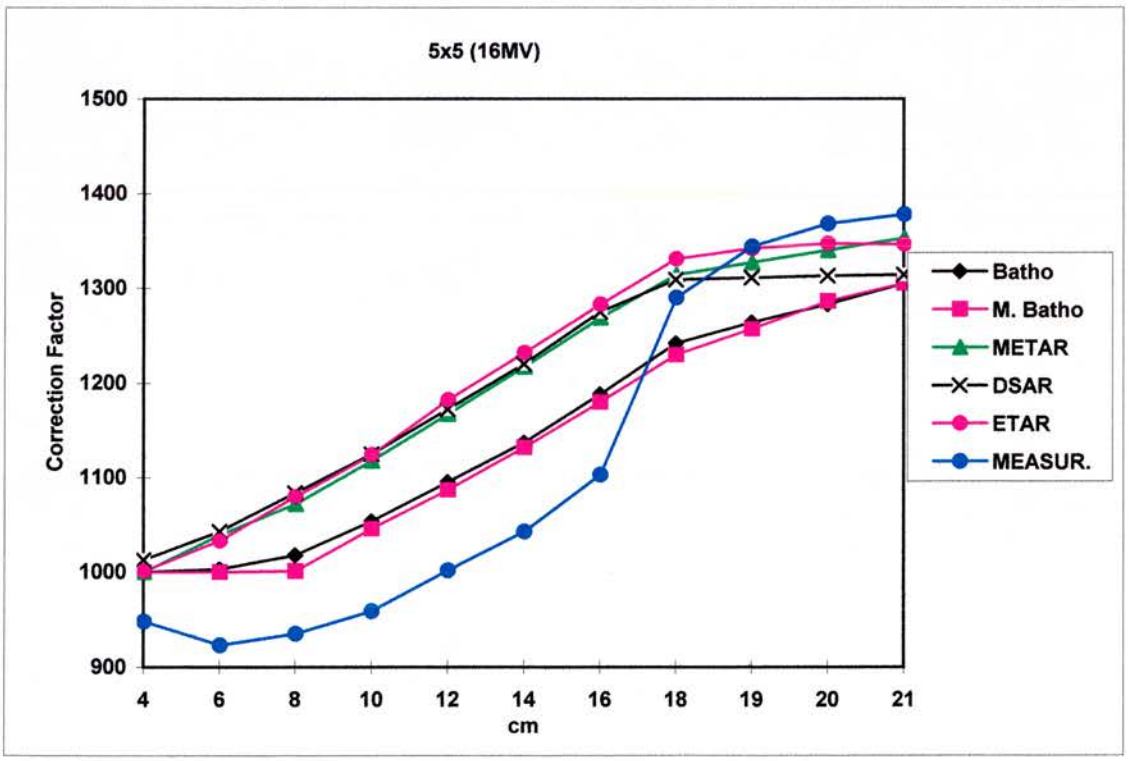

Fig. 6-7: Correction factors for points along the central axis lying both within a below 14cm cork inhomogeneity

6-5-Discussion

One significant source of uncertainty in treatment planning is related to the inhomogeneity algorithms used (see chapters 4 and 5). Two experimental situations were used as limited tests of the performance of the inhomogeneity algorithms available on different planning systems in the department, one to test the situation beyond a typically-sized lung inhomogeneity and one to test the situation close to interfaces. The correction factor was defined as the ratio of the dose in a heterogeneous phantom to dose at the same point in a homogeneous phantom. Table (6-I) shows that most values from power law, ETAR and METAR methods are within 2% (and mostly within 1.0%) of measured values for the total dose from 3-fields where only one passes through lung in this relatively simple situations. If no correction is made, errors according to Table (6-I) can be up to 6% in these situations. The analysis of single fields (Table 6-II) shows that discrepancies from field II, the field passing through the inhomogeneity can be up to 3.0% using the Batho method. These methods include those based on the assumption of separation of primary component and scattered radiation, but they do not take into account electronic non-equilibrium situations.

A slab interface phantom was designed according to figure (6-3) to test the performance of the inhomogeneity algorithms in electronic nonequilibrium situations. The ratio of the dose in the inhomogeneous phantom to that at the same point in a homogeneous phantom was determined as a correction factor. The doses were measured at points along the central axis. Figures (6-4 to 6-7) quantify the performance of different inhomogeneity algorithms against measured values. Batho and modified Batho methods (2D) show an underestimate by up to 8.0%, but ETAR, METAR and DSAR methods (3D) show an overestimate relative to measured values up close to the inhomogeneity boundary for 10x10 field sizes on 6 MV and 16 MV photon beams and for 5x5 field size on 6 MV photon beams (Figs. 6-4 to 6-6). All algorithms significantly overestimate relative to measured values up close to the

boundary for 5x5 field size on 16 MV photon beams (Fig. 6-7). The reason is that for the lower energy beam (6MV) the average projected range of electrons is about 1.5 cm in water and approximately 6 cm in cork with density 0.25, but for the higher energy beam (16MV) the average projected range of electrons is 3 cm in water and 12 cm in cork. If electrons are scattered from the edge of the field towards the central axis and from the central axis towards the edge by approximately 1/2 of this range as an estimate (3cm and 6cm), then for a 5x5 cm field size there is approximate lateral electronic equilibrium for 6MV but not for 16MV. Therefore the doses are reduced at 16MV. This effect is observed in figure (6-7).

At interfaces in the RMI/cork phantom, all algorithms show significant deviations from measured values. However, 3D algorithms (ETAR, METAR and DSAR) show better agreement with measured values in relation to other algorithms by up to 5.0%. Therefore, the use of 3D algorithms improve the dose calculation at inhomogeneity interfaces. All algorithms underestimate doses below the inhomogeneity, where there is an increase in scattered radiation beyond the interface. Again 3D algorithms, particularly the METAR methods show better agreement than 2D algorithms. If no correction is made, errors of up to 35% can be produced. It must of course be stated that any available inhomogeneity algorithm in treatment planning is better than using no correction at all.

In general it can be concluded that in simple situations both 2D and 3D algorithms show generally good agreement with measured values, but in complicated situations (electronic disequilibrium regions, interfaces, etc.) 3D conventional inhomogeneity algorithms show better agreement than 2D inhomogeneity algorithms. It must be stated that despite the advantages of conventional 3D algorithms, they still produce significant dose calculation errors in electronic disequilibrium regions particularly for high energy photon beams. Superposition methods can cope with situations of electronic nonequilibrium by using Monte Carlo calculations, but their application for treatment planning is not practical with present-day technology. Therefore, at present the ETAR and METAR methods are acceptable as being practical and more

accurate than other methods. Woo et al (1990) have compared the concept of the primary and scatter dose model to the condition of electronic disequilibrium by using Monte Carlo calculation methods. Recently, Haider and El-Khatib (1994) have proposed a modification of electronic disequilibrium without using the Monte Carlo method. They obtained all the necessary parameters from experimental measurements.

6-6-Conclusion

Two relatively simple experimental situations were used to test the performance of available 2D and 3D inhomogeneity algorithms in different planning systems by using the IPSM geometric phantom and a slab interface phantom and to give estimates of the magnitude of possible deviation due to of presence of inhomogeneity. The results can be summarised as follows:

- In simple situations where electronic equilibrium exists and the inhomogeneities stretch across the field, 2D and 3D algorithms (Batho, ETAR, METAR) show good agreement within less than 2.0% of measured values. Most values lie within 1.0% of measured values. Here these are deviations on total dose from 3-fields where only one passes through the inhomogeneity, for single fields passing through on inhomogeneity deviations are up to 3.0%.
- In electronic nonequilibrium situations e.g. the inhomogeneity interface between RMI/cork and inside the cork, all algorithms show significant deviations from measured values. 3D algorithms (ETAR, METAR, DSAR) show better agreement with measured values than 2D algorithms, to within 3.0% (mostly). 2D algorithms show significant deviations up to 8.0%.
- All algorithms underestimate below a low density inhomogeneity, where there is a sudden increase in scattered radiation beyond the interface. Within the unit density material, the correction factor increases for a few centimetre and then tends to level off. The reason is that progressively more of the scattered photons reaching the measurement point arise from unit density material than the cork. For points

well beyond the inhomogeneity, the correction factor depends on changes in the primary component of the radiation. For these points using a linear attenuation method can show good agreement for correction factors between measured and calculated values. Again 3D algorithms particularly METAR methods show better agreement than 2D algorithms with measured values, because they attempt to model this.

- If no correction is made, errors can be produced up to 6.0% for simple multifield situations, into 25% or so for single field through typical lung dimensions and 35% for interfaces and below the inhomogeneity. It is therefore stated that any available inhomogeneity correction algorithms in treatment planning are better than using no correction at all.

In general 3D algorithms show better agreement than 2D algorithms and they must be used if available. However, these methods still produce significant dose calculation errors in electronic disequilibrium situations. More complex algorithms or Monte Carlo methods will produce better agreement but at the expense of larger calculation times on current hardware.

Chapter 7

"Monitor Unit Calculation for High Energy Photon Beams"

7-Theory and Review

7-1-Introduction

One of the major sources of uncertainties associated with the absorbed dose delivered to the patient arises in treatment planning. This is partly due to the calculation of the dose distribution (previous chapter) and partly due to dose per monitor unit determination for the linac for the particular treatment conditions for the particular field and patient (dose per unit time for ^{60}Co treatment unit). There are two basic approaches to calculate monitor units: the isocentric approach and the fixed source-skin distance approach. The distance from the source to the point of measurement and to the plane in which field size is specified, are different for the two methods (Figs. 7-1, a and b). In the isocentric approach the measurement point is at isocentre, the depth of measurement point z_r is at some depths, e.g. 5cm or 10cm, and the collimator setting c_r is that to produce relevance field of 10cmx10cm and c for other field sizes at the isocentre. For the fixed FSD method the distance is defined from the source to the surface (set at isocentre) and reference field size c_r and other field sizes, c, are defined at the surface. The depth of the measurement point is defined normally at the dose maximum depth. The larger depth of measurement point (e.g. 5cm or 10cm) in the isocentre approach rather than depth of maximum dose in the fixed FSD approach can reduce uncertainties with measurement at a depth where contaminant electrons have negligible effect. Holt et al (1970) defined the output factor (O_r), or the total scatter factor ($S_{c,p}$), as the dose at a reference depth in phantom for a given field (c) divided by the dose at the same point and depth for a reference (10x10) field (c_r).

$$O_r(c) = D(z_r, c)/ D(z_r, c_r) \qquad (=S_{c,p}) \qquad \text{(Eq. 7-1)}$$

where z_r and c_r are reference depth and reference collimator setting respectively. Monitor unit calculations directly use output factors as follow:

-in the isocentric approach

$$MU = D(z, c)/ [D_0(z_r, c_r) . O_r(c) . TPR(z, c)] \quad \text{(Eq. 7-2)}$$

-for the fixed source-skin distance approach

$$MU = D'(z, c)/ [D_0'(z_r, c_r) . O'_r(c) . P(z, c)/100] \quad \text{(Eq. 7-3)}$$

where MU is the number of monitor unit, D(z,c) and D'(z, c) are the required absorbed doses for depth z and field size c. $D_0(z_r, c_r)$ and $D_0'(z_r, c_r)$ are the dose per monitor unit in the reference conditions. TPR(z, c) is tissue phantom ratio, P(z, c) is percentage depth dose for the appropriate conditions, $O_r(c)$ and $O'_r(c)$ are output factor. The use of the 'dash' is to distinguish the fact that the dose/MU and the output factors are different for the two approaches, being measured in conditions relevant to the different methods. The output factor is the combination of the relative effects of primary photons from the source and of the head scattered photons and of phantom scatter. Therefore, the output factor varies widely with the collimator setting.

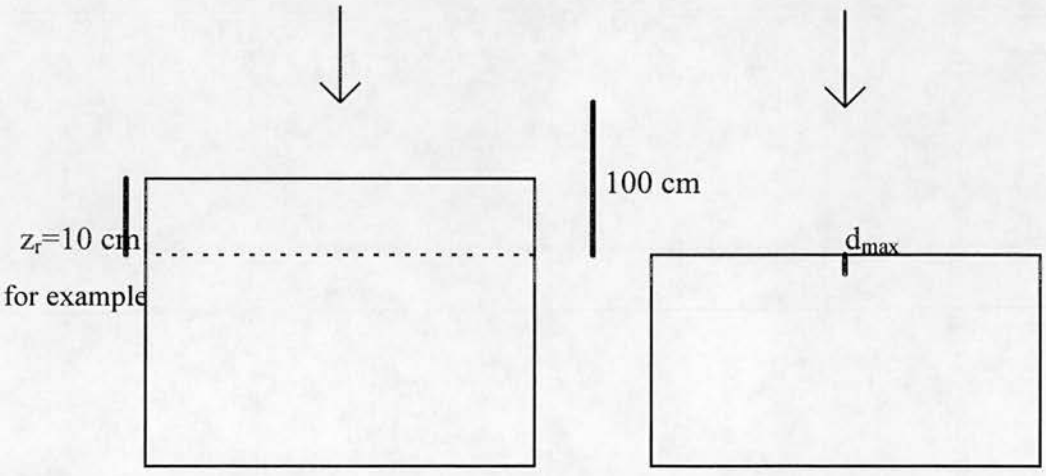

a) water tank for isocentric condition b) water tank for fixed SSD

Fig. 7-1: Geometry of dose calculation for a) isocentric condition b) fixed FSD

The output factor $O_r(c)$ or total scatter factor ($S_{c,p}$) can be separated into collimator scatter and phantom scatter as developed by Holt et al (1970) and extended by several authors (Khan et al 1980, Patterson and Shragge 1981, Krithivas and Rao 1987, Luxton and Astrahan 1988, and Spicka 1988). According to Fig. (7-2) it can be written that:

$$D_{air} = D_{primary} + D_{head\ scatter}$$

where $D_{primary}$ is the component direct from the source, or

$$D_{air} = D_{primary}\,(1+HS) \qquad \text{Eq. (7-4)}$$

in which HS is defined as $HS = D_{head\ scatter} / D_{primary}$. It should be noted that as it is dose per monitor unit which is the relevant parameter for a linac, the head scatter term includes the effect of scatter back into the monitor chamber. In phantom it can be written that:

$D_{phantom} = D'_{air} + D_{phantom\ scatter}$, where D_{air} is given a superscript 'dash' to make it plain that it is understood that the incident dose will be attenuated in the phantom and will vary with depth due to this. D_{air} is frequently referred to as primary dose. Here it is plain that it is composed of 'direct' primary plus head scatter components. It can be written that:

$$D_{phantom} = D'_{air}\,(1+PS) \qquad \text{Eq. (7-5)}$$

in which PS is defined as $PS = D_{phantom\ scatter} / D'_{air}$

the total dose can be written as:

$$D_{phantom} = D_{primary}\,(1+HS)\,(1+PS) \qquad \text{Eq. (7-6)}$$

The out put factor for field size (f) is defined as

$$OF\,(f) = D\,(f)/D\,(ref.) = [(1+HS)_f(1+PS)_f] \,/\, [(1+HS)_{ref}(1+PS)_{ref}]$$

where the direct primary component is the same in each case and so cancels in the ratio.

$$OF = [(1+HS)_f / (1+HS)_{ref}].[(1+PS)_f / (1+PS)_{ref}] = [S_c].[S_p] \qquad \text{Eq. (7-7)}$$

or $$S_{c,p} = S_c . S_p \qquad \text{Eq. (7-8)}$$

where S_c is the head scatter factor (relative to the reference field) measured in air and S_p is the phantom scatter factor (relative to the reference field).

One source of uncertainties can be introduced by algorithms which do not separate head scatter and phantom scatter in the calculated output factor (Mijnheer 1995) i.e. which take both factors applicable to one "field size". Separation of head scatter and phantom scatter is more important where they can be changed independently, for example when the field size on the phantom surface is different from the standard collimator setting e.g. blocked fields, wedged fields, asymmetric and irregular fields.

The phantom scatter (S_p) is calculated directly from equation (7-9). Both the Sc and the Sp can be defined at any depth, which should be specified. The phantom scatter at the depth of maximum is termed the peak scatter factor (PSF) (or strictly the normalised PSF, i.e. the NPSF, as it is normalised to the reference field size value).

$$S_p = S_{c,p} / S_c \qquad \text{Eq. (7-9)}$$

The head scatter factor is measured in air as a factor related to collimator opening. Kase and Svensson (1986) measured output factors in air for different machines using an ion chamber. Their results, except for a CGR Saturne 20 accelerator with a unique collimator design, showed that the main contribution to head scatter is due to the flattening filter, varying with the collimator opening. Air dose measurements from 5x5 to 40x40 cm field sizes led Luxton and Astrahan (1988) to conclude that head scatter can be analysed in terms of forward scatter from the central section of the flattening filter, back scatter from the collimators into the beam monitor chamber, and forward scatter from the collimator (Fig. 7-2). In addition, in small field sizes the apparent head scatter depend on penumbral effects (Bjarngard 1996). For field sizes less than 3 cm in high energy x-ray beams, the volume of flattening filter seen from the measurement position becomes small, so the effective 'scatter source' size becomes small. In addition the entire primary source can not be seen through the collimator opening from the point of measurement. The dose will therefore be reduced and this appears also as a reduced S_c (even though it is due to a reduction in primary). The width of the penumbra region at

reference depth and standard SSD or SCD is about 1.5cm, which for both sides of the beam is near 3cm hence this effect comes into play at field sizes less than this. But for larger field sizes' (c>3cm) this effect is not present and the variation of the head scatter factor is caused mainly by the effects related to the movable jaws and the flattening filter (Wu et al 1984, Dunscomb and Nieminen 1992, Zhu and Bjarngard 1994 and 1995).

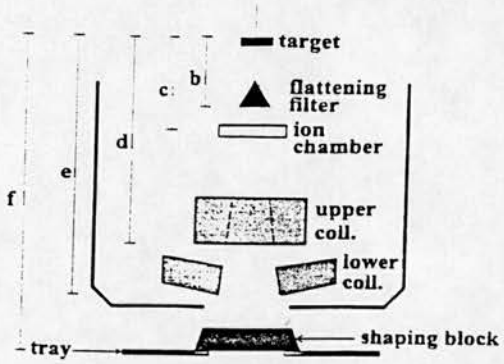

Fig. 7-2: Schematic geometries of the treatment head

Some authors (Patterson and Shragge 1981, Luxton and Astrahan 1988, Duzenli et al 1992) have concluded that backscattered radiation from the collimator jaws into the dose monitor chamber contributes to the field size dependence of relative radiation output. However, Haung et al (1986) and Dunscombe and Nieminen (1992) came to the opposite conclusion that backscattered radiation from the collimator jaws into the dose monitor chamber does not contribute to the variation of output with field size. Zhu and Bjarngard (1995) measured head scatter factors on a 6MV Philips SL 75-5 accelerator. They stated that if gun current and hence the photon output from the target is controlled through a feedback mechanism from the signal from the monitor chamber, then backscattered radiation is increased at smaller collimator settings giving an increase in signal and a corresponding decrease in the actual photon output. It is clear that the specific effects depend on the particular machine and head design.

7-2-Head Scatter Measurement

The head scatter factor can be written as:

$$S_c = D_{air}(c)/D_{air}(ref.) \qquad \text{eq.(7-10)}$$

Different methods have been used to measure head scatter in air. Some authors have used plastic build up caps of thickness equivalent to the depth of dose maximum (Dmax) using ionisation chambers (Holt et al 1970, Khan et al 1980, Patterson and Shragge 1981, Krithivas and Rao 1987, Luxton and Astrahan 1988, Spicka 1988). The depth of dose maximum is a function of energy and field size. For small field sizes (<4x4cm) the D_{max} increases with field size due to changing phantom scatter. For larger field sizes (>4x4cm) the D_{max} decreases slowly with field size due to contaminant electrons which are contributed by the flattening filter directly and by collimator jaws and air indirectly (Sixel and Podgorsak). In order to achieve a sufficiently effective depth of the measuring point taking account of electron equilibrium, a build up cap of thickness equivalent to maximum depth of dose maximum is appropriate. Such caps, built from plastic, become significantly large for smaller field sizes producing some "phantom scatter" component effect in the measurement. Therefore, many authors have used metal build up caps or longer focus to chamber distances to investigate factors for small fields (Evans 1968, Biggs et al 1979 and 1983, Schrader et al 1980, Pettit and Goodman 1983, Krithivas and Rao 1985, Dunscomb and Nieminen 1992, Zhu and Bjarngard 1995, Li et al 1995, Douglas et al 1995). To overcome the problems of contaminant electrons, various authors have used a miniphantom (Van Gasteren et al 1991, Tatcher and Bjarngard 1993, Li et al 1995, Douglas et al 1995, Zhu and Bjarngard 1995) with the chamber at a greater depth (see next section).

7-3-Electron Contamination and Electron Equilibrium for photon beams

Some secondary electrons will have ranges greater than electronic equilibrium depth (or thickness). Therefore if measurements are done at D_{max} or in equivalent thickness caps they will be affected by contaminant electrons originating from interactions outside the phantom or cap. It has already been stated that contaminant electrons are the cause of the shift of the depth of dose maximum to shallower depth when the field size is increased (Biggs and Russel 1979 and 1983, Ling et al 1982, Arcovito et al 1985, Thomadsen et al 1992, Sixel and Podgorsak 1994). Electron contaminants are introduced mainly by the flattening filter and partly by collimator jaws and air. Monte Carlo calculations at 220cm SSD give values of 66%, 23%, 11% for flattening filter, collimator jaws and air, respectively (Pettit et al 1983). They showed that the flattening filter and monitor chamber were the main sources of secondary electrons for short SSDs (80-100cm). However, at longer distances (300-400cm SSD) the main contributor of electrons was the air. Accelerators with different designs and materials in the beam also affect the electron contamination differently (Rao et al 1988, Li and Rogers 1995). It has been suggested (Li and Rogers 1995) that a 1mm-thick lead filter placed below the linac head can reduce contaminant electrons without noticeable changes in the photon beam quality.

Two methods have been proposed to remove the effect of electron contamination from head scatter factor measurements: (1)The first method includes using a sufficiently thick build up cap or miniphantom at depth far enough beyond D_{max} to diminish electron contamination. Krithivas and Rao (1985) came to the conclusion that a suitable depth to remove electron contamination is numerically equal to half the beam energy in cm of water or plastic close to water in response. A number of authors have recommended depths of 5cm and 10cm for low and high energy photon beams respectively. The publication proposed recently by an ESTRO working party on monitor unit calculations (1997) has recommended using a reference depth of 10cm for output factors in both a

large water phantom and a mini phantom for all MV photon qualities. (2)The second method is to use a magnet to separate photons and electrons (Krithivas and Rao 1985, Sjogren and Karlsson 1996).

For large field sizes, where the electron contamination contribution is more significant, the exclusion of contamination electrons can reduce the numerator of the ratio in equation (7-10) more significantly than the denominator, and Sc would be reduced. Therefore if contaminant electrons significantly affect the measurement, the apparent (measured) S_c values will be too high for larger field sizes (and conversely possibly too low for smaller field sizes).

In addition to contaminant electrons through the 'front' wall, the effects of electrons through the sidewalls must be considered. The sidewall thickness of the build up cap or width of the miniphantom must be large enough to assure lateral electron equilibrium and absorb contaminant electrons, and at the same time it must be smaller than the field sizes used. Li et al (1995) obtained the radius of lateral electron equilibrium for photon beams by Monte Carlo calculations as follow:

$$R_{Lee}[gr/cm^2] = 5.973\ (TPR\ ^{20}_{10}) - 2.688 \qquad \text{(Eq. 7-11)}$$

i.e. a linear relationship between R_{Lee} and $TPR(^{20}_{10})$, and concluded that the errors introduced by electron disequilibrium are not as significant as the errors due to electron contamination. It is clear that for smaller field sizes the miniphantom or build up cap can not satisfy both requirements on sidewall thickness. In fact as field size gets smaller, particularly for higher energy beams, lateral equilibrium may not be satisfied in a given clinical field anyway.

7-4-Phantom scatter

Phantom scatter is defined only by the area of the phantom being irradiated and should be independent of the collimators or other shielding used to define the field size. It can be determined from the quotient of the total scatter factor and the head scatter factor (equation 7-9). Van Gasteren et al (1991) and Storchi and Van Gasteren (1996) and found a strong relation between the phantom scatter factor and the quality index of a particular beam quality at 5cm and 10cm, as is expected. This should also be true at d_{max}, but the amount of scatter there is less, so it is not easy to see clear changes.

Phantom scatter at maximum depth has been known as peak scatter factor (PSF). BJR 25 (1996) has highlighted some problems in the measurement of PSF. In order to determine the PSF the total dose is measured at the peak depth in phantom, then the primary is measured using the same detector placed at the same point surrounded by a small mass of build up cap. Therefore, the amount of material above the measurement point should be the same as for the phantom measurement. However, the scatter from the small mass of the build up cap produces underestimates of around 2% in PSF (and also has a similar effect on TAR) (McKenzie 1997) for ^{60}Co beam. The use of normalised PSF can overcome this problem, defined (Day 1983) by the following formula:

$$NPSF(S) = PSF(S) / PSF(ST) \qquad \text{(Eq. 7-12)}$$

where S is any given field size, and ST is a standard (reference)field size, conventionally 10x10cm. This procedure and the resulting parameter (NPSF) remain useful as PSF_s are generally required in calculation as a ratio of values at different field sizes. For any given depth and field size the phantom scatter decreases with increasing beam energy, and for a given energy and field size it increases with increasing depth. But this is complicated for PSFs or NPSFs, because PSF is specified at Dmax and the depth of

maximum dose increases with beam quality. The two effects are in opposition to each other, and it depends on which effect predominates over the other as to the specific final behaviour.

7-5-Wedged Beams

Wedged beams are used for modifying the dose distribution in the patient. The output factor of the treatment machine decreases in wedged beams, which can be expressed in the wedge factor. The wedge factor is the ratio of the absorbed dose in water at a point along the central beam axis of the photon beam for the same number of monitor units with and without a wedge (ICRU 1976).

The wedge factor varies with field size and depth (Hughes et al 1972, Abrath et al 1980, Wu et al 1984, Palta et al 1988, McCullough et al 1988, Thomas 1990, Kalend et al 1990, Van Gasteren et al 1991, Knoos et al 1991, Heukelom et al $1994_{a,b}$, Cozzi et al 1996, Liu et al 1996). Heukelom et al ($1994_{a,b}$) observed an increase between 4% and 9% for the wedge factor for ^{60}Co γ-ray beams and for 4, 8, 16, 25 MV x-ray beams at depth of maximum dose when field sizes increased from 10x10 cm to 20x20 cm. Cozzi et al (1996) evaluated depth dependence of the wedge factor to be of the order of 5% for 6MV and less than 2% for 15MV from d_{max} to 30cm depth.

7-5-1-Field Size Dependence of Wedge Factors

The variation of wedge factor with field size has been reported due to the variation of head scatter, phantom scatter and backscatter radiation produced by the wedge and reaching the monitor chamber (Huang et al 1987, Heukelom et al $1994_{a,b}$). Wedge factors increase with increasing field size due to changes of the incident photon fluence by the wedge. When collimator size is increased, the scatter from the irradiated wedge volume and incident at the measurement point.is increased. The wedge also changes the

scatter from flattening filter or backscatter from collimators by attenuation, depending on wedge size and position. The amount of wedge factor increase is determined by the overall relative head scatter of wedged and open beams. Heukelom et al (1994) showed that the wedge factor (WF) at reference depth (depth of maximum dose) for a particular field size (v_c) can be written approximately.

$$WF(v_c, d_{ref}) \sim \frac{S_c(v_c, d_{ref}, w) \cdot S_p(v_c, d_{ref}, w)}{S_c(v_c, d_{ref}, o) \cdot S_p(v_c, d_{ref}, o)} \qquad \text{(Eq. 7-13)}$$

the wedge factor measured in an extended phantom (ext) and measured in a miniphantom (rod) can be written from Heukelom et al (1994_b) as follows

$$WF_{ext}(v, d) = \frac{H(v, d, w)}{H(v, d, o)} \times \frac{[1+(P(v, d, w)/H(v, d, w))]}{[1+(P(v, d, o)/H(v, d, o))]} \qquad \text{(Eq. 7-14)}$$

and

$$WF_{rod}(v, d) = H(v, d, w) / H(v, d, o) \qquad \text{(Eq. 7-15)}$$

Where 'w' and 'o' indicates the wedged and open photon beam, respectively. S_c is head scatter, S_p is phantom scatter, H and P are contribution of head scatter and phantom scatter, respectively. The measured values by Heukelom et al (1994_b) and extensive measured values from this work (chapter 8) indicate that the wedge factor from large phantom measurements [WF_{ext} (v, d)] is closely equal to the wedge factor from miniphantom measurements [WF_{rod} (v, d)]. Therefore, the second part of equation (7-14) is equal to unity. It means that the relative phantom scatter does not change between wedged and open beam. Knoos and Wittgren (1991) estimated a contribution of about 0.3% for phantom scatter effect on wedge factor between field sizes of 5x5 and 25x25

for 6MV and 18MV x-rays, and Palta et al (1988) based on computation obtained a contribution of less than 0.5% for phantom scatter and wedge factor. Therefore, the variation of the wedge factor is caused by a wedge-induced change in the head scatter, showing that head scattered photons produced from the wedge material play the main role in wedged beam variation. Heukelom et al (1994_a) showed that the magnitude of this variation was proportional to the irradiated wedge volume as viewed from the point of measurement. This can be altered if different wedge material or different wedge angles are used.

In some accelerators, wedges are situated beneath the collimator jaws and the variations of backscatter to the monitor chamber are equal for the open and wedged beams. For accelerators with wedges close to the monitor chamber, backscatter may also affect the wedge factor, however this effect is not generally significant (Cozzi et al 1996).

In general, it can be concluded that in the presence of a wedge, a field size dependent wedge factor or a separate output factor for wedged beams should be used.

7-5-2-The Depth Dependence of Wedge Factors

Wedge factor varies with phantom depth (McCullough et al 1988, Kalend et al 1990, Knoos and Wittgren 1991, Niroomand Rad et al 1992, Heukelom et al $1994_{a,b}$, Cozzi et al 1996). This variation is caused by a change in the energy spectrum of the photon due to preferential absorption of low energy photons in the wedge volume (beam hardening).

Heukelom et al ($1994_{a,b}$) showed that the ratio of head scatter and phantom scatter for wedged and open beams remain unchanged for all x-ray beams except for low energy (4MV) and high energy (25MV) photon beams. For 4MV photon beams, an increasing wedge factor with phantom depth was observed for a particular field size in a miniphantom, where the phantom scatter is absent (or minimal). Therefore, this increase

is due to wedge beam hardening and is independent of phantom scatter. For 25MV photon beams, an increasing wedge factor is observed in the first few centimetres of the irradiated phantom and is due to additional electron contamination produced in the head when the wedge is inserted. For both cases in low and high energy photon beams the variation of wedge factor with field size at different given depths is due to head scatter variation of wedged and open beams.

Knoos and Wittgren (1991) showed that at a clinically relevant depth e.g. 15cm, the changes in the relative wedge factors are about 2-3% for the 15°, 3-5% for the 30° and 5-7% for the 45° wedge filter compared to dmax for 6 and 18MV x-ray beams.. They concluded that errors could be produced in dose planning if depth dose data for open fields are used for fields with wedge filters. They showed that at large depth (>20cm) thicker wedges e.g. 45° could introduce errors of the order of 5-10%. Therefore, significant errors can be introduced in dose planning for centres which use only a single beam data set (depth dose) for both open and wedged beams. A modern dose planning system should consider wedged beam data separately from the open beams. One other important point in this is choosing an appropriate reference depth for clinical use. The choice of dose maximum depth may introduce significant dosimetry errors (Cozzi et al 1996). According to some international recommendations the relevant reference depth should be a depth where no contamination electrons are present. Recently the ESTRO working party on monitor unit calculations (1997) has recommended using a reference depth of 10cm for both percentage depth dose and output factor.

7-6-Output Factors for Fields Defined by Blocks, Asymmetric fields and Multi Leaf Collimator (MLC)

Separation of head scatter and phantom scatter is not critical in open fields, because the size of the irradiated phantom surface is the same as the collimator setting. But this separation is necessary where the field size on the phantom surface is different from the

standard collimator setting e.g. blocked fields, asymmetric fields, irregular and MLC fields. Uncertainties can be significant in each of those non-standard open field situations if head scatter and phantom scatter are not separated and considered independently.

7-6-1-Blocked Fields

Blocked fields are used to shield critical organs or healthy tissue. The area of the blocked field is different from the set collimator field size. In this case the output factor depends on both blocked and collimated field due in part to loss of phantom scatter, and also to a difference in scatter off the collimator and beam blocks.

Meli (1986) showed that output factors for a blocked field at 6MV are less than those for the set collimator field size due to differences in phantom scatter, but greater than those for a collimator limited (unblocked) field of the same surface field size due to differences in head scatter. Van Dam et al (1992_b) observed deviations between measured and expected values of 1% for 10MV and 5% for 25MV photon beams on a Philips SL25 accelerator for blocked fields. They concluded that the deviations are due to a balance between gain from block scatter and loss in head scatter. For low energy photon beams these two effects are approximately balancing each other and this was the reason that Meli (1986) came to the above conclusion. For higher energy photon beams the loss in head scatter is more important than the gain in block scatter. However, Tatcher and Bjarngard (1994) obtained less than 1% deviations for both miniphantom and large phantom for the same situations as Van Dam et al (1992_b). Their measurements were carried out in both low energy (6MV) and high energy (25MV) beams, therefore the observed deviations were independent of beam energy. They concluded that the difference in head scatter between open and blocked fields is not

significant. They stated that the results of Van Dam et al (1992_b) are incorrect, because they have been based on the use of peak scatter factors. Electronic equilibrium can be compromised at the depth of maximum dose with increasing beam energy, and to avoid this difficulty a larger depth is needed. Further work is necessary to observe the differences in head scatter and phantom scatter for blocked fields (see chapter 8).

7-6-2-Asymmetric Fields

Today manufacturers provide as standard, collimators with independent jaws which can be set asymmetrically. These are used as collimating blocks, to produce half-blocked fields and to match adjacent fields, etc. Independent jaws reduce the set up time and spare the radiographer from handling cumbersome heavy blocks.

Asymmetric collimation produces alteration in radiation output, depth dose and beam profiles (Khan et al 1986, Loshek and Keller 1988, Palta et al 1988, Thomas and Thomas 1990, Marinello and Dutreix 1992, Kwa et al 1994, and Cadman 1995). The dosimetric characteristics of asymmetric photon beams are different from symmetric fields. The main reason is due to change of head scatter factors for asymmetric fields relative to symmetric fields. In addition the 'central axis' of the asymmetric field shows dosimetry differences due to beam profile affects or hardening away from the symmetric axis position due to flattening filter effects.

Khan et al (1986 and 1993) defined the head scatter factor for a single pair of asymmetric collimators by

$$S_c(x, y, r) = \frac{\text{(output in air for asymmetric x.y field centred at a point)}}{\text{(output in air for symmetric 10x10cm field) .OAR (r)}} \qquad \text{(Eq. 7-16)}$$

where x and y are the collimated field openings for the lower jaws and upper jaws, respectively, r is the radial distance of the asymmetric field centre at a point to the collimator radiation axis in a plane perpendicular to that axis at isocentre, and OAR(r) is the off-axis ratio.

Cadman (1995) observed a maximum difference of 1% on Dose/MU between symmetric and asymmetric fields along both x and y axes in a 6MV x-ray beam. When OAR (off-axis ratio) was included in the asymmetric field values. The experimental values from Murray et al (1995) gave the same conclusion on output factors for asymmetric fields. They used a Varian Clinac 600C linear accelerator with four collimators which can be moved independently. All measurements were carried out with $0.6cm^3$ ion chamber in a phantom and the probe was placed at depth of 1.5cm in a polystyrene block large enough to provide sufficient scatter for all field sizes studied. The output factors for asymmetric fields were measured with field centres at radii of 2.5, 5, 7.5 and 10 cm from the isocentre axis. Factors were normalised to 1.0 for a symmetric 10x10 field and OAR were included. They concluded that output measured in air and at depth in a phantom are radially symmetric and each scatter component as a function of field size is independent of field position:

$$ROF\ (x_c, y_c, f_s) = OAR_{air}(x_c, y_c)\ .\ S_{c\sim ic}(f_s)\ .\ S_h(f_s)\ .\ S_p(f_s) \qquad \text{(Eq. 7-17)}$$

where ROF (x_c, y_c, f_s) is the relative output factor as a function of position of the field (x_c, y_c) and the field size (f_s) relative to a symmetric 10x10cm field at Dmax, $OAR_{air}(x_c, y_c)$ is the off-axis ratio measured in air for the point (x_c, y_c). Sc~ic (f_s) is backscatter from the collimator to the beam monitor chamber, $S_h(f_s)$ is head scatter, $S_p(f_s)$ is phantom scatter.

Niroomand Rad et al (1994) used two identical sets of manual wedges, one set of which are positioned centrally on the wedge plate whilst the other is positioned centrally to the

central ray of an asymmetric field. They used a Siemens Megatron 6745 which produces a 6MV x-ray photon beam. They observed that the wedge transmission factors for asymmetric fields are larger than for the corresponding symmetric situation. The reason can be due to the geometry of wedge filter and collimation and beam hardening effects of the flattening filter. The thin part of the wedge shows sharper dose gradients than the field placed on the thick part of the wedge (Palta et al 1988).

7-6-3-Multi-Leaf Collimators (MLC)

Currently multileaf collimators are in clinical development at many centres and by all manufacturers. They are now seen as a standard feature. A multileaf collimator can be used instead of blocks, to produce conventional field shaping and for conformal therapy (Galvin et al 1993, Jordan and Williams 1994). There are many advantages when a MLC is used instead of blocks, MLC remove the use of cumbersome shielding blocks, handling and storage. This can reduce the treatment time and minimise patient discomfort and movement, and therefore improve accuracy in treatment delivery. The design of MLCs allows beam delivery from any angle necessary to produce the optimum dose distribution for any shape without using trays (Heyler and Heisig 1995).

Conformal therapy pays close attention to matching the irradiated volume of tissue to the target volume (Takahashi 1965). As the aim of radiotherapy is to maximise dose to the target volume as accurately as possible and at the same time minimise dose to surrounding tissues as accurately as possible, then a multileaf collimator as a tool for conformal therapy can improve outcomes in radiotherapy. It allows a closer matching than standard blocks, but brings its own QC and potential in accuracies into the process.

Palta et al (1996) obtained characteristic dosimetric data e.g. field size dependence of output factors, depth doses, isodose distributions, and penumbra for a Philips SL18 with MLC. All data from MLC were similar to the standard set of collimator systems, with

the exception of output factors. In the Philips SL18 the MLC is positioned above the upper and lower jaws. When MLC is used for irregular shaped fields e.g. circle, ellipse and diamond (Palta et al 1996), the head scatter changes due to the scatter which reaches the monitor chamber and the measurement point being affected by the MLC. The difference between the MLC and standard jaws can be reduced with consideration of equivalent square irregular fields. This may not be valid for accelerators such as Varian, where the MLC has been situated below the standard jaws as a tertiary collimator. In these types of accelerators the regular collimator setting can be used as collimator jaws in addition to the MLC. A third type is for example, the MLC on a Saturne 43/series 800 linear accelerator which replaces the lower pair of jaws in the x direction and the distance of the collimator end from the isocentre is similar for the two designs (standard and MLC) (Georg et al 1997). Some authors have developed calculation schemes for MLC and some of these are discussed in chapter 9 where MLC calculations are investigated experimentally.

Chapter 8

"Monitor Unit Calculation for High Energy Photon Beams"

8-Assessment of Methods to Separate Total Scatter Factors into Head Scatter and Phantom Scatter Factors

8-1-Introduction

Phantom measurements are relatively straightforward, but to separate $S_{c,p}$ into S_c and S_p requires Sc measurements. The head scatter factor or collimator scatter factor as defined in chapter 7 can be measured in air by using an ionisation chamber with a suitable build up cap (Holt et al 1970, Khan et al 1980, Patterson and Shragge 1981, Krithivas and Rao 1987, Luxton and Astrahan 1988, Spicka 1988). For field sizes approaching the size of the cap or smaller, the cap provides significant scatter compared to a phantom measurement with the same field size and the measurement is not "free in air". The dimensions of the small mass of build up must be such as to produce a similar degree of secondary electron build-up as in a large phantom. Therefore, the amount of material above the measurement point should be the same as for a d_{max} phantom measurement. However the primary and head scatter factor is defined in free air, yet their experimental measurement includes an unwanted scatter from the small mass of the build up cap. This can overestimate the head scatter factor and then reduce the extracted peak scatter factor (PSF) as this is measured by the ratio of total scatter factor to head scatter factor. To reduce this error the thickness of build up cap must be as thin as possible, particularly for small field sizes but consistent with electron equilibrium. Even so the problems are not overcome at small field sizes. The head scatter factor for small fields can be measured by two methods i) using approximately water equivalent caps at a larger SSD

(Arcovito et al 1985), ii) or by using metal caps (Evans 1968, Biggs et al 1979 and 1983, Schrader et al 1980, Pettit and Goodman 1983, Krithivas and Rao 1985, Dunscomb and Nieminen 1992, Zhu and Bjarngard 1993 and 1995, Li et al 1995, Douglas et al 1995).

For newer approaches with reference depths of 5cm and 10cm, in order to avoid electron contaminants miniphantoms are necessary. A number of geometries of miniphantom, with different orientation of chambers have been compared and assessed. The frontwall thickness of a miniphantom must be large enough to avoid electron contaminants and the lateral thickness of the miniphantom must be thick enough to achieve lateral electron equilibrium. On the other hand it must be sufficiently small so that the miniphantom or cap be adequately covered by the field sizes required at the reference distance. This still gives problems for the small field sizes of interest (Van Gasteren et al 1991, Tatcher and Bjarngard 1994, Li et al 1995, Douglas et al 1995, Zhu and Bjarngard 1993 and 1995).

This chapter concentrates on measurements at three standard reference depths i.e. the depth of maximum dose using different thicknesses and materials (plastic and brass) of caps and 5cm and 10cm depths with brass (equivalent depth) and plastic miniphantoms at 100SCD (Source Chamber Distance), 100SSD (Source Surface Distance) and 150SCD for 6MV and 16 MV photon beams. All measurements were taken with beam axis vertically downwards. The purpose of this chapter is to investigate the effects of electron contaminants and electron equilibrium on collimator scatter factors and to assess and compare the methods of separation of total scatter factor into head scatter factor and phantom scatter factor. In the next chapter these methods will be used to measure head scatter and phantom scatter for blocked fields, irregular fields and MLC fields to assess the accuracy of output factors and monitor unit values for dose delivery to the patient.

8-2-Methods and Material

(I) Plastic Build up caps

The plastic build up caps were made of approximately water equivalent material mostly perspex but some were made of epoxy resin water substitute plastics (WT1) with different sidewall thickness (t) and different end thickness (d) which is listed in Table (8-I). These are used with chamber axis horizontal and to fit a 0.1cc PTW ionisation chamber. An epoxy cuboid shape cap with endwall thickness of 2cm and sidewall thickness of 1cm was also used (Fig. 8-1a).

(II) Brass build up caps

Brass build up caps with density 8.5 ($gr./cm^3$) were built with sidewall thickness of 2mm which is approximately equal to 1.7cm water equivalent material. The end thickness of the brass cap can be changed using brass discs each of 2mm thickness (Table 8-I). Therefore used with long axis vertical the end (now top) thickness can be varied to give brass miniphantoms of variable chamber depth. The diameter of the brass cap (1.1cm) is such that it allows to measure head scatter for small field sizes (>1cm). The internal diameter is again designed to fit the 0.1cc PTW chamber (Fig. 8-1a).

(III) Miniphantom

Two types of miniphantoms were built from epoxy resin water equivalent material (WT1) according to Fig. (8-1). A PTW ionisation chamber with air cavity 0.1cc was located at 5cm or 10cm water equivalent depth in an interchangable insert. The chamber was perpendicular to the beam axis for the first miniphantom and parallel for the other. Both miniphantoms are cylinders of diameter 4cm, which is smaller than (or at least equal to) the standard range of field sizes required at the reference distance and yet large enough to achieve lateral electronic equilibrium for x ray beams up to 16MV (Van Gasteren et al 1991, Tatcher and Bjarngard 1994, Zhu and Bjarngard 1993 and 1995, Douglas et al 1995, Dutreix et al 1997). The length of the first miniphantom is 20cm with measurement points at 5cm for low energy (6MV) and 10cm for high energy

(16MV) photon beams, beyond the range of contaminant electrons. The length of the second is 12.5cm.

The head scatter measurements were carried out in two geometry situations, horizontally and vertically, by caps and miniphantom according to figure (8-1). The collimator setting ranged from 4cm to 40cm for the linacs.

Table (8-I): The sidewall and top (or end) wall thickness of different build up caps, and miniphantoms

Caps# miniphantom	sidewall thickness (t, cm)		end wall thickness (d, cm)	
	true	equivalent	true	equivalent
perspex				
6	0.5	0.58	0.5	0.58
8	0.8	0.92	0.8	0.92
10mm	1.0	1.15	0.7	0.81
E7	1.4	1.61	0.5	0.58
16	1.6	1.84	1.8	2.07
E3	1.6	1.84	1.1	1.27
6MV	1.7	1.96	1.4	1.61
18	1.8	2.07	2.0	2.30
20	2.0	2.30	2.3	2.65
22 (16MV)	2.4	2.76	2.5	2.88
epoxy cap	2.0	2.0	1.0	1.0
	1.0	1.0	2.0	2.0
Brass cap	0.2	1.7	0.2	1.7
equivalent			0.4	3.4
thickness*			0.6	5.1
			0.8	6.8
			1.0	8.5
Miniphantoms	2.0	2.0	5.0	5.0
			10.0	10.0

** 2mm brass taken as 1.7cm equivalent*

 # the cap names are simply used as an identifier and are the names which have been given by the department at the time they were constructed

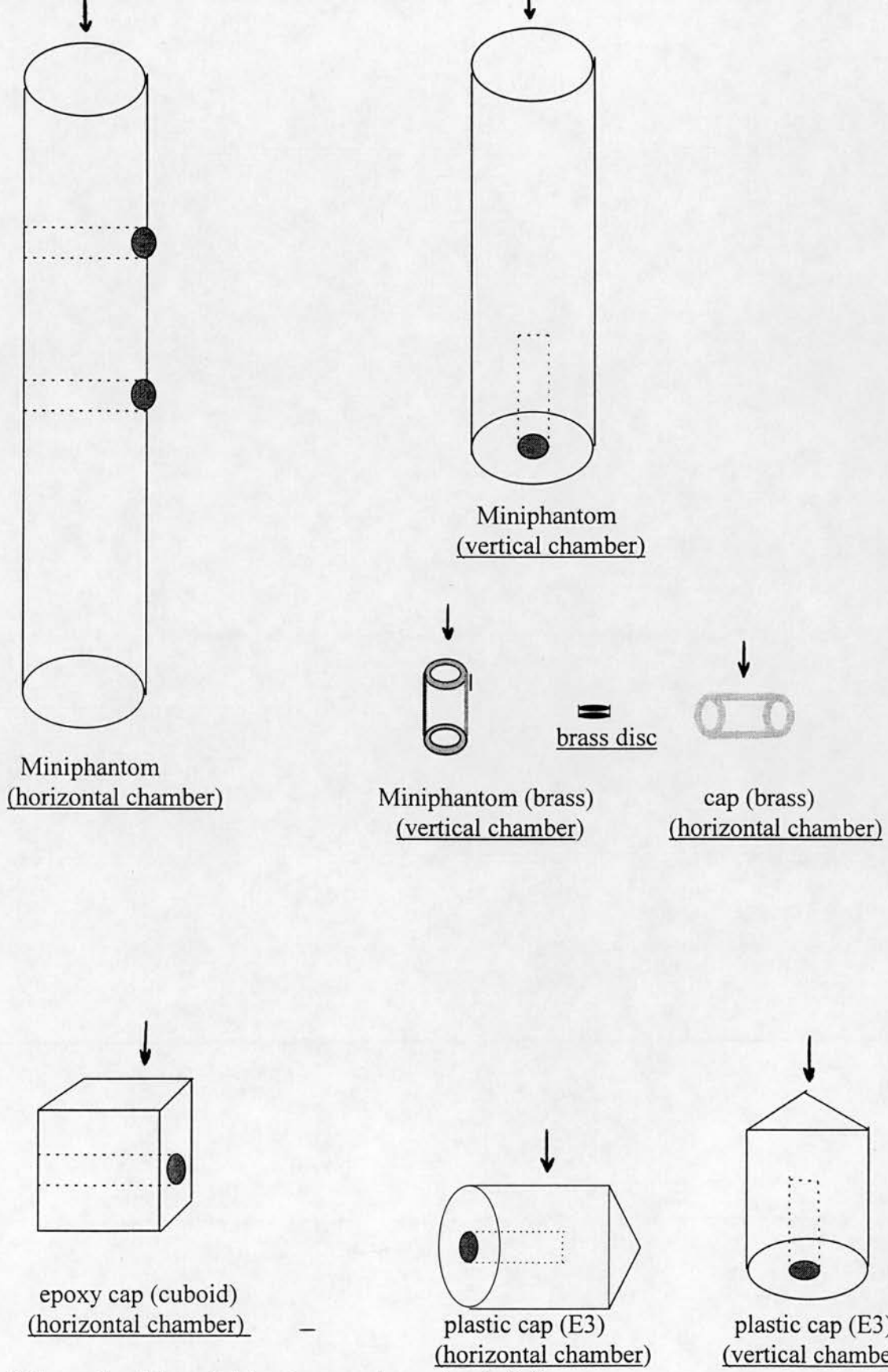

Fig. 8-1a: Schematic of the miniphantoms and caps (scale 0.5)
(all measurements done with beam pointing vertically down; therefore horizontal chamber, cap etc has chamber axis perpendicular to beam axis; vertical chamber, cap etc has chamber axis parallel to beam axis)

Measurements were carried out with photon beams of 6MV (QI = 0.665 and QI = 0.680) and 16MV (QI = 0.765). Charge was accumulated for 100 monitor unit irradiations for each field size and measurement situation. To consider the effect of SSD on measured head scatter factors, measurements were carried out at different distances i.e. 100SSD, 100SCD, and 150SCD.

IV-A new method for measuring head scatter factors

One RMI sheet (30x30cm) with thickness of 2cm was used for determination of head scatter factors. It has five holes (1cm diameter) to accept the PTW ionisation chamber at depths of 1, 4, 7, 10 and 15cm and was originally designed for interface scatter experiments. Two other sheets (30x30cm with thickness of 2cm) can be situated at the middle cross of the initial sheet to enable the excess scatter contribution from the first to be estimated and subtracted. Measurements were taken in the single sheet phantom (the upper sections of Figs. 8-1c and 8-1d) and then in the crossed sheets phantom (the lower sections of Figs. 8-1c and 8-1d) at 10cm depth and 100cm SCD for fields 4x4 to 40x40 for 6MV (CH6) and 6MV (Varian) photon beams. The difference between the two sets of values from these two sets of measurements were subtracted from the readings from the first set. This corrects the first set for the excess scatter from the size of the sheet (as the second set has an equal additional scatter component). The resulting ...values are equivalent to head scatter factors obtained by using an area of 2x2 cm^2 as a miniphantom. This method can reduce the mass scatter from the miniphantom and allows an effective miniphantom of 2x2cm, which is smaller than the miniphantoms used (Fig. 8-1c). The approach removes stem effects in the chamber measurements and compensates somewhat for lack of electron equilibrium in small miniphantoms. However horizontal chambers still limit the field size that can be measured with the method.

Fig. 8. 1b: Illustration of build-up caps and mini-phantoms

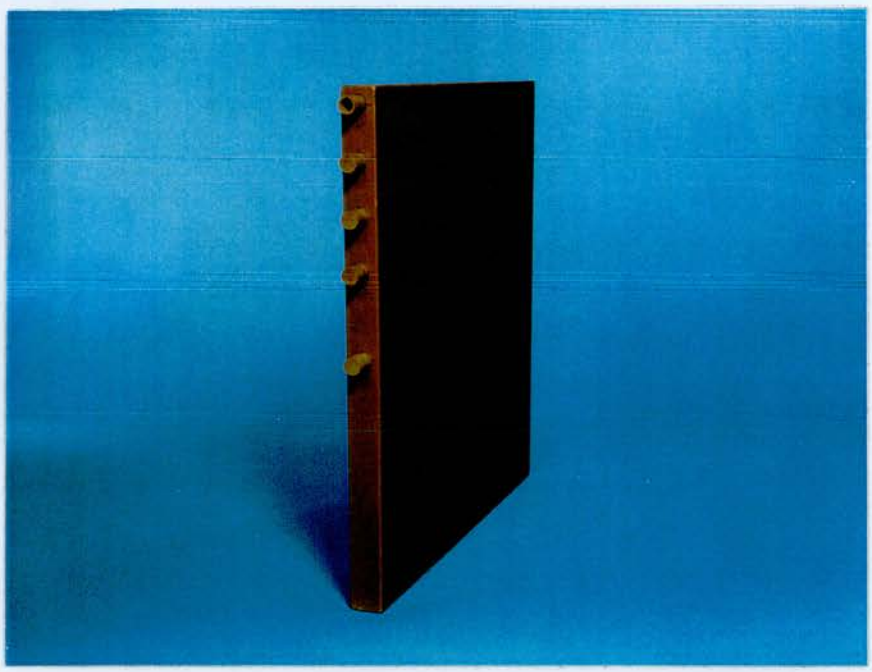

Fig. 8. 1c: Use of 'sheet' phantom to simulate small mini-phantom, by combining measurements in two situations.

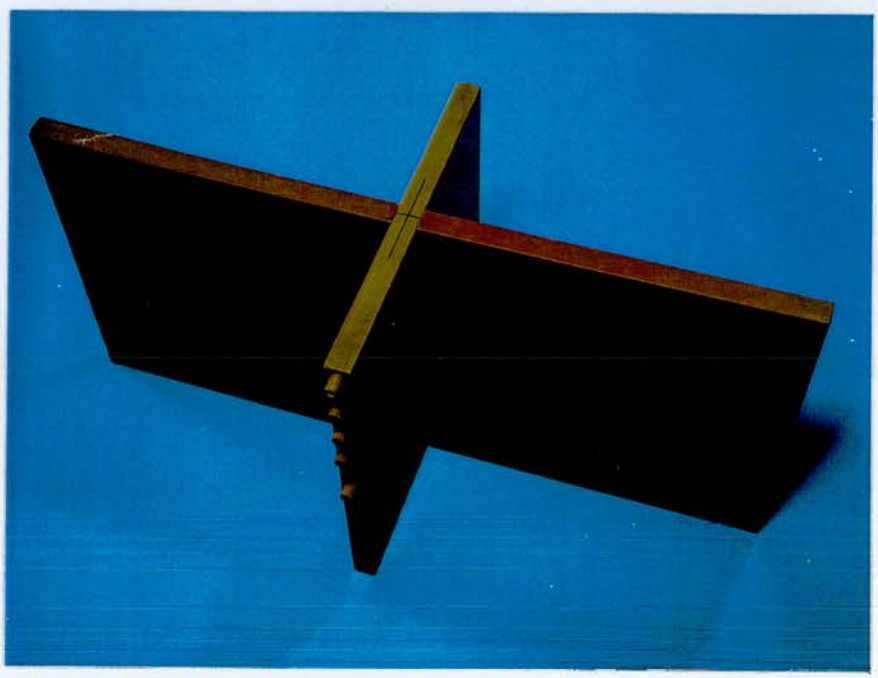

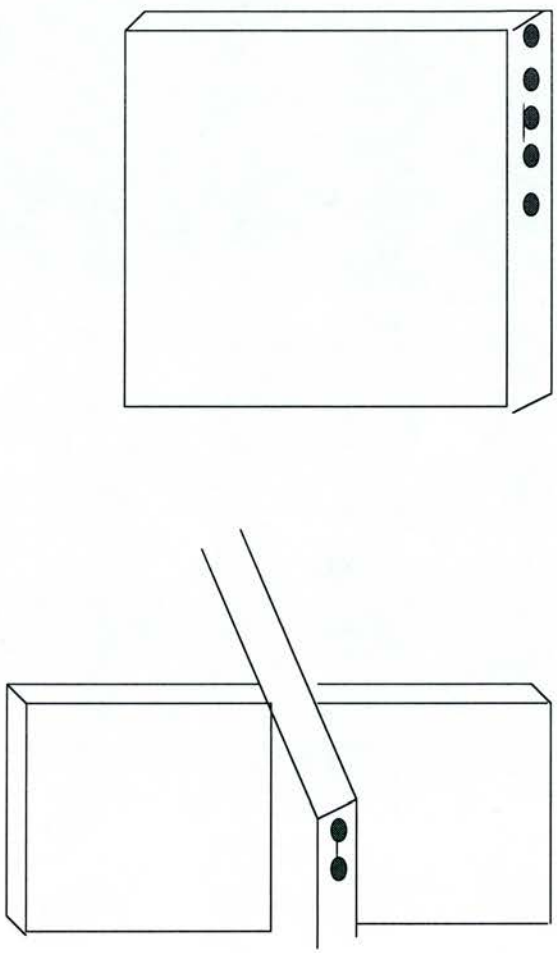

Fig. 8-1d: Schematic of "sheet" phantom to simulate mini-phantom,
by combining measurements in two situations

V-Uncertainties

Uncertainties for the measurements of head scatter factors are estimated at from 0.5% to 0.7% using caps and miniphantoms.

8-3-RESULTS

The measured head scatter factors, all normalised to a 10x10 cm field size, are illustrated in figures (8-2) to figures (8-7) for different plastic build up caps, brass caps and miniphantoms according to figure (8-1). These figures can indicate the effect of different thickness of caps in achieving electronic equilibrium in forward and lateral directions. Where the caps chosen were the standard range available in the department. All the results show that there are some significant differences between head scatter factors obtained with the different sidewall and top wall thickness caps. This is due to electron contaminants affecting measurements and to the lack of electronic equilibrium, particularly in too small thickness of caps. For example caps 6 and 8 (Fig. 8-3) and caps 10mm and E3 (Fig. 8-4) show the most marked differences to thicker caps. There were significant differences between head scatter factors obtained using the miniphantom and using thinner build up caps, because the measurements in miniphantoms are carried out beyond the range of electron contaminants. There was no significant difference between head scatter factors obtained by enough thickness of brass cap used as a brass miniphantom compared to the plastic miniphantom (Fig. 8-8). The end thickness of the brass cap can change from about 2cm to 8cm equivalent, this range of thickness is enough for 6MV photon beams (Fig. 8-8). According to Fig (8-8) there is no significant difference for different thicknesses of brass caps, because 2mm brass cap (1.7cm water equivalent) is enough to achieve electron equilibrium for 6 MV photon beam. Also

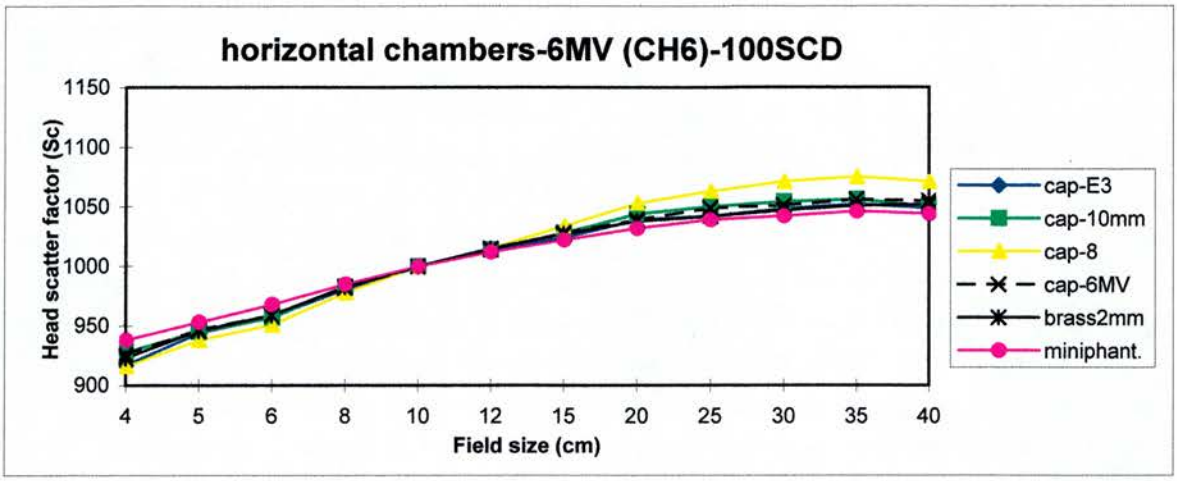

Fig. 8-2: Head scatter values for different horizontal caps and a miniphantom on 6MV (uncertainties on measured values are estimated at from (% to 0.7%, this applies to all subsequent figures up to Fig. 8-18)

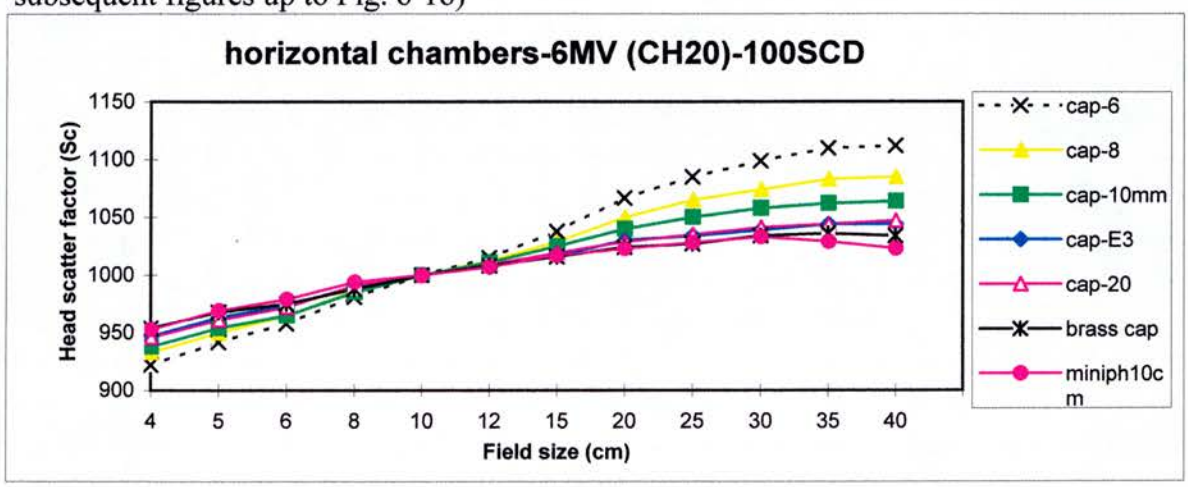

Fig. 8-3: Head scatter values for different horizontal caps on 6MV

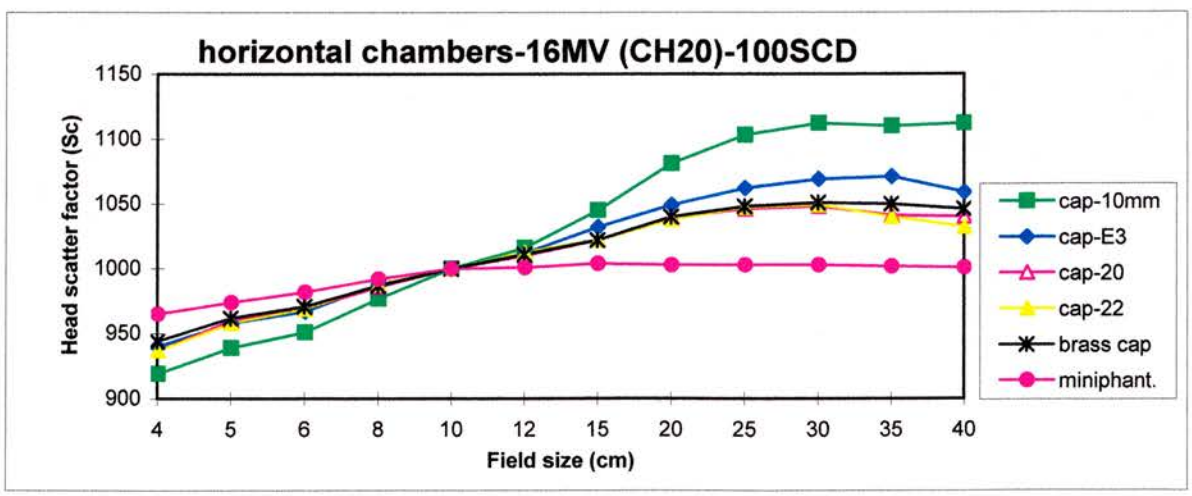

Fig. 8-4: Head scatter values for different horizontal caps and a miniphantom on 16MV

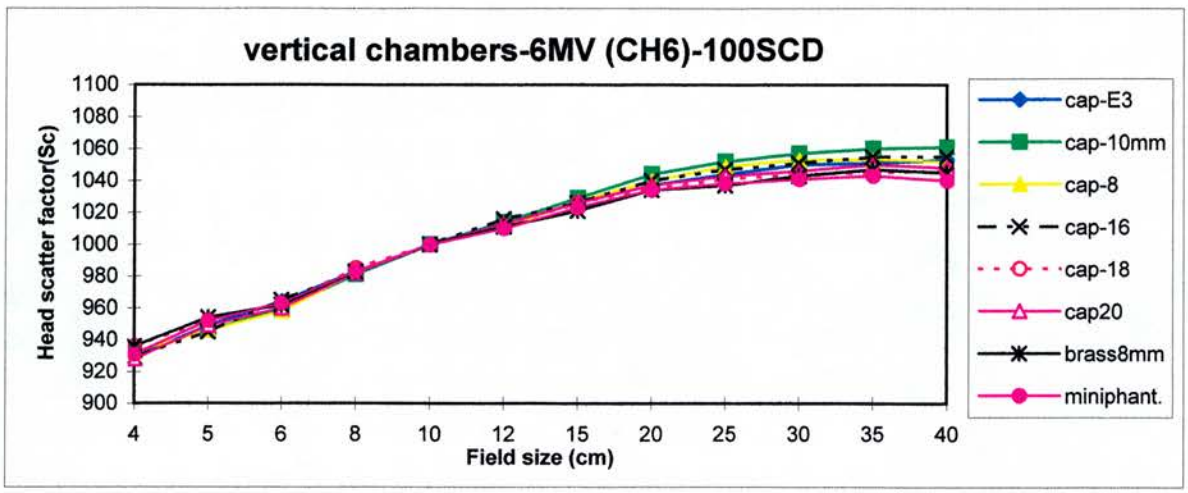

Fig. 8-5: Head scatter values for different vertical caps and a miniphantom on 6MV

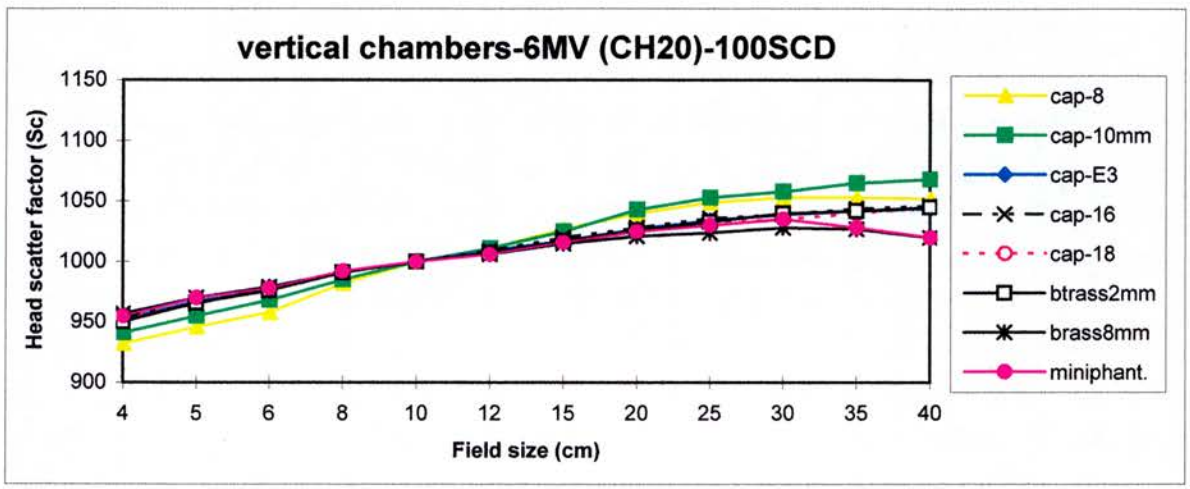

Fig. 8-6: Head scatter values for different caps and a miniphantom on 6MV vertically

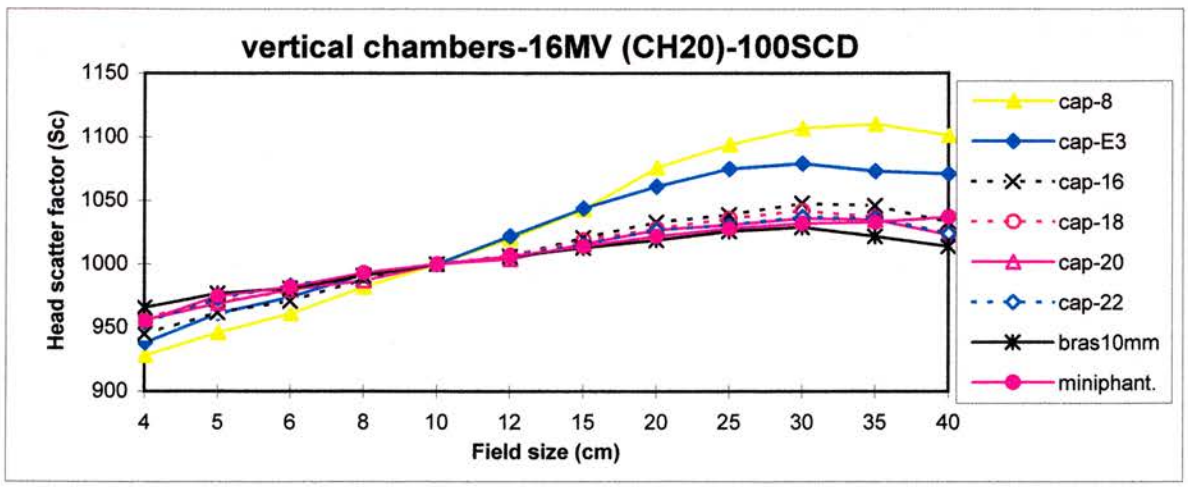

Fig. 8-7: Head scatter values for different caps and a miniphantom on 16MV vertically

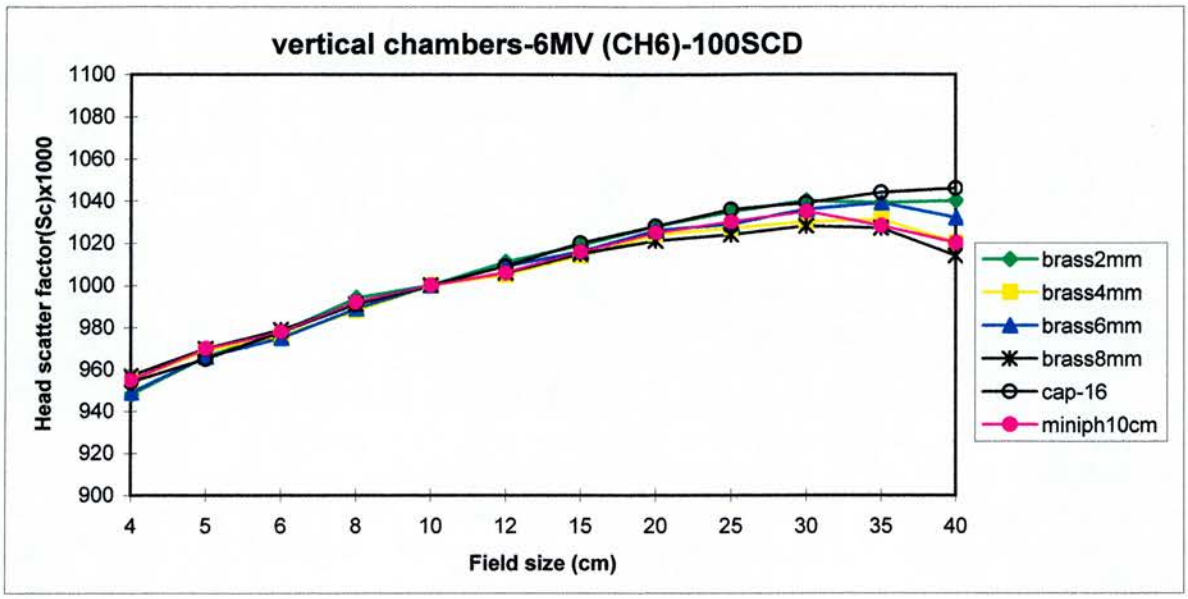

Fig. 8-8: Head scatter values for brass cap and miniphantom on 6MV photon beam

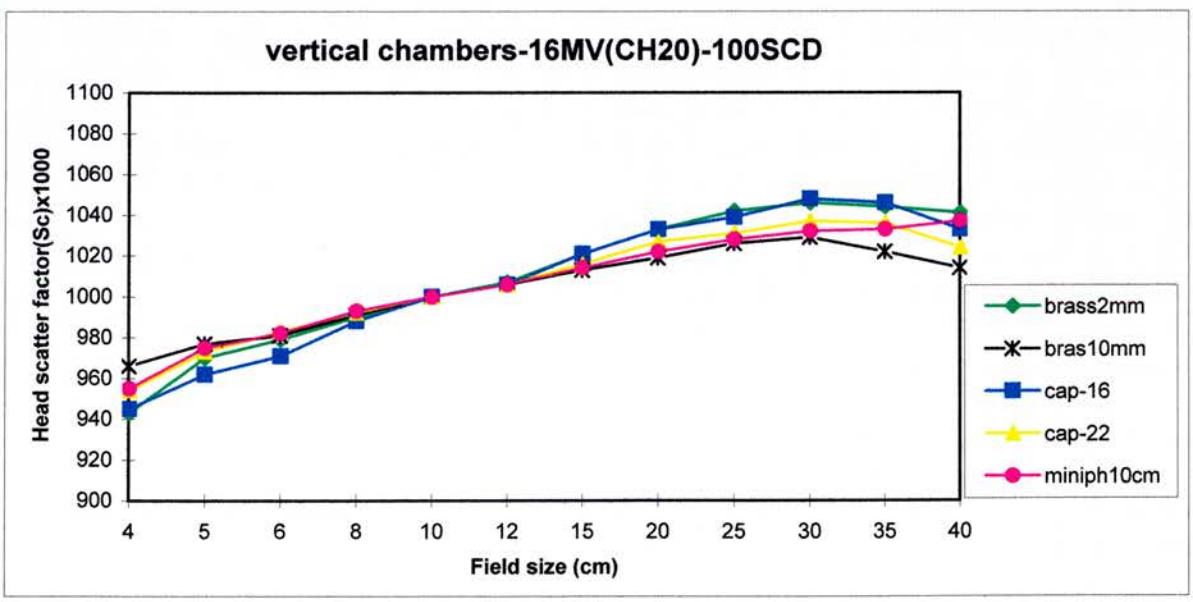

Fig. 8-9: Head scatter values for brass cap and miniphantom on 16MV photon beam

figures (8-8 and 8-9) show the head scatter factors measured using perspex caps which are the same as equivalent brass caps. However, a small thickness of brass cap e.g. 2mm is not enough for the 16MV photon beam, because the range of the most energetic electron contaminant is about 8cm (Fig. 8-9). So a 10cm equivalent depth is required to ensure the measurement point is beyond the largest ranges.

The influence of SSD or SCD on head scatter measurements with caps and miniphantoms were studied for 6MV and 16MV photon beams. The results obtained for 150SCD are shown in figures (8-10 to 8-12) comparing these to 100 SCD (Figs. 8-2 to 8-7), there was no significant difference between head scatter factors obtained for different distances. Similarly, the head scatter factors measured using caps showed some small differences, but not significantly, for 150SCD and 100SCD (Figs. 8-13 and 8-14). Also there was no observed significant difference between 100SSD and 100SCD head scatter measurements using the miniphantom (Fig 8-15).

For small field sizes (<4cm) the equilibrium mass (cap or miniphantom) is not fully covered by the fields at the 100SCD distance except for the brass cap. This means that the radiation did not cover the entire width of the caps (except brass cap) or miniphantoms which are constructed to these sizes to achieve electronic equilibrium. The plastic caps and miniphantoms are too large for these situations. Therefore, the measurements were carried out for all fields at 150SCD distance for build up caps (1.5 to 40 cm) and miniphantom (2.5 to 40 cm) to ensure they were fully covered. Figures (8-10 to 8-12) show the behaviour of the head scatter factors as a function of the field size. There was no significant difference between the head scatter obtained by the different caps used and the miniphantoms for small fields (1.5-4cm), according to figures (8-10 to 8-12). To display more clearly the differences between the head scatter factors measured using caps and using the miniphantom, the head scatter factors for small fields for the,

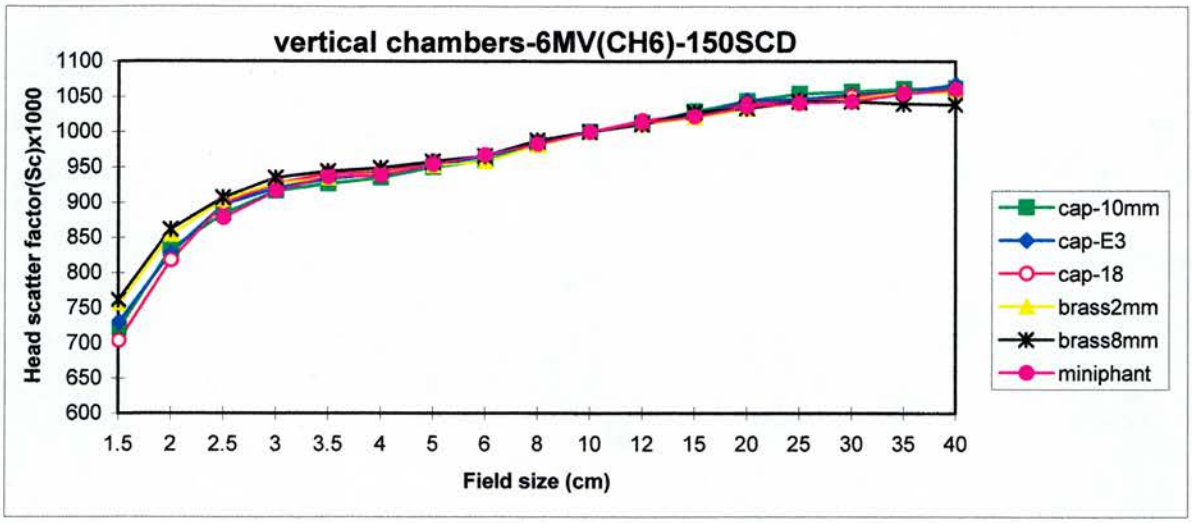

Fig. 8-10: Head scatter values for small ans large field sizes on 6MV photon beam

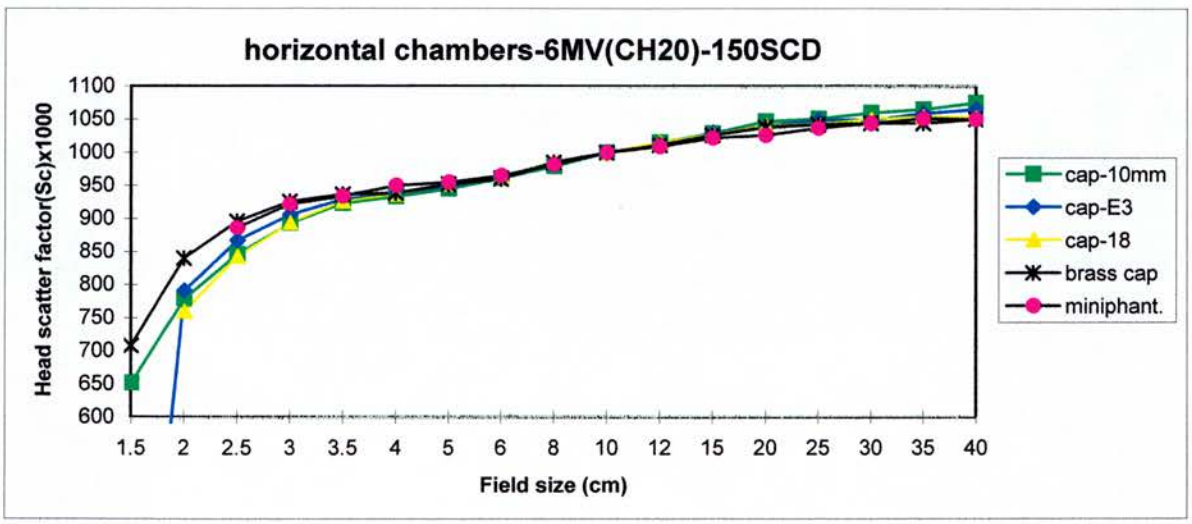

Fig. 8-11: Head scatter values for small and large field size on 6MV photon beam

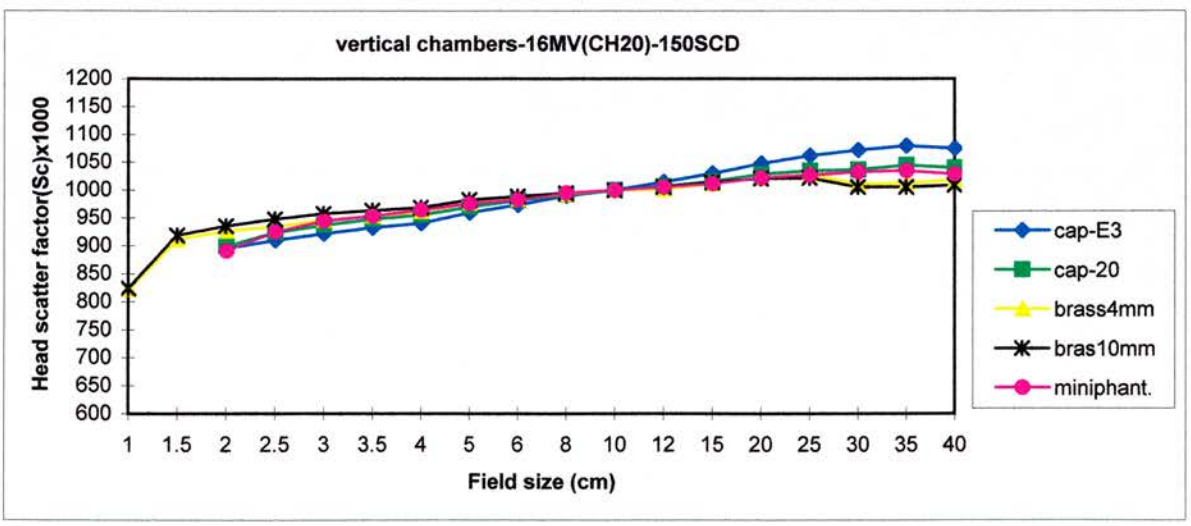

Fig. 8-12: Head scatter values for small and large field sizes on 16MV photon beam

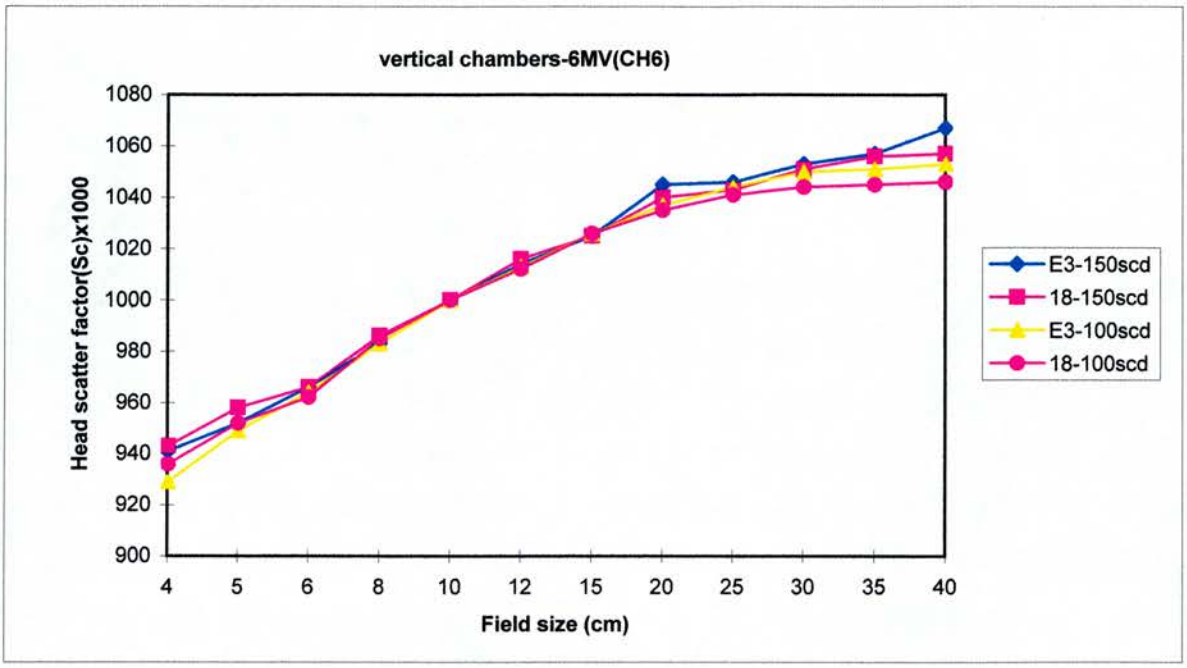

Fig. 8-13: The head scattervalues for 150SCD and100SCD on 6MV (CH6) photon beam

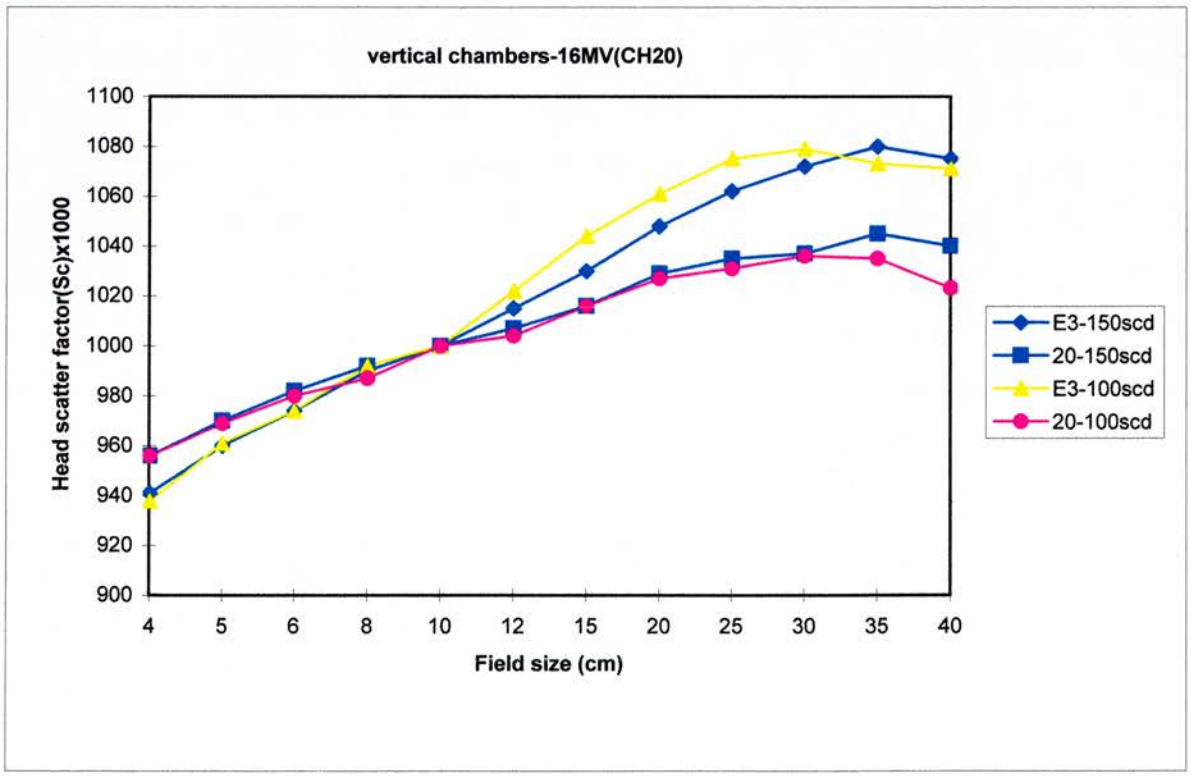

Fig. 8-14: The head scatter values for 150SCD and 100SCD on 16MV (CH20) photon bean

6MV beam, are displayed in larger scale in figure (8-16). The brass cap results showed that it was good enough to determine head scatter factors for small field sizes (down to 1cm) even at 100 SCD.

The influence of choice of reference depth relative to the range of possible electron contaminants on measurement of head scatter factors was studied for 6MV and 16MV photon beams at 5cm and 10cm depths. There was no significant difference for a change from 5cm to 10cm depths for 6MV photon beams, but there was a difference for 16MV photon beams (Figs. 8-17) although small. Therefore, a normalisation depth of 10cm would be sufficient for higher energy photon beams (at least up to 16MV beam in this department).

Fig. (8-18) compares the head scatter factors for the "6MV" cap and the epoxy cap with similar front wall (2cm), but thinner side walls (1cm rather than 2cm). There was no difference between them. This shows that the lateral electronic equilibrium can be achieved in a smaller thickness than the forward electronic equilibrium thickness. Therefore lateral electron equilibrium may not be too critical in these measurements.

Figure (8-19) compares the head scatter factors between the sheet phantom (2x2cm effective cross area) and the miniphantom (4cm diameter) for 6MV (CH6) and 6MV (Varian) photon beams at 10cm depth and 100cm SCD for field sizes 4x4 to 40x40. The results show that the sheet phantom with smaller effective diameter than the miniphantom can be used for head scatter factor measurements which agree were at field sizes where both can be used with those measured with a 'standard' miniphantom of greater width, giving confidence for its use at smaller field sizes. The agreement between the sheet phantom and the miniphantom is better for the newer Varian accelerator, reflecting the fact that this machine is very stable measurement to

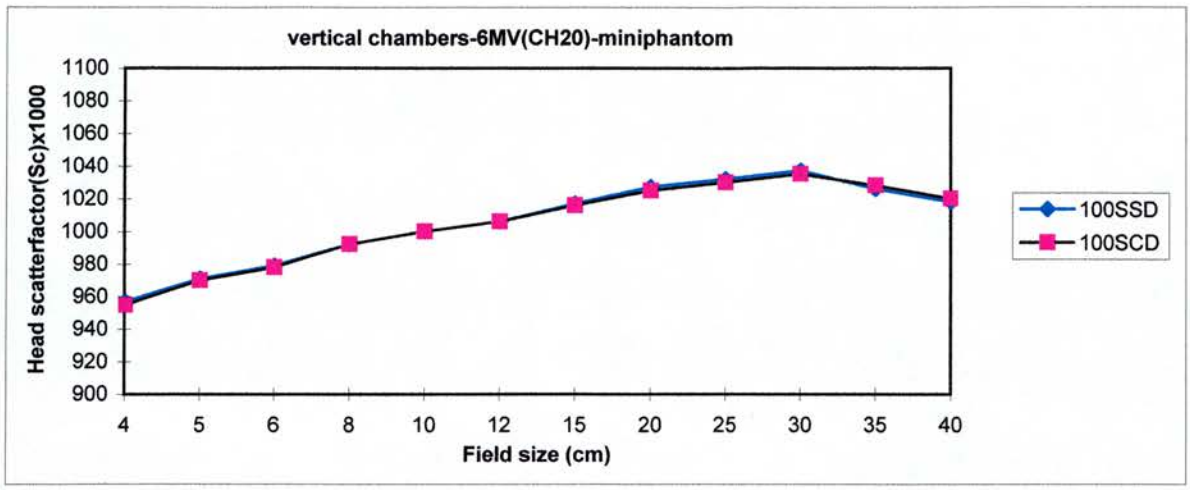

Fig. 8-15: Comparison of Sc values between SSD method and isocentre method

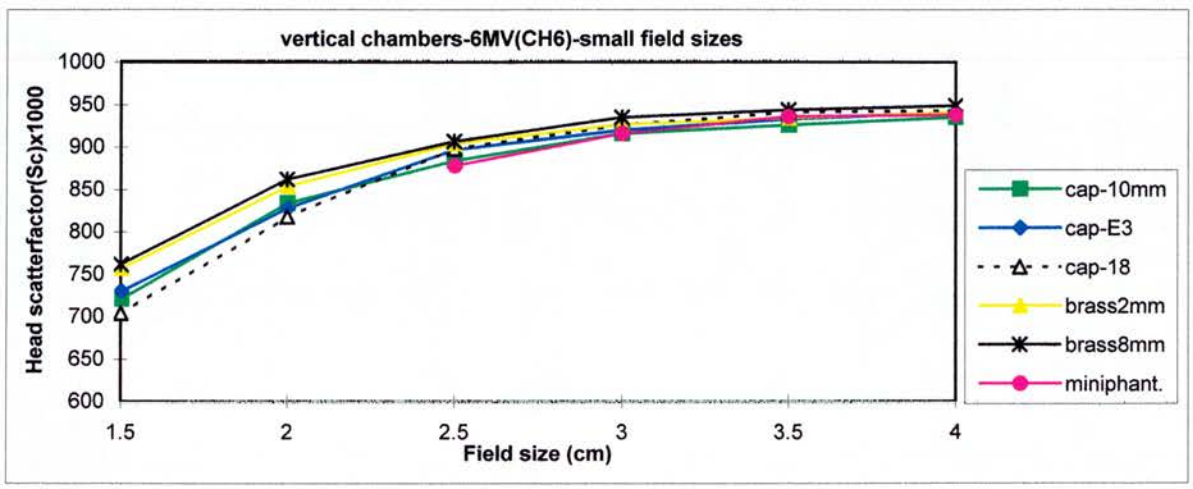

Fig. 8-16: Comparison of Sc values between brass cap and miniphantom

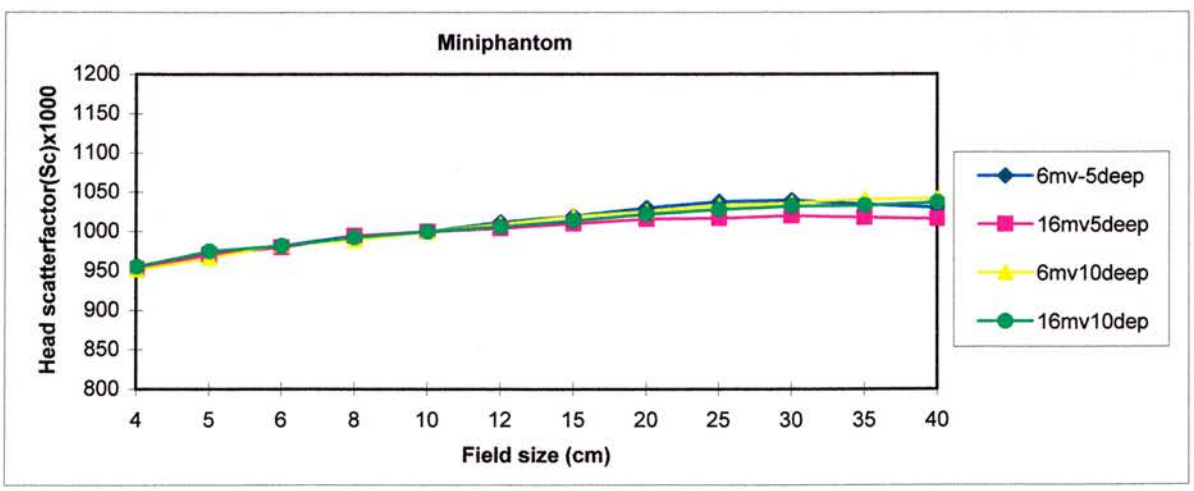

Fig. 8-17: Comparison of Sc values between different depths for different energy

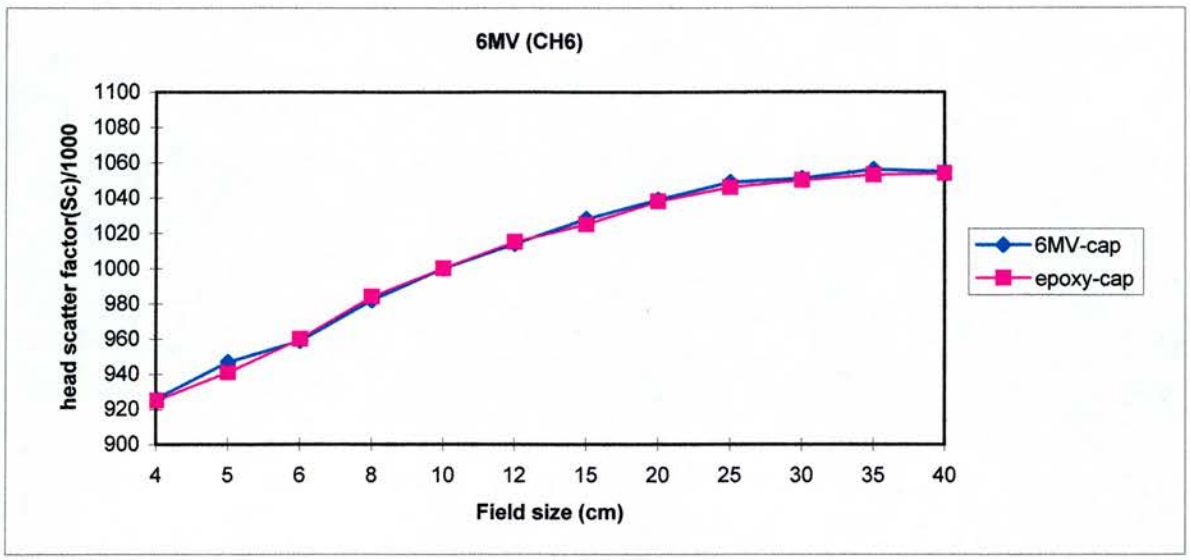

Fig. 8-18: Comparison of Sc values between 6MV-cap and epoxy-cap on 100SCD

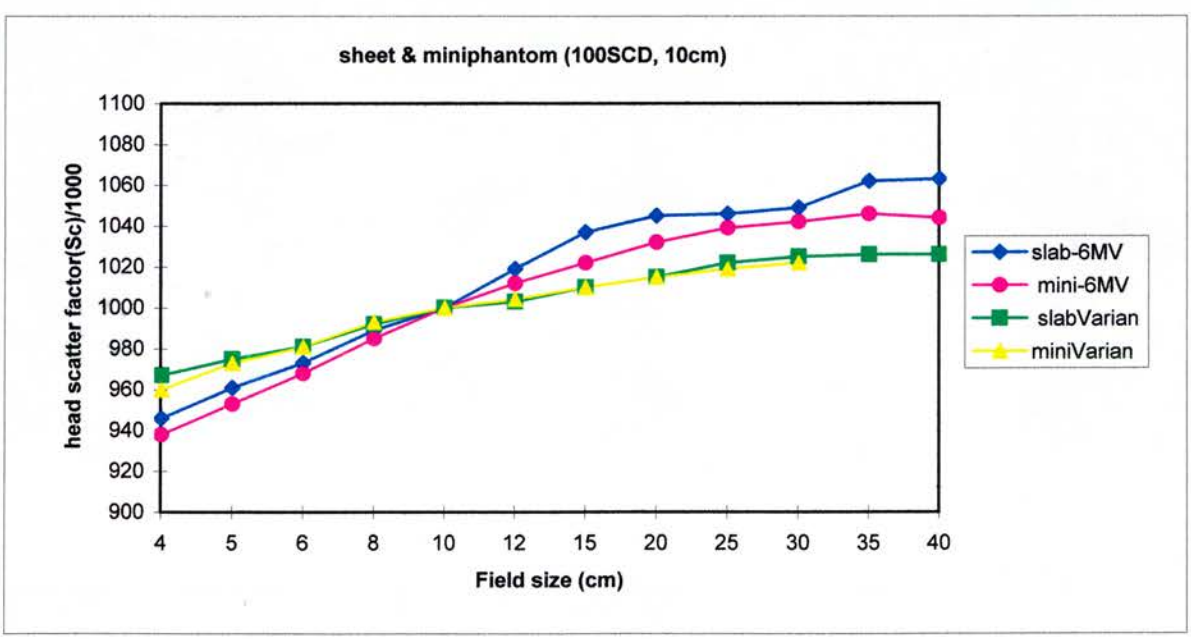

Fig. 8-19: Comparison Sc values between sheet phantom and miniphantom for 6MV (CH6) and 6MV (Varian) photon beams at 10cm depth and 100SCD

measurement. Because the sheet phantom approach requires two sets of measurements and subtraction of differences it has larger uncertainties which are effected by the particular machine stability.

8-4-Discussion

-Electron equilibrium

To study the effects of electron equilibrium and electron contaminants, measurements were carried out with several plastic build-up caps, with brass cap and with two miniphantoms for a range of 6 and 16 MV photon beams according to figure (8-1) and Table (8-I). According to figures (8-2 to 8-7) forward and lateral electron equilibrium can be achieved when the radius of the cap or 'front' thickness and radius of the miniphantom is large enough. The head scatter measurements against field size for caps 6, 8, 10mm (for 6MV photon beams) and caps 8, 10mm, E3 (for 16MV photon beams) show significant differences to measurement with large front wall thickness (t) and end wall thickness (d) of caps. The reason is that the radius and top wall thickness of these caps are not large enough to absorb contaminant electrons or to produce electronic equilibrium. For front wall, forward electron equilibrium is expected to be achieved when cap thickness is equivalent to d_{max} thickness, but for lateral electronic equilibrium the diameter of cap or miniphantom can be smaller than d_{max}. Recently Li et al (1995) studied the effects of lateral electron equilibrium (see chapter 7). They obtained the minimum beam radius required to achieve lateral electron equilibrium using EGS4 Monte Carlo simulation. They reported that the radii of electron equilibrium values have a linear relationship with the TPR^{20}_{10} values, according to equation (7-11). Based on this, the radius of lateral electron equilibrium values for the two beams investigated, 6MV and 16MV photon beams, is 1.4cm and 1.9cm, respectively. It can be seen that lateral electron equilibrium can be achieved in a smaller thickness than the range of

secondary electrons or of dose build up depth. This idea is useful to choose as small as possible side dimension of caps or lateral diameter of miniphantom. As discussed before the mass of cap or miniphantom can produce unwanted scatter, particularly for small field sizes. This can change the measured head scatter factors and therefore the derived phantom scatter factors. Therefore minimising the lateral dimensions is desirable. As an illustration of side wall differences Fig. (8-18) shows head scatter factors on the CH6 x-ray beam for the epoxy "cap" which has 2cm equivalent front wall build up, but 10mm equivalent side wall, compared to the cylindrical perspex cap "6MV" which has approximately 2cm thickness in all radial directions. There are no significant differences in the factors, indicating that the side wall thickness is not critical in measurement of head scatter factors, at least down to 1cm for 6MV.

-Sheet phantom method

Also Figure (8-19) shows no significant differences between head scatter factors obtained using the sheet phantom and the miniphantom. There are some small differences for the 6MV (CH6) photon beam, but given that the uncertainties increase with this method, these are not significant. This also illustrates the need to choose as small as possible dimensions of cap or miniphantom to remove the unwanted scatter due to the mass of material present. In addition this method is useful to check the determination of head scatter factors for small field sizes.

-Contaminant electrons; depth of measurement

The main reason for significant differences in the values of the head scatter factors obtained (Figs. 8-2 to 8-7) is due to the contaminant electrons generated outside the caps, for caps which are too thin as discussed above. Thomadson et al (1993) showed that contaminant electrons for high energy photon beams reach beyond the depth of dose

maximum and therefore recent recommendations are tending towards greater reference depths. Therefore, miniphantoms as described by Van Gasteren et al (1991) with depth of at least twice d_{max} thickness (Frye et al 1994) are needed to absorb contaminant electrons and make measurements independent of this. Alternatively the effect of contaminant electrons can be reduced by setting a 1.0mm thick lead filter below the linac head to remove such contaminants by attenuation, without noticeable changes in the photon beam quality (Sjogren and Karlsson 1996). It has been shown by these authors and other (Ling and Biggs 1979, Sjogren and Karlsson 1996) that the best position for a lead filter is between the upper and lower collimators. They found that electron contamination increased when the distance between the lead filter and the phantom surface decreased due to the fact that the lead filter has a dual effect on the one hand it acts as an absorber of secondary electrons and on the other hand it acts as an extended electron source closer to the patient with a strong SSD dependence of the electron contamination. Therefore, positioning between the upper and lower jaws is a good compromise considering both effects.

The head scatter factors measured with plastic miniphantoms and brass cap "miniphantom" (Figs 8-2 to 8-7) showed significant differences to thinner plastic build up caps as they removed contaminant electrons. This effect is clearer for the higher energy, 16MV, photon beam (Figs. 8-4 and 8-7). The top (end) thickness of the brass cap can be changed from 2cm to 8cm water/plastic equivalent, and whilst this is enough to use for the range of contaminant electrons in 6MV photon beams (Fig. 8-8), is not quite enough for 16MV photon beams. However there is little difference between head scatter factors obtained by the brass cap used as a brass miniphantom and the plastic miniphantom according to figure (8-9). In general there are not large differences between thicker (thick enough to give electronic equilibrium) buildup caps and miniphantoms, although this is less true for 16MV than for 6MV.

-SSD; small field sizes

The influence of SSD on head scatter factor measurements by caps or miniphantoms showed that the head scatter is almost independent of SSD. This can be seen by comparison between figures (8-10 to 8-12) with figures (8-5, 8-2, and 8-7), respectively. There were no significant differences between distances 150 SCD and 100 SCD (Figs. 8-13 and 8-14). Therefore, head scatter must be a fairly uniform distribution, or the largest effects are on the monitor chamber response. Also figure (8-15) shows that there were no differences between head scatter obtained by 100 SCD and 100 SSD distances. The head scatter measurements at the 100 SCD did not cover the entire caps (except brass cap) and miniphantoms for small field sizes. To consider further this problem, measurements were carried out for all fields at 150SCD distance for build up caps (1.5 to 40 cm) and miniphantom (2.5 to 40 cm) in order to give complete coverage. Figures (8-10 to 8-12) show the behaviour of the head scatter factors as a function of the field size. According to these figures the head scatter factors for small field sizes (1.5-4cm) drop sharply. This can be correlated to the effective source size, where the entire source is no longer seen from the measurement point, and also backscattered radiation from the collimators into the monitor chamber is larger for small field sizes. At the same time, for small field sizes electron contaminant effects are small or absent. However some of the steeper fall using horizontal chambers (Fig. 8-11) may be due to the chamber becoming large relative to the smaller field sizes (<2cm) resulting the whole chamber not being fully irradiated. At 150cm SCD a 2cm field size setting produces a 3cm (50% width) field size, but the chamber length is approximately 10mm meaning that is all in the field, but may be beginning to experience varying profile values along its length. The brass cap was good enough to determine head scatter factors for small field sizes (>1cm), according to figure (8-16) but the geometry must use vertical chambers to avoid the chamber size problem noted above. The use of either higher density (e.g. brass) cap, or longer distances, or the combination of both is shown to allow measurements to be readily extended to small field sizes. Any of these must be tied to standard measurements by overlapping the measurement range. The new method to effectively

achieve smaller miniphantoms can also be used for smaller field sizes, but still has the problem of detector size for the situation described, which used a horizontal ionisation chamber.

-Depth

Based on these measurements of Sc against field size, electron contaminants are shown to be field size dependent. For small field sizes (<10cm), the effects of contaminant electrons are smaller than for the normalisation field value according to equation (8-1), therefore the apparent head scatter factor is decreased. For larger field sizes contaminant electrons are more significant for the numerator of the ratio in equation (8-1) than the denominator, therefore head scatter is increased.

$$S_c = D_0(z_r, c)/D_0(z_r, c_r) \qquad \text{Eq. (8-1)}$$

where z_r, c_r are reference depth and reference collimator setting respectively, D_0 is absorbed dose in air. However, with the exclusion of the contaminant electrons for large fields using measurement systems putting the chamber beyond the range of electron contamination, the measured head scatter factors are reduced at larger field sizes (increased at smaller). These are the best estimate of true head scatter factors.

From the results it can be concluded that the main reason for errors introduced to Sc values is due to contaminant electrons from the head of the machine. The head scatter measurements obtained here showed that contaminant electrons can be absorbed by a sufficiently large thickness of cap wall or by using a miniphantom. To avoid the influence of contaminant electrons on head scatter measurements, depths of 5cm and 10cm were sufficient for 6MV and 16MV photon beams, respectively. The depth of dose maximum in build up caps is typically not suitable due to possible remaining variation of contaminant electron effects as illustrated in figures (8-2 to 8-7 and 8-10 to 8-12). Figure (8-17) shows the influence of depth beyond the contaminant electron

range on measurement of head scatter for 6MV and 16MV photon beams at 5cm and 10cm depths, respectively. There was no significant difference for a change from 5cm to 10cm depths for 6MV photon beams. However, a small difference was observed for 16 MV photon beams (Fig. 8-17). This indicates that as expected a 5cm depth is strictly not enough for higher energy photon beams. Therefore, a normalisation depth of 10cm would be appropriate for high energy photon beams. This is in agreement with recommendations of some dosimetry protocols (IAEA 1987). IAEA (1987) recommends a reference depth of 5cm for lower energy photon beams (Quality index<0.7) and 10cm depth for higher energy photon beams (Quality index>0.7). In comparison the most recent UK recommendations (IPSM now IPEM 1990) recommend 5cm up to QI= 0.75 and 7cm for QI= 0.75-0.81. Recently an ESTRO working party (1997) has recommended a reference and normalisation depth of 10cm, for all photon beam qualities (^{60}Co to 50MV). The head scatter measurements here have confirmed this depth at least up to 16 MV (QI= 0.765). The depth of 10cm may also give only minor errors at 50MV photon beams (Sjogren et al 1997).

Therefore, ideally separation of the field size dependent total scatter factor into a collimator scatter factor and a phantom scatter factor should be carried out beyond the depth of maximum by a miniphantom. This requires normalisation of all dosimetry procedures to a reference depth of 10cm and the use of TPR_s, etc. The accuracy of monitor unit determination or of the calculations of dose delivery to the patient can be significantly influenced by the determination of head scatter. This becomes more important where the standard collimator setting and field size on the phantom surface differ e.g. wedged beams, blocked fields, irregular and MLC fields. These aspects will be considered in the next chapter for symmetric, asymmetric, wedged, blocked, irregular and MLC fields by separation of total scatter factor into head scatter factor and phantom scatter factor for each case, to assess calculation uncertainties in treatment planning systems and treatment planning measurements.

8-5: Conclusions

The mass of buildup cap or miniphantom can produce unwanted scatter, particularly for small field sizes. Therefore, it is suggested to use as small as possible lateral dimensions of caps or miniphantom for measurement of head scatter factors. The measurements support equation (7-10), to obtain the minimum beam radius required to achieve lateral electron equilibrium. The measurements, however, imply that even thinner side walls can be used without problems. The front wall thickness needs to be at least equivalent to buildup depth. However this thickness is smaller than the range of the most energetic secondary electrons. Therefore, this is typically not sufficient to put the measured head scatter factors beyond the influence of contaminant electrons. Therefore, greater reference depths are recommended for head scatter factors not to be influenced by these effects, although thick enough buildup caps also give reasonable agreement with miniphantoms particularly at lower energies. Head scatter factors do not appear to depend on distance (at least from 100 to 150cm). Therefore, longer distances can be used to make smaller collimator setting measurements.

The miniphantom is a reliable and simple tool to measure and describe complex head scatter factors. For small field sizes (down to 1cm) the brass cap can be used as a miniphantom as long as it is normalised to plastic miniphantoms or caps at field sizes where both are appropriate (e.g. 10x10) and as long as vertical chambers are used for the smallest field sizes. These extensive measurements conclude that reference depths of 5cm and 10cm are appropriate for determination of head scatter factors. These depths are good enough to avoid contaminant electrons for lower energy and typical higher energy beams respectively. For a single depth, 10cm would have to be used. Head scatter factors will be strongly dependent on the machine head design and for a given

machine with different energies may them be dependent on energy, due to head changes as energy is changed as well as different scatter and interactions. Therefore no single sets of head scatter factors are appropriate. Best results for head scatter factors for standard fields at depths of 5cm and 10cm for the machines and different energy photon beams studied here are summarised in the next chapter for the derivation of phantom scatter factors.

The sheet phantom is a useful new method for determination of head scatter factors to obtain as small as possible the effect of scatter due to the mass of material present on the results and is useful for small field sizes. However it has increased uncertainties and it may need to be modified in terms of geometry (vertical chamber) or size of detector to be applicable to the smallest field sizes. The results suggest that using a 2x2 cm^2 miniphantom with a vertical chamber position will be useful for small field sizes.

Chapter 9

"Monitor Unit Calculation for High Energy Photon Beams"

9-Measurement and Calculation of Output Factors in air and in phantom and the evaluation of phantom scatter for symmetric, asymmetric, wedged, blocked, irregular and MLC fields

9-1-Introduction

Monitor unit calculation is a very important step in order to provide accurate dose delivered to the patient. The accuracy of monitor unit determination for dosimetry calculation can be significantly influenced by the determination of head scatter and phantom scatter. This becomes more important where the collimator setting and field size on phantom surface differ or where the beam distribution is altered from the standard e.g. wedged beams, blocked fields, irregular and MLC fields. The separation of total scatter factor into head scatter factor and phantom scatter factor was reviewed in chapter (7). Different methods to obtain head scatter measurements were compared in the previous chapter (8). The head scatter factors measured by using miniphantoms avoids the problem of contaminant electrons but their use must be in a system where other parameters are normalised in the same way. This chapter concentrates on the results obtained by separating total scatter factor into head scatter factor and phantom scatter factor for open and wedged beams, blocked field, MLC and irregular fields for both D_{max}-based systems and also at 5 and 10 cm. The output factors obtained in air and in phantom are investigated and compared to those used in the standard in-house treatment planning calculation approach and other approaches.

9-2-Experimental Methods

9-2-1-Open Field

The previous chapter showed the results of head scatter factor measurements for field sizes from 4x4 to 40x40 cm obtained by using miniphantoms and build up caps and indicated the optimum measurement conditions and values. The total scatter factors ($S_{c,p}$) were measured in a full scatter RMI epoxy resin water equivalent phantom, 30cmx30cm, at the different depths of interest i.e. the depth of maximum dose, 5cm and 10cm depths. Phantom scatter factors were then determined according to equation (7-9). All measurements were carried out in photon beams of 6MV (QI = 0.665 and QI = 0.680) and 16MV (QI = 0.765), using a PTW 0.1cc ionisation chamber. All subsequent factors in other measurement situations were measured in the same way. Estimated uncertainties on relative head scatter and total scatter factors are in the range 0.5%-0.7%, and for phantom scatter factors is 0.7-1.0%. This applies for these open field values and all the subsequent measurements described below.

9-2-2-Rectangular Fields

The total scatter factors and the head scatter factors for rectangular fields were measured on the same 6MV (CH6 and CH20) and 16MV photon beams using the RMI phantom, the miniphantom and the brass cap. The field size setting ranged from 4x40 to 40x4 cm. Firstly the upper collimator was fixed at 4cm width while the lower collimator was varied, and then the lower collimator was fixed at 4cm width while the upper collimator was varied. The head scatter values of these two sets of jaws setting were tested to investigate any differences (exchange effect).

9-2-3-Wedged Beam

For wedged beams, measurements were carried out on the same two accelerators with 6MV and 16MV photon beams. The wedge angle for both accelerators was 60° using the single motorised wedge for each. The variation of output with field size was measured in both air and phantom at 100cm SCD. The maximum field size for the wedged beam was 20x20, therefore the output factors were obtained for field sizes from 4x4 to 20x20 cm. The output factors in air and in phantom were measured using caps or miniphantoms and solid RMI phantom, respectively. The measured output factors were normalised to the 10x10 cm wedged field size. All other conditions of measurement were similar to those used for open fields. Thus, the variations observed in the open field due to flattening filter, collimator effects etc are excluded in the variations of wedge factors (W.F.). The observed variations are only due to wedge effects. This factor is a function of field size. It can be obtained from a ratio of the dose measured in a miniphantom or phantom at isocentre with and without the wedge for the same number of monitor units.

Phantom scatter factors were determined from total scatter factors and head scatter factors in a similar way to those for open fields according to equation (7-9).

9-2-4-Asymmetric fields

Output measurements were carried out for asymmetric fields for 6MV and 16MV photon beams. This work utilised accelerators with four independent jaws such that the jaws (x and y) can be moved independently making it possible to get asymmetrical fields. Measurements were carried out for two conditions, asymmetry along the x-axis and along the y-axis. At the first step one jaw from the x-jaws was kept constant at 4cm from the central axis, the other jaw setting was varied from 2 to 19cm, and the y-jaws were varied symmetrically such that the total y dimension was the same as the total x

dimension e.g. if x_1 and x_2 were set at 4cm and 2cm then y was set to be symmetric 6cm field. At the second step one jaw from the y-jaws was kept constant at 4cm, the other jaw setting was varied from 2 to 19cm, whilst the x-jaws were varied symmetrically. In order to assess the output variation with collimator positions, measurements were performed in air using a miniphantom at depth 10cm. The total scatter factor was obtained using the RMI phantom, 30x30 cm in size. All asymmetric field measurements were taken with the chamber on the normal field central axis (CAX).

The head scatter factors and total scatter factors also were measured for wedged asymmetric beams. A method was proposed and tested to calculate asymmetric output factors (see 9-2-7).

9-2-5-Conformal Blocked Fields

Some irregular conformal shaped fields for prostate and bladder patients are produced clinically using individually constructed blocks. All blocks were of 7.5 cm height placed on the standard tray. A number of these were selected from those being used for patients and measurements were carried out under them. Output factors for blocked fields in air and in phantom were measured for varying collimator settings using a build up cap, a miniphantom and the RMI phantom at the depths of dose maximum and 10 cm. To investigate the effect of blocks which may modify the head scatter but which may also present additional block scatter components (Van Dam et al 1992_b), different area blocks were irradiated.

All field size factors were normalised to a standard 10x10 field size, taken whilst the same tray as for the blocked field was still in the beam. In this way the effect of the tray, without correction factor, can be eliminated. The measured values were compared to calculated values (see 9-2-7).

9-2-6-Multileaf Collimator (MLC) Fields

Output factors were considered for regular and irregular fields set up on an MLC (Varian 600). The MLC consisted of 40 pairs of leaves where each leaf provided a 1-cm-wide projection at isocentre. The maximum field size used was 28x28cm. The leaves are arranged in two opposed leaf banks, A and B, below and moving in parallel with the X collimator jaws. The influence of the leaves on the output ratio was considered. The output factors in air and in phantom were measured for a series of square and rectangular fields using a build up cap, a miniphantom and the RMI phantom, 30cmx30cm, for 6MV photon beams (QI = 0.665).

To test the behaviour of the output factor for MLC irregular fields, the four corners of square fields set by the main photon jaws were blocked by MLC leaves. This reduced the field area to approximately 50% of the area set by the collimator jaws. The measured values were compared to calculated values (see 9-2-7).

9-2-7-Calculated prediction of factors

1.Asymmetric fields

For the standard in house planning approach output factors are taken to be the same as for the equivalent symmetric field. Here a method was used to calculate asymmetric output factors taking into account the changes introduced by asymmetric collimator positions (Rosenburg et al 1995). On the beam axis, the head scatter factor can be calculated for an arbitrary rectangular field that is given by the average of the value derived at the centre of the corresponding symmetrical fields according to equations (9-1 and 9-2) where the parameters are illustrated on the following diagram:

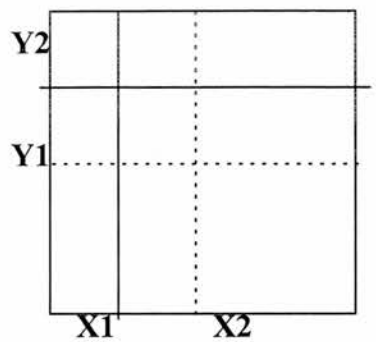

For asymmetry along the x-axis this is

$$S_c = 1/2\ S_c\ (2X1 \times 2Y) + 1/2\ S_c\ (2X2 \times 2Y) \qquad \text{eq. (9-1)}$$

where Y is assumed symmetric (field size 2Y) and for asymmetry along the y-axis it is

$$S_c = 1/2\ S_c\ (2Y1 \times 2X) + 1/2\ S_c\ (2Y2 \times 2X) \qquad \text{eq. (9-2)}$$

where X is assumed symmetric (field size2X). For a field asymmetric in both directions this extends to

$$S_c = 1/4\ S_c\ (2X1 \times 2Y) + 1/4\ S_c\ (2X2 \times 2Y) + 1/4\ S_c\ (2Y1 \times 2X) + 1/4\ S_c\ (2Y2 \times 2X)$$

Then phantom scatter factors are taken to be the same as for the same area symmetric field (see later) and total scatter factors (output factors) can be obtained by the combination of the S_c and S_p. Alternatively Sc,p can be obtained using a similar formalism to equations 9-1 and 9-2.

2.Conformal blocked field

For conformal blocked fields the measured total output factors were compared with calculated values from the standard in-house treatment planning approach and also to an approach which separates the head and phantom scatter components as equation (9-3).

$$D(FS) = MU \times OF(CS) \times [S_p(FS) / S_p(CS)] \quad \text{eq. (9-3a)}$$

or $$Sc,p = S_c(CS) \times S_p(FS) \quad \text{eq. (9-3b)}$$

where CS was the side of the equivalent square field determined from the collimator setting L and W by CS = 2LW / (L+W), FS was the length of the side of a square area equivalent to the blocked field. The output factor of the field defined by the collimator setting was OF (CS), and MU was monitor units set. The ratio of $[S_p(FS) / S_p(CS)]$ is the ratio of phantom scatter factor for the effective field size of the blocked field with size FS to the phantom scatter factor for the field defined by the jaws, CS. If the measurement is carried out at depth of dose maximum, the phantom scatter factor is the peak scatter factor. The assumption here is that the block does not change the head scatter factor significantly (see later).

3.MLC Field

The measured dose per monitor unit at the depth of maximum dose was compared with calculated values from the standard in-house treatment planning approach which uses values for the equivalent standard field, and with an approach as in equation (9-3) for MLC fields. The absorbed dose at the depth of 5cm and 10cm for different field sizes was compared with calculated values.

The standard in-house treatment planning approach for different situations is summarised as below:

-all data normalised to d_{max} measurements;

-all standard planning data (for output factors, wedge factors, tray factors and etc.) measured at d_{max};

-percentage depth dose used (normalised to d_{max});

-for rectangular fields, equivalent area used;

-for irregular fields, actual irradiated area used for output factors (but wedge factor from collimator setting);

-asymmetric field, use equivalent area as though the field is symmetric (with wedge factor for the actual asymmetric field).

9-3-Measurements and Calculations and comparison of factors: Results

9-3-1-Open Fields (symmetric)

9-3-1-1-Square Fields

Figures (9-1a to 9-1c and Table 9-I), (9-2a to 9-2c and Table 9-II) and (9-3a to 9-3c and Table 9-IIIa,b,c) show the total scatter factors, head scatter factors and phantom scatter factors, respectively, for depths of dose maximum, 5cm and 10cm. The larger spread of results between the machines for S_c at the depth of dose maximum (Fig. 9-2a) as compared to the miniphantom measurements may be due to the greater influence of contaminant electrons at this depth. The differences at larger depths for different accelerators are because of differences in head design. This was also observed by Kase and Svensson (1986), Luxton and Astrahan (1988), and Van Gasteren et al (1991). There are small differences for head scatter obtained at d_{max} for 6MV and 16MV photon beams produced in one machine with the same head design except for target and flattening filters (Fig. 9-2a). There are no differences between these two curves at depth 10cm (Fig. 9-2c), where contaminant electrons are absorbed. Figures (9-1a to 9-1c and Table 9-I) show the differences obtained for total scatter factor ($S_{c,p}$) for different machines.

Phantom scatter is defined only by the area of the phantom being irradiated and should be independent of the collimators used to define the field size. The results of this work confirmed the expected variations of the phantom scatter factors with beam quality and depths according to figures (9-3a to 9-3c). The results of phantom scatter at depth of dose maximum (PSFs) were in agreement with PSFs obtained from BJR (25, 1996) typically within 1.0% (Table 9-IIIa and Fig. 9-3a). Of course the PSF as denoted in this work are really $NPSF_s$ normalised to 10x10 field size and are compared here to $NPSF_s$ as given in BJR25 (1996).

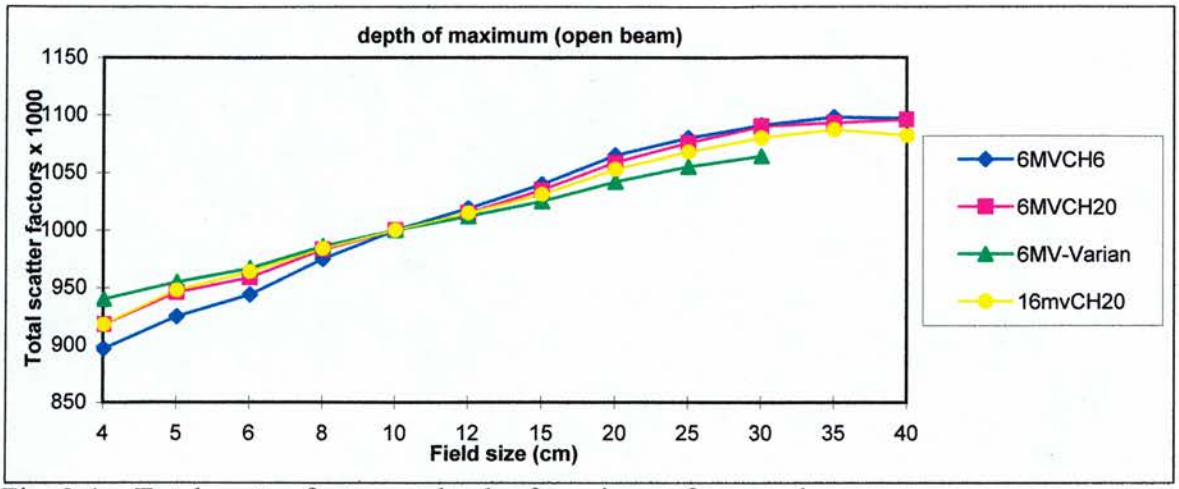

Fig. 9-1a: Total scatter factors at depth of maximum for open beams (uncertainties on measured values are estimated at from 0.5% to 0.7%)

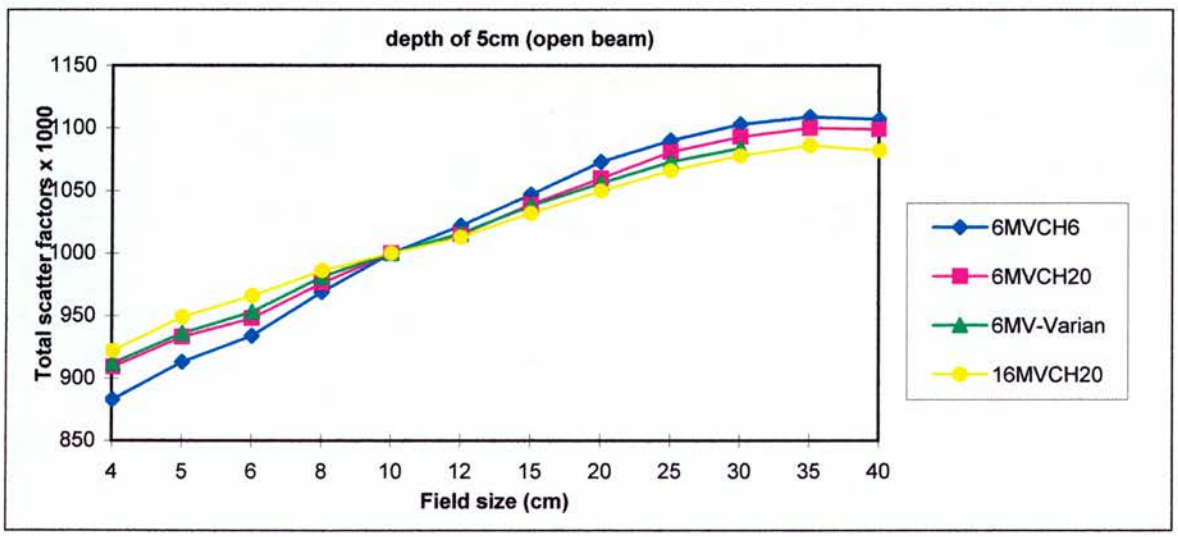

Fig. 9-1b: Total scatter factors at depth of 5cm for open beams

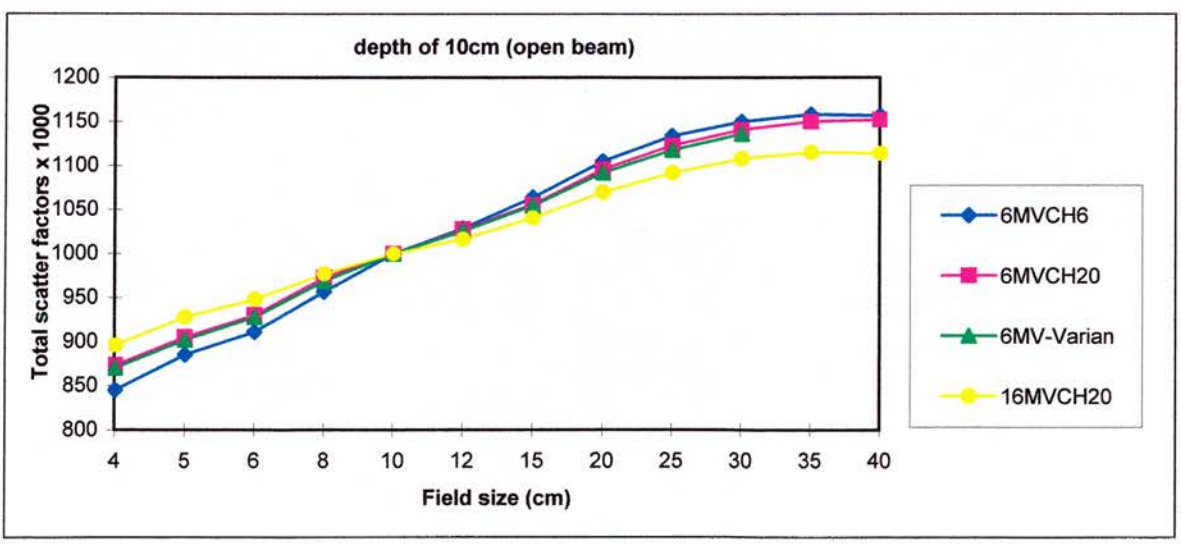

Fig. 9-1c: Total scatter factors at depth of 10cm for open beams

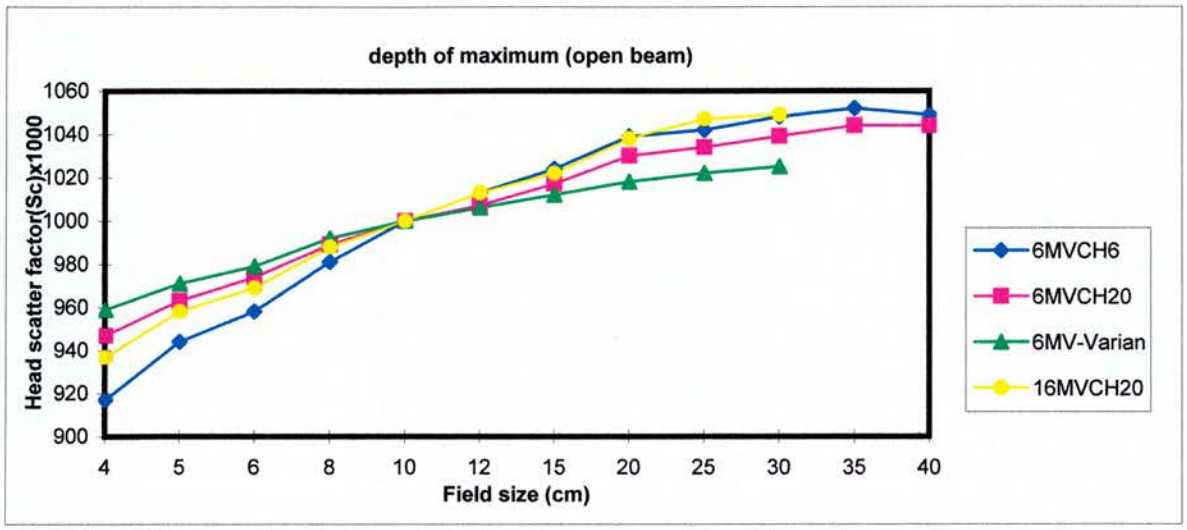

Fig. 9-2a: Head scatter factors at depth of maximum for different energies (uncertainties on measured values are estimated at from 0.5% to 0.7%)

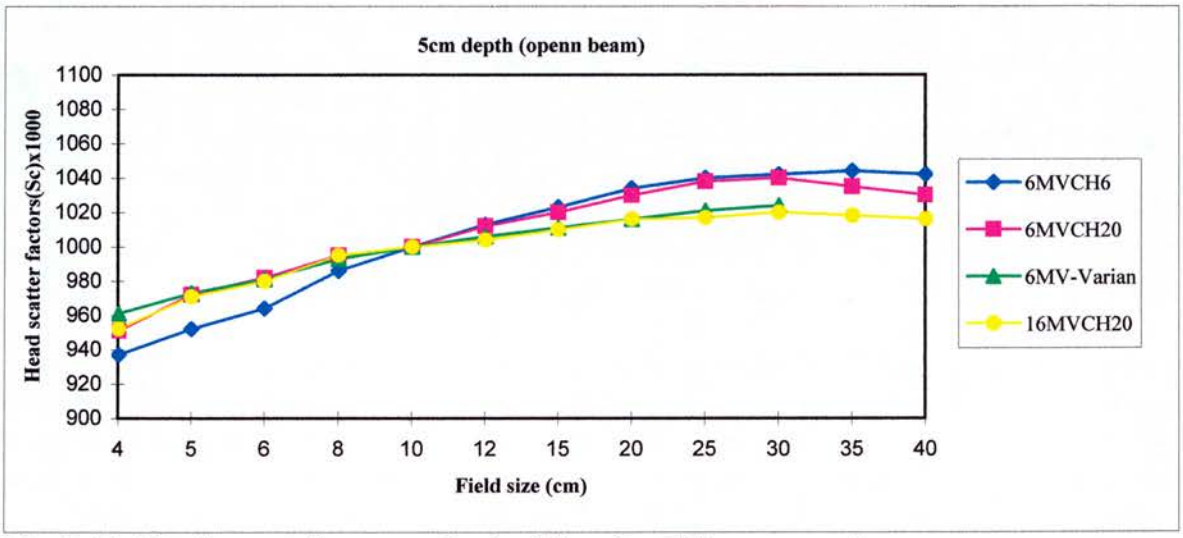

Fig. 9-2b: Head scatter factors at depth of 5cm for different energies

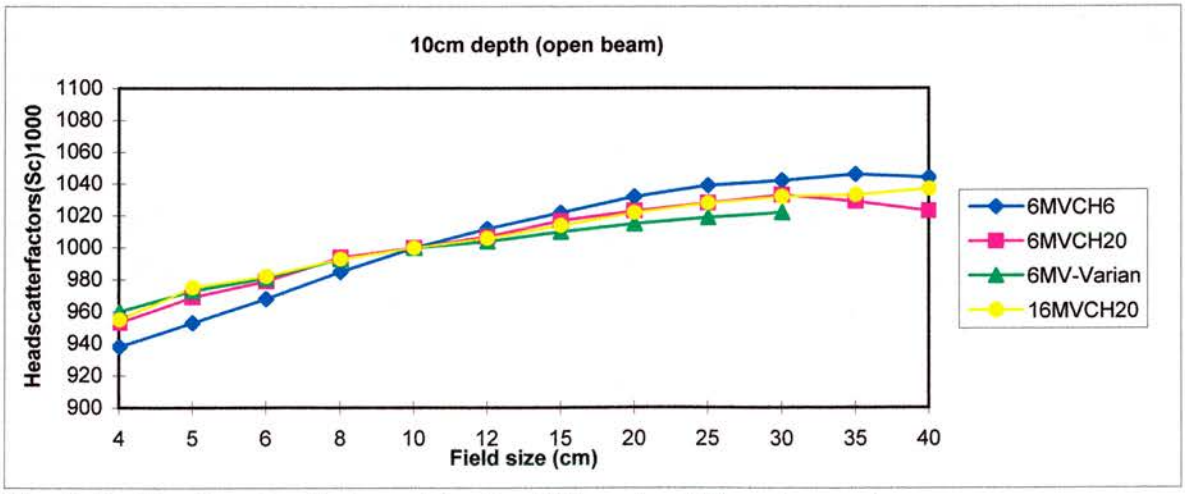

Fig. 9-2c: Head scatter factors at depth of 10cm for different energies

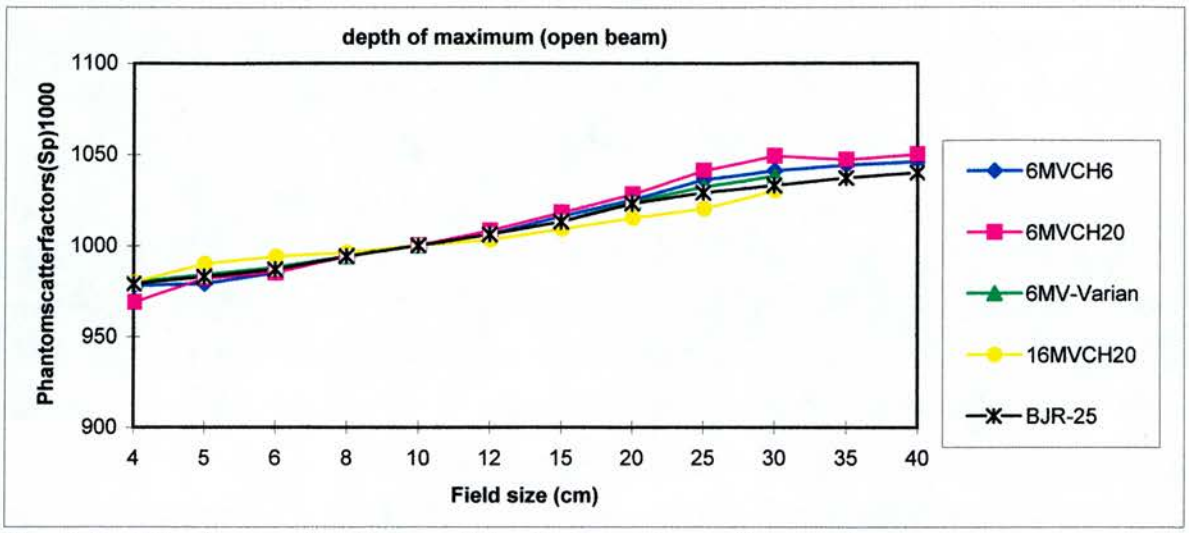

Fig. 9-3a: Phantom scatter factors at depth of maximum for open beams (uncertainties on derived values are estimated at from 0.7% to 1.0%)

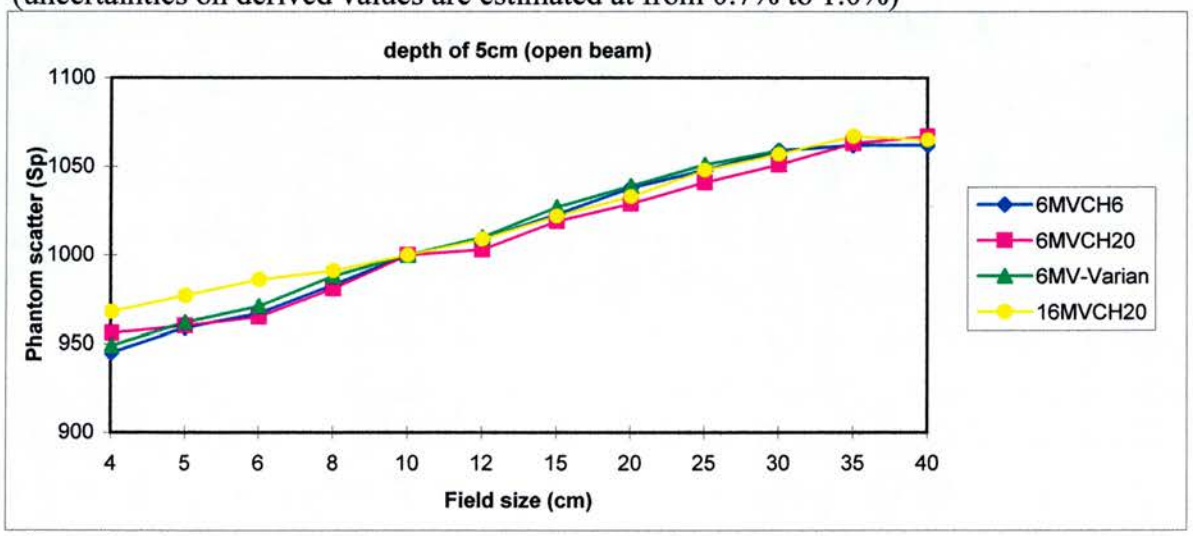

Fig. 9-3b: Phantom scatter factors at depth of 5cm for open beams

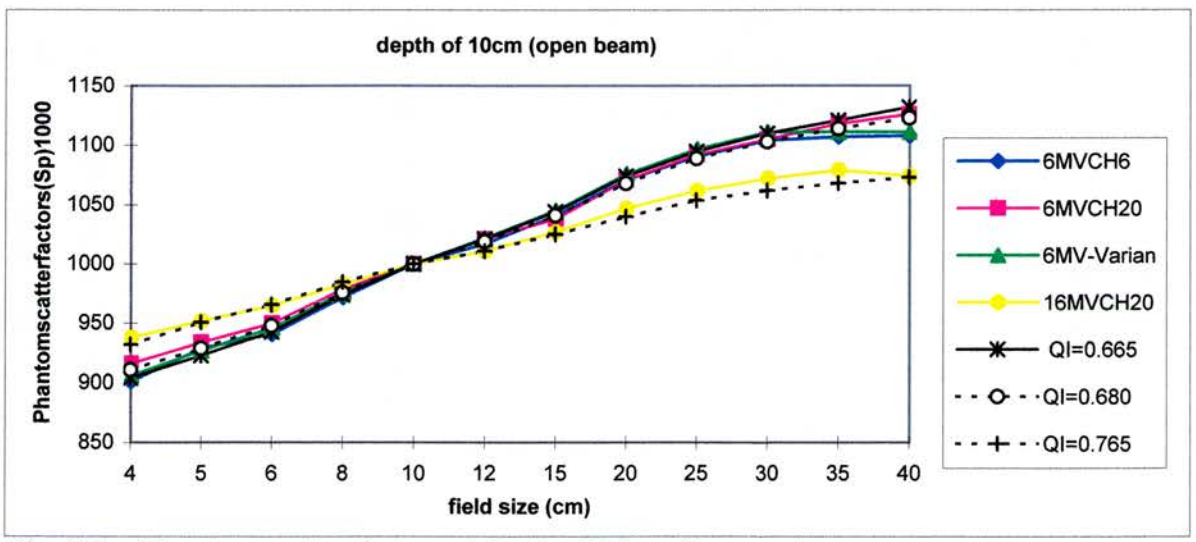

Fig. 9-3c: Phantom scatter factors at depth of 10cm for open beams

Also the phantom scatter factors obtained at depths 5cm and 10cm were in agreement with S_p values obtained by Van Gasteren et al (1991) and Storchi and Van Gasteren (1996) generally within 1.0% (Table 9-IIIb,c), respectively. From these results it can be concluded that the phantom scatter factors are consistent and the tabulated values are confirmed as applicable. It means that each radiotherapy centre can use phantom scatter factors from these tables selected by the appropriate quality indices and depths. The collimator scatter can be determined simply by these tables and total scatter factors measured for each machine in the centre according to equation (9-4).

$$S_c = S_{c,p} / S_p \qquad \text{Eq. (9-4)}$$

Table 9-I: Measured total scatter factors at depth of dose maximum, 5cm and 10cm for different energy photon beams

	6MV (Varian)			6MV (CH6)			6MV (CH20)			16MV (CH20)		
	d_{max}	5cm	10cm	d_{max}	5cm	10cm	d_{max}	5cm	10cm	d_{max}	5cm	10cm
4x4	0.940	0.912	0.870	0.897	0.883	0.845	0.918	0.909	0.873	0.918	0.922	0.896
5x5	0.955	0.936	0.902	0.924	0.913	0.885	0.946	0.933	0.905	0.948	0.949	0.928
6x6	0.967	0.953	0.928	0.944	0.934	0.911	0.959	0.948	0.930	0.964	0.966	0.948
8x8	0.986	0.981	0.969	0.975	0.969	0.957	0.983	0.976	0.973	0.984	0.986	0.977
10x10	1.00	1.00	1.00	1.00	1.00	1.00	1.00	1.00	1.00	1.00	1.00	1.00
12x12	1.012	1.016	1.026	1.019	1.022	1.029	1.015	1.015	1.028	1.015	1.013	1.017
15x15	1.025	1.038	1.055	1.040	1.047	1.064	1.035	1.039	1.056	1.031	1.032	1.041
20x20	1.045	1.056	1.092	1.065	1.073	1.105	1.059	1.060	1.096	1.053	1.050	1.070
25x25	1.055	1.073	1.118	1.080	1.090	1.134	1.076	1.081	1.123	1.068	1.066	1.092
30x30	1.064	1.084	1.136	1.091	1.103	1.150	1.090	1.093	1.141	1.080	1.078	1.108
35x35	-	-	-	1.098	1.109	1.158	1.093	1.100	1.150	1.087	1.086	1.115
40x40	-	-	-	1.097	1.107	1.157	1.096	1.099	1.152	1.082	1.082	1.114

-

Table 9-II: Measured head scatter factors at depth of dose maximum, 5cm and 10cm for different energy photon beams

	6MV (Varian)			6MV (CH6)			6MV (CH20)			16MV (CH20)		
	d_{max}	5cm	10cm	d_{max}	5cm	10cm	d_{max}	5cm	10cm	d_{max}	5cm	10cm
4x4	0.959	0.961	0.960	0.917	0.934	0.938	0.947	0.951	0.953	0.937	0.952	0.961
5x5	0.971	0.973	0.973	0.944	0.952	0.953	0.963	0.972	0.969	0.958	0.971	0.975
6x6	0.979	0.981	0.981	0.958	0.964	0.968	0.974	0.982	0.979	0.969	0.980	0.985
8x8	0.992	0.993	0.993	0.981	0.986	0.985	0.989	0.995	0.994	0.988	0.995	0.995
10x10	1.00	1.00	1.00	1.00	1.00	1.00	1.00	1.00	1.00	1.00	1.00	1.00
12x12	1.006	1.006	1.004	1.013	1.013	1.012	1.007	1.012	1.007	1.013	1.004	1.004
15x15	1.012	1.011	1.010	1.024	1.023	1.022	1.017	1.020	1.017	1.022	1.010	1.012
20x20	1.018	1.016	1.015	1.039	1.034	1.032	1.030	1.030	1.023	1.038	1.016	1.012
25x25	1.022	1.021	1.019	1.042	1.040	1.039	1.034	1.038	1.028	1.047	1.017	1.011
30x30	1.025	1.024	1.022	1.048	1.042	1.042	1.039	1.040	1.033	1.049	1.020	1.011
35x35	-	-	-	1.052	1.044	1.046	1.044	1.035	1.029	1.051	1.018	1.006
40x40	-	-	-	1.049	1.042	1.044	1.044	1.030	1.023	1.045	1.016	1.004

Table 9-IIIa: Derived phantom scatter factors at depth of dose maximum (NPSF) for different energies

	6MV -CH6	6MV -CH20	6MV-Varian	16MV-CH20	BJR (25)*
4x4	0.978	0.969	0.980	0.980	0.979
5x5	0.979	0.982	0.984	0.990	0.983
6x6	0.985	0.985	0.988	0.994	0.987
8x8	0.994	0.994	0.994	0.996	0.994
10x10	1.00	1.00	1.00	1.00	1.00
12x12	1.006	1.008	1.006	1.003	1.006
15x15	1.016	1.018	1.013	1.009	1.013
20x20	1.025	1.028	1.024	1.015	1.023
25x25	1.036	1.041	1.032	1.020	1.029
30x30	1.041	1.049	1.038	1.030	1.033
35x35	1.044	1.047	-	-	1.037
40x40	1.046	1.050	-	-	1.040

** for all MV x-ray qualities*

Table 9-IIIb: Derived Phantom scatter factors at depth 5cm for different energy photon beams

Quality Index	**6CH6 0.680**	**6CH20 0.680**	**6-Varian 0.665**	**Van G.* 0.650**
4x4	0.945	0.955	0.949	0.950
5x5	0.959	0.960	0.962	0.960
6x6	0.967	0.965	0.971	0.970
8x8	0.983	0.981	0.988	0.988
10x10	1.00	1.00	1.00	1.00
12x12	1.009	1.003	1.010	1.012
15x15	1.023	1.019	1.027	1.027
20x20	1.038	1.029	1.039	1.047
25x25	1.048	1.041	1.051	1.058
30x30	1.059	1.051	1.059	1.067
35x35	1.062	1.063	-	-
40x40	1.062	1.067	-	-

** the nearest quality value to these 6MV beams*

Table 9-IIIc: Derived phantom scatter factors at depth 10cm for different energy photon beams

Quality Index	**6CH6** **0.680**	**6CH20** **0.680**	**Van G.*** **0.680**	**6-Varian** **0.665**	**Van G.*** **0.665**	**16CH20** **0.765**	**Van*** **0.765**
4x4	0.901	0.916	0.911	0.906	0.904	0.938	0.932
5x5	0.929	0.934	0.929	0.927	0.923	0.952	0.951
6x6	0.941	0.950	0.948	0.946	0.943	0.965	0.966
8x8	0.972	0.979	0.976	0.976	0.974	0.983	0.985
10x10	1.00	1.00	1.00	1.00	1.00	1.00	1.00
12x12	1.017	1.021	1.019	1.022	1.021	1.011	1.011
15x15	1.041	1.038	1.041	1.045	1.044	1.027	1.025
20x20	1.071	1.071	1.068	1.076	1.074	1.047	1.040
25x25	1.091	1.092	1.089	1.097	1.095	1.062	1.054
30x30	1.104	1.105	1.103	1.111	1.110	1.072	1.062
35x35	1.107	1.118	1.114	-	1.121	1.079	1.069
40x40	1.108	1.126	1.123	-	1.132	1.074	1.073

** Storchi and Van Gasteren values*

9-3-1-2-Rectangular Fields (Symmetric)

a) Head Scatter Factors

Upper and lower jaws are at different distances from the source and from the dose monitor ionisation chamber, therefore the influence of lower jaws (X) on the head scatter component is different from upper jaws (Y). The results show the differences for head scatter factors obtained for the two sets of jaws for field sizes from 4x4 to 4x40 and 4x4 to 40x4 (Tables 9-IV at D_{max} and 9-V at 10cm). This shows means that the output factor in air for the field (X=a and Y=b) is different from that for the field (Y=a and X=b) by up to 3.0% depending on machine. A part of the output factor depends on backscatter from the collimators, particularly the upper collimator, into the beam monitor ionisation chamber. For this reason there was a range of differences between head scatter factors measured for rectangular fields where the different dimensions are set by upper or lower jaws according to figure (9-4). This also was observed by Kase and Svenson (1986), and Luxton and Astrahan (1988). However, Wu et al (1984) and Huang et al (1986) came to the conclusion that backscattered radiation from the collimator jaws into the dose monitor chamber does not change with field size and that this does not contribute to the change of photon output with field size.

Table 9-IV: Head scatter factors for rectangular fields at depth of maximum

	6MV(CH6)		**6MV (CH20)**		**6MV-Varian**		**16MV (CH20)**	
	x = c	**y = c**	**x = c**	**y = c**	**x = c**	**y = c**	**x = c**	**y = c**
4, 4	0.930	0.930	0.945	0.945	0.959	0.958	0.944	0.942
4, 6	0.941	0.941	0.964	0.954	0.966	0.961	0.960	0.955
4, 10	0.962	0.948	0.973	0.961	0.965	0.957	0.969	0.961
4, 15	0.969	0.954	0.978	0.962			0.976	0.964
4, 20	0.976	0.954	0.981	0.962	0.984	0.974	0.978	0.965
4, 30	0.979	0.950	0.985	0.961	0.984	0.974	0.983	0.963

- x=c (lower jaws fixed and upper jaws movable) *c=constant (in this case 4cm)*

- y=c (upper jaws fixed and lower jaws movable)

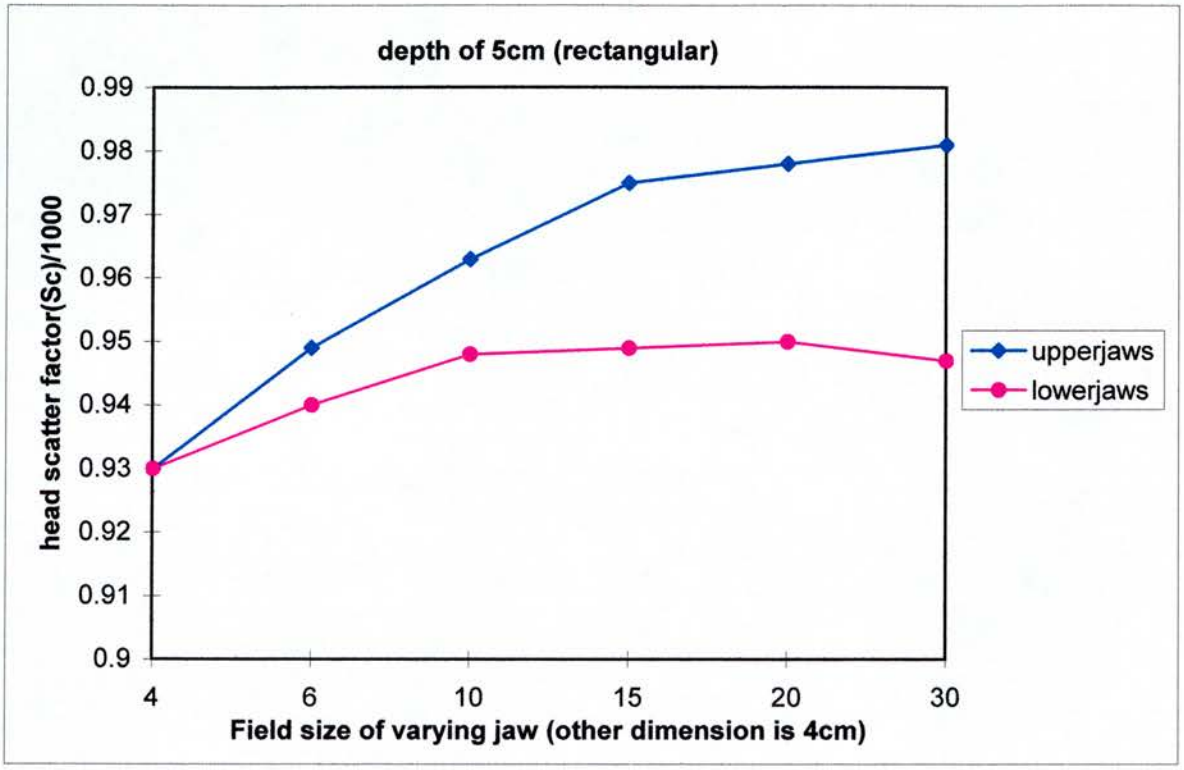

Fig. 9-4: Differences of Sc values on 6MV for upper and lower jaws where one jaw is fixed and the other jaw is variable (uncertainties in the measured values are estimated at from 0.5 to 0.7% as described earlier)

Table 9-V: Head scatter factors for rectangular fields at depth of 10cm

	6MV (CH6)		6MV (CH20)		6MV-Varian		16MV (CH20)	
	x = c	y = c	x = c	y = c	x = c	y = c	x = c	y = c
4, 4	0.930	0.930	0.953	0.953	0.961	0.961	0.968	0.964
4, 6	0.947	0.943	0.967	0.960	0.968	0.966	0.979	0.972
4, 10	0.965	0.951	0.979	0.965	0.981	0.972	0.987	0.974
4, 15	0.972	0.952	0.982	0.967			0.991	0.973
4, 20	0.978	0.951	0.987	0.967	0.984	0.976	0.993	0.972
4, 30	0.982	0.954	0.989	0.963	0.983	0.977	0.994	0.971

- x=c (lower jaws fixed and upper jaws movable)) c=constant (in this case 4cm)

- y=c (upper jaws fixed and lower jaws movable)

b) Equivalent Field size

In order to obtain an output factor for a rectangular field, the equivalent field size has been defined as that equivalent square field that has the same S_c value as the given rectangular field. Sterling et al originally (1964) proposed the equivalent field size as:

$$ES(x, y) = 2xy / x+y \qquad \text{Eq. (9-5)}$$

Where x, y is the width and length of the rectangular field, and ES (x, y) is the side of equivalent square. This equation works well when $|x-y|$ is small. However, it can introduce a significant error in calculated output factors when the rectangle is elongated.

Several authors (Szymczyk et al 1991, Vadash and Bjarngard 1993, and Yu et al 1995) have developed more complex equations to obtain more accurate equivalent field size.

c) Total scatter Factors

Table (9-VIa) compares the output factor values from treatment planning data according to equation (9-5) with rectangular measured values (upper and lower jaws) at depth of dose maximum with the same equivalent areas in different energy beams. The differences are more significant when output factors are obtained simply by considering the area and using standard treatment planning tables. The variation of output factors with the same field but different jaws (exchange effect) is up to 3.0% depending on machine, and the output factors obtained by the in-house treatment planning approach using equivalent square is situated between them i.e. to ±1.5%. The differences of output factors if simple field area is used (i.e. ignoring equivalent area) are up to 5% (Table 9-VIa). Table (9-VIb) shows the measured total scatter factors for rectangular fields at depth of 10cm for different energy photon beams.

Table (9-VIa): Comparison of rectangular output factors from measurement and from treatment planning tables (at d_{max})

	6MV (CH6)				6MV (CH20)				6MV (Varian)				16MV (CH20)			
	planning		Meas.		planning		Meas.		planning		Meas.		planning		Meas.	
	area	2ab/ a+b	upp. jaws x=c	low. jaws y=c	area	2ab/ a+b	upp. jaws x=c	low. jaws y=c	area	2ab/ a+b	upp. jaws x=c	low. jaws y=c	area	2ab/ a+b	upp. jaws x=c	lo. jw. y= c
4x6	**0.925**	**0.923**	**0.929**	**0.920**	**0.939**	**0.936**	**0.944**	**0.938**	**0.939**	**0.939**	**0.938**	**0.938**	**0.939**	**0.936**	**0.949**	**0.940**
4x10	**0.951**	**0.942**	**0.946**	**0.936**	**0.964**	**0.954**	**0.960**	**0.947**	**0.946**	**0.946**	**0.946**	**0.944**	**0.964**	**0.954**	**0.962**	**0.949**
4x15	**0.973**	**0.951**	**0.962**	**0.940**	**0.978**	**0.964**	**0.969**	**0.953**	**0.969**	**0.962**	**0.965**	**0.957**	**0.978**	**0.964**	**0.971**	**0.954**
4x20	**0.988**	**0.955**	**0.968**	**0.944**	**0.990**	**0.968**	**0.977**	**0.955**	**0.992**	**0.972**	**0.975**	**0.964**	**0.990**	**0.968**	**0.974**	**0.955**
4x30	**1.009**	**0.963**	**0.973**	**0.945**	**1.007**	**0.973**	**0.980**	**0.956**	**1.006**	**0.976**	**0.980**	**0.966**	**1.007**	**0.973**	**0.980**	**0.958**

- x=c (lower jaws fixed and upper jaws movable) *c=constant (in this case 4cm)*

- y=c (upper jaws fixed and lower jaws movable)

Table (9-VIb): The total scatter factors for rectangular fields at depth of 10cm for different energy photon beams

	6MV (CH6)		6MV (CH20)		6MV (Varian)		16MV (CH20)	
	x=c	y=c	x=c	y=c	x=c	y=c	x=c	y=c
4, 4	0.850	0.850	0.873	0.875	0.872	0.871	0.900	0.900
4, 6	0.879	0.871	0.901	0.897	0.886	0.884	0.926	0.920
4, 10	0.911	0.894	0.924	0.913	0.922	0.915	0.942	0.932
4, 15	0.924	0.905	0.939	0.925	-	-	0.953	0.943
4, 20	0.936	0.912	0.950	0.930	0.939	0.930	0.959	0.945
4, 30	0.943	0.914	0.951	0.935	0.947	0.935	0.963	0.948

- x=c (lower jaws fixed and upper jaws movable) *c=constant (in this case 4cm)*

- y=c (upper jaws fixed and lower jaws movable)

d) Phantom Scatter Factors

Tables (9-VII and 9-VIII) compare the equivalent square phantom scatter factors from this work with the phantom scatter obtained from BJR (25, 1996) at d_{max}, and Storchi and Van Gasteren (1996) at a depth of 10cm. The equivalent square field values for phantom scatter were determined according to equation (9-5). The agreement was good between the results and those obtained from BJR (25, 1996), and Storchi and Van Gasteren (1996) generally within 1.0% (Table 9-VII and 9-VIII).

Table 9-VII: Phantom scatter factors for rectangular fields at depth of maximum (PSF)

	6MV (CH6) x = c y = c	6MV (CH20) x = c y = c	6MV-Varian x = c y = c	16MV(cH20) x = c y = c	BJR (25)* Eq. Square
4, 4	0.976 0.977	0.979 0.981	0.978 0.979	0.983 0.985	0.979
4, 6	0.987 0.978	0.979 0.983	0.979 0.982	0.989 0.984	0.982
4, 10	0.983 0.987	0.987 0.985	0.985 0.986	0.993 0.988	0.986
4, 15	0.993 0.985	0.991 0.991		0.995 0.990	0.988
4, 20	0.992 0.990	0.996 0.993	0.991 0.990	0.996 0.990	0.989
4,30	0.994 0.995	0.995 0.995	0.996 0.992	0.997 0.995	0.990

**for all MV x-ray beam qualities*

- x=c (lower jaws fixed and upper jaws movable)

- y=c (upper jaws fixed and lower jaws movable)

Table 9-VIII: Phantom scatter factors for rectangular fields at depth of 10cm

	6-CH6 Q=0.680	6-CH20 Q=o.680	Van G. * Q=0.680	6Varian Q=0.665	Van G. * Q=0.665	16-CH20 Q=0.765	Van G. * Q=0.765
4, 4	0.914 0.914	0.916 0.918	0.911	0.907 0.906	0.904	0.934 0.934	0.933
4, 6	0.925 0.924	0.916 0.918	0.926	0.915 0.915	0.914	0.946 0.947	0.948
4, 10	0.944 0.940	0.944 0.946	0.942	0.940 0.941	0.938	0.954 0.957	0.961
4, 15	0.951 0.951	0.956 0.957	0.953			0.962 0.969	0.969
4, 20	0.957 0.959	0.962 0.962	0.958	0.954 0.953	0.953	0.966 0.972	0.972
4, 30	0.960 0.963	0.962 0.970	0.962	0.967 0.957	0.959	0.969 0.976	0.976

* using equivalent square values

9-3-2-Wedged Fields

The total scatter factors and head scatter factors for wedged beams are shown in Figs. (9-5a to 9-5c and Table 9-Xa) and Figs. (9-6a to 9-6c and Table 9-Xb) respectively, as a function of field size for 6MV and 16MV photon beams. The output measurements were carried out at different depths dose maximum, 5cm and 10cm. Figures (9-5 a-c and

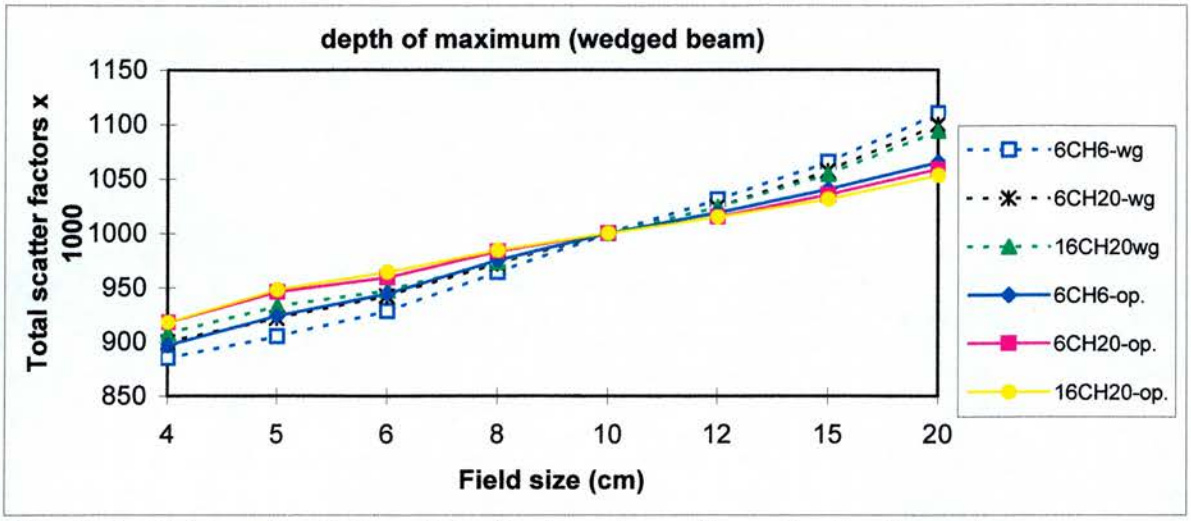

Fig. 9-5a: Total scatter factors at depth of maximum for wedged and open beams

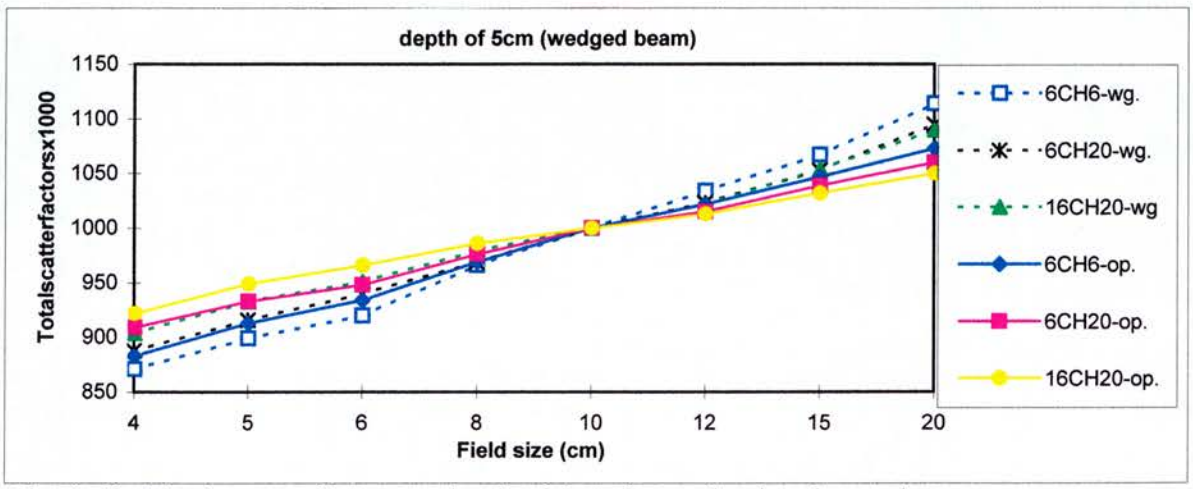

Fig. 9-5b: Total scatter factors at depth of 5cm for wedged and open beams

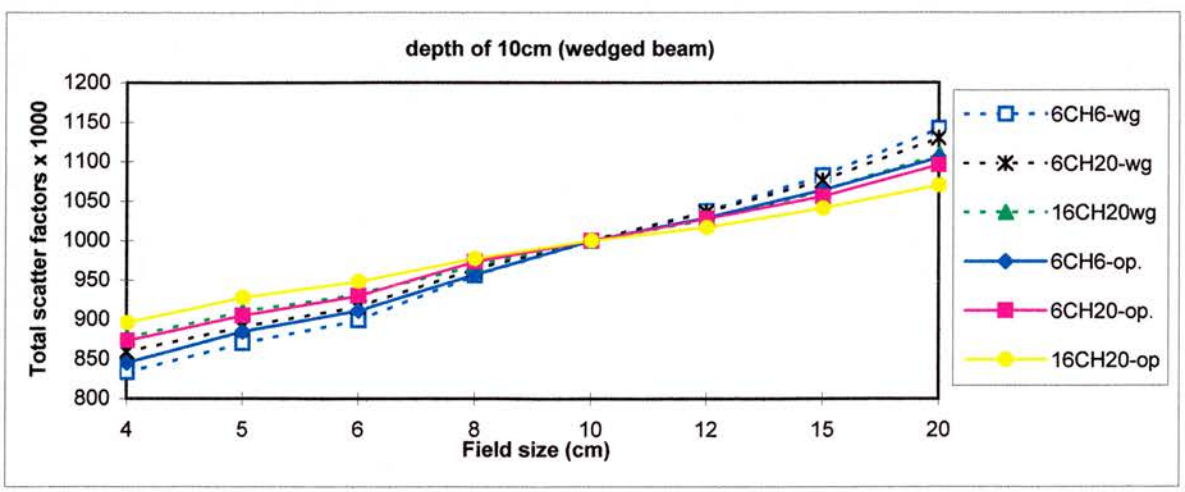

Fig. 9-5c: Total scatter factors at depth of 10cm for wedged and open beams

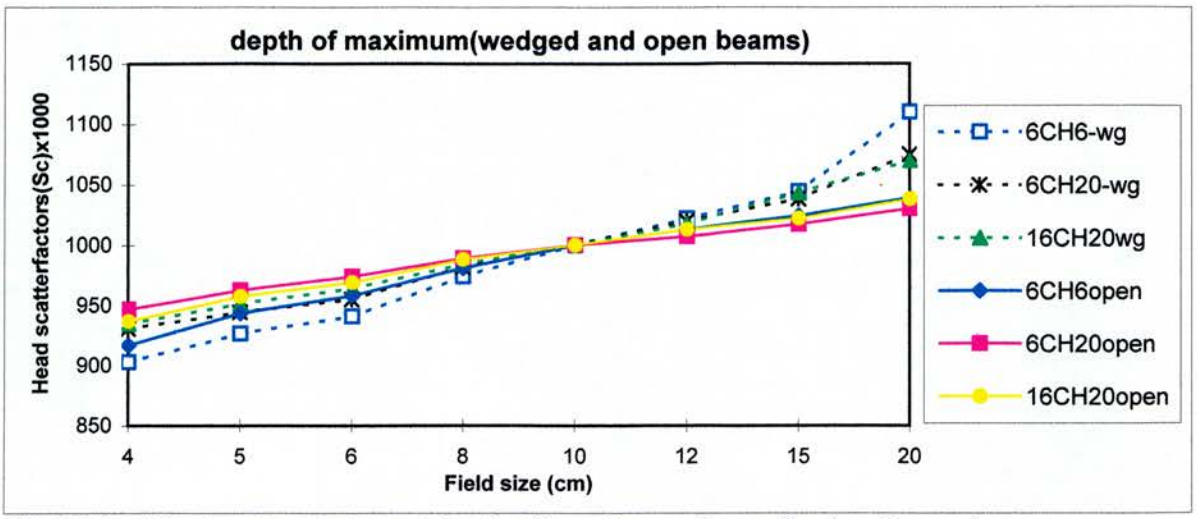

Fig. 9-6a: Head scatter factors at depth of maximum for wedged and open beams

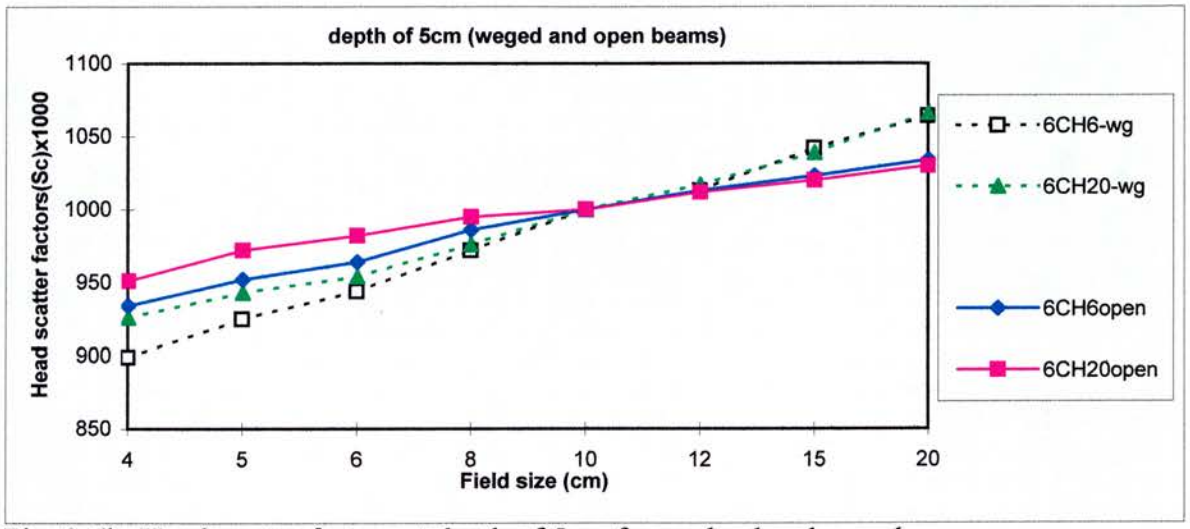

Fig. 9-6b: Head scatter factors at depth of 5cm for wedged and open beams

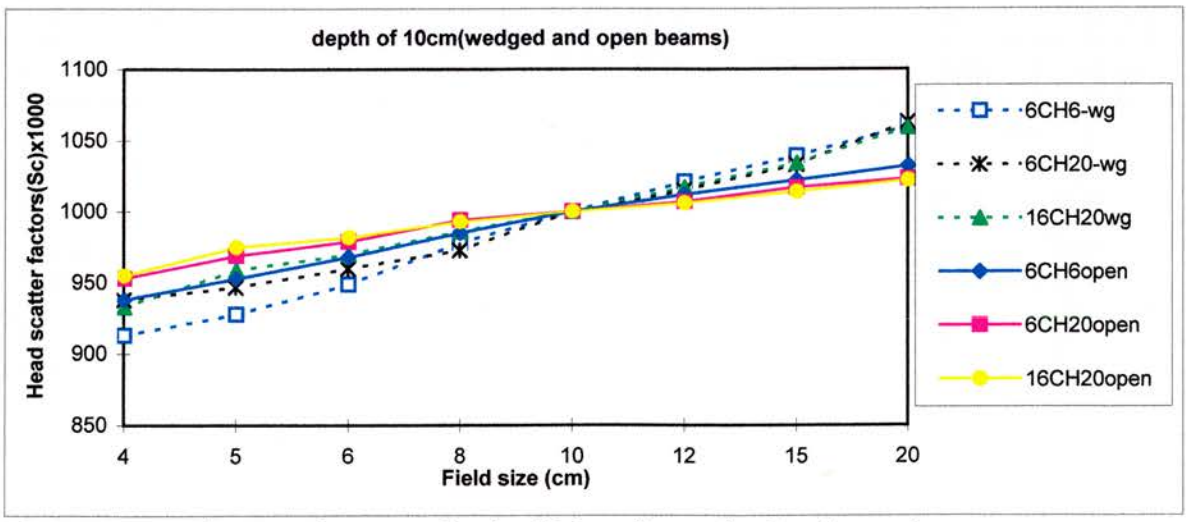

Fig. 9-6c: Head scatter factors at depth of 10cm for wedged and open beams

9-6a-c) compare the total and head scatter measured values with wedge (dashed line) and without wedge (solid line). For all measurements an increase in the variation of total scatter and head scatter with field size is shown, when the wedge is inserted in the photon beam. This can be due to changes of scatter fluence produced by the wedge, and also differences in the amount of backscatter to the monitor chamber for open and wedged photon beams. There was also observed an increase in the variation of the head scatter factor with field size for rectangular fields, when the wedge is inserted in the photon beam (Fig. 9-7).

The results confirmed the variation of wedge factors with field size and depth according to Table (9-IX). They show deviations of 6% and 3% for wedge factors with field size and depth respectively, for the various stated energy beams. The variation of wedge factor with field size can be due to the variation of head scatter and backscattered radiation produced by the wedge. However, the last two effects may be negligible (Cozzi et al 1996) in linacs of some designs. However, the machines in this centre (CH6 and CH20) have a motorised wedge set above the collimators with a significant amount of backscatter to the monitor chamber. The variation of wedge factor with depth can be due to changes in the energy spectrum of the photons (beam hardening), because of absorption of low energy incoming photons in the wedge volume. Another reason can be due to scattered radiation produced in the wedge volume as low energy photons (Huang et al 1987, Knoose and Witgren 1991, Tatcher and Bjarngard 1992, Heukelom et al $1994_{a,b}$, and Cozzi et al 1996).

Table (9-Xc) shows the phantom scatter factors obtained for wedged beams for different energy photon beams and depths. These values are in good agreement within combined experimental uncertainties with the phantom scatter factors obtained for open fields in this work generally within 1.0% (compare to Tables 9-IIIa,b,c). It shows that the increasing variation of total scatter factors for wedged beams compared to open beams is

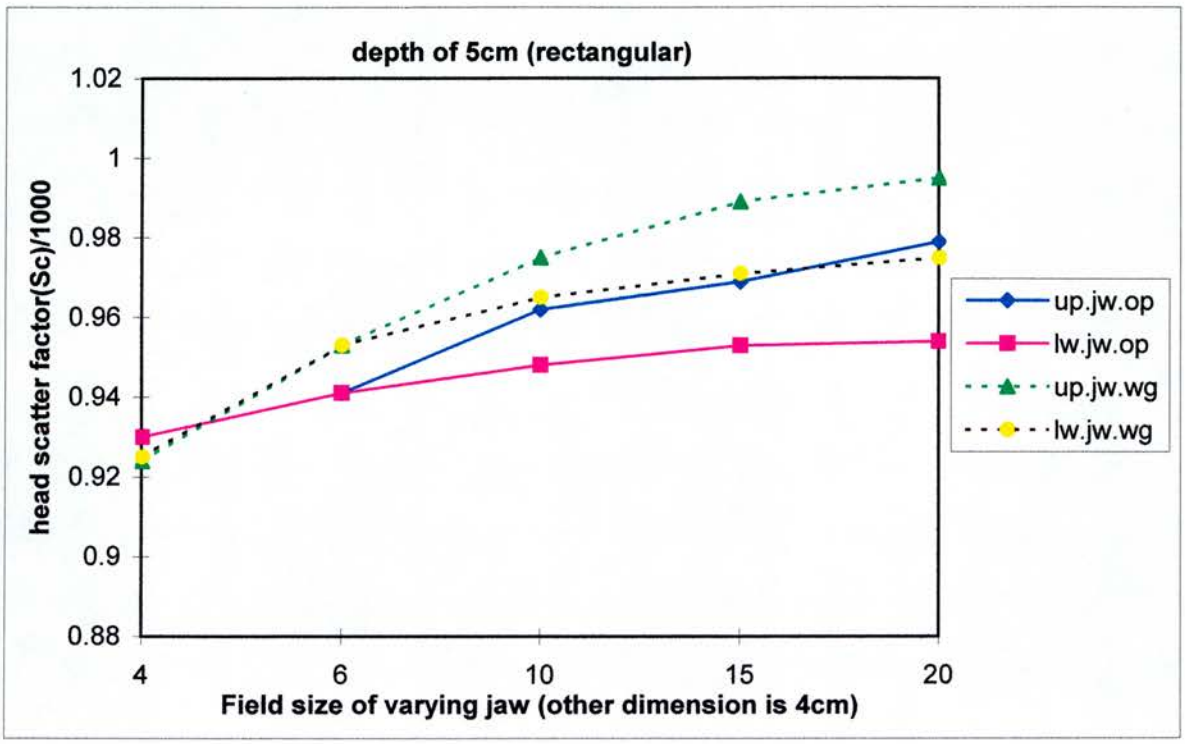

Fig. 9-7: differences of Sc values between wedged and open beams for rectangular field when one jaw is fixed and the other jaw is variable (uncertainties in the measured values are estimated at from 0.5 to 0.7% as described earlier)

essentially due to head scatter factor changes. The effect of change of phantom scatter is negligible.

Table 9-IX: Variation of wedge factors with field size and depth for different energy photon beams

	Maximum depth	**5cm depth**	**10cm depth**
	6MV*6MV#16MV	**6MV*6MV#16MV**	**6MV*6MV#16MV**
4x4	2.748 2.793 2.654	2.731 2.777 2.672	2.685 2.720 2.667
5x5	2.767 2.815 2.670	2.735 2.761 2.665	2.693 2.718 2.664
6x6	2.756 2.792 2.673	2.735 2.737 2.665	2.684 2.718 2.657
8x8	2.742 2.775 2.699	2.702 2.732 2.638	2.650 2.702 2.636
10x10	2.710 2.742 2.626	2.692 2.713 2.621	2.647 2.677 2.611
12x12	2.677 2.719 2.605	2.663 2.692 2.599	2.628 2.657 2.585
15x15	2.648 2.685 2.569	2.643 2.678 2.568	2.603 2.628 2.557
20x20	2.600 2.640 2.526	2.593 2.625 2.530	2.561 2.597 2.522

** CH6 # CH20*

Table (9-Xa): Total scatter factors for wedged beams at depths maximum, 5cm and 10cm for different energy photon beams

	6MV (CH6)			**6MV (CH20)**			**16MV (CH20)**	
	d_{max}	**5cm**	**10cm**	**d_{max}**	**5cm**	**10cm**	**d_{max}**	**10cm**
4x4	0.885	0.871	0.833	0.900	0.888	0.859	0.908	0.877
5x5	0.905	0.899	0.870	0.922	0.916	0.891	0.933	0.910
6x6	0.928	0.920	0.899	0.942	0.940	0.916	0.947	0.932
8x8	0.964	0.966	0.956	0.972	0.969	0.964	0.973	0.968
12x12	1.031	1.034	1.037	1.024	1.023	1.036	1.024	1.027
15x15	1.065	1.067	1.082	1.057	1.053	1.076	1.054	1.063
20x20	1.110	1.114	1.142	1.100	1.095	1.130	1.094	1.109

Table (9-Xb): Head scatter factors for wedged beams at depths maximum, 5cm and 10cm for different energy photon beams

	6MV (CH6)			6MV (CH20)			16MV (CH20)	
	d_{max}	5cm	10cm	d_{max}	5cm	10cm	d_{max}	5cm
4x4	0.903	0.899	0.913	0.931	0.926	0.938	0.935	0.933
5x5	0.927	0.925	0.928	0.945	0.943	0.947	0.952	0.959
6x6	0.941	0.944	0.949	0.955	0.954	0.960	0.964	0.970
8x8	0.974	0.972	0.978	0.982	0.976	0.973	0.984	0.986
12x12	1.022	1.013	1.021	1.020	1.017	1.015	1.018	1.017
15x15	1.044	1.042	1.039	1.038	1.039	1.033	1.043	1.034
20x20	1.073	1.064	1.060	1.075	1.066	1.063	1.070	1.059

Table 9-Xc: Phantom scatter factors for wedged fields at depths of maximum, 5cm and 10cm for different energy photon beams

	depth of max. (PSF)			**5 cm depth**		**10 cm depth**		
	6MV*	**6MV#**	**16MV**	**6MV***	**6MV#**	**6MV***	**6MV#**	**16MV**
4x4	0.980	0.967	0.973	0.969	0.959	0.912	0.916	0.940
5x5	0.976	0.976	0.980	0.972	0.971	0.938	0.941	0.949
6x6	0.986	0.986	0.982	0.975	0.985	0.947	0.954	0.961
8x8	0.990	0.990	0.989	0.994	0.993	0.978	0.991	0.982
12x12	1.009	1.004	1.006	1.021	1.006	1.016	1.021	1.010
15x15	1.020	1.018	1.011	1.024	1.013	1.041	1.042	1.028
20x20	1.034	1.023	1.022	1.047	1.027	1.077	1.063	1.047

** CH6 # CH20*

9-3-3-Asymmetric Fields

In air and in phantom output measurements were carried out for various square open and wedged fields using the dual asymmetric collimators. Head scatter factors and total scatter factors were determined on the geometric central axis but with collimator variations along the x and y axes asymmetrically as described in section 9-2-4.

a) Total scatter and head scatter factors (open fields)

The measured total scatter and head scatter factors for asymmetric fields along the x and y axes are shown in Tables (9-XI and 9-XII) respectively. The head scatter factors were also calculated using equations (9-1 and 9-2) as described in section 9-2-7. Total scatter factors were obtained using a similar formalism to these equations as noted in section 9-2-7. Tables (9-XI and 9-XII) compare the measured head scatter factors with calculated values as above for asymmetric fields with asymmetry along the x and y axes. The agreement between calculated and measured values is good, within 1.0% and 0.7% for total scatter and head scatter factors respectively, showing the usefulness of the proposed calculation scheme to within ±1.0%. Differences between measured asymmetric head scatter factors and symmetric field values (same dimension) are up to 2.0% (Table 9-XII).

b) Total scatter and head scatter factors (wedged fields)

The total scatter and head scatter factors for asymmetric wedged fields is shown in Tables (9-XIII$_a$ and 9-XIII$_b$) respectively. These tables show an increase in the variation of in air and in phantom output values for wedged beams as also seen for symmetric fields. Asymmetry along the direction of the wedge (x-asymmetry) might be expected to show differences due to different effects on head scatter factors of thin or thick part of the wedge. This is due partly to changes in scatter produced in the wedge and partly to

attenuation of existing head scatter by the wedge and both of these would be different for different thicknesses of wedge. This has been observed by Hounsell and Wilkinson (1996), who showed that the overall head scatter effects with wedges are greater over thinner part of the wedge than over thicker parts. The results here show a tendency to support this, but the difference is not very significant. It may be expected that this will be dependant on wedge design and position.

Table 9-XI: Total scatter factors for asymmetric fields at different energies (at 5cm for 6MV beams and 10cm for 16MV beam)

jaws@ posn.	6MV (CH6) meas. open	6MV (CH6) calc.$ open	6MV (CH20) meas. open	6MV (CH20) calc.$ open	16MV (CH20) meas. open	16MV (CH20) calc.$ open
X-as.*						
4, 2	0.931	0.929	0.948	0.950	0.943	0.943
4, 6	0.997	0.999	1.00	1.003	0.996	0.998
4,8	1.014	1.017	1.013	1.010	1.011	1.013
4, 11	1.035	1.036	1.031	1.027	1.028	1.031
4, 16	1.052	1.055	1.047	1.041	1.046	1.050
4, 19	1.059	1.063	1.051	1.041	1.051	1.054
Y-as.#						
4, 2	0.926	0.928	0.943	0.967	0.933	0.940
4, 6	0.999	0.995	0.998	1.001	0.996	0.999
4, 8	1.015	1.012	1.017	1.010	1.013	1.013
4, 11	1.035	1.026	1.027	1.025	1.030	1.032
4, 16	1.048	1.044	1.048	1.040	1.047	1.049
4,19	1.055	1.049	1.055	1.043	1.055	1.054

@ The dimensions given are the two. position of the asymmetric jaws. The other set of collimators are symmetric to give the same total field width (see section 9-2-4)

X-as. asymmetry along the X-axis Y-as# asymmetry along the Y-axis*

$calculation following the formalism of equations 9-1 and 9-2

Table 9-XII: Head scatter values for asymmetric fields at different energies (at depths beyond the range of contaminant electrons, 10cm)

jaws@ posn. X-as.*	6MV (CH6) meas. open	calc.$ open	meas. sym.&	6MV (CH20) meas. open	calc.$ open	meas. sym.&	16MV (CH20) meas. open	calc.$ open	mea. sy.&
4, 2	0.961	0.960	0.964	0.980	0.974	0.982	0.981	0.986	0.982
4, 6	0.998	1.001	1.00	1.00	0.996	1.00	0.998	0.998	1.00
4,8	1.007	1.010	1.013	1.002	1.001	1.012	1.003	1.005	1.006
4, 11	1.017	1.019	1.024	1.013	1.009	1.020	1.009	1.010	1.014
4, 16	1.023	1.024	1.034	1.018	1.016	1.030	1.013	1.015	1.022
4, 19	1.025	1.027	1.037	1.020	1.018	1.035	1.014	1.017	1.026
Y-as.#									
4, 2	0.957	0.958	0.964	0.972	0.974	0.982	0.977	0.977	0.982
4, 6	0.998	0.999	1.00	0.998	0.999	1.00	0.998	0.998	1.00
4, 8	1.007	1.006	1.013	1.008	1.001	1.012	1.002	1.002	1.006
4, 11	1.014	1.011	1.024	1.009	1.007	1.020	1.008	1.007	1.014
4, 16	1.018	1.025	1.034	1.017	1.013	1.030	1.013	1.012	1.022
4,19	1.017	1.021	1.037	1.019	1.018	1.035	1.016	1.017	1.026

@ The dimensions given are the two positions of the asymmetric jaws. The other set of collimators are symmetric to give the same total field width (see section 9-2-4)

X-as. asymmetry along the X-axis, Y-as# asymmetry along the Y-axis*

& symmetric field of same dimension (overall)

$ calculation following the formalism of equations 9-1 and 9-2

Table 9-XIII$_a$: Total scatter values for asymmetric wedged fields at different energies (at depths beyond the range of contaminant electrons, 10cm)

Asymmetric fields (jaw position[@])	**6MV(CH6)-wedge**	**6MV(CH20)wedge**	**16MV(CH20)weg**
x-axis*			
4, 2	0.908	0.927	0.926
4, 6	1.00	1.00	1.00
4, 8	1.028	1.022	1.025
4, 10	1.049		1.047
y-axis[#]			
4, 2	0.916	0.924	0.927
4, 6	1.00	1.00	1.00
4, 8	1.026	1.020	1.025
4, 11	1.051	1.048	1.055
4, 16	1.076	1.082	1.083

X-axis asymmetry along the X-axis, Y-axis[#] asymmetry along the Y-axis*

@ The dimensions given are the two positions of the asymmetric jaws. The other set of collimators are symmetric to give the same total field width (see section 9-2-4)

Table 9-XIII$_b$: Head scatter values for asymmetric wedged fields in different energy (at depths beyond the range of contaminant electrons, 10cm)

Asym. jaw pos.@	6MV(CH6)-wedge		6MV(CH20)wedge		16MV(CH20)wedge	
	ß=90°+	ß=270°$	ß=90°+	ß=270°$	ß=90°+	ß=270°$
x-axis*						
4, 2	0.933	0.932	0.956	0.964	0.971	0.962
4, 6	1.00	1.00	1.00	1.00	1.00	1.00
4, 8	1.015	1.017	1.007	1.015	1.010	1.011
4, 10	1.025	1.031	1.022	1.027	1.022	1.023
y-axis#	x	x	x	x	x	x
4, 2	0.946	0.938	0.960	0.959	0.970	0.970
4, 6	1.00	1.00	1.00	1.00	1.00	1.00
4, 8	1.019	1.016	1.012	1.014	1.010	1.014
4, 11	1.037	1.042	1.033	1.029	1.023	1.027
4, 16	1.049	1.047	1.050	1.048	1.035	1.041

X-axis asymmetry along the X-axis, Y-axis# asymmetry along the Y-axis*

@ The dimensions given are the two positions of the asymmetric jaws. The other set of collimators are symmetric to give the same total field width (see section 9-2-4)

+ the 4cm off-axis collimator to over the thin end of the wedge, the normalise collimator to over thick part of the wedge

$ the 4cm off-axis collimator over the thick part of the wege, the variable collimator is on the thin part of the wedge

x y-asymmetry is perpendicular to the wedge angle, therefor this simply moves the field to opposite sides of the same wedge shape

c) Differences between output factors for symmetric and asymmetric fields

Table (9-XIV) compares the total scatter factors between symmetric and asymmetric beams of the same dimensions. The first column in the table gives the dimensions where for the asymmetric fields the dimensions are x = 4, x_2 (asymmetric)by y = 4+ x_2 (symmetry) for x-axis asymmetry and y = 4, y_2 (asymmetric) by x = 4+ y_2 (symmetric) for y-axis asymmetry. Treatment planning in the standard department approach uses symmetric field output factors instead of asymmetric ones. Comparing values of total scatter factors from treatment planning tables with measured values for symmetric square fields at d_{max} shows agreement to within experimental uncertainty (typically less than 0.5%). The next columns in the table compare measured asymmetric field values to measured symmetric field values at 5cm and 10cm for three energies, assuming these symmetric field values are in similar agreement to planning calculated values. The asymmetric values are shown separately for x-axis asymmetry and y-axis asymmetry.The differences between total scatter factors along the x and y axes in this work for asymmetric fields and the total scatter factors from symmetric fields (measured values) are up to 2.5%. For many simpler situations agreement is within 1.0%, indicating that symmetric field factors can be used to within ±1.0% where asymmetry is not too extreme. However, for more complicated asymmetric situations the differences are increased. Therefore, for complicated asymmetric situations using output factors directly from symmetric field data produces increased errors and uncertainties for dose calculation. In all situations tested the formalism of equations 9-1 and 9-2 give good prediction of measurement to within ±1.0%.

Table 9-XIV: Comparison of asymmetric field output factors with measured and calculated symmetric field planning values at the stated depths

	6MV (CH6)			6MV (CH20)			16MV (CH20)		
field dimen.	asym.* x-axis (5cm)	asym.* y-axis (5cm)	sym. meas. (5cm)	asym.* x-axis (5cm)	asym.* y-axis (5cm)	sym. meas. (5cm)	asym.* x-axis (10cm)	asym.* y-axis (10cm)	sym. meas. (10cm)
5x5			0.913			0.933			0.928
6x6	0.931	0.926	0.934	0.948	0.943	0.948	0.943	0.933	0.948
8x8			0.969			0.976			0.977
10x10	0.997	0.999	1.00	1.00	0.998	1.00	0.996	0.996	1.00
12x12	1.014	1.015	1.022	1.013	1.017	1.015	1.011	1.013	1.017
15x15	1.035	1.035	1.047	1.031	1.027	1.039	1.028	1.030	1.041
20x20	1.052	1.048	1.073	1.047	1.048	1.060	1.046	1.047	1.070
25x25			1.090			1.081			1.092
30x30			1.103			1.093			1.108

** asymmetric fields are 4, x_2 (asymmetry) by $y = 4 + x_2$ (symmetry) or 4, y_2 (asymmetry) by $x = 4 + y_2$ (symmetry)*

d) Phantom scatter factors

Derived phantom scatter factors for asymmetric fields have been compared with phantom scatter factors from symmetric fields in Table (9-XV). The agreement between symmetric and asymmetric phantom scatter factors was good, as expected, typically within 1.0% within combined experimental uncertainties. This means that the phantom scatter values are dependent only on irradiated field size, and not on the collimator position. This was also observed by Palta et al (1988) and Murray et al (1995).

Table 9-XV: Comparison of phantom scatter values between symmetric and asymmetric fields for 5cm deep for 6MV beams and 10cm deep for 16MV beam

asym. jaw position*	6MV (CH6) asymmet.	6MV (CH6) symmet.+	6MV (CH20) asymmet.	6MV (CH20) symmet.+	16MV (CH20) asymmet.	16MV (CH20) symm.+
4, 2	0.969	0.967	0.967	0.965	0.961	0.965
4, 6	0.999	1.00	1.00	1.00	0.998	1.00
4, 8	1.007	1.009	1.011	1.003	1.008	1.011
4, 11	1.018	1.023	1.018	1.019	1.019	1.027
4, 16	1.028	1.038	1.029	1.029	1.033	1.034

** see tables 9-XI and 9-XII* *+ symmetric field of same dimension*

9-3-4-Conformal Blocks

a) Head scatter factors

Head scatter factors for blocked and unblocked fields are presented in Tables (9-XVI and 9-XVII) for various square and rectangular collimator setting at depths of dose maximum and 10 cm. The area of the blocked fields (as described under the tables) are 85cm^2, 92.5cm^2, 69cm^2, and 55cm^2 which are shown in Figs. (9-8a to 9-8d) respectively. These were selected from typical blocks being used on patients at the time of the work. The head scatter measurements were carried out for varying collimator sizes larger than the blocked field area, but smaller than the overall dimension of the outer edge of the block, i.e. a relatively narrow possible set of values. This was based on typical clinical situations where the collimators would be closely fit to the blocked size so that real differences are small between the collimator setting and irradiated area, as the blocks shapes are not very irregular or elongated.

There was no significant difference for these open and blocked fields between their measured head scatter factors at the depth of 10 cm (Table 9-XVII) showing that basic head scatter effects are not changed significantly (within less than 0.5%) by the presence of these blocks. However, there were differences of up to approximately 2.0% at the

Fig. 9-8a: Illustration of patient conformal block used to form blocked fields (area = 85cm^2)

Fig. 9-8b: Illustration of patient conformal block used to form blocked fields (area = 92.5cm^2)

Fig. 9-8c: Illustration of patient conformal block used to form blocked fields (area = 69cm^2)

Fig. 9-8d: Illustration of patient conformal block used to form blocked fields (area = 55cm^2)

depth of dose maximum. This is due to the changed contribution of secondary electron contaminants produced by blocks, effective at this depth, but not at 10cm.

Table 9-XVI: Head scatter factors for conformal blocks and compared to open (unblocked) fields at depth of dose maximum

collim. setting	6 MV block	6 MV unblo-cked	16 MV block	16 MV block	16MV unblo-cked	16MV block
Field I	*		$	*		
10x10	0.994	1.00	0.986	0.990	1.00	
8.5x8.5			0.978			
14x11				1.012	1.016	
15x15				1.017	1.022	
Field II	#		@	#		
10x10	0.997	1.00	0.976	0.988	1.00	0.992

*Blocked field area: *=85cm^2 #=92.5cm^2 $=69cm^2 @=55cm^2*

Table 9-XVII: Head scatter factors for conformal blocks and compared to open (unblocked) fields at depth of 10 cm

collim. setting	6 MV block	6 MV unblo-cked	16 MV block	16 MV block	16MV unblo-cked	16MV block
Field I	*		$	*		
10x10	1.00	1.00	1.00	0.999	1.00	
8.5x8.5			0.994			
14x11				1.006	1.006	
15x15				1.016	1.014	
Field II	#		@	#		
10x10	0.999	1.00	0.999	1.001	1.00	0.998
8x8			0.993			

*Blocked field area: *=85cm^2 #=92.5cm^2 $=69cm^2 @=55cm^2*

b) Total scatter factors

The total scatter factors for conformal blocked fields and open fields with the same collimator settings, measured at depth of dose maximum and at 10cm are shown in Tables (9-XVIII and 9-XIX) respectively. The differences are up to 3.0% (but mostly within 1.0%). Table (9-XVIII) also compares the total scatter factors for conformal blocked fields with calculated values from the standard planning approach in the department. The differences are up to 3.0%. This is due to the standard planning approach using the effective irradiated field area to select an output factor for calculation, i.e. ignoring any differences between a conformal blocked field of this area and a standard open field of the same area.

Table 9-XVIII: Comparison of conformal block output factors ($S_{c,p}$) to those for unblocked fields and calculated values, using equation (9-3)and by the standard planning approach at depth of dose maximum

	6 MV				16 MV				16 MV			
coll. set.	un-b meas	conf meas	cal. eq9-3	st. p$^+$	un-b meas	conf meas	cal. eq9-3	st.p$^+$	un-b meas	conf meas	cal. eq9-3	st.p$^+$
F. I	**open**	*	*			*	*			$	$	
10x10	1.00	0.997	0.995	0.993	1.00	0.997	0.997	0.993	1.00	0.993	0.997	0.984
8.5x85	0.987	0.984	0.987	0.993	0.988	0.985	0.986	0.993	0.988	0.984	0.988	0.984
14x11					1.019	1.009	1.010	0.993				
15x15					1.031	1.018	1.020	0.993				
F.II	**open**	#	#			#	#			@	@	
10x10	1.00	0.998	0.997	0.996	1.00	0.997	0.998	0.996	1.00	0.986	0.996	0.976
8x8	0.983	0.979	0.986	0.996	0.984	0.981	0.986	0.996	0.984	0.976	0.984	0.976
F. II	**wedg**	#	#			#	#					
10x10	1.00	0.997	0.998	0.996	1.00	0.999	0.998	0.996				

*Blocked field area: *=85cm^2 #=92.5cm^2 $=69cm^2 @=55cm^2*

+ standard planning values

Table 9-XIX: The measured output factors (Sc,p) for blocked and unblocked fields at 10cm depth

collimator setting	6MV blocked	6MV unblocked	16MV blocked	16MV unblocked	16MV blocked	16MV unblocked
field I op.	*		*		$	
10x10	0.990	1.00	0.994	1.00	0.987	1.00
8.5x8.5					0.977	0.983
14x11			1.00	1.020		
15x15			1.008	1.041		
field II op.	#		#		@	
10x10	0.992	1.00	0.996	1.00	0.981	1.00
8x8					0.970	0.977
field II wg.	#		#			
10x10	0.995	1.00	0.995	1.00		

*Blocked field area: *=85cm^2 #=92.5cm^2 $=69cm^2 @=55cm^2*

Table (9-XVIII) then presents calculated total output factors for the blocked fields using the approach of equation (9-3) as described in section 9-2-7 showing close agreement with measured total output factors within 1.0%. This equation considers phantom scatter independently of collimator size. The phantom scatter is taken to be that appropriate to the area of the phantom being irradiated, whilst the head scatter

is selected appropriate to the collimator positions. This approach then is shown to give better prediction of measurement in these situations than the standard planning approach and shows the typical errors present for such typical conformal blocks.

c) Phantom scatter factors

The differences between the derived phantom scatter factors, presented by collimator size (open fields), or by irradiated area (blocked fields) are shown in Table (9-XX). Some blocked fields show greater phantom scatter factors than unblocked, but this simply reflects the experimental uncertainties (<1.0%). These results support the previous statement that phantom scatter factors are solely dependent on irradiated area within experimental uncertainties.

Table 9-XX: Phantom scatter factors for blocked and unblocked fields at depths of maximum and 10cm

	6MV				16MV				16MV			
	PSF-dmax		10cm-dep.		PSF-dmax		10cm-dep.		PSF-dmax		10cm-dep.	
coll. set.	blo. *	unbl ock.	blo. *	unbl ock.	blo. *	unbl ock.	blo. *	unbl ock.	blo. $	unbl ock.	blo. $	unbl ock.
8.5									1.006	0.997	0.983	0.987
10	1.002	1.00	0.992	1.00			0.995	1.00	1.007	1.00	0.987	1.00
14x11					0.997	1.003	0.994	1.011				
15x15					1.001	1.009	0.992	1.027				
fieldII	#		#		#		#		@		@	
8x8									1.002	0.996	0.977	0.996
10	1.001	1.00	0.990	1.00	0.999	1.00	0.995	1.00	1.010	1.00	0.982	1.00

Blocked field area: *=$85cm^2$ #=$92.5cm^2$ $=$69cm^2$ @=$55cm^2$

9-3-5-MLC and Irregular Fields

a) Regular MLC Fields

To assess the influence of multi-leaf collimators (MLC) on output factors for regular fields, the jaw field definition was replaced with MLC definition. Table (9-XXI)

compares the MLC head scatter factors with standard collimator head scatter factors at the depth of dose maximum and at 10cm. Firstly the head scatter factors for the MLC were obtained where the standard collimators (jaws) were fixed at 30x30. These are shown in column 3 normalised to the 10x10 MLC setting (jaws set fixed at 30x30). The results show a much smaller variation with MLC setting than with jaw setting, typically around half the difference from unity for the same defined area. The absolute difference between the two situations can be seen from the results of measurements for a 10x10 field defined by the MLC with jaws at 30x30 to the measurement for a 10x10 field defined by the jaws. This was measured to be 1.024 (reflecting the collimator scatter factor for the 30x30 jaws positions). Secondly head scatter factors were measured where the X-jaws are constant (X = 30) but the y-jaws were varied to equal the MLC field set. It should be noted here that the MLC leaves move in the same direction as the X jaws, i.e. each square field was defined by the MLC jaws in the x-direction (with back-up x-jaws left at 30cm setting) and by the y jaws in the y-direction. The results show that differences are not significant between this situation and the normal jaw situation except for the constant multiplying factor which is the ratio of 10x10 fields defined in each way (1.006) Both these experiments show that MLC on its own has a significantly smaller effect on head scatter factors by amounts which are typically half the difference (or less), than for the jaws themselves. This is due to the fact that in this linac design the multi-leaf collimator is located farther from the source than the jaws and therefore gives less backscatter to the monitor chamber. Therefore this MLC can be considered in the same way as blocks for regular fields in terms of head scatter factors changes i.e. the head scatter factors are essentially defined by the jaw settings. Nevertheless, for more accurate dose calculation, the effect of leaf setting could be taken into account. For large jaw settings the variation is typically within ±1.5%. For the X jaw set large, but the Y jaw following the MLC closely the variations are small. Typically in clinical practice the jaws will be brought in as close as possible to the MLC setting and so changes in factors would be expected to be small. As a test of this, Table (9-XXII) shows the total scatter factors with different collimator jaw settings varying for

leaf size 10x10 and leaf size 24x24cm, compared to calculated values using equation 9-3b and compared to calculated values using a standard unmodified approach (i.e. the latter depending only on irradiated area).

Table 9-XXI: The head scatter factors for various MLC and collimator jaw settings at depths of dose maximum and 10cm

	depth of maximum			10cm depth		
	MLC=out*	X=Y=30$	X=30cm$	MLC=out*	X=Y=30$	X=30cm$
X, Y, MLC						
4x4	0.959	0.977	0.967	0.960	0.979	0.969
5x5	0.971	0.984		0.973		
6x6	0.979	0.990	0.986	0.981	0.991	0.987
8x8	0.992	0.995		0.993	0.996	
10x10	1.00+	1.00#	1.006+	1.00+	1.00#	1.006+
12x12	1.006	1.002		1.004	1.003	
15x15	1.012	1.007	1.015	1.010	1.007	1.013
20x20	1.018	1.013	1.022	1.015	1.010	1.019
25x25	1.022	1.013		1.019	1.009	
28x28	1.024	1.012	1.028	1.021	1.008	1.024
30x30	1.025			1.022		

** normal jaws field definition*

+ normalised to 10x10 defined by jaws

 # normalised to 10x10 defined by MLC (with jaws at 30x30)

$ x jaws fixed, field defined by MLC only

Table 9-XXII: Total scatter factors for different collimator jaws with constant MLC field at the depth of maximum, compared to calculated values using equation 9-3b

	MLC fixed field (10x10)			MLC fixed field (24x24)		
x, y jaws size	meas.	calc. (eq. 9-3b)	standard planning	meas.	calc. (eq. 9-3b)	standard planning
8x8	0.985	0.985	0.984			0.984
10x10	1.00	1.00	1.00	1.00	1.00	1.00
12x12	1.009	1.006	1.00			1.011
15x15	1.015	1.012	1.00			1.025
20x20	1.020	1.018	1.00	1.035	1.042	1.040
25x25	1.022	1.022	1.00	1.057	1.054	1.049
30x30	1.024	1.025	1.00	1.066	1.056	1.049

Tables (9-XXIII and 9-XXIV) compare the total scatter factors and phantom scatter factors for MLC fields with collimator defined fields, when X and Y jaws are constant (X=Y=30cm) and when only X-jaws are constant (X=30cm). In all conditions the derived phantom scatter factors are equal for the same irradiated area defined by MLC or by collimator jaw within experimental uncertainties. The phantom scatter factors at d_{max} produced by MLC fields are in agreement with phantom scatter data from BJR (25, 1996) within 1.0%. Therefore, when only regular fields are considered with jaws set closely to the MLC setting, the dosimetric characteristics of the MLC fields are similar to the standard fields in situations where MLC is situated below the jaws (as in this Varian machine). This maynot be the case for other MLC designs e.g. Philips.

Table 9-XXIII: Total scatter factor values for MLC and collimator defined fields at depth of dose maximum and at 10 cm

	depth of maximum			10 cm depth		
	MLC=out	X=Y=30	X=30cm	MLC=out	X=Y=30	X=30
X, Y, MLC						
4x4	0.940	0.957	0.949	0.870	0.892	0.882
6x6	0.967	0.978	0.975	0.928	0.939	0.936
8x8	0.986	0.989		0.969	0.973	
10x10	1.00+	1.00#	1.008+	1.00+	1.00#	1.008+
12x12	1.012	1.009		1.026	1.022	
15x15	1.025	1.021	1.032	1.055	1.049	1.060
20x20	1.042	1.035	1.049	1.092	1.082	1.097
25x25	1.055	1.043		1.118	1.103	
28x28	1.061	1.044	1.064	1.129	1.110	1.132

 # normalised to 10x10 defined by MLC (with jaws at 30x30), to convert to a true output factor, multiplying by 1.024. *+ normalised to 10x10 defined by jaw*

Table 9-XXIV: The derived phantom scatter values for MLC and collimator jaws, comparing with BJR(25) and Van Gasteren values at depth of maximum and 10cm respectively

	depth of maximum (PSF)				depth of 10cm			
	mlcout	x=y=30	x=30	BJR25	mlcout	x=y=30	x=30	V.G.
xy,MLC								
4x4	0.980	0.980	0.981	0.979	0.906	0.911	0.910	0.904
5x5	0.984	0.984		0.983	0.927			0.923
6x6	0.988	0.988	0.989	0.987	0.946	0.948	0.948	0.943
8x8	0.994	0.994		0.994	0.976	0.977		0.974
10x10	1.00	1.00	1.002	1.00	1.00	1.00	1.002	1.00
12x12	1.006	1.007		1.006	1.022	1.019		1.021
15x15	1.013	1.014	1.016	1.013	1.045	1.042	1.045	1.044
20x20	1.024	1.022	1.026	1.023	1.076	1.072	1.076	1.074
25x25	1.032	1.030		1.029	1.097	1.094		1.095
28x28	1.036	1.032	1.034	1.033	1.105	1.102	1.105	1.104

b) Irregular Fields

For MLC irregular fields a diamond shape was used as illustration Fig. 9-9, this reduced the field area approximately by 50% as compared to the jaw setting. The measured output factors for the diamond shapes were compared with the in house treatment planning approach calculations and with calculated values using the approach in equation (9-3b) at depth of dose maximum according to Table (9-XXV). The results showed up to 2.0% and 0.6% differences with standard planning calculations and equation (9-3b) calculated values, respectively. This shows that it is necessary to separate the dose component coming from the head and from phantom for accurate calculations. Equation (9-3b) was used also for depths' 5cm and 10cm, with consideration of phantom scatter factors from the MLC field area. Table (9-XXVI)shows good agreement for absorbed dose values between measured and calculated values within less than 0.5% for 5cm and 10cm. These differences are less than those obtained for blocked fields.

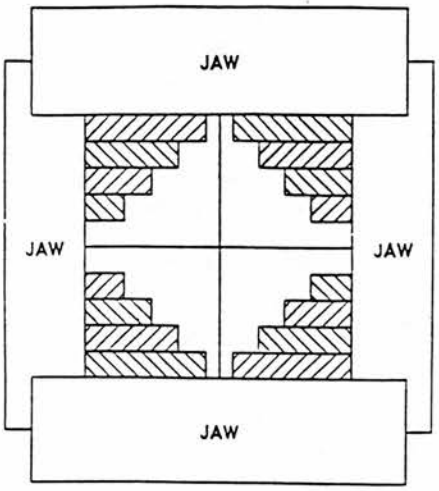

Fig. 9-9: Illustration of the MLC leafs set to form a diamond shape blocking that reduced the field area to approximately 50% of that area covered by collimator jaws

Table 9-XXV: Comparison of measured and calculated output values at depth of dose maximum using MLC fields to give diamond shaped fields

jaws	MLC*	Mea.#	st. planning	differenc.%	calculat. &	differenc%
6x6	4.3	0.958	0.941	1.8	0.960	0.2
10x10	7.0	0.991	0.975	1.6	0.991	0.0
15x15	10.6	1.016	1.002	1.4	1.014	0.2
20x20	14.2	1.033	1.021	1.2	1.030	0.3
26x26	18.5	1.049	1.037	1.2	1.044	0.5
30x30	21.2	1.058	1.043	1.4	1.052	0.6

** equivalent square (cm^2)* *& calculation by equation 9.3b*

 # Normalised to 10x10 defined by jaws

Table 9-XXVI: Comparison of total scatter factors between measured and calculated values for MLC fields at depth of 5cm and 10cm for diamond shaped fields using equation 9-3b

jaws	5 cm depth			10 cm depth		
	MLC* field area	meas.	calc. eq. 9-3b	MLC* field area	meas.	calc. eq. 9-3b
6x6	4.3	0.934	0.935	4.3	0.893	0.896
10x10	7.0	0.982	0.980	7.0	0.964	0.961
15x15	10.6	1.016	1.014	10.6	1.019	1.016
20x20	14.2	1.039	1.039	14.2	1.057	1.055
26x26	18.5	1.060	1.057	18.5	1.090	1.088
30x30	21.2	1.071	1.067	21.2	1.106	1.105

* *equivalent square* (cm^2)

9-4-Discussion

Monitor unit calculation is an important step in radiotherapy treatment preparation. The accuracy of monitor unit determination for specific patients can be significantly influenced by the determination and application of appropriate output factors. This work discusses separating the contributions of head scatter and phantom scatter to the dose. Total output factors and head scatter factors have been determined in a large phantom and a build up cap or a miniphantom, respectively at depths of dose maximum and 10cm. The previous chapter (8) showed that there is no significant differences between in air output factors determined for isocentric conditions and fixed source surface distance conditions. All measurements for output factors in phantom and in air in this chapter were carried out isocentrically.

9-4-1- Open Fields

Output factors in phantom and air are field size dependent (Figs. 9-1a-c to 9-2a-c and Tables 9-I and 9-II). The variations of head scatter factors with field size from 4x4 to 40x40 cm^2 for 6MV photon beams (CH6), 6MV (CH20), 6MV (Varian) 16MV (CH20) are summarised in Table (9-XXVII) at depths of maximum, 5cm and 10cm respectively, for open beams, wedged beams (4x4 to 40x40 cm^2) and rectangular fields (field variation as described in section 9-3-1-2 from 4x40 to 40x4 cm^2). The larger differences observed for S_c at depth of dose maximum as compared to 5 and 10cm are due to the additional effect of contaminant electrons at this depth. For depths beyond the range of contaminant electrons, S_c is essentially independent of depth. Table (9-XXVIII) gives a similar summary of the percent average changes in total scatter factors over the same range of conditions.

Table 9-XXVII: Variations of head scatter factors for different situations (see text)+

	6MV (CH6) %			6MV (CH20) %			6MV (Varian) %			16MV (CH20) %		
	d_{max}	5cm	10	d_{max}	5cm	10	d_{max}	5cm	10	d_{max}	5cm	10
open	13	11	11	10	8	7	7	6	6	11	6	4
wedg	17	17	15	14	14	12	-	-	-	14	-	13
rect.	5	5	5	4	4	4	3	3	2	4	4	3

+ overall variations are given as percentage changes normalised to the reference field (10x10) value

Table 9-XXVIII: Variations of total scatter factors for different situations (see text)+

	6MV (CH6) %			6MV (CH20) %			6MV (Varian) %			16MV (CH20) %		
	d_{max}	5cm	10	d_{max}	5cm	10	d_{max}	5cm	10	d_{max}	5cm	10
open	20	22	31	18	19	28	12	17	27	16	16	22
wedg	23	24	31	20	21	27	-	-	-	19	19	23
rect.	6	8	9	6	6	8	4	6	5	5	5	6

+ overall variations are given as percentage changes normalised to the reference field (10x10) value

Phantom scatter factors at depth of dose maximum (PSF) and 10cm were consistent with published tabulations (Figs 9-3a to 9-3c). Their values were in agreement with PSF_s obtained from BJR (25, 1996) and 10cm S_p from Storchi and Van Gasteren (1996) values respectively within 1.0% (Tables 9-IIIa and 9-IIIc). The phantom scatter factors at depth of 5cm were in agreement with Van Gasteren et al (1991) typically also within 1.0% (Table 9-IIIb). Therefore, the differences of total output factors $S_{c,p}$ (Figs. 9-1a to 9-1c) for different machines of the same energy are due to differences in collimator scatter effects. Uncertainties on the measurements of total scatter factors and head scatter factors are estimated at from 0.5% to 0.7%, and for the derived phantom scatter factors obtained are from 0.7% to 1.0%.

9-4-2- Rectangular Fields

Head scatter factors for rectangular fields are different from square fields of the same equivalent areas, because upper and lower jaws are at different distances from the source and monitor ionisation chamber with different influence of scatter (exchange effects). This can be seen from the results for rectangular fields for different energy at depth of dose maximum and 10cm according to Tables (9-IV, 9-V and 9-VI). Considering these tables the measured output factor values could vary up to 3.0% for the same field size when interchanging the collimator settings. Therefore, the standard head scatter measurements for square fields must be replaced by measurements for different collimators. Table (9-VI) compares the head scatter values for upper and lower jaws with the Sterling formalism (eq. 9-5) which does not take account of exchange effects. The differences between measured and calculated values are within 1.0% when the upper jaws change and the lower jaws are fixed and 2.5% when the lower jaws change and the upper jaws are fixed. Therefore, the side of the equivalent square should be obtained using different weights for the upper and lower collimators. (Vadash and Bjarngard, 1993). Of course the most accurate method is to use head scatter data, which have been directly measured for combinations of width(W) and length (L) for each particular

machine in a clinic, however too many measurements are required for this approach so a systematic use of symmetric field data is preferable and has been shown here to be appropriate.

The differences of output factors using simple field area are up to 5.0% showing the well-recognised necessity of at least using equivalent area (Table 9-VI).

Phantom scatter values for rectangular fields are approximately the same within experimental uncertainties when the upper jaws or the lower jaws are changed but producing the same field sizes. These values are in agreement with BJR (25, 1996) and the Van Gasteren (1996) values at depth of dose maximum and 10cm, respectively (Table 9-VII and 9-VIII). This clearly confirms that phantom scatter factors are determined only by the area of the phantom being irradiated, and are not dependent on collimator jaw position. Therefore, the total output value differences for the same equivalent areas of rectangular fields but using different jaws (Table 9-VI) are only affected by collimator scatter factor differences.

9-4-3- Wedged Beams

Figures (9-5 and 9-6) show the total scatter factors and head scatter factors for wedged beams as a function of field size. Comparisons of these figures with figures (9-1 and 9-2) for open fields show that there is an increase in the variation of output factors with field size, when the wedge is inserted in photon beams. This is also observed clearly for rectangular fields in Fig. (9-7). Therefore a wedge factor can be defined which increases with field size. The results showed 6.0% changes in wedge factors over field size from 4x4 to 20x20 (Table 9-IX). Similar observations have been reported with up to 3.5-9.0% changes by other workers (Wu et al 1984, Palta et al 1988, and Heukelom et al 1994). This variation is caused by a wedge-induced change of the photon fluence of both primary photons and scattered photons.

The contributions to phantom scatter factors due to a change in photon fluence for wedged beams is negligible (Table 9-X). The phantom scatter factors at d_{max} for wedged beams are in good agreement with phantom scatter factors obtained for open fields and to BJR values (BJR25, 1996) within 1.0%. They are also in agreement with other works (Brown et al 1987, Heukelom et al $1994_{a,b}$, and Cozzi et al 1996). Also the phantom scatter factors for wedged beams at 10cm depth are in good agreement with phantom scatter values obtained by Storchi and Van Gasteren (1996) within 1.0%. The effect of backscattered radiation produced by the wedge and reaching the monitor chamber may be large or small depending on the distance of the monitor chamber from the wedge.

The depth dependence of wedge factors is also observed in Table (9-IX) at depths of dose maximum, 5cm and 10cm. The variation of wedge factors with depth was within 3.0% for all fields. This was also reported at 4.0% and 2.0% up to 25cm depth for 4 and 10 MV units (McCullogh et al 1988), and between 2.0% and 7.0% at 15 cm depth (Knoos et al 1991) for a range of energies. The variation of wedge factor with depth can be due to a change in the energy spectrum of the photon beam (beam hardening) as described in section 9-3-2. For higher energy photon beams in particular it can also be due to contaminant electrons in the primary photon beam influencing the wedge factor at small phantom depths (Heukelom et al $1994_{a,b}$). Therefore, the variation of wedge factor requires careful study consistent with the implementation and use of wedge data in a given centre's planning calculation approach.

Based on these measurements it is suggested that the reference depth for planning data measurements should be taken to be similar to the reference depth defined in dosimetry protocols (IAEA 1987). This depth also can be used for other measurements such as output factors. Recently, an ESTRO working party on monitor unit calculations (1997) has recommended using a reference depth of 10cm for normalising percentage depth dose and output factors. It is also suggested from the measurements that algorithms

should consider wedged beams separately from corresponding open ones for depth dose. A field size dependent wedge factor or a separate output factor for wedged beams should be used.

9-4-4- Asymmetric Fields

Asymmetric collimation allows the independent movement of separate jaws or collimators. The total scatter factors and head scatter factors have been measured along the x-axis and y-axis asymmetrically (Tables 9-XI and 9-XII). The behaviour of the parameter S_c for asymmetric fields is different from symmetric fields because of the flattening filter design and jaw positions. The differences in output factors (total scatter factors) for symmetric and asymmetric fields can introduce non-negligible errors in calculation if only the equivalent areas are considered.

Table (9-XIV) shows the differences between measured total scatter factors and those obtained by the routine treatment planning calculations approach in the department. For the situations considered, there were up to 2.0% differences between measured and calculated value. The reason is that symmetric output values are used for asymmetric fields without correction. This can produce uncertainties for dose calculation.

A method calculating the output of the asymmetric field relative to the output for symmetric fields according to equations (9-1 and 9-2) was investigated as described in section 9-2-7. The calculations require only available data obtained from measurement on symmetric fields and use appropriate half field (or quarter field) scatter factors for each half or quarter of the asymmetric field, thereby accounting for the individual jaw positions. Measured and calculated output values based on this scheme agree to typically within 1.0% (Table 9-XIV). This can also be seen for total head scatter factors according to Tables (9-XI and 9-XII). Therefore, it is possible to determine output factors for asymmetric fields from symmetric beam values using equations (9-1 and 9-2) with good accuracy.

Phantom scatter factors for asymmetric fields were in good agreement with symmetric field phantom scatter values of the same area (Table 9-XV). This confirms again that phantom scatter is determined only by the irradiated volume (area) of the phantom.

9-4-5- Blocked Fields

Van Dam et al (1992) reported significant deviations between measured and calculated output values for blocked fields. They concluded that deviations are due to differences in the balance between gain in block scatter and loss of head scatter. The output factors in air (head scatter factors) for different clinical conformal block shielded areas were measured for 6MV and 16MV beams at depth of dose maximum and 10cm according to Tables (9-XVI and 9-XVII). Considering these values the differences between blocked and unblocked fields are generally not significant. The reason may be due to the fact that for the smallest block opening (4 and 5.5cm), only peripheral parts of the flattening filter are obscured from the measurement point and therefore only small changes in that component of head scatter are produced. Also the blocking is not very irregular or elongated so the jaw settings are not very different to the edges of the blocks. However, differences were observed for blocked and unblocked head scatter values at depth of dose maximum. This can be due to contaminant electrons produced by blocks affecting the situation at this depth. For total output factors the differences between blocked and unblocked head scatter values were up to 3.0% (but mostly within 1.0%). These results agree with results obtained by Tatcher and Bjarngard (1994). They also obtained less than 1.0% differences between measured output values and predicted values for blocked fields.

Table (9-XVIII) compares the output values for conformal blocked fields with calculated values from the standard planning approach in the department. The differences were significant, at up to 3.0%. The reason for these differences is due to the fact that the standard planning calculations use the effective irradiated field size area for monitor unit

determination. An approach based on separating head and phantom scatter was investigated, where the calculated values showed differences of less than 1.0% with measured values (Table 9-XVIII). The main differences in total scatter factor between blocked and unblocked fields of a given collimator setting are due to differences for phantom scatter values (Table 9-XX), i.e. the block does not significantly affect the head scatter factors, so S_c should be selected by jaw settings and S_p by blocked field area.

9-4-6- Multi Leaf Collimator (MLC) Fields

Multileaf collimators (MLC) are becoming increasingly available and can be used instead of blocks for field shaping and conformal therapy. A MLC removes the need for cumbersome shielding blocks, handling and storage. It allows beam delivery from any angle to produce the optimum dose distribution for any shielding shape without a tray. It can also reduce the treatment time and minimise patient discomfort and movement, and therefore also improve accuracy in dose delivery from this point of view. Output factors were measured for a constant jaw setting (x = y =30cm) and variable MLC field setting according to Table (9-XXI). The results show only small changes of head scatter values (generally in clinical situations expected to be < 1%). This is due to the MLC being located further from source than the jaws, and producing scatter contributions which are smaller than those from jaws. Therefore, in this unit (Varian 600) the MLC can be considered similar to a block in this context. For more accurate dose calculation, the effect of particular leaf settings can be taken into account (Table 9-XXI).

The scatter characteristics of a given MLC system is similar to a standard set of collimators in a similar position, therefore depending on head design, the output factors can be different. For example in the accelerator investigated (Varian 600) the results are in agreement with expectation for a MLC which is a tertiary collimator (Tables 9-XXI and 9-XXII). In this type of machine the MLC is located below the collimator system and therefore farther from the source and the monitor chamber. The phantom scatter produced by regular MLC fields are in agreement with phantom scatter obtained from

BJR (25, 1996) and Storchi and Van Gasteren (1996) for depths of maximum and 10cm respectively within 1.0% (Table 9-XXIV), showing again that there is no difference between phantom scatter obtained for MLC fields or for collimator defined fields.

The measured output values for MLC fields which are significantly modified from the collimator jaws shape (e.g.diamond shape) were in agreement with calculated values within 0.6% at depths of maximum, 5cm and 10cm (Table 9-XXV and 9-XXVI) where the calculations separated head and phantom scatter and combined appropriate values for the particular irradiated situation. The head scatter is defined by the collimator jaw settings and the phantom scatter is defined by the MLC field (irradiated area). For different designs of machine e.g. Philips linacs/MLC this may not be appropriate, because the MLC is located higher in the head replacing the upper set of jaws. Therefore, the amount of head scatter that reaches the point of measurement and the monitor chamber is more significantly affected by the MLC position. This means that the collimator scatter should probably be considered as that for an equivalent square of the irregular field (Palta et al 1996).

The standard treatment planning approach in this department uses the effective field (blocked beam) area for monitor unit calculation. The differences between measured output values and calculated values using the standard planning approach were up to 2.0% (Table 9-XXV). This shows larger differences than the algorithms proposed and investigated above relative to measured values. Therefore, significant uncertainties can be produced where collimator setting and field size on the phantom are not treated separately in monitor unit calculations for blocked and MLC fields.

9-5-Conclusion

The accuracy of monitor unit determination can be significantly influenced by the determination and application of output factors. Various configurations of open,

wedged, blocked and MLC beams for symmetrical and asymmetrical situations have been studied. From the extensive results the following points are concluded.

-It is necessary to separate scatter components from the linac head (head scatter) and from within the phantom (phantom scatter) when the collimator setting and irradiated area are significantly different.

-The phantom scatter factors are determined only by the irradiated volume of the phantom. These values are consistent for symmetric, asymmetric, rectangular, and wedged beams of the same equivalent areas. This means that phantom scatter factors are consistent in all such situations, and can be defined by tabulated data at the appropriate reference depth for the beam quality of interest;

-Head scatter factors for rectangular fields are different from square fields of the same equivalent areas . Upper and lower jaws are at different distances from the source and monitor ionisation chamber, with different influence of scatter (exchange effect). Therefore the exchange effect should be considered in the calculation of equivalent square, etc. (Vadash and Bjarngard 1993);

- Estimated uncertainties on measurements of total scatter factors and head scatter factors are from 0.5% to 0.7%, and for the derived phantom scatter factors are from 0.7% to 1.0%.

-Wedge factors are field size and depth dependent. Algorithms should consider wedged beams separately from corresponding open ones for depth dose. A field size dependent wedge factor or a separate output factor for wedged beams should be used;

-A reference depth beyond the depth of maximum should be considered to avoid the influence of contaminant electrons. A recent ESTRO working party on monitor unit

calculation (1997) has recommended using a reference depth of 10cm for both percentage depth dose and output factors and this is shown to be adequate for energy of at least up to 16MV. Such an approach however has many implications for planning and dosimetry procedures and requires very careful discussion and implementation. If may be better to run it as an alternative, as a check system, in parallel with the established approach in a department.

-It is possible to determine output factors for asymmetric fields from symmetric beam values for some simple situations. A calculation method was proposed and tested that requires only available data obtained from measurement on symmetric fields, and predicts generally to within 1%.

-There were no observed significant differences for head scatter values between blocked and unblocked fields. The main differences between blocked and unblocked fields are due to differences for phantom scatter values (change in irradiated area). The algorithms should consider head scatter and phantom scatter separately. The equation (9-3) showed good agreement with measured values mostly within 1.0%;

-For the Varian MLC the change of head scatter factors was smaller than for the standard collimator system values. For this MLC design (Varian) the MLC can be considered as a block in its effect on output factors. However for more accurate dose calculations the effect of particular leaf settings could be taken into account.

-To define monitor unit and output factor for MLC fields, the contribution of head scatter factor and phantom scatter factor for such irregular fields should be separated. The calculated values following this approach showed good agreement with measured values for both MLC and blocked fields to within 1%. It considers head scatter defined by collimator jaws and phantom scatter by MLC setting. This might not be appropriate for Philips machine, because there the MLC is located above the collimator system. For

this type of accelerator the head scatter should probably be considered as an equivalent square of the irregular field. Therefore the appropriate approach for a given MLC depends on the design.

In summary it can be concluded that the extensive measured and calculated values show that separating head scatter and phantom scatter for regular and irregular fields provides an acceptably accurate method to calculate monitor units for standard and conformal radiotherapy treatments certainly to within ±1.0% and provides an improvement over simpler approaches which in the range of situations investigated here give differences up to 3.0% compared with measurement.

Chapter 10

10-Summary of Experimental Assessment of Achievable Accuracy in Radiotherapy

Table (10-I) summarises the uncertainty values from basic dosimetry to the patient dose delivery. The measured values are compared with those obtained from estimated values (chapters 3, 4, 5, and 6). All uncertainties in the table, as in the rest of the section are given as 1 standard deviation.

Table (10-I): The uncertainties from standards laboratory to the patient dose delivery (1SD)

	Estimated values		**Measured values**	
	airkerma based dosimetry % Brahme(1988)	**D_w based dosimetry % Thwaites(1993)**	**D_w based dosimetry (This work) %**	**sources**
beam calibration				
1	0.5	-	-	
2	0.3	0.7	0.7	NPL
3	0.3		0.25	records & exp.
4	0.5			
5	0.5	0.6	0.2	records
6	2.5*			
7	1.0	0.8	0.6	records & exp.
8	1.5	1.0	1.0	records
total (beam calibration)	**3.3**	**1.6**	**1.4**	
other single-field parameters determination		**2.0**	**1.0**	experimental
Treatment plann.				
9		2.0	1-2	experimental
10			1-2	experimental
11		2.0	1-2	experimental
convolution (2D)				3.0 (from the
pencil beam(3D)				3.0 literature)
superposition(3D)				3.0
12		1.0[$]	0.5-1.0[$]	experimental
(planning)Total		**>3.6**	**1.9-3.7**	
		(total)3.8	(entrance) 3	in-vivo
Dose delivery			(exit) 3.5	dosimetry
			(total) 3.25	
Total (end)		**5-6**	**4-5**	**1 S.D.**

**later replaced as 1.4% from Monte Carlo calculation (Andreo 1991)*

+assuming all contributions are included as tabulated

 # using 2.5% for target volume dose delivery instead of 3.25% (field data) decreases these final figures by approximately 0.5% (see text)

$ for conventional fields; also for irregular, blocked, asymmetric, MLC, etc provided S_c and S_p are accounted for correcting (if not uncertainties are greater)

1-physical constants, 2-calibration: secondary standard, 3-calibration: reference instrument, 4-transfer K_{air}, 5-calibration: field instrument, 6-physical constants and user factors, 7-field instrument, 8-dose/monitor unit variation, 9-patient data, 10-different planning system in simple situations, 11-additional uncertainties due to inhomogeneity algorithms, 12-MU calculation

Table (10-II) shows the consistency obtained in a quality audit programme between centres (Scottish+ group). Also the results for a single department are summarised (chapters 4 and 5).

In general, Tables (10-I and 10-II) show that the clinical requirements on dosimetric precision can be achieved in optimum conditions within a given centre and also in simplified conditions centre-to-centre. Following the arguments in section 5-4-2 and using an estimate of 2.5% for the uncertainty on target volume dose delivery from all fields (consistent with the single field in vivo figures given here) would change the total values from 4-5% to 3.4-4.5%. However, analyses of the results point by point and field by field (Table 5-IV) show potential problems in treatment planning system, algorithms and particular treatment situations, in particular around inhomogeneities, interfaces, due to lack of scatter, etc. Therefore, it is not possible to achieve the clinical requirements on accuracy unless the whole set of conditions are optimal and potentially, particularly for complex situations, uncertainties may be larger than 5.0%.

Table (10-II): Accuracy achievable (1sd) in a single department and consistency achievable between Scottish+ centres in the quality audit programme

	uncertainties at the different levels of radiotherapy	
	single department (%)	centres (Scottish+ group) %
geometric phantom		
reference point	0.8	1.3
other single field factors	1.0	1.0
homogeneous phantom	1.3	1.7
inhomogeneous phantom (all points)	1.6	2.4
semi-anatomic phantom		
2D- TPS (TV)	1.3	
2D- TPS(all points)	2.0	
3D- TPS (TV)	1.3	
3D- TPS (all points)	1.4	
Thorax (TV)	1.0	1.6
Thorax (all points)	1.2	3.6
Breast	1.8	3.6
in-vivo dosimetry		
Breast	entrance (2.5)	
Head and Neck	entrance (3.0) exit (3.5)	

Table (10-III) shows the increasing uncertainties from basic dosimetry to patient dose delivery in optimum situations for one single centre and between centres. In-vivo dosimetry measurements using diodes for head and neck treatments show 3.25% (1sd) variation. Some components of the preceding uncertainties (e.g. patient data, TPS, etc) may already be included here. Dose delivery uncertainties may be increased for other sites, depending on the particular situation and conditions. Summing all these uncertainties for a worst-case (but still all conditions optimised) total gives 4-5% (Table 10-I). Table (10-III) then compares the summed uncertainties for one single department with that for all centres.

Uncertainties are increased moving from one department to many departments according to Table 10-III (last column). If all centres use the same calibration laboratory and protocol, then some systematic uncertainties are removed from consideration of dosimetry consistency (columns 3 and 4). This the second column gives an estimate of overall achievable accuracy, whilst column 3 gives an estimate of achievable departmental precision. Column 4 gives an estimate of achievable inter-departmental precision. Column 5 gives the quadrature-subtracted differences between the single department and multi-department figures. The final row of figures uses the realistic best case in vivo estimate of multiple field target volume dose delivery uncertainty of 2.5%, rather than the row single field data.

Table 10-III: Cumulative uncertainties up to and including each listed stage from basic dosimetry to patient dose delivery in optimum situations for one single centre and between centres (1sd)

	uncertainties with one standard deviation level			
up to and including	**NPL to dose delivery %[+]**	**single centre[x] %**	**all centres[x] %**	**differences %**
basic dosimetry	1.4	0.8	1.3	1.0
single field	1.7	1.3	1.6	1.0
treatment plan.	2.6-4.0	1.6-2.4	2.3-4.0	1.7-3.2
dose delivery	4 to 5%*	3.5 to 4%*	(4 to 5%)*	-
dose delivery	3.6-4.5%#	3.0-3.5%#	3.4-4.5%#	

**using 3.25% for dose delivery (direct field data)*

#using 2.5% for dose delivery to target volume (estimated target volume value)

+ overall absolute accuracy

x consistency (reproducibility), i.e. remaining common systematic differences e.g. due to basic physical data values

For one single department random uncertainties within the department are important. If other centres are involved, systematic uncertainties between centres can again contribute to

the inconsistency as systematic uncertainties in parameters involved in a given set of measurements in a particular centre may be effectively randomly distributed across different centres.

In general Table (10-I) combining estimated uncertainties on the listed stages shows a good view of achievable accuracy up to patient dose delivery within a single department, with achievable sd on the target volume dose just matching the 3-3.5% clinically required value in optimum situations. Also Tables (10-II and 10-III) show that an achievable sd on target volume dose (precision) can be less than this 3-3.5% both single centre and centre to centre in optimum conditions. Therefore, the answer to the question "can we achieve the required accuracy at the end point of patient dose delivery in radiotherapy dosimetry?" is yes, in optimum conditions within a centre and centre to centre. However this requires very careful attention to procedures and quality control at all stages. Also potentially larger uncertainties may be present for more complex situations and non optimal conditions, particularly in conditions of poor quality assurance at all stages.

11-Summary and Conclusion

11-1-Introduction and Required Accuracy in Dosimetry

The purpose of treatment of cancer is to remove, kill or prevent growth of the cancer cells. This can be carried out by surgery, radiotherapy, chemotherapy or a combination of modalities. In radiotherapy, tumour cells are killed or damaged by ionising radiation. The dose required to achieve cell killing is variable, because the cells have different sensitivity to radiation. The radiation tolerance of the normal tissues inside the irradiated volume generally limits the absorbed dose values needed for adequate tumour control to ensure they are below those which cause unacceptable complications. The tumour cells are surrounded by the normal tissues, and the tumour mass may also spread and infiltrate some normal tissues. Therefore, it is not possible to kill all tumour cells without some normal cells receiving a high dose and this restriction is due to the narrow relationship between the probability of local tumour control or normal tissue injury and total absorbed dose. The aim of radiotherapy is to maximise the dose to tumour cells and at the same time minimise dose to normal tissue cells.

Accuracy of radiotherapy dosimetry and treatment delivery is vital to produce effective quality in treatment, because of the steepness and small separation of the dose responses of local tumour control and normal tissue complications. Based on clinical data on these dose-effect relationships, an accuracy is recommended of ±3% on absorbed dose delivered at the specification point and ±5% at other points in the target volume (Mijnheer et al 1987, Brahme et al 1988, Thwaites et al 1992). This is a requirement at the one standard deviation level and applies to final patient doses, incorporating all contributing uncertainties up to and including treatment delivery. It is generally taken to be consistent with the ICRU (1976) requirement of ±5% on delivered dose.

In order to achieve these requirements, quality assurance and quality control programmes have an obviously important role in reducing uncertainties and improving accuracy and there are many national and international recommendations concerned with this, for example the recent guidelines from ESTRO (Thwaites et al 1995_a). Recently, many of these have been framed within guidelines for formal quality systems. In-vivo dosimetry, portal imaging and internal and external quality audit are additional complementary systems which can assist in identifying and quantifying errors and uncertainties. This work has comprehensively examined the achievable accuracy and consistency in radiotherapy dosimetry in one single radiotherapy centre in conditions that are expected to be close to optimal and between centres in the surrounding region.

The accuracy achieved in practice can be estimated either by a priori methods or by measurement-based investigations, including dose intercomparison, which can be carried out at various levels of the technical radiotherapy process to define errors and uncertainties at each of those stages. This work investigates the experimental analysis of achievable accuracy in the different steps up to and including dosimeter and treatment machine calibration and some aspects of treatment planning. Specific studies have been carried out to separate out effects at different stages. The experimentally assessed values have been compared to estimated a priori values from previous studies.

11-2-Uncertainties in Basic Dosimetry up to and including Beam Calibration

The uncertainties in different protocols based on air kerma calibration and water absorbed dose calibration have been compared. One of the major sources of discrepancies between protocols is in the different sets of stopping power ratios. However, there is generally good agreement between modern protocols to within approximately 1%. The development of dosimetry techniques at standards labs e.g. calorimetry at the NPL in the UK, permit considerable improvements in the direct determination of the absorbed dose to water in a water phantom. Different standards labs approaches are in agreement typically to within a

few tenths of a percent giving good confidence in the underlying basis of the dosimetry chain.

Here each possible step in the basic chain has been investigated either directly or using data from quality control records. The analysis and comparison between the uncertainty values obtained and the estimated values based on both air kerma calibration and water absorbed dose calibration by different authors showed that there is good agreement in most cases between measured and estimated values. This agreement is better for dosimetry based on the N_w calibration and the IPSM code of practice (1990) than for that based on an air kerma calibration and N_d protocols. In general, from the comprehensive results based on measurements and historical records, compared with estimated values, it can be concluded that the experimentally obtained uncertainties in the UK basic dosimetry chain and the estimated values based on water absorbed dose calibration and protocols support each other. Also the basic dosimetry based on water absorbed dose calibration protocols is more accurate than air kerma calibration based dosimetry. Overall uncertainties in basic dosimetry, up to and including beam calibration, for megavoltage x-ray beams are measured at 1.4% (implying also a consistent value for ^{60}Co should be approximately 1%) for UK procedures. This can be compared to an estimated values (Thwaites 1993) of 1.6% and to estimated values for air kerma based dosimetry of 2.5-3.5%.

11-3-Uncertainties in Clinical Dosimetry; Audit using a geometric phantom

A previously-designed geometric phantom, developed for a UK national dosimetry intercomparison and audit system (Thwaites et al 1992), has been used to extensively test achievable accuracy of dosimetry including some basic treatment planning parameters and processes in one department in conditions which are expected to be close to optimal. This has also been used as the first step in the development of an inter-departmental audit in Scottish and other radiotherapy centres (the so called Scottish+ audit group, within the UK radiotherapy dosimetry audit network). There was overall good agreement between

measured and calculated values in the single department for 3field planned irradiations and for single fields. The overall mean being 0.997±0.006 for homogeneous situations and 0.994±0.008 for inhomogeneous. However, analysis field by field showed that wedged beams produced generally larger uncertainties. The reason may be due to planning algorithms for wedged beams, misalignment of central beam axis with wedged axis, and small uncertainties in wedge position with time. Other sources of uncertainties from analysis field by field can be linked to the presence of inhomogeneities and the performance of inhomogeneity algorithms.

The mean ratio of measured to calculated values from interdepartmental audit at the reference point was obtained as 0.998 with a standard deviation of 1.3% (Table 4-IV), which is smaller than previously reported studies. This may be due to using one single standards laboratory and one clear code of practice in all centres. However, in addition the better precision found in this audit compared to the previous UK dosimetry intercomparison shows that dosimetry audit itself provides a basis for improving quality in treatment dosimetry and delivery. Similar improvements were seen in this round of multi-field audit. For both homogeneous and inhomogeneous situations, no systematic error was observed (means of 1.00 and 0.998 respectively), with standard deviations of 1.8% and 2.5% respectively.

In general, all stated values in these centres are in agreement with audit measured values within the audit system's predetermined tolerances and are therefore satisfactory within the terms of audit. Some reports (e.g. EORTC 1989 and IAEA/WHO 1980) have shown much larger uncertainties than this work and it therefore can be concluded that quality assurance and quality control programmes are vital and must be focused on all steps of radiotherapy. The overall results here both in the single centre and in multicentres give support for the stated expectation that the dosimetric and quality control structure of the centres involved is close to optimal, in that the figures obtained are close to estimated values (i.e. there are no

unforeseen uncertainties). If anything the values are less than estimated. Also the uncertainties obtained are at the lower end of the range of reported values from other intercomparisons.

11-4-The Development and Use of a Semi-anatomic Audit Phantom

Following this step of audit, a semianatomic phantom has been developed and constructed for more complicated situations in treatment planning. It has shapes and structures similar to some common sites, e.g. breast, thorax, head and neck, etc. but is still relatively simple. It is made from epoxy resin tissue substitute materials, contains "lung" and "bone" and is drilled to take small ionisation chamber inserts.

It has been extensively tested before interdepartemental audit use, by measuring the whole range of possible irradiation situations on five megavoltage photon beams, calculating dose distributions using the Edinburgh in-house treatment planning system and using Cadplan, and comparing measured results to expected values. This initial testing gives general overall confidence in the phantom and methodology. It also allows an extensive assessment of planning in this centre. There are no significant systematic discrepancies due to the phantom. The mean ratio of measured to calculated doses, using the Edinburgh in house TPS and Cadplan, for points in the target volume for all sites and energies has been obtained at 0.990 with a standard deviation of 1.3% (for individual sites s.d. varies from 0.3% to 2.0%). When points outside the target volume of the thorax were considered, uncertainties were increased (overall to s.d. between 1.4 and 2.0%). The analysis of results point by point and field by field showed that the major discrepancies can be linked to problems in the way that planning systems cope with some treatment situations, in particular around inhomogeneities, interfaces, edges of beams, etc. Others can be linked to small discrepancies in the department's dosimetry or processes, for example in planning data, machine performance, etc.

The phantom has also been used in two rounds of interdepartmental audit for thorax and breast sites. The mean ratio of measured to calculated values obtained were 0.982 and 0.997 with standard deviations of 1.6% and 3.6% for thorax and breast respectively. This shows that there is general agreement of doses within the specified audit tolerances, and generally satisfactory performance within the terms of the audit.

The audit system has been shown to be effective in use in interdepartmental studies, drawing attention to problem areas. It is cost effective. The hierarchical cycle system, coupled with visits and ion chamber measurements, allow a wide range of modalities and parameters to be tested in a reasonable time with one annual visit. The semi-anatomic phantom allows modified future audits, for example by incorporating additional inhomogeneities, by adding additional measurement points inside inhomogeneities, etc. and also by possibly modifying the external shape.

11-5-Uncertainties in Treatment Planning Inhomogeneity Algorithms

Analysis of single field results in both geometric phantoms and semianatomic phantoms showed that inhomogeneity algorithms are one significant source of uncertainty in treatment planning. Two relatively simple experimental situations were used to test the performance of available 2D and 3D inhomogeneity algorithms in different planning systems by using the IPSM geometric phantom and a slab or sheet interface phantom. One of these tested doses and algorithm performance beyond a reasonably large inhomogeneity (lung) and one close to a cork (lung) and tissue interface. The results can be summarised as follows:

-In simple situations where electronic equilibrium exists, 2D and 3D algorithms (Batho, ETAR, METAR) show good agreement within less than 2.0% of measured values. Most values are within 1.0% of measured values.

-In electronic nonequilibrium situations e.g. the inhomogeneity interface between RMI/cork and inside the cork, all algorithms show significant deviations from measured values. 3D

algorithms (ETAR, METAR, DSAR) show better agreement with measured values than 2D algorithms, to within 3.0% (mostly). 2D algorithms show significant deviations up to 8.0%.
-All algorithms underestimate below the inhomogeneity in the interface situation, where there is a sudden increase in scattered radiation beyond the interface. Again 3D algorithms particularly METAR methods show better agreement than 2D algorithms with measured values, because they attempt to model this.
-If no inhomogeneity correction is made, errors can be produced up to 6.0% for typical simple three field situation where one field passes through lung and up to 25% for the individual field passing through the typical lung dimensions. Larger errors may be present close to interfaces. It is therefore stated that any available inhomogeneity correction algorithms in treatment planning are better than using no correction at all.

In general 3D algorithms show better agreement than 2D algorithms and they must be used if available. However, these methods still produce significant dose calculation errors in electronic disequilibrium situations. More complex algorithms or Monte Carlo methods will produce better agreement but at the expense of larger calculation times on current hardware.

11-6-Overall uncertainties in patient Dose Delivery

Optimal uncertainties in patient dose delivery can be considered by using best case in-vivo dosimetry results in a single department with good quality control. For example Blyth et al (1997) measured entrance and exit doses with diodes on patients treated for head and neck malignancies. The standard deviation on the results of both entrance and exit dose measurements obtained were 3% and 3.5% respectively for field by field data. For multiple field target volume uncertainties a figure of 2.5% (1sd) was estimated. These results, coupled with the results for basic dosimetry uncertainty and those from geometric phantom and semianatomic phantom measurements (Table 11-I) gives a good estimate of achievable accuracy within a single department in optimal conditions. In general, from the values in

Tables (10-I, 10-II, and 10-III) it can be concluded that the clinical requirements on accuracy can be achieved in optimum conditions within a given centre and also in simplified conditions centre-to-centre.

However, analyses of the results point by point and field by field in both the geometric phantom and the semianatomic phantom measurements shows some larger uncertainties in particular treatment situations, in particular around inhomogeneities, interfaces, due to lack of scatter, etc. Therefore, at the present, the clinical requirement on accuracy is only achievable in optimal conditions and this requires very careful attention to procedures and processes and quality control at all stages. Potentially larger uncertainties may be present and therefore the clinically required accuracy may be unachievable for non optimal situations and complex situations, where uncertainties can be larger than 5%. In particular some international intercomparisons have shown much larger uncertainties in some countries or regions, even for basic dosimetry at the level of beam calibration.

11-7-Head and Phantom Scatter Separation for MU Calculation

One of the significant source of uncertainties associated with the absorbed dose delivered to the patient is due to dose per monitor unit determination and calculation in treatment planning for complex situations for linacs (or dose per unit time for ^{60}Co treatment unit). The accuracy of monitor unit determination for patient dosimetry calculations can be significantly influenced by the determination and use of head scatter and phantom scatter and their separate application. This becomes more important where the beam distribution is altered from the standard e.g. wedged beams, blocked fields, asymmetric fields, irregular and MLC fields.

To assess and compare the various measurement methods, head scatter factors were measured using plastic build up caps, brass caps, and brass and plastic miniphantoms for different situations. In addition these measurements were intended to investigate the effects

of secondary and contaminant electrons. For small field sizes (<4cm) the equilibrium mass is not fully irradiated at the 100SCD distance except for brass caps, and therefore for these smaller field sizes measurements were also carried out at a longer (150SCD) distance for both build up caps and miniphantoms.

Lateral electron equilibrium can be achieved when the radius of cap or miniphantom is large enough to produce secondary electrons balance, as a first approximation equal to the thickness required for forward electron equilibrium (build-up thickness). However, the measurements showed that lateral electron equilibrium can be achieved in smaller thicknesses. This is useful in order to choose as small as possible side wall thickness of cap or lateral diameter of miniphantom, because the small mass of cap or miniphantom can produce unwanted scatter, particularly for small field sizes, which can change the measured values. The use of either higher density caps, or longer distances, or both can be used for small field sizes. Any of these must be linked to standard measurements by overlapping the measurement range. In addition a new method was tried for small fields using a difference methods in sheet phantoms to effectively simulate a thinner miniphantom. This gave promising results but needs further development. This method can reduce the effect of scatter due to the mass of material present on the results. However, the uncertainties in the measured scatter factors are increased. The shortcoming of the method as initially implemented is the size and orientation of the detector to fit small field sizes. To solve this problem the sheet phantom method could be used with a PTW ionisation chamber in the vertical position, i.e. parallel with the beam (in fact it is possible that a 2x2 cm^2 miniphantom with a vertical chamber could also be used).

The head scatter factor measurements showed differences for different front wall thickness of caps due to contaminant electrons generated outside the caps reaching the chamber. However, miniphantoms showed they were of sufficient thickness to absorb contaminant electrons (e.g. 5cm for 6MV and 10cm for 16MV) for photon beams which reach beyond

the depth of dose maximum. The contaminant electrons are field size dependent, therefore the effect of contaminant electrons on small field sizes is small. In general thicker build up caps (thick enough for electronic equilibrium) give similar results to miniphantoms for 6MV beams, but this is not as true for 16MV.

The measurements at different distances showed that head scatter factors are essentially independent of SSD or SCD. There was no also significant difference for a change from 5cm to 10cm depths for 6MV photon beams, but differences were observed for the 16MV photon beam. Therefore, a normalisation depth of 10cm would be appropriate for high energy photon beams. This is in agreement with recommendations of some dosimetry protocols (IAEA 1987) and recently an ESTRO working party (1997) and Dutreix et al (1996) have recommended a reference and normalisation depth of 10cm, for all photon beam qualities (^{60}Co to 50MV). Therefore, ideally separation of the field size dependent total scatter factor into a collimator factor and a phantom scatter factor should be carried out beyond the depth of maximum using a miniphantom. This requires normalisation of all dosimetry procedures to this depth 10cm and the use of TPRs, etc. It needs very careful introduction and implementation as it affects other processes in radiotherapy. One solution may be to keep the usual approach, but use this other approach in parallel as an independent check for complex situations.

11-8-Head and Phantom Scatter Separation in Clinical situations

Various configurations of open, wedged, blocked and MLC beams for symmetrical and asymmetrical situations have been studied. From the extensive results the following points are concluded.

-It is necessary to separate scatter components from the linac head (head scatter) and from within the phantom (phantom scatter) when the collimator setting and irradiated area are significantly different.

-The phantom scatter factors are determined only by the irradiated volume of the phantom. These values are consistent for symmetric, asymmetric, rectangular, and wedged beams of the same equivalent areas. This means that phantom scatter factors are consistent in all such situations, and can be defined by tabulated data at the appropriate reference depth for the beam quality of interest;

-Head scatter factors for rectangular fields are different from square fields of the same equivalent areas . Upper and lower jaws are at different distances from the source and monitor ionisation chamber, with different influence of scatter (exchange effect).

-Estimated uncertainties on measurements of total scatter factors and head scatter factors are obtained from 0.5% to 0.7%, and for phantom scatter factors are obtained from 0.7% to 1.0%.

-Wedge factors are field size and depth dependent. Algorithms should consider wedged beams separately from corresponding open ones for depth dose. A field size dependent wedge factor or a separate output factor for wedged beams should be used;

-A reference depth beyond the depth of maximum should be considered to avoid the influence of contaminant electrons. A recent ESTRO working party on monitor unit calculation (1997) has recommended using a reference depth of 10cm for both percentage depth dose and output factors and this is shown to be adequate for energy of at least up to 16MV. Such an approach has many implications for planning and dosimetry and may be better used as an independent alternative (see above);

-It is possible to determine output factors for asymmetric fields from symmetric beam values for some simple situations. A calculation method was proposed and tested that

requires only available data obtained from measurements on symmetric fields and predicts to within 1.0%;

-There were no observed significant differences for head scatter values between blocked and unblocked fields at a depth of 10cm, where the collimator settings stay the same. It should be noted have that these are not very irregular or elongated conformal blocks. However there were observed differences for head scatter factors between blocked and unblocked fields at the depth of maximum, due to contaminant electrons produced by the blocks. The main differences between blocked and unblocked fields are due to the differences for the appropriate phantom scatter values (change in irradiated area). The algorithms for these situations should consider head scatter and phantom scatter separately. Equation (9-3) which does this showed good agreement with measured values to within 1.0%;

-For the Varian MLC the changes of head scatter factors with field size were smaller than for the standard collimator system values . For this MLC design, i.e. with the MLC added below the standard collimators, the MLC can be considered as a block in its effect on output factors particularly where the standard collimators are set not far outside the MLC which would generally be the case clinically. However for more accurate calculations the effect of particular leaf settings could be taken into account;

-To calculate monitor units or output factors for MLC (or conformally blocked) fields, the contribution of head scatter factor and phantom scatter factor for such irregular fields should be separated. The calculated values following this approach showed good agreement with measured values for both MLC and blocked fields to within 1%. The approach selects head scatter factors as defined only by collimator jaw settings and phantom scatter factor by MLC setting (or blocked field area). This might not be appropriate for Philips machine for example, because there the MLC is located above the collimator system

replacing the upper set of jaws. For this type of accelerator the head scatter should probably be considered as an equivalent square value of the irregular field. Therefore the appropriate approach for a given MLC depends on the design.

In general the extensive measured and calculated values show that separating head scatter and phantom scatter for regular and irregular fields provides a more accurate method to calculate monitor units for standard and conformal radiotherapy treatments than standard planning approaches (in the range of situations studied here to within 1.0% compared to within 3.0%).

11-9-Summary

In summary, it can be concluded that uncertainties are produced in all the different steps of radiotherapy treatment. The required clinical accuracy can be achieved in practice but only in optimum conditions within a centre and simplified conditions centre-to-centre, showing the need for careful quality control at all stages. For more complex situations and non optimal situations this may not be achievable as larger uncertainties have been noted in many studies. Further work is needed in this area to improve the situation. The pilot work has established the audit approach and methodology as a valuable system and has provided a baseline set of data for subsequent ongoing routine audit, building on the methods developed. Overall the continued improvement in accuracy will develop and should be encouraged. World-wide there is a lot of scope through improved quality control and the extension of international quality audit programmes to help all centres to achieve the levels of accuracy that have been demonstrated as achievable. This will have a significant impact on tumour control rates achieved, while maintaining normal tissue complication rates at acceptable levels.

Appendix I

"Publications and Presentations"

-Allahverdi M and Thwaites D I (1996_a). An experimental investigation of achievable accuracy in radiotherapy dosimetry, Proc. 3rd Biennial Radiotherapy Physics Meeting (Leeds, 1996) (York: IPEM) pp 69, Phys. Med. Biol. to be submitted.

-Allahverdi M and Thwaites DI (1996_b). A Semi-anatomic phantom for use in interdepartmental Audit, Proc. 3rd Biennial Radiotherapy Physics Meeting (Leeds, 1996) (York: IPEM) pp 13.

-Allahverdi M, Nisbet A, Thwaites D I (1996_c). An investigation of commercial epoxy-resin phantom materials for Megavoltage photon dosimetry, Proc. 3rd Biennial Radiotherapy Physics Meeting (Leeds, 1996) (York: IPEM) pp 13.

-Thwaites D I and Allahverdi M (1995_b). The development of interdepartmental audit methods, Radiotherapy and Oncology, vol. 37 (suppl. 1), 152.

-Allahverdi M, Thwaites DI (1996_d). Accuracy in radiotherapy Dosimetry, the 9th International Congress of Geographic Medicine (Oncology), Shiraz, Iran, 68.

-Allahverdi M and Thwaites DI (1997). Testing a Semi-anatomic phantom for use in interdepartmental Audit, Radiotherapy & Oncology, vol. 40 (suppl. 1), 570.

-Thwaites D I and Allahverdi M (1995_c). Evaluation of commercial epoxy-resin water-substitute phantom materials for MV photon beam use, Radiotherapy & Oncology, vol.37 (suppl. 1), 150.

-Allahverdi M and Thwaites D I (1996_e). Experimental Audit of Radiotherapy Dosimetry, 3rd. Iranian Medical Sciences Meeting, Manchester, session C, 2.

-Thwaites D I and Allahverdi M (1997). The use of a semi-anatomic phantom in Interdepartmental dosimetry audit, World Congress on Medical Physics and Biomedical Engineering, XIth International Conference on Medical Physics, Nice, France, 140-PSI.02.

-Nisbet A, Thwaites D I, Allahverdi M, Davison A (1997). An Evaluation of Commercial Epoxy-resin phantom materials in Dosimetry, World Congress on Medical Physics and Biomedical Engineering, XIth International Conference on Medical Physics, Nice, France, 132-PSI.34.

Appendix II

"An Evaluation of Epoxy Resin Phantom Materials for Megavoltage Photon Dosimetry"

M. Allahverdi, A. Nisbet* and D.I. Thwaites
(First draft)

Department of Medical Physics and Medical Engineering
University of Edinburgh
Western General Hospital
Crewe Road
Edinburgh EH4 2XU

(* Corresponding Author, present address: Department of Medical Physics, Sandringham Building, Leicester Royal Infirmary NHS Trust, Leicester, LE1 5WW)

Short Title: Epoxy Resin Phantom Materials in Photon Dosimetry

Abstract

Epoxy resin phantom materials have been available for some time and are widely used for dosimetry purposes, not least in audit phantoms. Information on their behaviour is partly available in the literature, but there are different mixes and formulations often given similar names and it may not be appropriate to transfer information from one material to another. Four commercially available water-substitute materials have been evaluated for use in megavoltage photon beams. They are the original White formulation, WT1, and a development of this to produce an electron beam formulation, WTe, both of which are available commercially by Radiation Physics at St. Bartholomew's Hospital, London; and two plastics produced by RMI, Wisconsin, the original 'solid water' mix, RMI 451, and the later version which replaced it, RMI 457. Four independent experiments were carried out to compare these materials to water in Megavoltage photon beams ranging in energy from cobalt-60 to nominal 16 MV X-rays and some general conclusions are drawn from the results as to their use. All are suitable for relative dosimetry in megavoltage photon beams. However, differences of up to 1% are observed for absolute measurements. The newer formulations, developed for electron beam use, are also closer to water for megavoltage photon beams.

1. Introduction

The 1990 Institute of Physical Sciences in Medicine (IPSM) Code of Practice for megavoltage photon beam dosimetry recommends that a water phantom be used in the calibration of megavoltage photon beam treatment units. It is recognised however that this may be time consuming and that the use of a perspex phantom may be more convenient for routine use. Today there are a number of epoxy resin water substitute phantom materials available and their use is becoming more widespread, both for routine dosimetry and in dosimetry intercomparisons (Thwaites et al 1992, Nisbet and Thwaites 1997). There is however little published data on the differences in dosimetry between water and these materials. The matter is complicated by the fact that there are different mixes and formulations often given similar names and it may not be appropriate to transfer information from one material to another.

Four commercially available water substitute materials have been evaluated for use in the routine calibration of photon beams. They are the original White formulation, WT1, (White 1977, Constantinou 1978) and a development of this to produce an electron beam formulation, WTe, both of which are available commercially by Radiation Physics at St. Bartholomew's Hospital, London; and two plastics produced by RMI, Wisconsin, the original 'solid water' mix, RMI 451, and the later version which replaced it, RMI 457. The results for the two RMI mixes are compared to other recently published results (Tello et al 1995).

2. Experimental Methods

Four independent experiments were carried out to compare these materials to water in megavoltage photon beams ranging in energy from cobalt-60 to nominal 16 MV x-rays. The nominal qualities were cobalt-60, 4 MV, 6 MV, 9 MV and 16 MV, with quality indices for the latter four of 0.63, 0.68, 0.72 and 0.765 respectively. The treatment units employed to produce the photon beams were a TEM mobaltron cobalt-60 unit, a Radiation Dynamics Dynaray 4, an ABB Dynaray CH6, a Radiation Dynamics Dynaray 10 and an ABB Dynaray CH20 respectively. All the measurement in the accelerators were made at 1 m FSD, the measurements in the cobalt-60 unit were made at 80 cm FSD.

An NE2571 graphite walled cylindrical ionisation chamber and NE2620A electrometer assembly was employed for techniques 1,2 and 3 and a NACP design plane parallel ionisation chamber was employed for technique 4. One 20 mm sheet from each of the solid phantom materials was machined to hold the NE2571 chamber with its central axis at 10 mm depth. In addition one 10 mm sheet of each material was machined to hold the NACP chamber with its front face flat against the phantom material. For all the measurements at least 150 mm of the appropriate phantom material was positioned behind the chamber to provide backscatter. The WTe phantom consisted of 250 mm x 250 mm sheets with thickness varying from 1 mm to 50 mm. The RMI 457 and RMI 451 phantom materials consisted of 300 mm x 300 mm sheets with thickness varying from 1 mm to 50 mm. The sheets were measured with a micrometer and found to be within ±0.1 mm of the nominal thickness. An IPSM geometry phantom (Klevenhagen et al 1983) constructed of WT1 was also employed . This had an insert for an NE2571 chamber at 50 mm depth in the material. Two water tanks were

employed: an automated Radiation Field Analyser (RFA) produced by Scanditronix and an in-house water tank constructed of perspex. A schematic diagram of this tank is shown in Figure 1. A permanent cavity constructed of perspex enabled the NE2571 to be positioned at 50 mm or 250 mm depth in water for a horizontal beam. The thin perspex wall was 2 mm thick.

Technique 1: The WT1 phantom was set up with the NE2571 chamber at 50 mm depth and the surface of the phantom at 1m FSD. A field size of 100 mm x 100 mm was used throughout. At least three readings were taken. The water tank was then set up with the surface of the phantom at 1m FSD. The surface level of the water tank was continuously monitored for water evaporation to ensure a constant FSD was maintained. The NE2571 chamber was positioned at 50 mm depth in a thin water proof sheath and at least three readings taken. The WT1 phantom was then set up once more with the NE2571 chamber at 50 mm depth and again at least three readings taken. The water phantom measurements were thus bracketed by two sets of measurements in the WT1 phantom.

Another cylindrical ionisation chamber was mounted on a clamp stand throughout the course of the measurements to act as a reference chamber. The tip of the reference chamber was positioned just within the light field to ensure negligible perturbation of the photon field. The reading obtained from the NE2571 chamber was divided by the reference chamber reading thus minimising the effects of drift in the output of the linear accelerator throughout the course of the experiments. A variation of $\pm 0.1\%$ is estimated. The temperature of the phantoms, as well as the pressure, were continually monitored throughout a series of

measurements and the results converted to a common temperature for all phantom materials.

The standard deviation of each set of readings was of the order of ±0.1%. The positional uncertainty of the chamber in the water tank was ±0.5 mm, i.e. ±0.2% in the readings. The same front pointer was used throughout the measurements to set the FSD in order to minimise differences in setting the FSD. The uncertainty in setting this is ±0.5 mm i.e. ±0.1% in reading. The uncertainty in temperature and pressure may be estimated as being ±0.1% from ±0.25^{0}C and ±0.1 mm Hg. The phantom ratios may therefore be estimated to have an uncertainty of ±0.3%.

Given the lower positional uncertainties associated with the plastic phantoms the WTe, RMI 451 and RMI 457 phantom materials were compared in turn to the WT1 phantom as above and phantom factors relative to water derived.

Technique 2: A horizontal photon beam was employed. The in-house water tank was set up with the chamber at 250 mm depth, and an FSD of 1 m. The water tank was not filled to capacity but sufficient water was placed in the tank to provide adequate coverage of the photon field. At least 3 readings were taken. 50 mm of a phantom material was then placed in the water tank perpendicular to the photon beam, i.e. the epoxy resin phantom material displaced the water, and at least 3 measurements were taken. The epoxy resin phantom material was then removed and at least 3 readings taken in the water phantom. Using this technique the only uncertainties to be considered are the variation in chamber readings for each set of measurements and the uncertainty in the drift in the output of the linear

accelerator throughout the course of the experiment, i.e. a total uncertainty of ±0.2%.

Technique 3: A horizontal photon beam was used throughout. The in-house water tank was set up with the chamber at 50 mm depth and the front pointer was again used to set an FSD of 1 m to the surface of the phantom. At least 3 readings were again taken. This measurement was bracketed by 2 sets of measurements in the epoxy resin phantom material under investigation. The slabs were positioned vertically on the couch i.e. perpendicular to the photon beam, with the chamber at 50 mm depth and with an FSD of 1 m.

The uncertainties involved are as with technique 1 except that the positional uncertainty of the chamber in the water tank is negligible. However, one requires a correction for the persex wall and sheath with an associated uncertainty of ±0.5%. The phantom ratios may therefore be estimated to have an uncertainty of ±0.5%.

Technique 4: This is a repeat of technique 1 except employing an NACP design plane parallel chamber. As with technique 1 the phantom ratios may be estimated to have an uncertainty of ±0.3%.

3. Results and Discussion

The phantom correction factors necessary to correct the readings in the epoxy resin phantom materials to equivalent readings in water are tabulated in Table 1 for all the experimental techniques. In determining small differences, confirmation of results by different experimental techniques is important. The phantom

correction values obtained using the methods agree within the measuring uncertainties. The mean phantom correction factors obtained from the techniques are tabulated in Figure 2 for WT1; Figure 3 for WTe; Figure 4 for RMI 451; and Figure 5 for RMI 457. The error bars represent the maximum spread in values between the experimental techniques.

There is little other data available in the literature, however, the mean values may be compared with those quoted in Tello et al (1995) for an equivalent measuring technique, (technique V in that paper) . For RMI 457 Tello et al obtained phantom correction factors of 0.999, 1.003 and 1.004 for cobalt-60, quality index 0.682 and quality index 0.762 respectively. The corresponding values reported in this paper are 0.999, 1.004 and 1.007 respectively. For RMI 451 Tello et al obtained phantom correction factors of 1.005 and 1.011 for quality indices of 0.682 and 0.777 respectively. Corresponding values reported here are 1.0025 and 1.0065 for quality indices of 0.68 and 0.765 respectively. That is to say that there is agreement within the measuring uncertainty for both of these mixes.

In conclusion the results indicate that an assumption of unity for the phantom correction factors of epoxy resin phantom materials may introduce a systematic uncertainty of the order of 1% in megavoltage photon beam dosimetry, dependent upon both the beam quality and the actual epoxy resin phantom material used. Furthermore it can be stated that the newer formulations, WTe and RMI 457, developed for electron beam use are also closer to water for use in the routine calibration of megavoltage photon units.

References

Constantinou C 1978 Tissue substitutes for particulate radiations and their use in radiation dosimetry and radiotherapy. Ph.D. thesis, London University.

Klevenhagen S C, Putney R and Hanson M 1983 A solid water phantom for dose distribution intercomparison in radiotherapy. Presented at Proc. 2nd Ann. Meeting of ESTRO (Bordeaux, 1983)

Institute of Physical Sciences in Medicine (IPSM) 1990 Code of practice for high energy photon therapy dosimetry based on the NPL absorbed dose calibration service *Phys.Med.Biol.* **35** 1355-1360

Nisbet A and Thwaites D I 1997 A dosimetric intercomparison of megavoltage electron beams in UK radiotherapy centres *Phys.Med.Biol.* **42** 2393-2409

Tello V M, Tailor R C and Hanson W F 1995 How water equivalent are water equivalent solid materials for output calibration of photon and electron beams *Med. Phys.* **22** 1177-1189.

Thwaites D I, Williams J R, Aird E G, Klevenhagen S C and Williams P C. 1992 A dosimetric intercomparison of megavoltage photon beams in UK radiotherapy centres. *Phys.Med.Biol.* **37** 445-461

White D R 1977 The formulation of tissue substitute materials using basic interaction data *Phys.Med.Biol.* **22** 889-899.

List of Figures.

	QI	0.568 (^{60}Co)	0.63 (4MV)	0.68 (6MV)	0.72 (9MV)	0.765 (16MV)
WT1	Technique 1	0.995	0.999	0.999	0.998	1.002
	Technique 2		0.999	1.002	1.003	1.009
	Technique 3		0.999	0.999	1.000	1.003
	Technique 4	1.001	0.999	0.999	1.000	1.003
WTe	Technique 1		1.002	0.998	0.999	0.998
	Technique 2		0.999	0.999	0.998	0.997
	Technique 3		0.997	0.998	0.995	0.991
	Technique 4	0.999	0.999	0.996	0.995	0.991
RMI 451	Technique 1	0.992	0.996	0.997	0.997	1.007
	Technique 2		0.999	1.006	1.004	1.009
	Technique 3		0.995	0.999	1.000	1.004
	Technique 4	0.996	0.994	0.999	1.000	1.004
RMI 457	Technique 1	0.992	0.997	0.998	0.999	1.003
	Technique 2		1.005	1.008	1.007	1.008
	Technique 3		1.000	1.000	1.003	1.006
	Technique 4	0.999	0.999	1.000	1.003	1.006

Table 1: Phantom Correction Factors (water/solid water) for WT1, WTe, RMI 451, RMI 457 at calibration depth

Figure 1. Schematic diagram of the in house water tank employed.

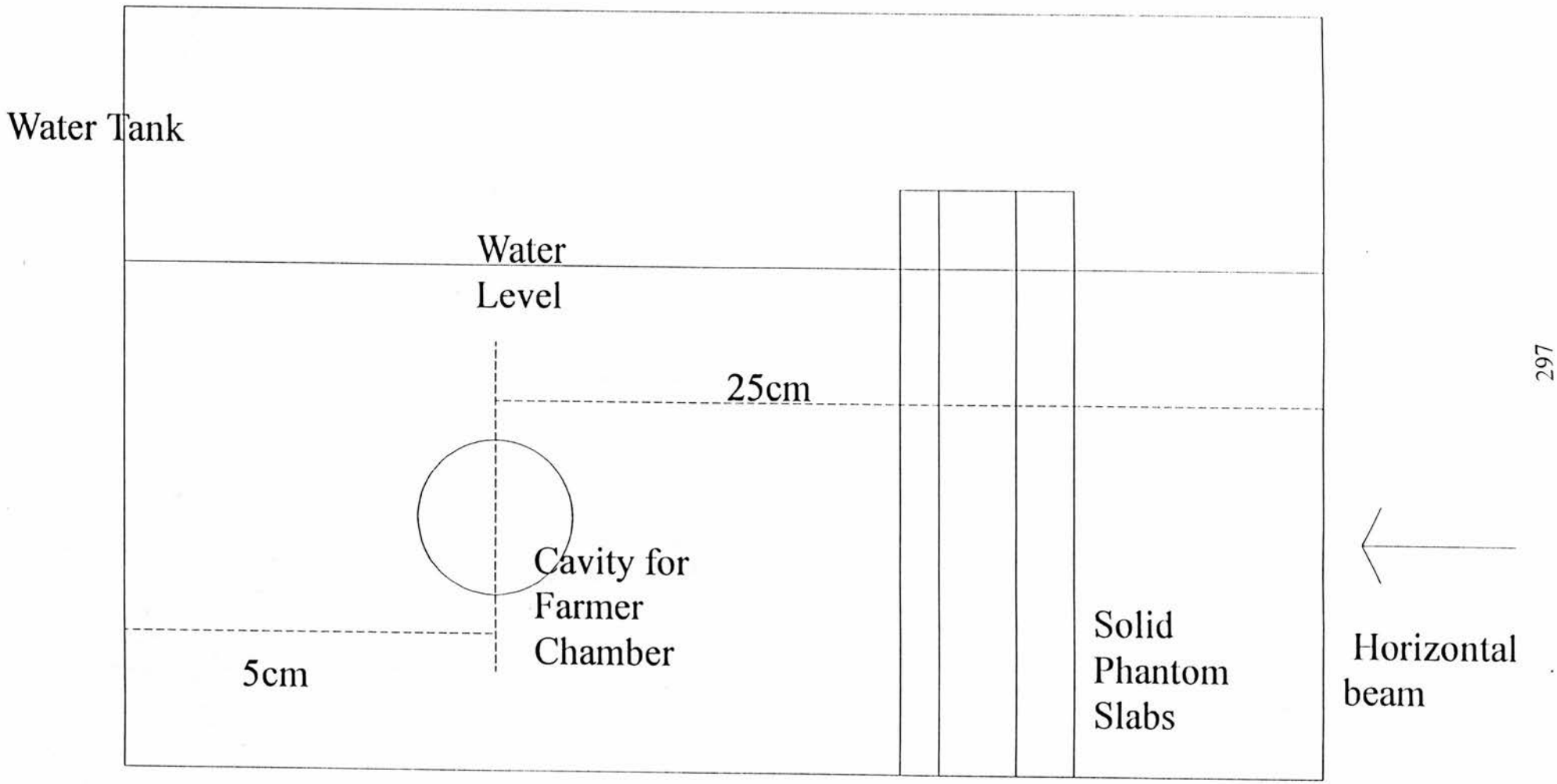

Figure 2. Phantom Correction Factors for WT1

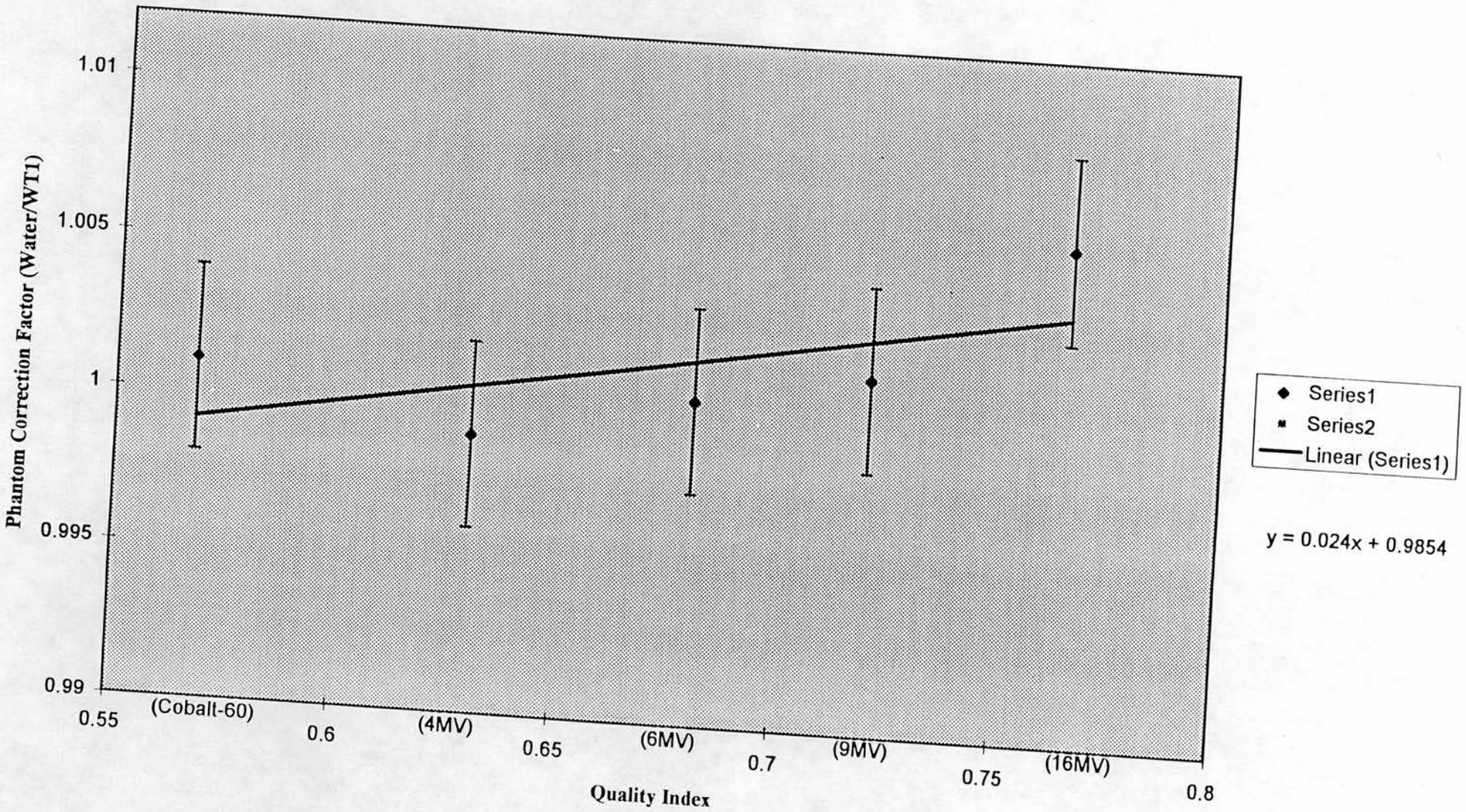

Figure 3. Phantom Correction Factors For WTe

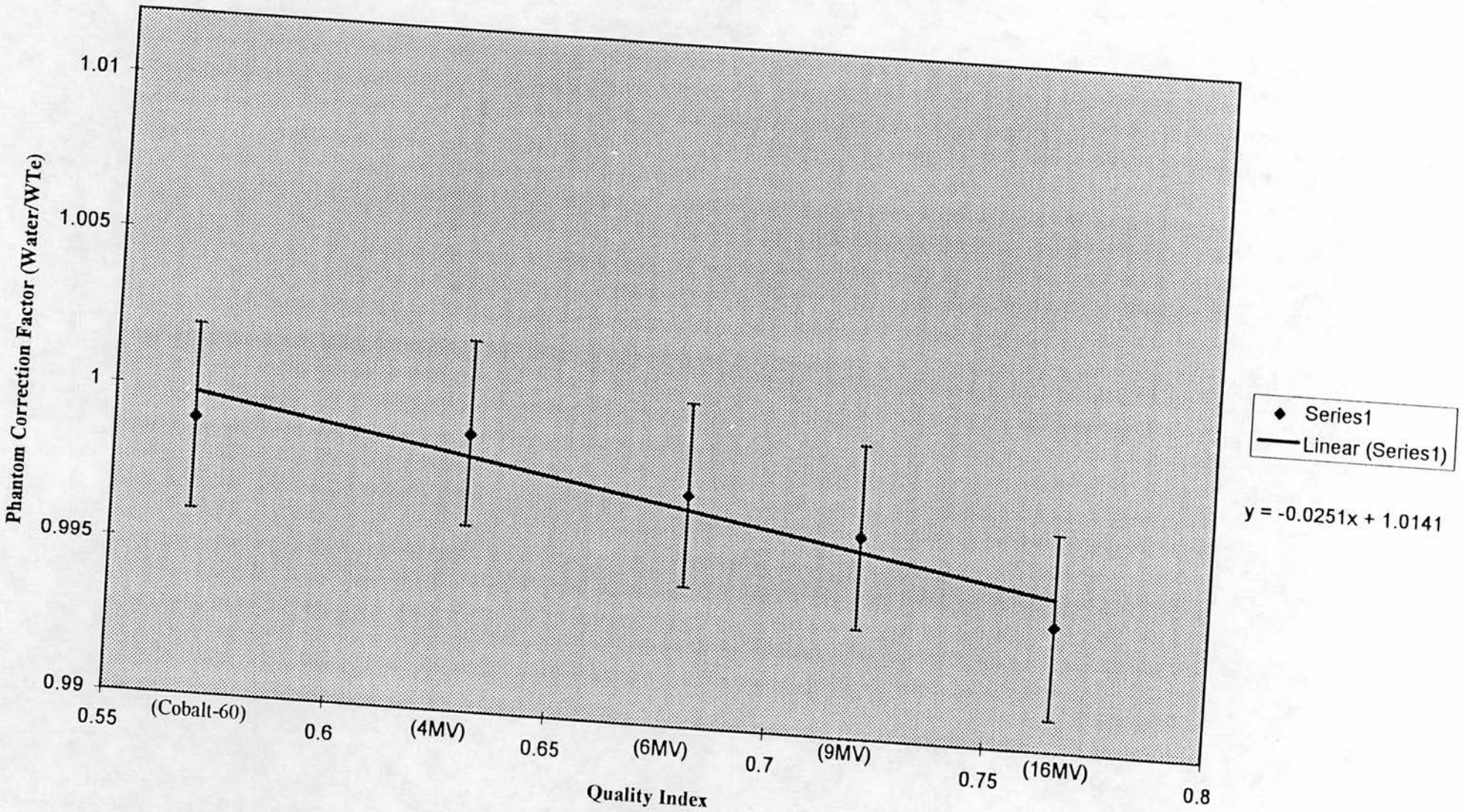

Figure 4. Phantom Correction Factors for RMI 451

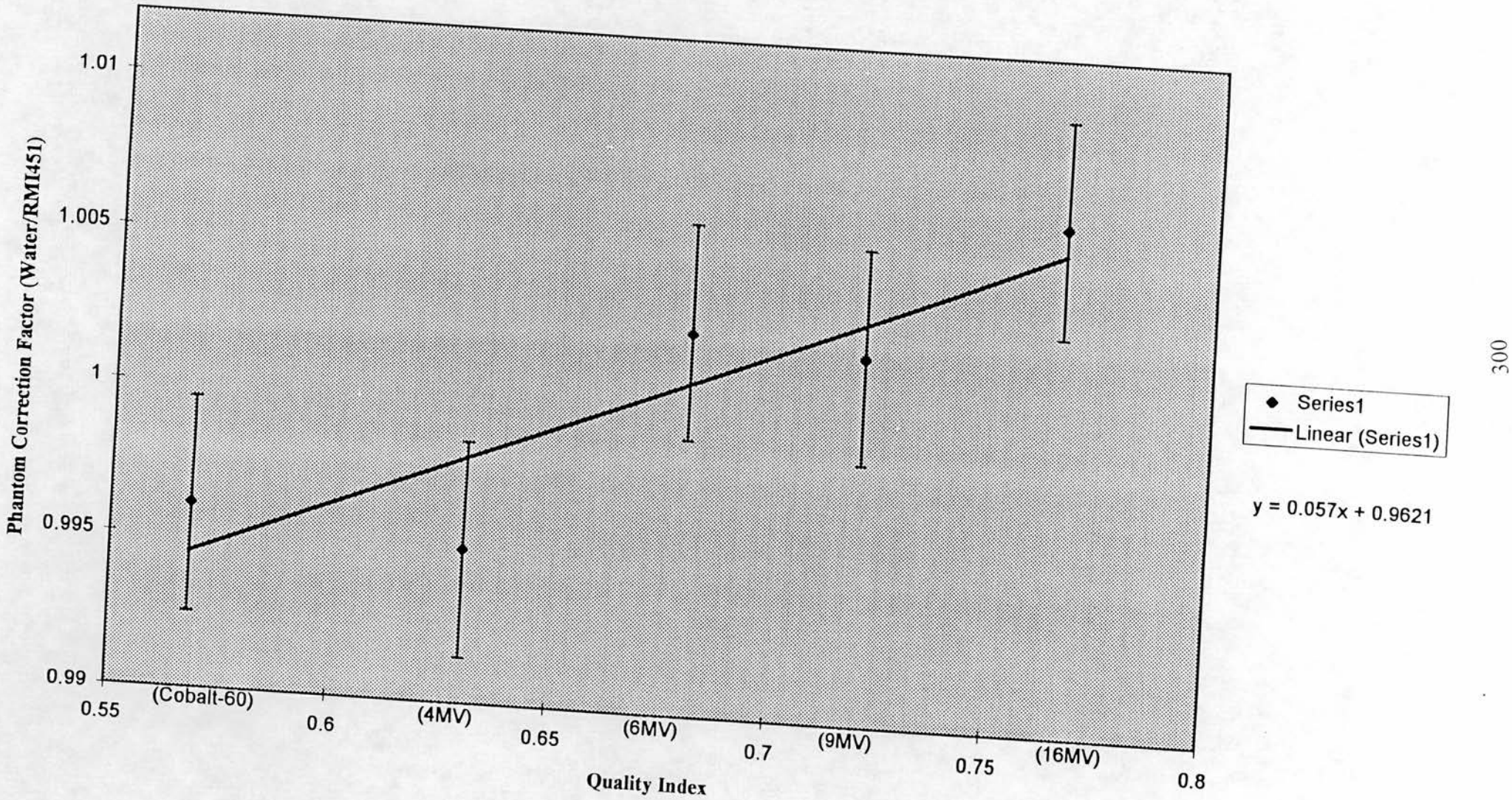

Figure 5. Phantom Correction Factors for RMI 457

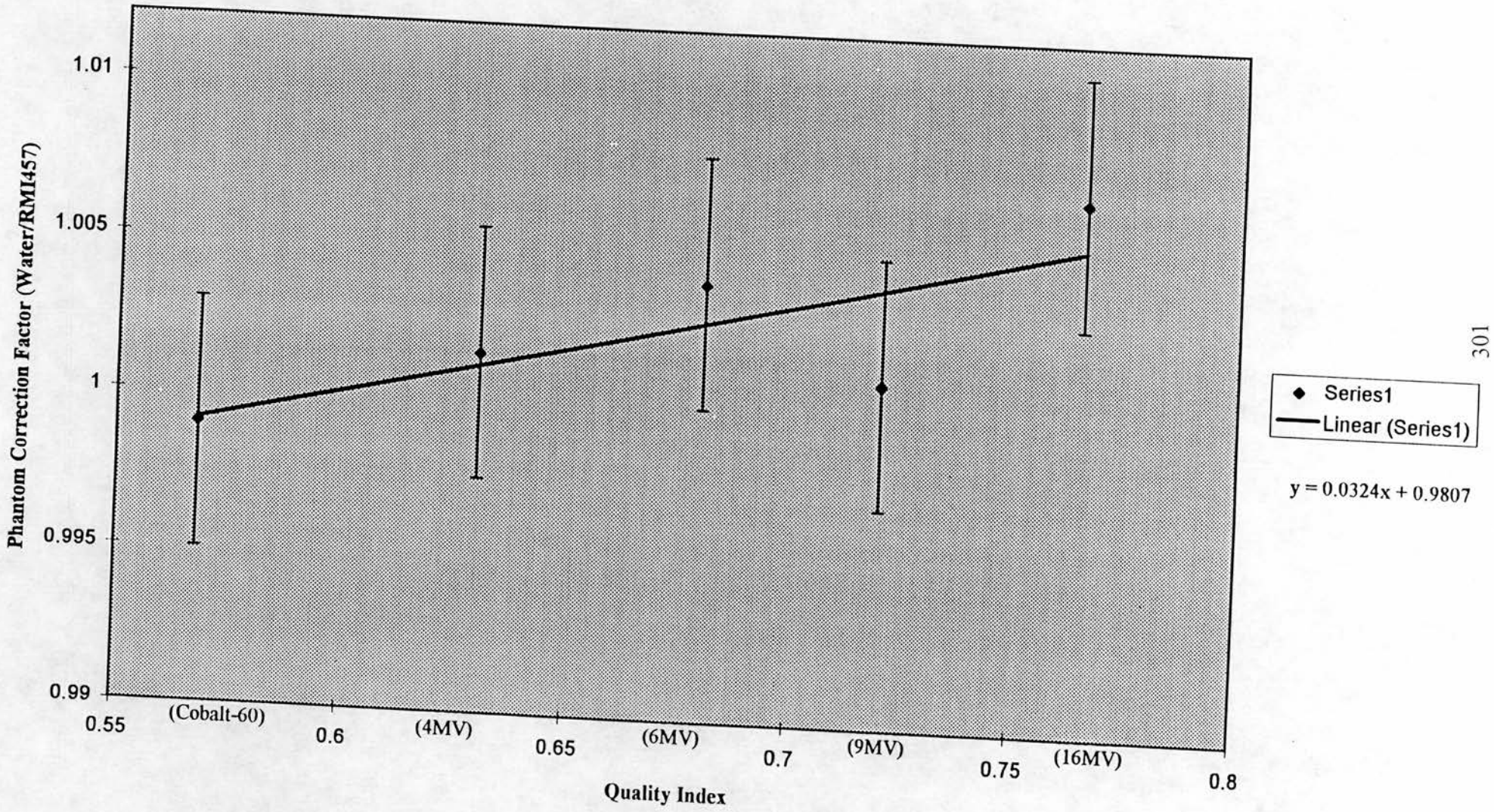

References :

-Abrath F, Purdy J (1980), Wedge design and dosimetry for 25 MV x-rays. radiology 136: 757-762.

-Acrovito G, Piermattei A, D'Abramo G, Andreasi F (1985), Dose measurements and calculations of small radiation fields for 9-MV x-rays, Med. Phys. 12 (6), 779-784.

-Ahnesjo (1991), Dose calculation methods in photon beam therapy using Energy Deposition Kernels, Ph. D. thesis, Stockholm University.

-Aird E G, Williams C, Mott G T, Dische S, Saunders M I (1994), Quality assurance in the CHART clinical trial, Radioth. Oncol, in press.

-Allahverdi M and Thwaites D I (1996_a). An experimental investigation of achievable accuracy in radiotherapy dosimetry, Proc. 3rd Biennial Radiotherapy Physics Meeting (Leeds, 1996) (York: IPEM) pp 69, Phys. Med. Biol. to be submitted.

-Allahverdi M and Thwaites DI (1996_b). A Semi-anatomic phantom for use in interdepartmental Audit, Proc. 3rd Biennial Radiotherapy Physics Meeting (Leeds, 1996) (York: IPEM) pp 13.

-Allahverdi M, Nisbet A, Thwaites D I (1996_c). An investigation of commercial epoxy-resin phantom materials for Megavoltage photon dosimetry, Proc. 3rd Biennial Radiotherapy Physics Meeting (Leeds, 1996) (York: IPEM) pp 13.

-Allahverdi M and Thwaites DI (1997). Testing a Semi-anatomic phantom for use in interdepartmental Audit, Radiotherapy & Oncology, vol. 40 (suppl. 1), 570.

-Almond P R, Law J, and Svensson H (1972), Comparison of radiation dosimetry between Houston (USA), Edinburgh (UK), and Umea (Sweden) Phys. Med. Biol. 1, 64-70.

-American Association of Physics in Medicine (1984), Physical aspects of Quality Assurance in Radiation Therapy, Rep. 13, AAPM New York.

-American Association of Physics in Medicine (1994), comprehensive QA for Radiation Oncology; Report of AAPM Radiation Therapy Committee task Group 40.

-American Association of Physicists in Medicine (AAPM, 1983). A protocol for the determination of absorbed dose from high energy photon and electron beams. Task Group 21, Radiation Therapy committee, AAPM, Med. Phys., 10, 741-771.

-Andreo P, and Brahme A (1986). Stopping power data for high energy photon beams. Phys. Med. Biol., 31, 839-858.

-Andreo P (1990), Uncertainties in dosimetric data and beam calibration, Int. J. Radiation Oncol. Biol. Phys., 19, 1233-1247.

-Asparadix M (1996), A study to assess and improve dose computations in photon beam therapy, Ph.D. thesis, Univesity of Edinburgh.

-Batho H F (1964), Lung correction in cobalt 60 beam therapy, J. Can. Assoc. Radiol., 15, 79-83.

-Battista J J, Rider W D, Van Dyk J (1980), Computed Tomography for Radiotherapy planning, Int. J. Radiol. Oncol. Biol. Phys. 6, 99-108.

-Beaudion L (1968), Analytical approach to the solution of the dosimetry in heterogeneous media, M.Sc. thesis, University of Toronto.

-Berger M, Seltzer S (1982). Stopping powers and ranges of electrons and positrons. Gaithersburg: NBS; Report NBSIR, 82-2550A.

-Biggs P, Ling C (1979), Electron as the cause of the observed d_{max} shift with field size in higher energy photon beams. Med. phys. 6:291-295.

-Biggs P, Russel M (1983), An investigation into the presence of secondary electrons in megavoltage photon beams. Phys. Med. Biol., 28:1033-1043.

-Bjarngard B E et al. (1990), Doses on the central axes of narrow 6-MV x-ray beams, Med. Phys., 17(5), 794-799.

-Bjarngard B E (1993), Scatter factor for a 25 MV x-ray beam, Med. Phys., 20(2), 357-362.

-Blyth C, McLeod A, Thwaites D (1997), A pilot study of the use of in vivo diode dosimetry for quality assurance in radiotherapy, Radiography, 3, 131-142.

-Bonnett D E, Mills J A, Aukett R J, and Martin Smith P (1994). The development of an interdepartmental quality assurance programme for external beam therapy Brit. J Radiology, 67, 275-82.

-Bortfeld T, Schelegel W, Rhein B (1993), Decomposition of pencil beams kernels for fast dose calculation in three dimensional treatment planning, Medical Physics, 20 (2), 311-318.

-Boutillon M, Coursey B, Hohlfeld K, Owen B, Rogers D (1993), Comparison of primary water absorbed dose standards, Measurement Assurance in Dosimetry, Vienna, May 1993, 95-112.

-Boyer A, Mok E (1984), A photon dose calculation model employing convolution calculations, Medical Physics, 12 (2), 169-177.

-Brahme A (1988), Accuracy requirements and quality assurance of external beam therapy with photons and electrons, Acta Onc., 15, suppl I.

-Bridier A, et al (1993), Check of a multipurpose phantom to be used in the frame of a quality assurance network, in proc. 2nd Biennial ESTRO meeting on Physics in Clinical Radiotherapy, Prague, May 1993 (abst. p 117).

-British Journal Radiology (BJR, 1996), suppl. 25.

-Brown L, Siddon R, Bjarngard B (1987), Scatter dose for wedged fields. Phys. Med. Biol. 32: 1321-1326.

-Cadman P (1995), A dosimetric investigation of scatter conditions for dual asymmetric collimators in open fields, Med. Phys., 22(4).

-Cassel K, Hobday P, Parker R (1981), the implementation of a generalised Batho inhomogeneity correction for radiotherapy planning with direct use of CT numbers. Phys. in Medicine and Biology, 26 (4), 825-833.

-Comte Francais "Measure des Rayonnements Ionisants" (CFMRI. 1987), Recommendations pour la measure de la dose absorbee en radiotherapie dans les faisceaux de photons et d'electrons d'energie comprise entre 1MeV et 50 MeV (Rep. CFMRI No. 2) Chiron, Paris.

-Ciocca M, Landoni C, Italia C, Montanaro P, Canesi P, and Valdagni R (1991), Quality control in the conservative treatment of breast cancer: Patient dosimetry using silicon detectors, 22, 304-307.

-Clarkson J R (1941), A note on depth dose in fields of irregular shape, BR. J. Radiol., 14, 265-268.

-Cozzi A, Cozzi L, Garavaglia G (1996), Wedge Factors: Dependence on depth and field size, Radiotherapy and Oncology, 39, 31-34.

-Cunningham J (1972), Scatter -air ratios, Phys. Med. Biol., 17 (1), 42-51.

-Cunningham J, Beaudion L (1973), Calculations for tissue inhomogeneities with experimental verification, XII International Congress of Radiology, 653-657.

-Cunningham J and Schultz R (1984), On the selection of stopping power and mass energy-absorption coefficient ratios for high energy x-ray dosimetry, Med. Phys., 11, 618-623.

-Davis B, Faessler P (1993), Quality audit of megavoltage radiotherapy units: intercomparison of dose at a reference point using a mailed TL-dosimetry system, Radiotherapy and Oncology, 28, 79-81.

-Day M (1983), The normalised peak scatter factor and normalised scatter functions for high energy photon beam in British Journal of Radiology, supl 17, 131-136.

-Denham J W, Dally M J, Hunter K, Wheat J, Fahey P, Stat M, and Hamilton C S (1993), Objective decision making a portal film: the results of a pilot study, Int. J. Radia. Oncol. Biol. Phys., vol. 26, 869-876.

-Douglas M D, Bhudatta R, Bruce R, and Paul J (1995), Intercomparison of normalised head scatter factor measurement techniques, Med. Phys., 22 (2), 249-253.

-Dunscombe P, Nieminen J (1992), on the field size dependence of relative output from a linear accelerator, Med. Phys. 19 (6), 1441-1444.

-Dunscombe P B, Fox K, Loos S, and Leszczynski K (1993), The investigation and rectification of field placement errors in the delivery of complex head and neck fields, Int. J. Radia. Oncol. Biol. Phys., vol. 26, 155-161.

-Dutreix A, Van der Schueren E, Derreumax S, Chavaudra J (1993), Preliminary results of a quality assurance network for radiotherapy centres in Europe, Radiother. Oncol. 29, 97-101.

-Dutreix A, Svensson H, Bjarngard B, Bridier A, Mijnheer B, Shaw J (1996), Considerations by the ESTRO (IAEA) working party on monitor unit calculations, ESTRO, Austria, Viena, 89, S25.

-Dutreix A, Bjarngard B, Bridier A, Mijnheer B, ShawJ, Svensson H (1997), Monitor unit calculation for high energy photon beams, world congress on Medical Physics and Biomedical Engineering, Nice, France, 132-TU3.01.

-Duzenli C et al (1992), Backscatter in to the beam monitor chamber: implications for dosimetry of asymmetric collimators, Med. Phys., 20(2), 363-368.

-El-Khatib E, Battista J (1984), Improved lung dose calculation using tissue-maximum ratios in the Batho correction, Med. Phys., 11(3), 279-286.

-El-Khatib E and Battista J (1986), accuracy of lung dose calculations for large field irradiation with 6-MV x-rays, Med. Phys., 13(1), 111-116.

-El-Khatib E, et al (1989), Evaluation of lung dose correction methods for photon irradiations of Thorax phantom, Int. J. Radiation Oncol. Biol. Phys., vol 17, pp 871-878.

-EORTC (1989), proc. EORTC Meeting on quality control (Leuven 1989) (Amestelveen, the Netherlands: EORTC).

-ESTRO (1995), Monitor unit calculation and verification for therapy machines 3rd biennial meeting on a physics in clinical radiotherapy, Gardone Riviera, Italy, 1-137.

-Evans D, (1968), x-ray and Gama-ray interactions. In: Radiation Dosimetry, vol I, 93-155. Academic press, New York.

-Fertil B, Malaise E (1981), Inherent cellular radiosensitivity as a basic concept for human tumor radiotherapy , Int. J. Radiat. Oncol. Biol. Phys. 7: 621-629.

-Frye D, Paliwal B, Thomadsen R, Jursinic P (1994), intercomparison of normalised head scatter factor measurement techniques, Med. Phys. 22 (2), 249-253.

-Galvin J, Smith A, Lally B (1993), Characterization of a multileaf collimator system, Int. J Radiation Oncol. Biol. Phys. 25, 181-192.

-George D, Dutreix A (1997), A formalism to calculate the output ratio in a mini-phantom for a GE multileaf collimator, Phys. Med. Biol. 42, 521-536.

Goiten M (1979), The utility of computed tomography in radiation therapy: an estimate of outcome. Int. J. Radiot. Oncol. Biol. Phys., 5, 1799-1807.

-Haider T, El-Khatib E (1994), Differential scatter integration in regions of electronic non-equilibrium, Phys. Med. Biol., 31-43.

-Hansson W F, Stovall M, and Kennedy P (1991_a), Review of dose intercomparison at a reference point , IAEA 1994.

-Hansson W F (1991_b), Planned quality audit network in the USA, IAEA-Tecdoc-734, Leuven.

-Hansson U, and Johansson K A (1991_c), Quality audit of radiotherapy with EORTC mailed in water TL dosimetry,Radiother. Oncol.,20, 191-196.

-Hansson W F, Shalek R J, and Kennedy P, (1991_d), Dosimetry Quality assurance in the U S from the experience of the Radiological Physics Centre proc. Quality assurance symposium (Galveston, 1991) (American college of Medical Physics).

-Hansson U, Johansson K A, Horiot J C, Bernier J, Mailed (1993), TL dosimetry programme for machine output check and clinical application in the EORTC radiotherapy group , Radiother. Oncol. ,29, 85-90.

-Hansson W F and Jarvinen H (1994), The world-wide quality audit network, ESTRO, radiation dose in Radiotherapy from prescription to delivery, IAEA-TECDOC-734, Leuven, 321-323 (in press).

-Heyler S, Heisig S (1995), Multileaf collimation versus conventional shielding blocks: a time and motion study of beam shaping in radiotherapy, Radiotherapy & Oncology, 37, 61-64.

-Heukelom S, J H Lanson, B J Mijnheer (1994_a), wedge factor constituents of high energy photon beams: field size and depth dependence, Radioth. and Oncol., 30, 66-73, 1994.

-Heukelom S et al. (1994_b), Wedge factor constituents of high-energy photon beams: head and phantom scatter dose components, Radioth. & Oncol. 32, 73-83.

-Heukelom JS, Lanson J H, Mijnheer B J (1992), In vivo dosimetry during pelvic treatment, Radiother. & Oncol., 25, 111-120.

-Heukelom S, Lanson J H, and Mijnheer B J (1991_a), Comparison of entrance and exit dose measurements using ionisation chambers and silicon diodes, Phys. Med. Biol., 36, 47-59.

-Heukelom S, Lansn G H, van Tienhoven G, Mijnheer B J, (1991_b), In vivo dosimetry during tangential breast treatment , Radiother. & Oncol., 22, 269-279.

-Hobday P, Hodson J, and Husband J (1979), Computed Tomography applied to Radiotherapy treatment planning, Techniques and results, Radiology, 133, 477-482.

-Holt J, Laughlin J, Morony J (1970), The extension of the concept of tissue air ratios (TAR) to high x-ray beams. Radiology 96: 437-446.

Hoornaert M, Van Dam J, Vynckier S and Bouiller A (1993), A dosimetric quality audit of photon beams by the Belgian Hospital Physicist Association, Radiother. Oncol. 28, 37-43.

-Hounsell A and Jhon Wilkinson (1996), The variation in out put of symmetric, asymmetric and irregularly shaped wedged radiotherapy fields, Phys. Med. Biol., 41, 2155-2172.

-Huang P, Chu J, Bjarngard B (1987), The effect of collimator backscatter radiation on photon output of linear accelerators, Med. Phys. 14 (2), 268-270.

-Hughes D, Karzmark C, Levy R (1972), Letter to the editor, Br. J. radiol. 45, 868.

-Huq M and Nath R (1990), Comparison of IAEA 1987 and AAPM 1983 for dosimetry calibration of Radiotherapy beam, Med. Phys., 18 (1), 26-35.

International atomic Energy Agency (IAEA, 1987). Absorbed dose determination in photon and electron beams: an international code of practice. Technical rep. Ser. No. 277, IAEA, Vienna, pp 1-98.

-IAEA proc. EORTC meeting on Quality control (Leuven, 1989) (Amstelveen, the Netherlands: EORTC).

-International Commission on Radiation Units and measurements (ICRU, 1976), determination of absorbed dose in a patient irradiated by beams of X and Gamma rays in radiotherapy procedures, ICRU report 24.

-ICRU (1987), Use of computers in external beam radiotherapy procedures with high-energy photons and electrons. Report 42, Washington DC, 20014, USA.

- Institute of Physical Sciences in Medicine (IPSM now IPEM, 1988), Commissioning and quality assurance of linear accelerators IPSM Report 54 (York: IPSM).

-Institute of Physical Sciences in Medicine (IPSM now IPEM, 1990), Code of practice for high energy photon dosimetry radiotherapy based on the NPL absorbed dose calibration service, Phys. Med. Biol., 35, 1355-1360.

-Institute of Physics and Engineering in Medicine (IPEM, 1994), Commissioning and quality control of treatment planning systems, IPEM, Report No. 68, 1-44.

-Johansson K A (1982_a), Studies of different methods 0f absorbed dose determination and a dosimetric intercomparisons at the Nodric radiotherapy centres, Ph D Thesis university of Goteborg.

-Johansson K A, Mattson L O and Svenson H (1982_b), Dosimetric Intercomparison at the Scandinavian radiation therapy centres, Acta Radiology Ther. Phys. Biol., 21, 1-10.

-Johansson K A et al (1986), Quality assurance control in the EORTC co-operative group of Radiotherapy. 2, Dsimetry Intercomparisons, Radiother. Oncol., 7, 269-279.

-Johansson K A, Horriot J C (1987), Quality assurance control in the EORTC co-operative group of radiotherapy. 3, Dosimetry Intercomparisons in an anatomical phantom, Radiother. Oncol., 9, 289-298.

-Jordan T, Williams P (1994), The design and performance characteristics of a multileaf collimator, Phys. Med. Biol. 39, 231-251.

-Kalend A, Andrew Wu, Maitz A (1990), Separation of dose gradient effect from beam hardening effect on wedge factors in photon fields, Med. Phys., 17 (4), 701-704.

-Kase K and G K Svensson (1986), Head scatter data for several linear accelerators (4-18 MV), Medical Physics, 13(4), 530-532.

-Khan F et al (1980), revision of tissue-maximum ratio and scatter-maximum ratio concepts for cobalt 60 and higher energy x-ray beams, Med. Phys., 7(3), 230-237.

-Khan F et al (1986), Dosimetry of asymmetric x-ray collimators, Med. Phys., 13(6), 936-942.

-Khan F (1993), dosimetry of wedged fields with asymmetric collimation, Med. Phys., 20(5), 1447-1452.

-Knoos T, Wittgren L (1991), Which depth dose data should be used for dose planning when wedge filters are used to modify the photon beam, Phys. Med. Biol. vol. 36, No 2, 255-267.

-Krithivas G, Rao N (1985), A study of the characteristics of radiation contaminants within a clinically useful photon beam, Med. Phys., 12 (6), 764-768.

-Krithivas G, Rao N (1987), Dosimetry of 24 MV x rays from a linear accelerator, Med. Phys. 14 (2), 274-281.

-Kwa W, Kornelsen R, Harrison R, El-Khatib E (1994), dosimetry for asymmetry x-ray fields, 21 (10), 1599-1604.

-Larson K, Prasad S (1978), Absorbed dose computation for inhomogeneous media in radiation treatment planning using differential scatter air ratios. In 2nd annual symposium on computer applications in Medical care, 93-99, IEEE, NY.

-Leavitt D (1982), Dosimetry of photon inhomogeneities. AAPM Monograph No 9 (AIP, New York).

-Lebesque J V, Bel A, Bijhold J, and Hart A (1992), Detection of systematic patient set up errors by portal film analysis, Radiotherapy and Oncology, letter to editors, 23, 98.

-Leunens G, Van Dam J, Dutreix A, and van der Schueren (1990_a), Quality assurance in radiotherapy by in vivo dosimetry. 2. determination of the target absorbed dose, Radiother. & Oncol., 17, 73-87.

-Leunens G, Van Dam J, Dutreix E, and van der Schueren (1990_b), Quality assurance in radiotherapy by in vivo dosimetry. 1. Entrance dose measurements, a reliable procedure, Radiother. & Oncol. 17, 141-151.

Leunens G, Verstraete J, Van Dam J, Dutreix A, van der schueren (1991), In vivo dosimetry for tangential breast irradiation: role of the equipment in the accuracy of dose delivery, Radiother. & Oncol., 22, 285-289.

-Li X A et al. (1995), Lateral electron equilibrium and electron contamination in measurements of head scatter factors using miniphantoms and brass caps, Med. Phys., 22(7), 1167-1170, 1995.

-Ling C and Biggs P (1979), improving the build up and depth-dose characteristics of high energy photon beams by using electron filters, Med. Phys., 6, 296-301.

-Ling C, Schel M, Rustgi S (1982), Magnetic analysis of the radiation components of a 10MV photon beam, Med. Phys. 9, 20-26 (1982).

-Liu C, Zhu T, Palta J (1996), Characterzing output for dynamic wedges, med. Phys. 23 (7), 1213-1218.

- Loshek D, Keller K (1988), Beam profile generator for asymmetric fields Med. Phys. 15, 604-610.

-Lovinger R, Loftus T (1977). Uncertainty in the delivery of absorbed dose. In: Casnati E, ed. Ionising Radiation Meteorology, 141-162.

-Lulu B, Bjarngard B (1982), Batho's correction factor combined with scatter summation, Med. Phys., 9 (3), 372-377.

-Luxton G and Melvin A Astrahan (1988), Output factor constituents of a high- energy photon beam, Med. Phys., 88- 91.

-Mackie T R et al (1985), A convolution method of calculating dose for 15MV x-rays, Med. Phys., 12, 188-189.

-Mackie T R (1990), applications of the Monte Carlo method in radiotherapy. The dosimetry of ionising radiation, vol. III, Chapter 6. N. Y. academic press.

-Mackie T R, El-Khatib (1984), Lung dose corrections for 6 and 15 MV x-rays. Med. Phys. 12 (3), 327-332.

-Marinello G, Dutreix A (1992), A general method to perform dose calculations along the axis of symmetrical and asymmetrical photon beams, Med. Phys. 19 (2), 275-281.

-Matsson, (1985), Comparison of different protocols for the dosimetry of high-energy photon and electron beams, Radiother. Oncol., 4, 313-318.

-McCullough E C et al. (1988), A depth dependence determination of the wedge transmission factor for 4-10 MV photon beams, Med. Phys., 15(4), 621-623.

-McKenzie A, (1997), What is the explanation for the changes to cobalt-60 tissue air ratios in BJR supplement 25. Phys. Med. Biol. 42, 1055-1064.

-Meli J A (1986), Output factors and dose calculations for blocked x-ray fields, Med. Phys., 13(3), 405-408.

-Mijnheer B, Wittkamper F, (1986), comparison of recent codes of practice for high energy photon dosimetry. Phys. Med. Biol., 31 (4), 407-416.

-Mijnheer B J, Batterman J J and Wamberise A W (1987), what degree of accuracy is required and can be achieved in photon and neutron therapy? Radiotherapy and Oncology, 8, 237-252.

-Mijnheer B J (1995), Monitor unit calculation and verification for therapy machines, workshop, IAEA code of practice for monitor unit calculations, ESTRO, third Biennial meeting, Gardon Riviera, Italy, 130-133.

-Milan J and Bently R (1974), The storage and manipulation of radiation dose data in a small digital computer, Brit. J. Radiology, 47, 115.

-Mills J A, Aukett R J, Bonnett D E, and Martin Smith P (1992), A pilot interdepartmental audit: description, results and recommendations (pro. Quality in Radiotherapy, York, July 1992), Scope, 1, 12.

-Millwater C J (1993), The role of in vivo dosimetry as part of quality assurance in a Radiotherapy department, a feasibility study, M.Sc. dissertation, University of Edinburgh.

-Millwater C J, McLeod A M, and Thwaites D I (1994), The role of in vivo dosimetry in optimising radiotherapy treatment, Proc. Brit. Oncol. Ass. meeting 1994.

-Millwater C J, McLeod A S, and Thwaites D I (1998), In vivo semiconductor dosimetry as part of routine quality assurance, The British Journal of Radiology, 71, 661-668.

-Mitine C, Leunens G, Verstraete N, Blankaert N, Van Dam J, Dutreix A, van der Schueren E (1991), Is it necessary to repeat quality control procedures for head and neck patients? Radiother. & Oncol., 21, 201-210.

-Mitine C, Dutreix A, and van der Schueren E (1993), Black and white in accuracy assessment of megavoltage images: the medical decision is often grey, Radither. & Oncol., 28, 31-36.

-Mohan R, Chui C, Lidofski L (1986), Differential pencil beam dose computation model for photons. Med. Phys. 13, 64-73.

-Murray B et al, (1995), Out put factors for fields defined by four independent collimators, Med. Phys., 22(30), 285-290.

-Nederlands Commissie voor stralingdosimetric (NCS, 1989), (Netherlands Commission in Radiation Dosimetry). Code of practice for the dosimetry of high energy electron beams. NCS Report 5.

-Niroomand Rad A et al. (1992), Wedge factor dependence on depth and field size for various beam energies using symmetric and half-collimated asymmetric jaw settings, Med. Phys., 19(6), 1445-1450.

Niroomand Rad A, Rodgers J, Taylor P, and Hames B (1994), Dosimetric parameters of a modified set of wedges for use with asymmetric fields of a 6MV linear accelerators, Med. Phys., 21 (9), 1405-1408.

Nisbet A (1994), The dosimetric accuracy of megavoltage photon and electron beams in radiotherapy, Ph. D. thesis, University of Aberdeen.

-Nisbet A and Thwaites D I (1997), A dosimetric intercomparison of electron beams in UK Radiotherapy centres, Phys. Med. Biol., 42, 2393-2409.

-Nordric association of Clinical Physics (NACP, 1980). Procedures in external radiation therapy dosimetry with electron and photon beams with maximum energies between 1 and 50 MeV. Acta. Radiol. Oncol. 19: 55-79.

-O'Connor J (1957), The variation of scattered x-ray with density in an irradiated body. Physics in Medicine and Biology, 1: 352-369.

-Owen B (1991), NPL absorbed dose to water calibrations for ^{60}Co and 4 to 19 MV x-rays, CCEMRI (I)/ 91-3, BIPM.

Palta J R et al (1988), Dosimetric characteristics of a 6MV photon beam from a linear accelerator with asymmetric collimator jaws, Int. J. radiation Oncology Biol Phys., vol 14, pp 383-387.

-Palta J et al, (1996), dosimetric considerations for a multileaf collimator system, Med. Phys., 23(7), 1219-1224.

-Patterson M S and Shragge P C (1981), Characteristics of an 18 MV photon beam from a Therac 20 Medical linear Accelerator, Med. Phys., 8(3), 312-318.

-Pettit P, Goodman M (1983), Investigation of build up dose from electron contamination of clinical photon beams. Med. Phys., 10: 18-24.

-Prasad S C, Glasgow G P, and Purdy J A (1979), Dosimetric evaluation of Computed Tomography treatment planning system, Radiology, 130, 777-781.

-Purdy J (1992), Photon dose calculation for three dimensional radiation treatment planning, seminars in Radiation Oncology, vol2, No 4, 235-245.

-Purdy J, Prasad S (1983), Current methods and algorithms in radiation absorbed dose calculation and the role of computed Tomography: A review, Computed Tomography in Radiation Therapy, New York.

-Rao B, Prasad S, Parthasaradhi K, Ruparel R, Garces R (1988), Investigations on the near surface dose for three 10MV x-ray beam accelerators with emphasis on the reduction of electron contamination, Med Phys. 15, 246-249.

-Redpath A T et al (1977), A comprehensive radiotherapy planning system implemented in Fortran on a small interactive computer, 1977, British J. of Radiology, 50, 51-57.

-Redpath A T, Wright D H (1981), Beam modelling techniques for Computerised Therapy planning. In Burger, G., editor, treatment planning for external beam therapy with neutrons. Urban and Schwarzenberg, Munich, p. 54.

-Redpath A T and Thwaites D I (1992), A three dimensional scatter correction algorithm for photon beams, Phys. Med. Biol., vol. 36, No 6, 187-197.

-Redpath A T, Williams J R, and Thwaites D I (1993), Treatment planning for external beam therapy. Radiotherapy Physics in practice, Williams J R and Thwaites D I, Oxford university press, ch. 8, 135-185.

-Redpath A T (1995), A beam model for three dimensional Radiotherapy, The British Journal of Radiology, 68, 1356-1363.

-Rice R K et al. (1987), Measurements of dose distributions in small beams of 6MV x-rays,., Phys. Med. Biol., vol 32, No 9, 1087-1099.

-Rosenberg I et al (1995), Calculation of monitor units for a linear accelerator with asymmetric jaws, Med. Phys., 22(1), 55-63.

-Scharder R, Maschuw R (1980), Reduktion der oberflachen-dosis von ^{60}Co strahlen in der gewbetiefe von 0 bis 3 mm mit einem magnetichen feld. Strahlentherapie, 156: 257-263.

-Sharp M B et al (1995), Extrafocal radiation: A unified approach to the prediction of beam penumbra and out put factors for megavoltage x-ray beams, Med. Phys., 22(12).

-Shaw J E (1993), Quality assurance of treatment planning systems, Scope (Dec. 1993 - IPSM).

-Sipila P (1992) Quality assurance of treatment planning systems in proc. Radiotherapy Dosimetry, Radiation dose from prescription to delivery (Leuven, Sept. 1991), IAEA Tech Doc. 734, in press.

-Sixel K, Podgorsak E (1993), Buildup region of high-energy x-ray beams in radiosurgery, Med. Phys. 20 (3), 761-764.

-Sixel K, Podgorsak E (1994), Build region and depth of dose maximum of megavoltage x-ray beams, Med. Phys. 21 (3), 411-417.

-Sjogren R, Karlsson M (1996), Electron contamination in clinical high energy photon beams, Med. Phys., 23 (11), 1873-1881.

-Sjogren R et al (1997), Depth for dose calibration in high energy photon beams, Radiotherapy and Oncology, 43, 311-313.

-Sontag M R, Cunningham J R (1977), Corrections to absorbed dose calculations for tissue inhomogeneities, Med. Phys. 4 (5), 431-436.

-Sontag M R, Cunningham J R (1978), The Equivalent Tissue Air Ratio method for making absorbed dose calculation in a heterogeneous medium, Radiotherapy, 129, 787-794.

-Spicka J MS et al. (1988), Separating output factor into collimator factor and phantom scatter factor for Megavoltage photon calculations, Medical dosimetry,13, 23-24, 1988.

-SSRBMP (1984) unpublished, as reported in Johansson et al (1987).

-Sterling T D, Perry H, and Katz L (1964), Automation of radiation treatment planning, The British Journal of Radiology, 37, 544-550.

-Storchi P, Van Gasteren J (1996), A table of phantom scatter factors of photon beams as a function of the quality index and field size, Phys. Med. Biol., 41, 563-571.

-Svenson H, Hansson G, Zadanszky K (1990), The IAEA/WHO at dosimetry service for radiotherapy centres (1969-1987), Acta Oncologica 29, Fasc. 4.

-Szymczyk W, Goraczko A and Lesiak J (1991), Prediction of Saturne II + 10MV and 23MV photon beam output factors, Int. J. Radiol. Oncol. Biol. Phys., 21, 789-793.

-Takashi S (1965), Conformation radiotherapy rotation techniques as applied to radiography and radiotherapy of cancer, Acta Radiology, suppl. 242, 1-142.

-Tatcher M, Palti S (1981), Evaluation of density correction algorithms for photon-beam dose calculations, Radiology, 141, 201-205.

-Tatcher M and Bjarngard B E (1992), Head-scatter factors in rectangular photon fields Morris, Med. Phys., 20(1), 205-206.

-Tatcher M, Bjarngard B E (1994), Head scatter factors in blocked photon fields Radioth. & Oncol., 33, 64-67.

-Tawfique K and El-Khatib E (1995), Differential scatter integration in regions of electronic non-equilibrium, Phys. Meed. Biol., 40, 31-43.

-Thomadsen B, Kubsad S, Paliwal B, Sahabi S and Mackie T (1993), On the cause of the variation in tissue maximum ratio values with source to detector distance, Med. Phys. 20, 723-727.

-Thomas S (1990), The variation of wedge factors with field size on a linear accelerator. Br. J. Radiol. 63: 355-356.

-Thomas S (1991), A modified power-law formula for inhomogeneity corrections in beams of high energy x-rays. Med. Phys. 18 (4), 719-723.

-Tienhoven G, Lanson J H, Crabeel D, Heukelom S, and Mijnheer B I (1991), Accuracy in tangential breast treatment set up: a portal imaging study, Radiother. & Oncol., 22, 317-322.

-Thilander A, Johanson K A (1994), Absorbed dose intercomparison in Sweden, IAEA , Leuven, 143-158.

-Thwaites D I (1988), Review and analysis of accuracy required and achievable in Radiotherapy, Phys. Med. Biol., 34, 1989, 639 (abstract).

-Thwaites D I (1991), Accuracy requirement in Radiotherapy: A practical and theoretical course in Radiotherapy Physics (part II), Royal Marsden Hospital, London, 1-17 (chapter 12).

-Thwaites D I et al (1992), A dosimetric intercomparison of megavoltage photon beams in the U K Radiotherapy centres, Phys. Med. Biol., 37, 445.

-Thwaites D I (1993), Uncertainties at the end point of the Basic Dosimetry Chain, Proceeding of an International Symposium on Measurement Assurance in Dosimetry, Organised by the International Atomic Energy Agency and held in Vienna, 24-27 May 1993.

-Thwaites D I, Williams J R (1994_a), " Radiotherapy Dosimetry Intercomparisons " , Radiation dose in Radiotherapy from prescription to Delivery, IAEA-TECDOC-734, IAEA, Vienna (in press).

-Thwaites D I (1994_b), The role of Quality Audit in Radiotherapy.

Thwaites D I, Scalliet P, Leer JW, Overgaard J (1995_a), Quality assurance in radiotherapy, European society for Therapeutic Radiology and Oncology Advisory Report to the Commission of the European Union for the "Europe Against Cancer Programme" Radiotherapy and Oncology, 35, 61-73.

-Thwaites D I and Allahverdi M (1995_b), The development of interdepartmental audit methods, Radiotherapy and Oncology, vol. 37 (suppl. 1), 570.

-Thwaites D I and Allahverdi M (1995_c), Evaluation of commercial epoxy-resin water-substitute materials for MV photon beam use, Radiotherapy and Oncology, vol. 37 (suppl. 1), 150.

-Thwaites D I (1996), External audit in radiotherapy dosimetry in 'Radiation Incident (Brit. Inst. Radiol., London).

-Thwaites D I and Allahverdi M (1997), The use of semianatomic phantom in interdepartmental dosimetry audit, World Congress on Medical Physics and Biomedical Engineering, XI th International conference on Medical Physics, Nice, France, 140-PSI-02.

-Vadash P, Bjarngard B (1993), an equivalent-square formula for head scatter factors, Med. Phys. 20 (3), 733-734.

-Van Bree N A et al (1991), Results of quality control of breast cancer irradiation in the Netherlands, IAEA, Leuven.

-Van Bree, Van Battum H, Huizenga H, Mijnheer B (1994), results of quality control of breast cancer irradiations in the Netherlands, IAEA-TECDOC-734, Leuven.

-Van Dam J, Vaerman C, Blankaert N, Leunens G, Dutreix A, and van der Schurren E (1992_a), Are port films reliable for in vivo exit dose measurements Radiother. & Oncol., 25, 67-72.

-Van Dam et al (1992_b), influence of shielding blocks on the out put of photon beams as a function of energy and type of treatment unit, Radiotherapy and oncology, 24, 55-59.

-Van de Geijn J (1972). Computational methods in beam therapy planning. computer programmes in Biomedicine, 2: 153-168.

-Van Dyk J, Barnett R B, Cygler J, and Shragge C (1993), Commissioning and quality assurance of treatment planning computers, Int. J. Radiation Oncol. Biol. Phys., 26, 261-273.

-Van Gasteren J M et al. (1991), The determination of phantom and collimator scatter component of the output of megavoltage photon beams : measurement of the collimator scatter part with a beam-coaxial narrow cylindrical phantom, Radiotherapy and Oncology, 20, 250-257.

-Weatherburn H, and Nisbet A (1991), The protocols and codes of practice used for the determination of absorbed dose in megavoltage photon and electron beams. Critical review in Biomedical Engineering 19 (2, 3), 147-180.

-Webb S, Fox R (1980), Verification by Monte Carlo methods of power law TAR algorithm for inhomogeneity corrections in photon beam dose calculations. Physics in Medicine and Biology, 25 (2) :225-240.

-Webb S, Cassel K (1985), Comment on 'Generalised Batho correction factor' Physics in Medicine and Biology, 30 (8), 859-860. Letters to editor.

-Weltens C, Leunens G, Dutreix A, Cosset G M, Eschwege F, van der Schueren E (1993), Accuracy in mantle field irradiations : irradiated volume and daily dose, Radiother. & Oncol., 29, 18-26.

-Westerman C, Mijnheer B, Kleffens H (1984), Determination of the accuracy of different computer planning systems for treatment with external photon beams, Radiotherapy and Oncology, 1, 339-347.

-Williams J R and Thwaites D I, editors (1993). Radiotherapy Physics in Practice. Oxford University Press, Walton Street, Oxford, OX2 6DP.

-Withers H and Peters L J (1980), Basic principles of Radiotherapy, 3rd edn., pp 103-180, editor; G.H. Fletcher. Lea and Febiger, Philadelphia.

-William Kwa et al, (1994), dosimetry for asymmetric x-ray fields, Med. Phys., 21(10).

-Wittkamper F W et al, (1987), Dose intercomparison at the Radiotherapy centres in the Netherlands. 1, Photon beam under reference conditions and for Prostatic cancer treatment , Radioth. Oncol., 9, 33-44.

-Wittkamper F W et al, (1988), Dose intercomparison at the Radiotherapy centres in the Netherlands. 2, Accuracy of locally applied computer planning systems for external photon beams, Radioth. Oncol., 11, 405-414.

-Wong J, Henkelman R (1982), Reconsideration of the power law (Batho) equation for inhomogeneity corrections. Medical Physics, 9 (4), 521-530.

-Wong J, Henkelman R, (1983), A new approach to CT pixel-based photon dose calculation in heterogeneous media. Medical Physics, 10,199-208.

-Wong J, Purdy J (1990), On methods of inhomogeneity correction for photon transport. Medical Physics, 17, 807-814.

-Wong J et al (1991), Role of inhomogeneity corrections in three-dimensional photon treatment planning. Int. J. Radiation Oncology Biol. Phys. (1991), 21 (1), 59-69. Photon Treatment Planning Working Group.

-Woo M, Cunningham J, Jezioranski J (1990), Extending the concept of primary and scatter separation to the condition of electronic disequilibrium, Med. Phys. 17 (4), 588-595.

-World Health Organisation (1988), Quality Assurance in Radiotherapy (Geneva, WHO).

-Worsnop B R, (1968), Phantom thermoluminescent dosimeter comparison for a co-operative Radiotherapy trial, Radiology, 91, 545-553.

-Wu A, Zwicker R, Krasin F, Sternick E (1984), Dosimetry characteristics of large wedges for 4 and 6 MV x-rays, Med. Phys. 11: 186-188.

-Young M, Gaylord J (1970), Experimental tests of corrections for tissue inhomogeneities in radiotherapy, Br. J. Radiol., 349-355.

-Yu MK, Murray B, and Sloboda R (1995), parametrization of head scatter factors for rectangular photon fields using an equivalent square formalism, Med. Phys., 22 (8), 1329-1332.

-Zhu T C and Bengt E Bjarngard (1994), The Head scatter factor for small field sizes, Med. Phys., 21(1), 65-68.

-Zhu T C, Bjarngard B, and Shackford H (1995), x-ray source and the output factor, Med. Phys., 22 (6), 793-798.